Formation Flight

analysis of wake sensitivity, drag and control in trimmed flight

E.R.G. Windels B.Sc.

Master Thesis

TU Delft Delft University of Technology

Faculty of Aerospace Engineering

Master of science thesis

For the degree of master of science in Aerospace Engineering at
Delft University of Technology

FORMATION FLIGHT

ANALYSIS OF WAKE SENSITIVITY, DRAG AND CONTROL IN TRIMMED FLIGHT

August 24, 2015

E.R.G WINDELS B.SC.

Delft University of Technology
Faculty of Aerospace Engineering – Systems Engineering and Aircraft Design
thesis id no. 256#15#MT#SEAD-FPP
Picture title page by S. Ramadier for AIRBUS S.A.S. 2014

Delft University of Technology

Delft University of Technology
Department of Systems Engineering and Aircraft Design

The undersigned hereby certify that they have read and recommend to the Faculty of Aerospace Engineering for acceptance a thesis entitled

Formation Flight analysis of wake sensitivity, drag and control in trimmed flight

in partial fulfilment of the requirements for the degree of Master of Science Aerospace Engineering

Dated: August 24, 2015

Chairman exam committee
Supervisor:

Prof. Dr.Ir. L.L.M. VELDHUIS

Supervisor:

Dr. Ir. M. VOSKUIJL

Reader:

Dr. Ir. R. DE BREUKER

Reader:

Ir. O. STROOSMA

ACKNOWLEDGEMENTS

The research as presented here provided me with many insights and interesting thoughts concerning aerospace engineering. This would not have been possible without the help of the people surrounding and supporting me. First of all I would like to express my sincere appreciation for both my supervisors, dr.Ir. Mark Voskuijl and prof. dr.Ir Leo Veldhuis, for their critical feedback and assistance during my master graduation project. I would also like to express my gratitude to the friends who have read and corrected my report for spelling and consistency. Furthermore a special thanks to my close friends, room mates and family for supporting me during this long and hard final period of my master study in aerospace engineering.

24th of august, 2015

E.R.G. Windels B.Sc.

ABSTRACT

A research simulation model was created to perform extended research into formation flight dynamic behaviour. The principle of aircraft flying in formation is to lower the induced drag and fuel flow. A trail aircraft that flies within the wake vortex field of a lead aircraft encounters an increased effective angle of attack, reducing the induced drag component. This benefit is accompanied by induced interference effects, most pronounced in roll and pitch. Control deflections are required to retain a predefined flight path within the formation flight (trim). These deflections during cruise flight diminish the benefit of drag reduction. This research focuses on quantifying this reduction in benefit. The test case investigated was an Airbus A330-300 in an assumed cruise flight at Mach 0.6 at an altitude of $11,000$ meters with a lift coefficient of 0.623. An extended vortex lattice method combined with a simulation model of non-linear equations of motion based on rigid multi body dynamics was used. The aerodynamic results showed a margin of error of 10% around the vortex core. The position for highest induced drag reduction, the sweet spot, was located at $-0.15y/b$ and $0.1z/b$, where the lead aircraft vortex is located at $-0.107y/b$ and $0z/b$. In close proximity of the vortex, variations in loads with position remained small compared to the deeper wakefield. The untrimmed aircraft had a reduction in induced drag of 52.6%, where the trimmed aircraft had a reduction of 47.5%. The benefit is effectively lowered by 5.1%, and possibly more of the benefit is lost by compressibility and viscous effects that are not within the scope of this thesis. The aileron deflection at the sweet spot is $2.32^{\cdot}$ degrees. The trail aircraft at the sweet spot showed unstable behaviour in pitch and roll. The aileron hinge moments caused by deflection during cruise formation flight were estimated. When compared to the design limit in solo flight condition, loads were shown to exceed the limit by 6.8% for deep wake field positions. At the sweet spot, the hinge moments were well within the limit. A study on the design of the aileron control surfaces revealed that an increase in area, by using both inboard and outboard ailerons, negatively affects the stability of the formation. Nevertheless the hinge moments are reduced by using both ailerons. A positive effect on trim in formation flight was identified by deflecting the ailerons non-differential, through application of a predefined deflection on the in-vortex aileron to remove the rolling moment. The total benefits for the trail aircraft in formation flight at the sweet spot are 16.59% in total drag and 18.27% in fuel flow. Important to note is the absence of pressure drag for the total drag determination.

LIST OF SYMBOLS

Symbol	Description	Unit
Γ	Circulation strength of a vortex	m^2/s
Γ_0	Total circulation	m^2/s
Δ	Change between formation flight and solo flight condition	-
Λ	Sweep angle	deg
Λ_H	Hinge sweep angle	deg
∇	Gradient value	-
$\nabla\phi$	Velocity potential	-

Table 1: List of symbols: greek symbols capital

Symbol	Description	Unit
α	Angle of attack, with relation to body reference frame	deg
β	Side-slip angle, with relation to earth reference frame	deg
δ	Change in value of angle/coefficient	-
δa	Aileron deflection angle	deg
δe	Elevator deflection angle	deg
δr	Rudder deflection angle	deg
ϵ	Drag fraction	-
η	Semi-span of wing	m
η_i	Span-wise distance from center-line to inboard limit of aileron, over semi span	-
η_n	Span-wise distance from center-line to outboard limit of aileron, over semi span	-
θ	Pitch angle, with relation to earth reference frame	deg
ϕ	Roll angle, with relation to earth reference frame	deg
$\dot{\phi}$	Derivative to time of roll angle, roll rate	
ρ	Density	kg/m^3
τ	Trailing edge sweep angle	deg
ψ	Yaw angle, with relation to earth reference frame	deg
ω	Radial velocity	-

Table 2: List of symbols: greek symbols

Symbol	Description	Unit
AR	Aspect ratio, b^2/S	-
C_L	Lift coefficient	-
C_D	Drag coefficient	-
C_H	Hinge moment coefficient	-
C_X	Total aerodynamic force coefficient in X direction	-
C_Y	Side force coefficient	-
C_Z	Total aerodynamic force coefficient in Z direction	-
C_f	Friction coefficient	-
C_l	Rolling moment coefficient	-
C_m	Pitching moment coefficient	-
C_n	Yawing moment coefficient	-
C_p	Pressure coefficient	-
D	Drag	-
$G_{1,2,3}$	Functions used for induced camber contributions during hinge moment estimation	
L	Lift	-
M	Mach number	$Mach$
Re	Reynolds number	-
S	Total wing area	m^2
S_{wetted}	Total wetted area of aircraft model	m^2
$\mathbb{T}_{ve}$	Transformation matrix, from earth to vortex system	-
U	Speed	m/s
V	Speed	m/s
V_r	Radial velocity	m/s
V_θ	Circumferential velocity	m/s
W	Aircraft weight	kg
X	Total aerodynamic force in X direction	-
Y	Side force	-
Z	Total aerodynamic force in Z direction	-

Table 3: List of symbols: latin letters capital

Symbol	Description	Unit
a	Speed of sound	m/s
a_1	$\frac{dC_H}{d\alpha}$, Rate of change of lift due to angle of attack	rad^{-1}
a_2	$\frac{dC_H}{d\delta a}$, Rate of change of lift due to aileron deflection angle	rad^{-1}
b	Wing span	m
b_1	Hinge moment derivative with relation to the angle of attack	rad^{-1}
b_2	Hinge moment derivative with relation to the aileron deflection angle	rad^{-1}
c	Wing chord	m
c_f	Flap chord	m
d	Change in value of distance	m
h	Altitude	m
l	Rolling moment	-
m	Pitching moment	-
$\dot{m}$	fuel flow	-
n	Yawing moment	-
p	Roll rate	deg/s
q	Pitch rate	deg/s
r	Yaw rate	deg/s
r_c	Vortex core radius	m
t	Thickness	m
v	Horizontal velocity component	m/s
w	Vertical velocity component	m/s
$\mathbf{x}$	location vector	m
x	Longitudinal distance	m
y	Lateral distance	m
z	vertical distance	m

Table 4: List of symbols: latin letters

Symbol script	Description
i	Induced drag component
∞	free stream component
ref	Reflecting on reference value
v	Vortex reference frame
b	Body reference frame
E	Earth reference frame
α	Derivative to change of angle of attack
β	Derivative to change of side-slip angle
δa	Derivative to change of aileron deflection angle
δe	Derivative to change of elevator deflection angle
δr	Derivative to change of rudder deflection angle
p	Derivative to change of roll rate
q	Derivative to change of pitch rate
r	Derivative to change of yaw rate
$trim$	Reflecting on the aircraft in trimmed condition
FF	Reflecting on the aircraft in formation flight
$solo$	Reflecting on the aircraft in solo flight
0	Two dimensional wing in an incompressible flow assumed
T	Theoretical value used (instead of empirical)
$\star$	Standard plain section assumed

Table 5: List of symbols: subscripts and upperscripts

CONTENTS

CHAPTER

ONE

INTRODUCTION

Today's world poses a wide variety of challenges to the aviation industry: Noise problems around airports, pollutant emissions, fossil fuel depletion, all of which require smart solutions. Perhaps one of the most problematic and complex issues to tackle is reducing the usage of fossil fuels, or even find other fuels for aircraft. The use of fuel today automatically means emitting pollutants into the atmosphere, directly or indirectly. Besides design and configuration alterations of current aircraft, e.g. research into aero engines, wing-body fuselage configurations, also operational aspects are explored. The main advantage of operational changes is that they can potentially be implemented fast and easily using the existing aircraft fleet, however there are operational aspects that have not been exploited already.

Since the beginning of the twentieth century, research into flight in a formation has been carried out. Birds travelling long distances fly in V shaped or echelon formations. In 1914 it was identified by Wieselberger that it is more than just an optical benefit for the flock of birds [1]. Nowadays it is already scientifically proven that formation flight can offer a drag reduction of around 25%, using computational models [2]. Ranging from low order methods all the way to sophisticated Euler and Navier-Stokes codes, all identify the benefit. The drag reduction benefit in formation flight creates the opportunity to use less fuel during cruise flight. During a test flight, using two C-17 aircraft in a longer duration formation flight condition, an average fuel flow reduction of $5 - 10\%$ was attained during formation flight [3]. From an operational point of view, Flanzer et al. did research on the possible impact of formation flight on the entire fleet of C-17 aircraft of the U.S. Air Force [4]. Using existing data on flight paths and patterns of the C-17 aircraft for the U.S. Northern Command, it was identified that several percent per year in fuel could be saved, by allowing formation flights to be flown when possible and/or desired.

These reductions offer significant fuel savings, achieved by flying in formation. However the question rises what effect the formation has on the aircraft. Within a formation, a lead and trail aircraft are identified. The trail aircraft positions itself within the wake vortex field of the lead

aircraft. The mutual interference of the wake vortex field on the trail aircraft creates a beneficial region with respect to induced drag, creating a reduction in induced drag leading to an overall decrease in drag and fuel flow. The wake vortex field will also create disturbances however, where the rolling and pitching moment are the highest [5], which need to be counteracted. The aircraft is subjected to a new range of forces and moments, which it needs to cope with. Computational models and test flights have already proven that current aircraft are able to fly in formation, although the impact on the control systems is not specifically investigated or defined. The research study by Kless et al. [6] investigated the inclusion of compressibility effects within the formation flight benefit. It was identified that a complex behaviour existed between control deflections and the wake field, reducing the induced drag benefit in transonic conditions by $9 - 11\%$. Despite the results were inconclusive, further investigation was recommended.
This research will focus on the effect of balancing the aircraft forces and moments into a steady state straight flight, further referred to as trimming the aircraft. Quantifying the impact on formation flight benefits and providing a method to analyse current aircraft and the possibility to use them within a formation flight.

The research goal is to provide a quantitative analysis of aircraft trim on the trail aircraft and its lateral control system when flying within the wake vortex generated by a lead aircraft during formation flight. To reach this goal, five questions need to be answered. First, the interference effects within the wake field need to be quantified and understood. The variation of the interference effects needs to be mapped to identify regions of interest. Second, the effect on trail aircraft, when placed within the wake field, needs to be determined. A full understanding of the wake vortex field and the forces/moments it induces upon the trail aircraft is required. Third, the effect of trimming the trail aircraft can be investigated by making use of standard conventions. Fourth, the effect of the wake induced rolling moment upon the aileron deflection and aileron hinge moment is investigated. Finally it will be investigated what the effects of the aileron surface and their deflection angles are upon the trimming of the aircraft and the total formation flight benefit. A list containing the overview of the five questions, plus the research question, is given below:

The research goal is *to provide a **quantitative analysis** of **aircraft trim** on the trail aircraft and the impact on the **lateral control system** when flying within the wake vortex generated by a lead aircraft during a **formation flight***

- Analysis of wake vortex field sensitivity, as generated by the lead aircraft
- Analysis of trail aircraft positioned within wake vortex field
- Analysis and quantification of trim on the trail aircraft positioned within the wake vortex field
- Sensitivity of aileron surface and control allocation on the aircraft trim

Figure 1.1 shows the outline of the analysis tool that will be created. The report outline is built up similarly. Three major parts can be identified: The wake field analysis, the aerodynamic analysis and the flight dynamic and load analysis. Two iterations can be seen where the aileron surface and aileron deflection are varied, covering all research questions.

Within this report, first an outline and overview of the history of formation flight is given. Afterwards an overview of the research already performed concerning the topic of formation flight is provided, divided into perspectives on aerodynamics, flight dynamics and a combined overview. These first topics form the second chapter with background information. The third and fourth chapter consist of the aerodynamic and flight dynamic and load analysis respectively. Both chapters first identify requirements for analysis tools that need to be developed, after which tools are chosen for analysing the aerodynamic and flight dynamic and load aspects. These tools are extended to meet the specific requirements and are then validated. Finally analyses are performed on aerodynamic and flight dynamics and loads of the formation flight. A data sensitivity analysis is presented in chapter five. The data sensitivity analysis consists of two case studies, where the aileron area and deflection angles are varied to measure the impact upon the formation flight condition. Finally the sixth chapter provides a feasibility study of formation flight for commercial air transport. The impact of a trimmed formation flight is covered and compared to state-of-the-art studies performed today.

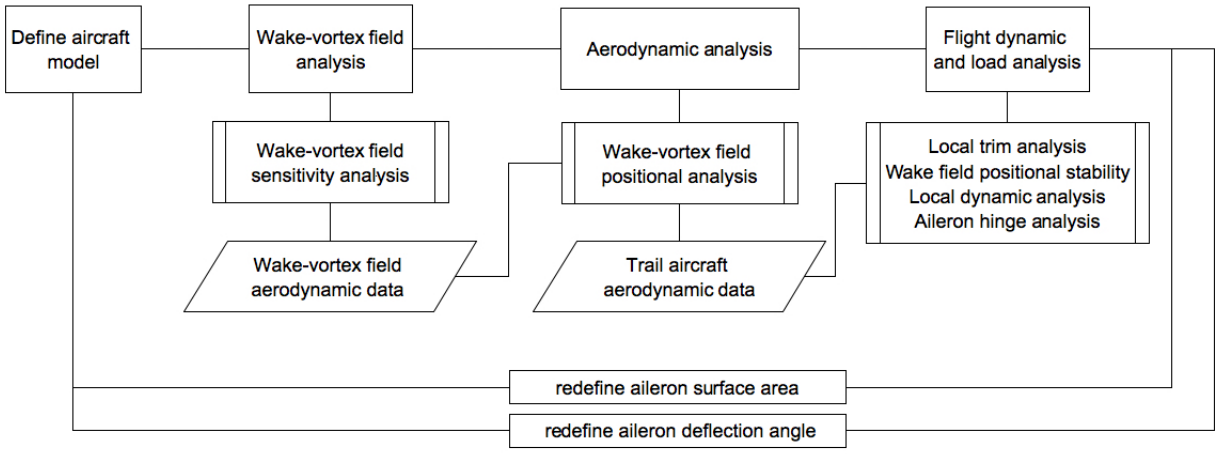

Figure 1.1: Outline of research into different topics

CHAPTER

TWO

BACKGROUND RESEARCH

This chapter contains the background literature research performed into the topic of trimmed formation flight. First the history and development of the formation flight is discussed. Subsequently the aerodynamic and flight dynamic aspects deemed relevant for the analysis of the trimmed formation flight are elaborated. Finally a general flight description of the formation flight condition is given to obtain a test case, which will be analysed within this research.

First of all some conventions are defined, which are used throughout the report. All graphs and figures presented here will make use of the vortex reference frame (indicated in red) and body reference frame (indicated in blue) shown in figure 2.1. The drag reduction values can be represented in two manners, the percentage of benefit of the formation condition or by means of the drag fraction. Both equations and symbols are shown in equations 2.1 and 2.2.

$$\Delta D = 100 \left[1 - \frac{D_{trailaircraftinformation}}{D_{trailaircraftoutformation}} \right] \tag{2.1}$$

$$dragfraction = \epsilon = \frac{\sum D_{i,formation}}{\sum D_{i,out-of-formation}} \tag{2.2}$$

2.1 History and development

The birds that fly around us, gave an incentive for man to investigate and create a way for mankind to fly. Ever since the first manned flight by the Wright brothers, the manner of flight by birds fascinated us. In 1914 Wieselberger formulated that when birds fly in a V formation, the trailing birds take advantage of the lead bird and thus use less energy for flight [1]. This theory

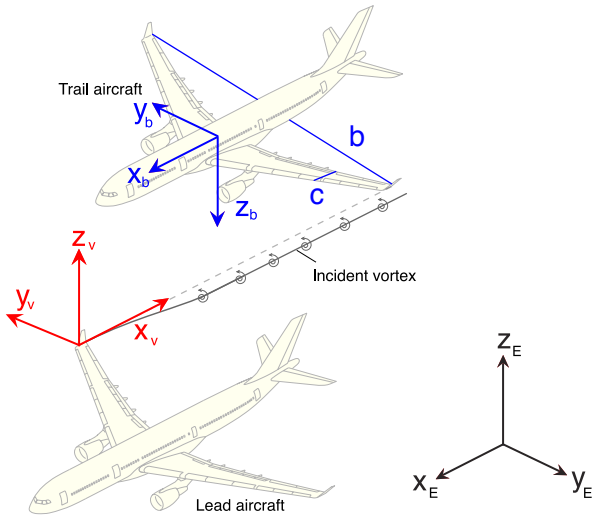

Figure 2.1: Clarification aircraft axis system and aircraft positioning

was created by observing and investigating three birds flying in a V-formation. A simplified analysis only showed small energy savings though. Throughout the coming decades several research investigated the mechanisms of drag reductions by formation flight. Stated here is a list of known studies: Stresemann in 1934, Stolpe and Zimmer in 1939, Storer in 1948 and Dorst in 1956. Most of their research was not quantitative however. The aerodynamic benefit principle was not properly understood at that time.
In 1942 Schlichting with Turckenbrodt [7] described the aerodynamics of the wake field behind an aircraft, with the regions of up- and down-wash together with the vortex pair, identifying that the up-wash region has a drag reduction when flown in. Schlichting subsequently investigated these drag reductions for a symmetrical V-shaped formation flight [8]. Hummel extended this theory in 1973-1978 to include formation of arbitrary shape, meaning different span, weight and aspect ratio [9] [10]. The theoretical investigations showed a mechanism of aerodynamic interference, where each wing (except the lead) of the formation flies in a region of up-wash generated by the preceding wing. It was identified that the angle with relation to the lift force, induced angle of attack α_i, was tilted creating a force which counteracts the induced drag component, $C_{D,i}$. This principle is shown in figure 2.2. The results of Hummel where in accordance with the findings of Lissaman et al., who performed a study on the optimal formation shape [11].

In 1982 Hummel published a theoretical study, calculating the total flight power reduction attainable by flying in formation, for arbitrarily shaped formations of any number of wings, both homogeneous and inhomogeneous. Homogeneous formation implies all aircraft to be the same within the formation, were an inhomogeneous formation allows multiple aircraft types to form a formation. A strong relation with the lateral distance between the wings was found. Like the study of Lissaman, the goal was to analytically describe the drag reduction and its link to the

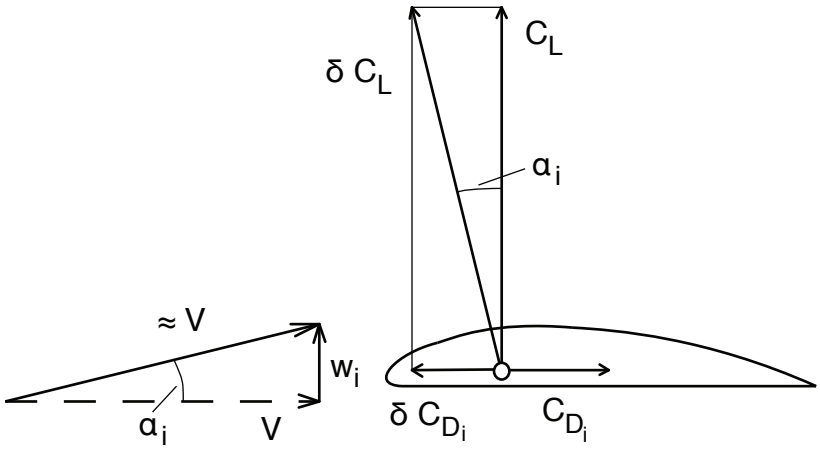

Figure 2.2: Forces acting upon the aerofoil for incoming flow under an upwash angle [12]

shape of the formation.

In 1990 Hummel and Beukenberg performed sample calculations of the formation flight benefit, related to the Dornier Do-28 aircraft, using horseshoe vortex representations to model the wings. These calculations included the effect of control deflections required to fly within the formation. A rolling moment was identified, created in addition to the drag benefit within the wake field due to an asymmetric wing loading. The wake sheet and tip vortices emanating from a lead aircraft were also studied for movements and roll-up effect [13]. In 1995 Hummel published the results of the theoretical prediction and a flight test of the two Dornier Do-28 aircraft. The results are shown in figure 2.3. The figure represent the theory, for a constant longitudinal separation and multiple lateral separation distances. The flight test results consist of three lateral separations, all with slight difference in longitudinal separation. The results showed a good agreement, although these small differences were present.

In parallel to the research concerning the benefits of formation flight and the up-wash region in the wake of a lead aircraft, research was done to investigate the negative behaviour occurring when encountering the wake field of an aircraft. The encounter of a wake vortex from an aircraft by another aircraft, especially during landing, was unwanted due to the vortex induced effects. The aircraft encountering a wake vortex field could have a sudden drop in altitude due to a change in lift, or a sudden change in rolling and/or pitching moment due to the asymmetric local lift distribution. During the landing phase the aircraft is at a low speed in close proximity to the ground. A sudden change, affecting the lifting capability of the aircraft could possibly result in a collision into terrain. Theoretical programs, wind tunnel tests and test flights where performed to measure and quantify the effects of a wake vortex flow field on an aircraft, without considering the benefits. The research into these vortex-induced effects would later be of interest when further investigating the formation flight condition. The results of these studies could be used to further quantify the unwanted effects, next to the desired drag reduction. Examples are the wind tunnel studies by McMillan [14] and Rossow [15]. The amount of studies and reports

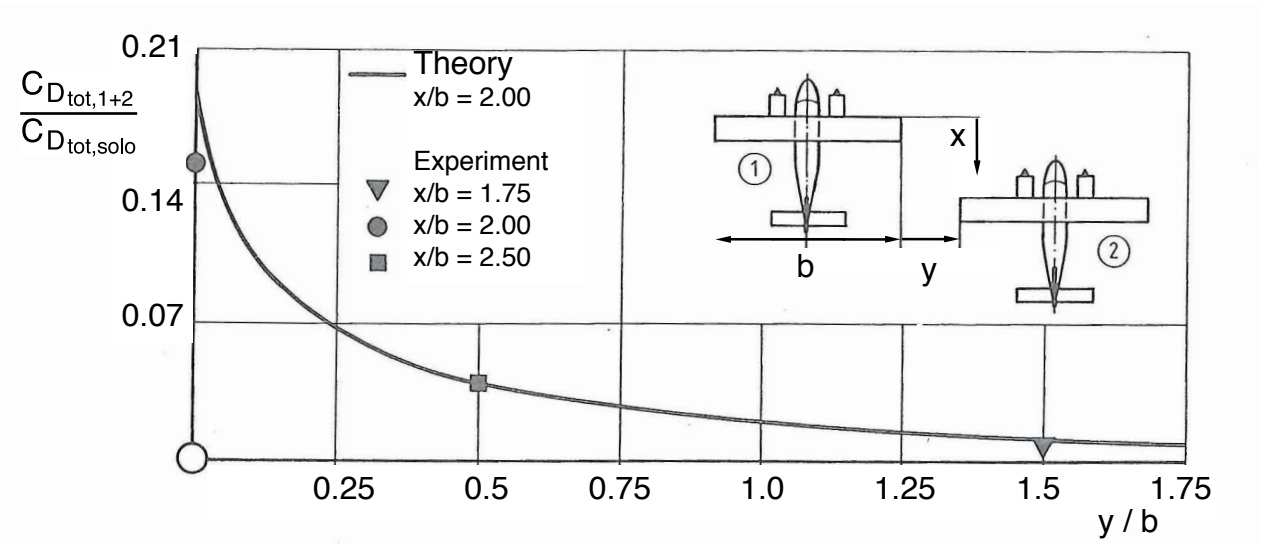

Figure 2.3: Relative power reduction for the trail Dornier Do-28 aircraft theoretically and experimentally measured as a function of the lateral separation distance, y/b (flight parameters: $C_{L,1} = 0.84$, $C_{L,2} = 0.93$ and $(C_{D_0})_{1,2} = 0.0489$)

concerning wake vortex interactions are vast and only of partial interest, therefore no great attention will be paid to the history, development and understanding.

Formation flight was not only investigated from a drag reducing perspective, but also for a control and tactical advantage during 'aerial delivery' missions [16]. During the first and second world war techniques for tactical formation patterns of fighter aircraft were developed and refined. During those days, the aircraft were flown without additional help with regards to positioning with relation to the other aircraft in the formation. Although the task of flying in a formation pattern was tedious, the task was deemed simple once the techniques were mastered by the pilot. The term Station Keeping was ascribed to the task of flying within a formation, stemming from the Navy describing their techniques to retain a tactical position with relation to one another.
Lockheed started to develop flight systems for station keeping in 1962. In 1965 a patent was distributed by them describing aircraft station keeping and terminal navigation systems [17]. The system developed, consisted of a series of transponders mounted on each aircraft to obtain relative positions to each other within the formation. The system was further refined towards a vector positioning station keeping system in 1968 [16]. The pilot could now accurately position the aircraft along three orthogonal axes, relative to a lead aircraft. The system was implemented in military aircraft and helicopters and remained a topic of further research. Not all studies concerning station keeping are included here, just a brief introduction upon the start of the research topic is given. Further information can be found by research into proceedings from Lockheed and the United States Air Force concerning the topic.

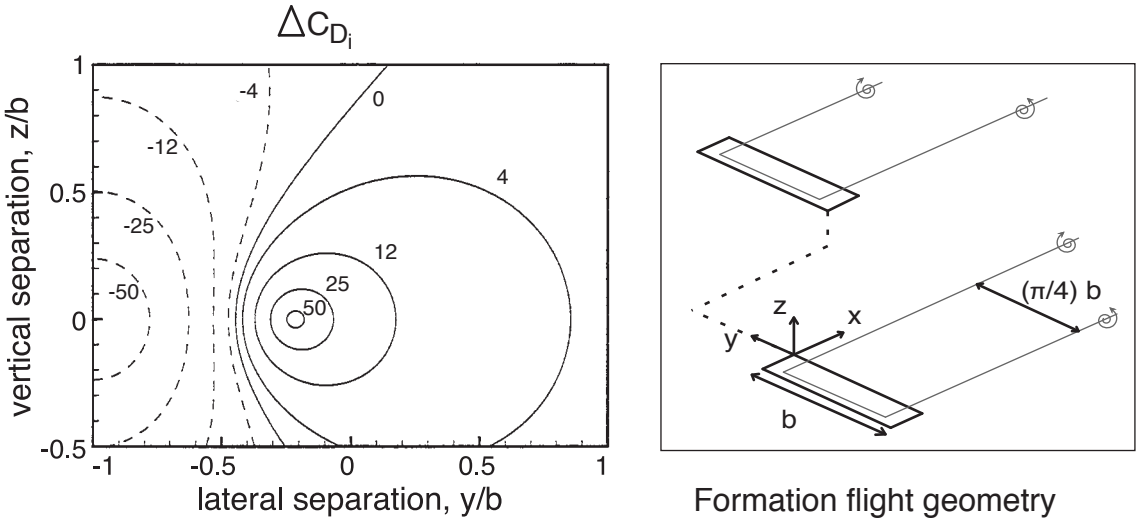

Figure 2.4: Induced drag reduction with relation to solo flight condition of two straight wing models (horseshoe vortex models) with relation to their their vertical and lateral separation[18]

The station keeping systems and studies of the wake field dynamic (in)stabilities by the US Air Force triggered Blake to reinvestigate the aerodynamic benefit as identified by Hummel in 1998 [18]. The advances made within the station keeping systems opened the possibility to fly aircraft in a close formation flight to significantly increase their range. Blake, using horseshoe vortex models to theoretically describe the formation flight, unveiled large induced drag reductions when flying at a specific spot with relation to a lead aircraft. Figure 2.4 shows the total drag reduction as obtained by Blake. The drag reduction is represented as a percentage related to the solo flight condition.

The formation flight condition also created changes in lift, side-force and the three moments. Blake already points out that the trim required to balance these forces and moments might degrade the drag benefit attained. In 2000 Blake investigated a tailless delta wing configuration mathematically, using a vortex lattice method, validated by wind tunnel test [19]. The goal was to identify the aerodynamic coupling and interference within the wake field, as created by a lead aircraft in the formation flight. The positional stability derivatives, for the three forces and moments, did not show a stable region within the wake field for the tailless delta aircraft. One or more derivatives was always unstable. This meant that flying in a close formation flight would never be inherently stable, for the tailless delta wing studied here. The aircraft would always try to move out of the wake field and out of the formation flight pattern. Studies on the drag reduction of aircraft flying in formation continued, comparing multiple methods with wind tunnel data, like Wagner did in 2001 for multiple T-38 aircraft [20]. Most studies are performed by the US Air Force in corporation with the NASA Dryden research center.
The analytical approaches and wind tunnel testing eventually lead to the flight test of two F/A-18 aircraft in 2002 [21] [22]. The results affirmed the analytical models, despite the effect of trim

and control of the aircraft in formation were not modelled. It was demonstrated however that the pilots were able to compensate the vortex-induced effects within the wake field to retain the formation flight manually. The task was cumbersome however, as the relation to the changes in forces and moments was highly dependent on the relative position of the trail aircraft in the wake field. A better understanding in how trim and control affect the formation flight together with an analytical model would be of interest. The pitching moment and rolling moment are the most pronounced. By increasing the longitudinal separation distance, the yaw and side-force become of interest with a decrease in rolling and pitching moment. Increasing the velocity from subsonic to transonic also weakened the vortex induced effects, although not making them negligible.

Nangia et al. published his study on the variations in size and spacing of commercial aircraft flying in formation and the relation to the induced effects and control in 2007 [23]. This started the interest of using the principle of formation flight on commercial aircraft, instead of only for military purposes. The results of Nangia showed again the importance of positioning the trail aircraft within the wake field of the lead aircraft, due to the sensitivity of forces and moments present within the wake field. Ning et al. started to research the effect of compressibility on transport aircraft and their related drag penalties in 2011, using an Euler solver method [24]. It was identified that the vortex interaction, in close proximity cases, create formation induced shocks. These shocks do not immediately imply a large drag increase, but do show a strong potential for flow separation and buffet. Although not entirely understood, Ning poses that further and more extensive research into these compressibility effects is required. It is also identified that further research into the effect of trim and control for the formation flight condition is advisable, to model and quantify the effect upon the drag reduction. Up until now only results of drag reduction from test flights include the effect of trim and control.
Fransen created an aerodynamic analysis tool, based on a vortex lattice method, which can analyse the formation flight for multiple aircraft [25]. The tool also incorporates an option to model, recreate and analyse wind tunnel tests analytically. A wind tunnel test concerning formation flight could thus first be mathematically modelled, analysed and refined before actually performing it. Van der Kleij investigated and developed a flight control system to trim and control the aircraft in the formation flight condition [26]. The research makes use of a basic aerodynamic estimation method, the lifting line theory. This data is used as input for an extensive flight simulation model, specific to the Boeing B-747 aircraft. Both Fransen and van der Kleij make an excursion to the effect of trim and control during the formation flight. Although different and inconclusive results are shown, a good impression is given upon the effect of trim during the formation flight. Figure 2.5 shows the drag reduction attained and the local wing loading for an Airbus A330 aircraft in trimmed condition throughout the wake field as obtained by Fransen. The maximal drag reduction value is marked with the red star and has a value of 61.78%. The highest drag reduction in untrimmed condition was shown to be 65.56%.

The effect of trim upon the formation flight was specifically researched by Kless et al. in 2013, using an Euler solver method [6]. Similar to the research of Ning, Kless identified the potential danger of formation-induced shocks creating flow separation and buffet. The research shows a loss in drag benefit of $3 - 5\%$ in subsonic and $9 - 11\%$ in transonic conditions.

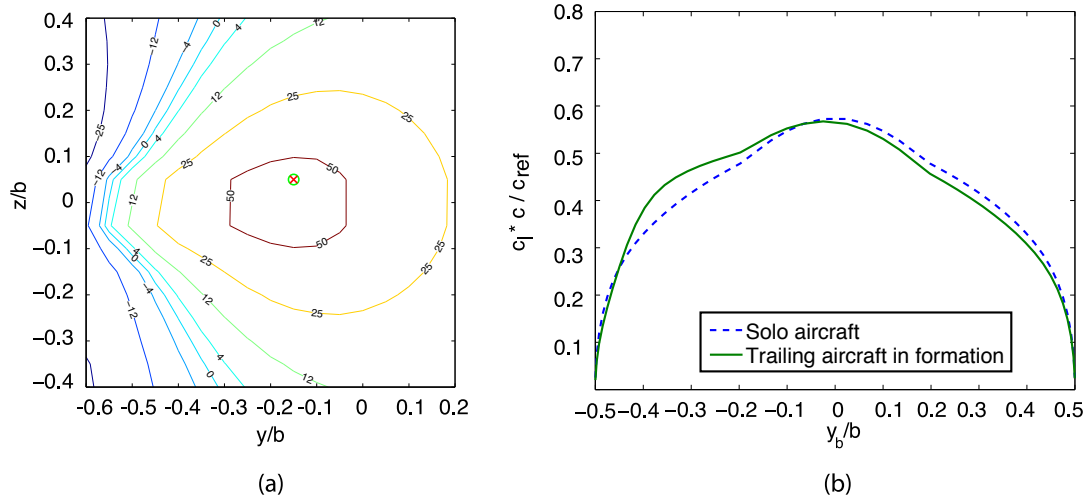

Figure 2.5: Formation Flight Results Fransen: (a) Induced drag reduction within wake field (b) wing loading at sweet spot [25]

It was pointed out that further research is required into the physics of the wake vortex field when encountering a trail aircraft, also recommended by Ning. Garmann et al. [27] and Barnes et al. [28] started to analyse the wake vortex and a lifting surface when one encounters the other. A validated high order Navier Stokes solver was used to attain a clear picture of the flow behaviour and force/moment variations. Their results are invaluable to further analyse, understand and develop techniques to investigate the formation flight.

The NASA Dryden research center and the US Air Force kept on researching and developing the formation flight principle, now also for larger transport aircraft instead of just fighters. The Surfing Aircraft Vortices for Energy (SAVE) program was started in 2012, to provide a platform for the analysis of the formation flight concept. Within SAVE an initial test flight was performed using a C-17 Hercules military transport aircraft [29]. The aircraft was chosen for its excellent station keeping capabilities, from pre-installed software of earlier tactical formation flights. The purpose was to gain insights to be used in further development of a formation flight control system, as well as to create a simulation and validation tool for analytical analysis.
The period of 2012 up and till 2014 was used to develop simulation tools, software systems, automated flight control systems and an enhanced autopilot; all tailored to the formation flight. Details on the wake propagation and movement were included in simulation models and within the flight control system to accurately track the wake vortex and position the trail aircraft perfectly. A wake-crossing prevention tool was developed to automatically prohibit the aircraft from moving into parts of the wake field where disturbance forces and moments are highest [5]. A final series of test flights were performed using the systems, for validation purposes. The flight control system proved to be satisfactory for station keeping within the wake field, as well as preventing the aircraft from crossing the wake field, encountering the highest disturbances

[3]. The fuel flow was also measured to determine how much could be reduced during the formation flight condition. The result of fuel flow reduction with relation to vertical and lateral separation for two C-17 aircraft is shown in figure 2.6

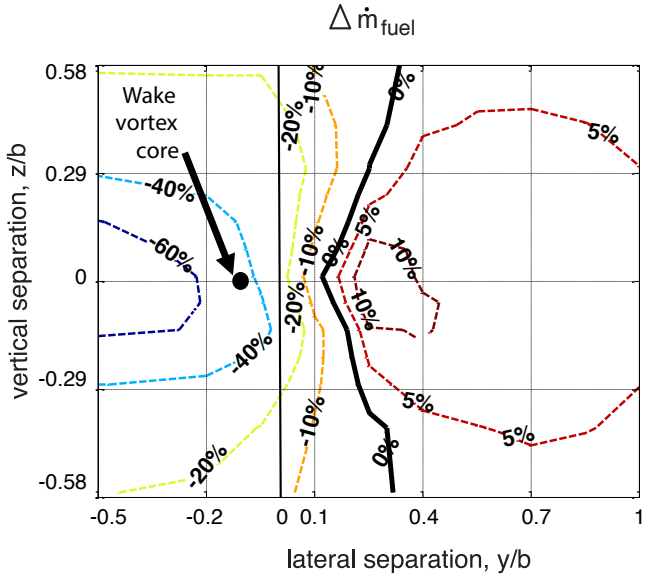

Figure 2.6: Fuel flow reduction, with relation to solo flight condition, obtained form test flight of two C-17 aircraft in formation flight condition[3]

2.2 Aerodynamics

The former section provided the history and development of the concept of formation flight form basic principle until the elaborate research studies executed now. This section will move into some more detail concerning certain aerodynamic aspects of interest for the wake field analysis and the trimmed formation flight. First of all the wake vortex sheet and its behaviour will be discussed, as it is crucial for the formation flight. The interaction of the trail aircraft wing with incident vortices and wake vortex sheets is discussed afterwards followed by a general wake field analysis.

2.2.1 Wake vortex sheet

An aircraft that is flying generates lift over its wings. This lift generation influences/disturbs the flow behind the aircraft, creating a wake field. Due to the three dimensionality of the wings, two tip vortices are created on either side of the aircraft. Between the two tip vortices a region of down-wash is generated and directly outside of the tip vortices, a region of up-wash is

generated by the airflow. Figure 2.7 shows the flow field behind an aircraft. The two vortices flow downstream to form a stable vortex pair. Whilst forming this vortex pair they both move inward and down-ward, known as the wake roll up effect. The effect of the creation and movement of the vortex pair was investigated and described by Jacquin et al.[30] and Veldhuis et al. [31]. Downstream, approximately three to nine wingspans, the wing tip vortices become two concentrated vortices in the flow field. At hat point the total inboard movement (meandering) of the vortices was theoretically determined and experimentally validated to be around $(\pi/4)b$ separation distance between the two vortex cores, which remains during dissipation. The downward movement does not have a set value and depend on the flow conditions. After nine wingspan they start to slowly decay in vorticity when propagating further downstream.

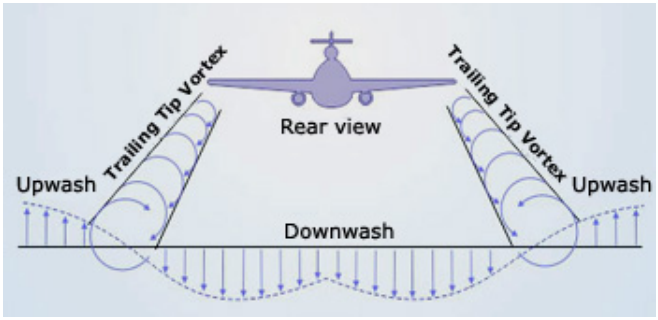

Figure 2.7: Flow field behind an aircraft [32]

In reality the wake vortex sheet is also influenced by the atmospheric winds. The sheet can be pushed up or down and left or right. Generally speaking it is assumed that the distance between the vortex pair remain constant. The wind influence was described by Halaas et al. when creating the simulation and validation model for the C-17 aircraft station keeping system within the SAVE program [5]. The purpose was not to fix the position of the trail aircraft with relation to the lead aircraft, but with relation to the wake vortex sheet. The movement of the vortex pair was therefore determined to identify the optimal position. A simulation model was created to describe the wake dynamics, using the knowledge from the existing wake vortex encounter studies, e.g. Rossow [15]. The model used atmospheric data and was incorporated within the station keeping flight control system, to determine the wake vortex sheet in real-time. The system was tested in a test flight and proved to be accurate enough.

It is important to know that the wake vortex sheet does not remain fixed in space, although for the current investigation of wake field sensitivities and the effect of trim, it is of minor importance. The actual position with relation to the wake vortex sheet is important as the position in the field determines the forces and moments. The wake vortex system was therefore fixed in space at a certain altitude, flowing parallel to the free stream velocity. The position was determined according to the wake-roll-up effect (laterally), neglecting the self-induced downward movement and the possibility of atmospheric interferences.

2.2.2 Wing vortex interactions

Another topic of interest was unveiled earlier, namely the interaction between the wing and the incident vortex system. What happens more precise in that region is elaborated within this part. Only a quantitative analysis is given to obtain insight in the behaviour of the vortex when it encounters the wing.
Garmann [27] and Barnes [28] both investigated the direct wing-vortex behaviour using the extensively validated high-order Navier-Stokes solver FDL3DI. The results of their studies will be used to gain insight into this complex flow behaviour. Afterwards the wind tunnel research of Inasawa [33] will be used to verify the results of the Navier-Stokes solver. The analysis in all cases is that of a rectangular wing. Garmann uses a predefined vortex were Barnes and Inasawa make use of a lead rectangular wing to create the vortex. The basic set-up for the trail aircraft with relation to the vortex is shown in figure 2.8, the lead aircraft and/or vortex generator is omitted in the sketch.

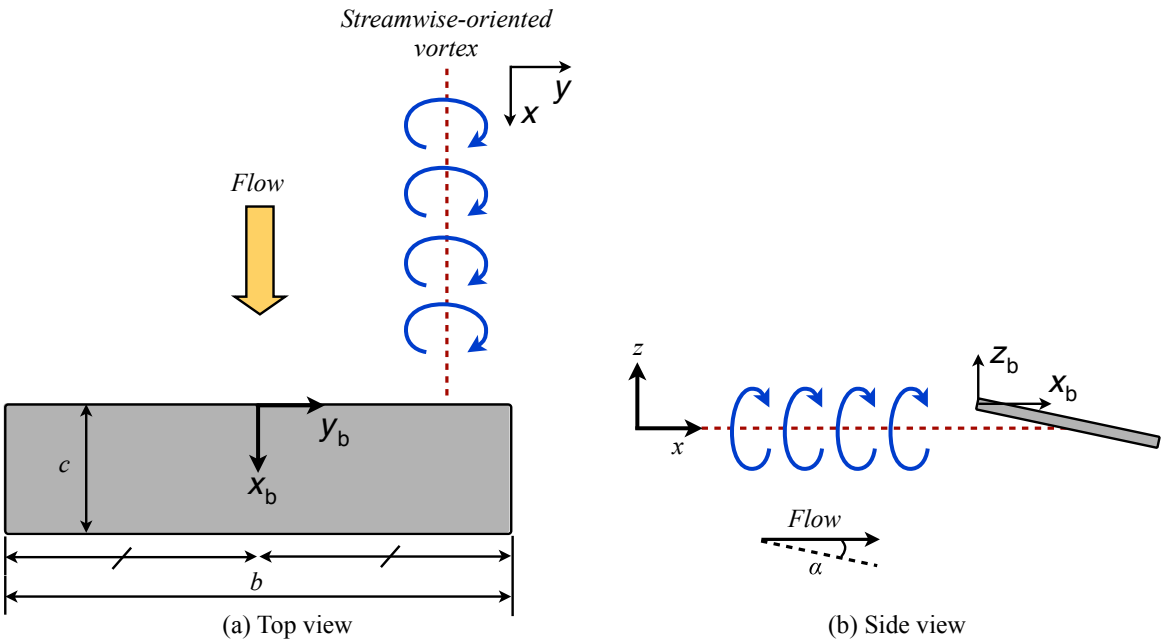

(a) Top view (b) Side view

Figure 2.8: Situation sketch of rectangular wing positioned in flow field with incident vortex [27]

First the results of Garmann will be discussed. Garmann created simulations of an analytical defined vortex superimposed on a free-stream, which is convected toward a rectangular wing at an angle of attack. Figure 2.9 shows the vorticity contours as determined by the Navier-Stokes solver for no vortex (a), close proximity (b), aligned to wing tip (c) and direct interaction (f). The vorticity contours are within dissecting plans perpendicular to the free stream at multiple longitudinal distances. These different positions coincide with the numbering within figure 2.10,

which is discussed later. The case of direct vortex interaction in figure 2.10e and 2.10d where excluded within figure 2.9, therefore they do not appear.

The situation for no impinging vortex is assumed to be self explanatory, the free stream creates a flow field over the wing profile and a tip vortex is created. When looking at the close proximity case figure 2.9b it can be seen that the impinging vortex core remains intact as it convects past the wing tip. At the end of the wing profile and after the wing, the tip vortex will interact with the impinging vortex and form a dipole. This dipole moves upward as it is propelled in the wake field. Both vortex cores remain distinguishable but due to the interaction they do become susceptible to spiralling disruptions.

When the wing tip is aligned, figure 2.9c, it can be seen how the incident vortex is drawn to the upper side of the wing profile as it flows past the tip. The upper side of the wing profile shows an increase in vorticity due to the interaction of the vortex with the outer shear layer on the wing profile. The vortex will entrain the tip vortex on the wing profile. At the trailing edge, both vortices still have distinct and coherent cores. However when being propagated behind the wing, the disrupted feeding sheet (shed off the wing) and entrainment of two opposite-signed vortices on the wing, make that the cores start to loose their coherency and strength. The upward movement behind the wing profile is still distinguishable. A deflection at the wing tip trailing edge, by for example the ailerons, could induce flow separation, disrupting the wake field and the coherency of the incident vortex core. This also holds for the final case, where the incident vortex travels over the wing surface.

This final case of direct interaction, figure 2.9f, shows how the impinging vortex alters the flow over the wing profile.The wing profile bifurcates the vortex into two almost equal vortices.
On the upper side of the profile a region of down-wash is present between the incident vortex to the wing tip, effectively reducing the effective angle of attack, enhancing the recirculation of the separated boundary layer (due to the vortex encounter), making the flow reattach to the surface again. This attached flow suppresses the formation of the tip vortex. A trailing edge deflection could impose flow separation, thus counteracting the initial effect of suppressing the tip vortex however. The region between incident vortex to fuselage sees a region of up-wash with an inboard movement of the bifurcated vortex flow, due to the vortex entrainment with the separated boundary layer.
On the lower side an outboard movement of the bifurcated vortex flow is distinguished (a mirror flow image to the upper side). Behind the wing, both upper and lower vortex cores dissolve within the wake sheet. As the tip vortex strength was almost annihilated by the upper bifurcated vortex flow field, no discernible vortex core is present any longer within the wake field.

Garmann create a three dimensional representation of the flow using the results from the instantaneous iso-surfaces from the Navier-Stokes solver. These representations are shown in figure 2.10, where for the direct wing-vortex interaction case enhancements are shown of the region of impingement.

The numbers in figure 2.10 coincide with those of figure 2.9 as was stated before. The spiralling undulations in figure 2.10b are the interaction between tip vortex and impinging after which they form the dipole downstream. The entrainment of figure 2.9c becomes clear in figure 2.10c.

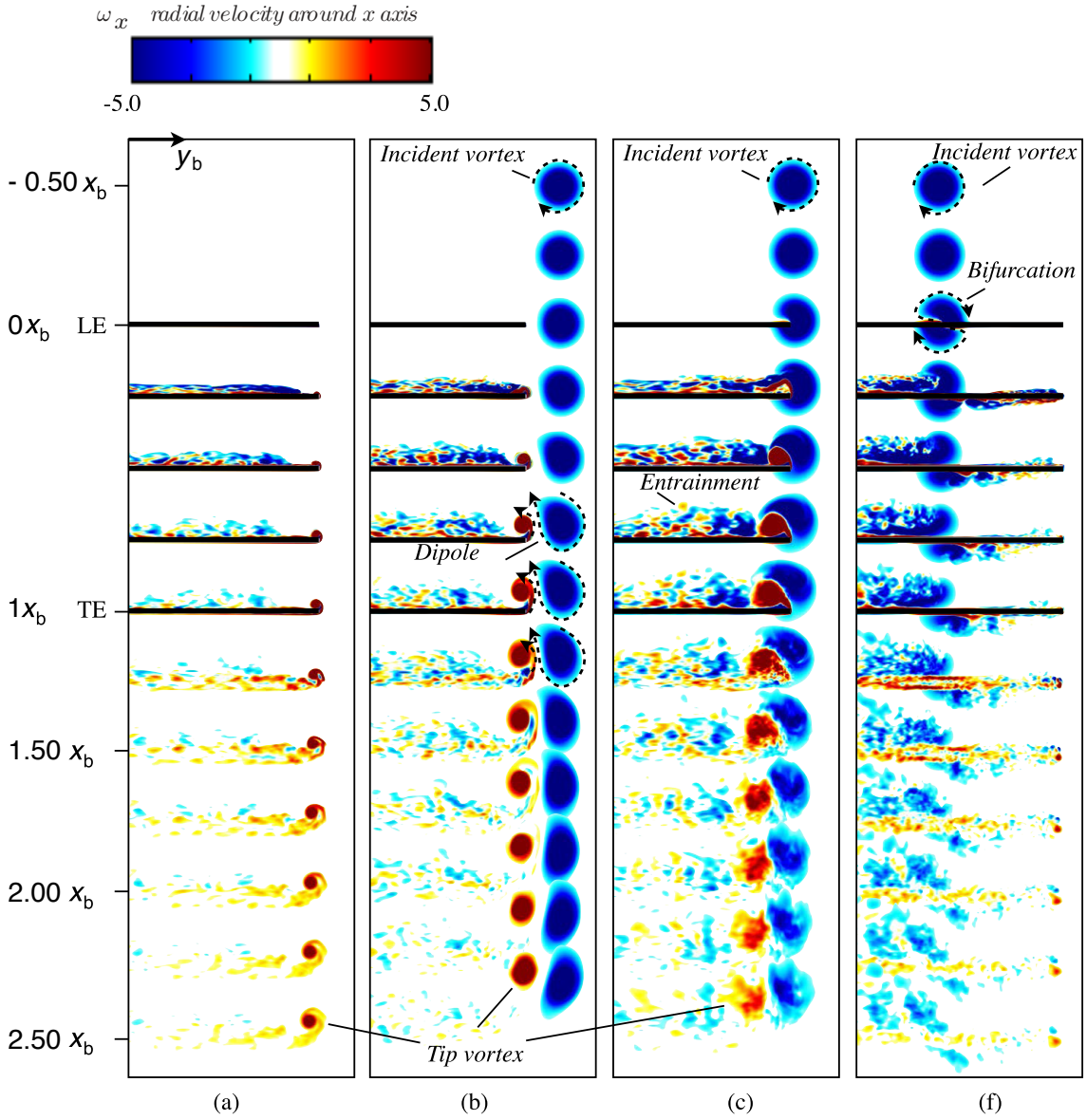

Figure 2.9: Interaction of wing-vortex and consequent decay with relation to vortex positions relative to the wing (a) no vortex (b) vortex in close proximity (c) vortex on wing tip (f) direct wing-vortex interaction [27]

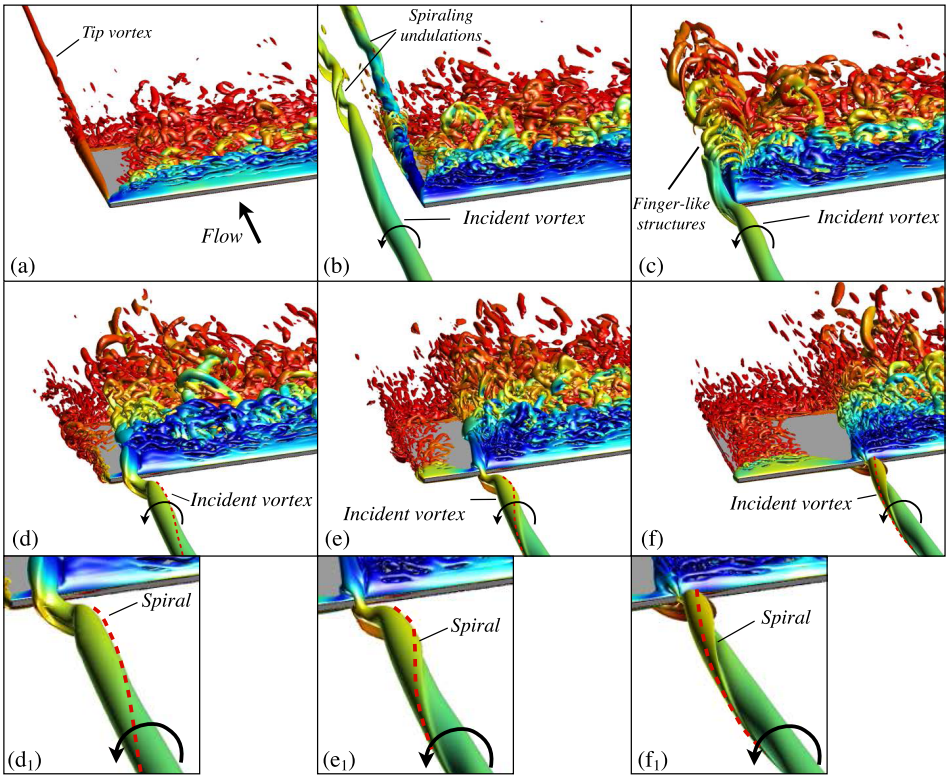

Figure 2.10: Snap shots of instantaneous flow structure simulations through iso-surfaces of the Q-criterion using validated high order Navier-Stokes solver FDL3DI (a) no vortex (b) vortex in close proximity (c) vortex on wing tip (d-f) direct vortex wing interaction for inboard moving vortex (impingement details are provided for the direct wing vortex interaction case, denoted by subscript 1)[27]

The impinging vortex entrains the tip vortex by finger-like substructures of opposite vorticity that create a loss in vortex core coherency downstream of the wing, as was stated before. Figure 2.10e to 2.10d do not have equivalents in figure 2.9, as the behaviour is similar to condition 2.10f in both. When looking at the direct interaction condition in figure 2.10e, the incident vortex encounters an upstream influence of the wing, which promotes a spiralling motion opposite to the sense of vortex rotation. Just before the vortex encounters the wing, the vortex re-orients and becomes perpendicular to the leading edge. The three figures of direct interaction also show a separation bubble next to the incident vortex on the wing profile (flat region). The separation bubble is due to the downwash region which creates a reattachment of the flow over the profile. Due to the reattachment of the flow, the tip vortex feeding sheet loses vorticity and the tip vortex is almost annihilated.

The pressure distributions over the suction (upper) and pressure (lower) side, for which the result graphs were omitted here, were also investigated by Garmann. The results showed, in corroboration with previous results, that the wing interaction induces flow separations but provide more suction over a larger chord-wise extent on the profile. The close proximity and tip-vortex interaction case strengthen the tip vortex feeding sheet due to the increase effective angle of attack in the tip region. The entanglement, dipole and entrainment, of the incident vortex and tip vortex also contribute to a more pronounced wake field. Once the incident vortex moves inboard on the wing, the tip vortex feeding sheet is suppressed by the down-wash region outboard of the impingement, resulting in two small separation bubbles on either side and a weak wake field. Both effects where only investigated on one side of the wing, the effect on the entire aircraft and wake field where omitted.

Inasawa [33] performed a wind tunnel research case of a rectangular wing interacting with a vortex generated by an identical lead wing. Figure 2.11 shows the flow visualization results of the test. For both conditions the dipole and entrainment effect can clearly be distinguished. The strength of the vortex pairs becomes also clear, from strong at the trailing edge for close proximity to weak for tip-vortex interaction. This partially confirms the research done by Garmann.

Barnes [28] used the same solver as Garmann, the FDL3DI Navier-Stokes based solver, again for a rectangular wing. Similar results where found to those of Garmann. The study also investigated the aeroelastic effects on a wing-vortex interaction. Figure 2.12 shows the direct vortex interaction case (similar to figure 2.9f) for three types of flexibility. The difference lies in a slight elevation fo the incident vortex.

Due to the flexibility of the wing in figure 2.12b, the vortex is forced to bifurcate or is even forced to one side of the wing, figure 2.12c. In the rigid wing case, the incident vortex approaches the wing, entangles with the tip vortex, is propelled upwards and propagates downstream. Expected behaviour as to what was discussed earlier. The flexible wing however shows a bifurcated vortex for the same relative position of the wing to the incident vortex. The upper part of the bifurcated vortex moves inboard, entangles with the separated boundary layer and dissipates. The lower surface bifurcated vortex however moves outboard and upward to create

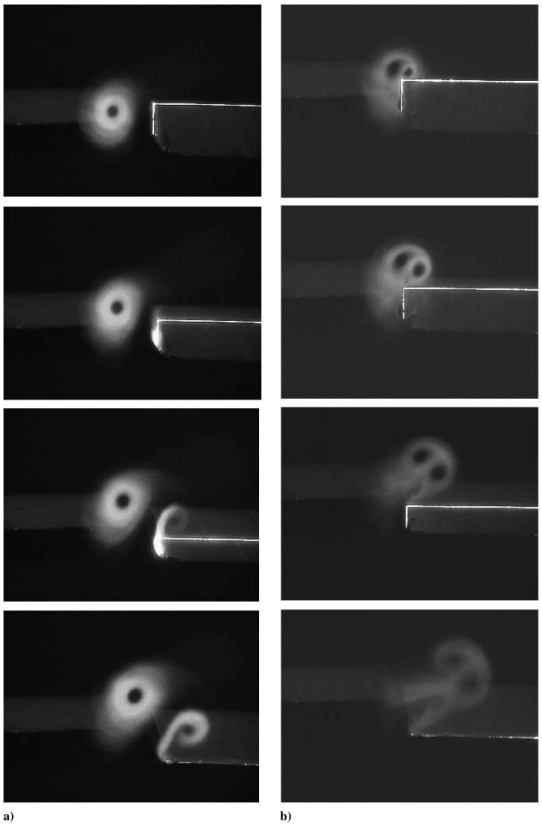

Figure 2.11: Wind tunnel study of wing-vortex interaction over a wing profile from top to bottom, leading edge to the trailing edge (a)vortex close proximity (b)vortex on wing tip [33]

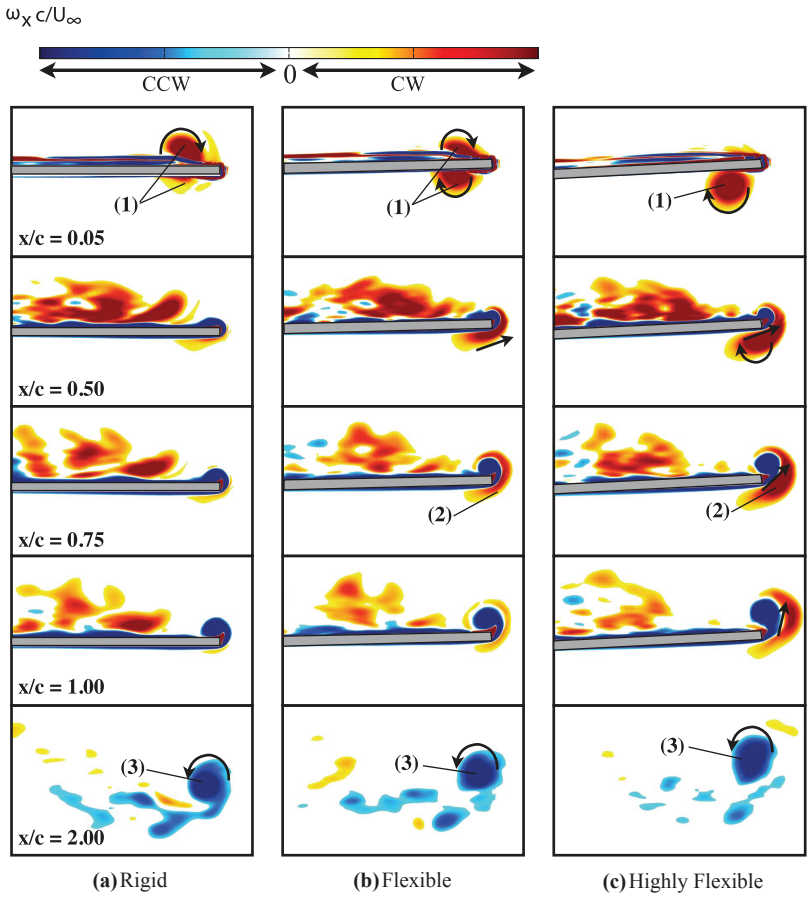

Figure 2.12: Interaction of wing with impigning vortex with relation to wing flexibility (a)rigid wing (b)flexible wing (c)Highly flexible wing [28]

a new tip vortex. When the entire vortex is forced to flow underneath the wing, as is the case for the highly flexible wing, the same effect occurs. The difference lies in the absence of the upper side vortex counterpart to lower the tip vortex feeding sheet. The incident vortex will now merge with the tip vortex as it moves outboard and upward over the pressure side of the wing, resulting in a stronger tip vortex. The behaviour is similar to what was expected when looking at the rigid wing case.
During the formation flight, these three cases could occur shortly after each other however due to small movements between lead and trail aircraft, creating a completely different interaction between the wing, the incident vortex and consequently the formation of the trail aircraft wake sheet. Briefly Barnes touches the situation where direct interaction of a flexible wing and vortex is present, this with relation to differences in pressure over upper and lower side. On the lower side alternating packets of positive and negative pressure are present, resulting in an amplified twist of the wing and fluctuating pressures near the leading edge, which is not desirable. This effect was not observed for the close proximity case nor for the rigid wing case. The aeroelastic effects could thus severely damage the trail aircraft wing parts that are submersed within the tip vortex of the lead. Further research into these effects is required.

The (approximated) reality of the interaction of a wing with a vortex system and/or wake field, as is the case during the formation flight condition, proves to be complex and shows instabilities. The location of the wing with relation to the vortex system determines how the flow field over the wing is affected. The flexibility of the wing is also important for the actual position with relation to the vortex system. The three studies of Garmann, Inasawa and Barnes show the strong relation and interaction between the incident vortex and the trail wing.
The complex flow behaviour shows that for a deflection of a surface at the trailing edge of the wing will create pressure gradients over the wing profile, making vortex-induced flow separation probable. As was identified by Kless and Ning, a complex vortex-induced shock wave system will be created at high subsonic and transonic velocities, possibly inducing buffet. Further research into the actual behaviour of the wing-vortex-deflection is required to gain a better insight into the aerodynamic behaviour for the trimmed flight condition.

2.2.3 Wake field analysis

After discussing the wake vortex sheet together with the wing-vortex interactions, it is time to now look at the overall picture for aircraft flying close proximity and within the wake field. Past research studies clearly showed the instability in forces and moments within the wake vortex field. Although the disturbance and interference effects can be overcome, they do impose strain on trim and control of the aircraft within the formation flight condition.

The research of Blake and Saban on a delta wing aircraft showed the influence of lateral and vertical positioning. Both used the same test configuration, which is shown in figure 2.13. The research was focussed towards the variations in forces and moments throughout the wake field, meaning for different vertical and lateral separation distances. Both used different theoretical methods, Blake the vortex lattice method and Saban the extended lifting line theory. They

validated their results with the same wind tunnel data and found a good match for the close proximity region of the wake vortex interaction. The direct interaction, where the vortex travels over the wing span, showed an underestimation of the benefits and interference effects (rolling and pitching moment) in both studies. The results of Saban will be discussed, omitting those of Blake as they are similar.

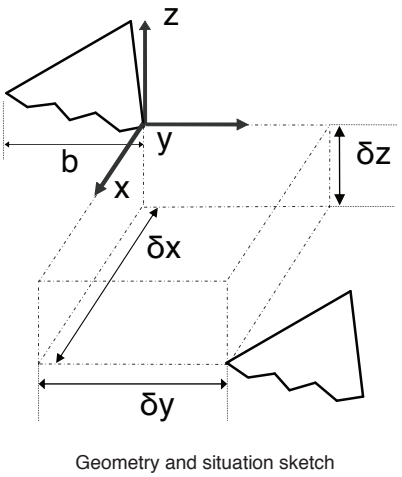

Figure 2.13: Configurational set-up for two delta wings in formation flight condition, as used in the research of Blake and Saban [19][34]

The results are shown in figure 2.14. The test set-up used by Saban are two delta wing aircraft positioned in an echelon formation, where the lateral and vertical separations where varied to create the test data. The two delta wings are separated longitudinally by two wingspans, with the trail aircraft thus within the wake vortex sheet as it is rolling up and forming into one stable tip vortex system. The data presented in figure 2.14 shows the forces and moments acting on the trail delta wing positioned at multiple lateral and/or vertical separation distances.

Figure 2.14a and 2.14b show the benefits due the up-wash region, positioned in the centre of the graphs. The left hand side shows that the disturbance effects within the down-wash create an unfavourable region for flight. The wake down-wash significantly reduces the lift, creating flow separation over the tips spreading fast creating more drag. This increase in drag and local decrease in lift also induces a sudden switch to a negative rolling moment, due to the unbalance in wing loading. When the vortex is not on the wing tip yet, but in close proximity of it, the up-wash region creates extra lift over the wing tip inducing a positive rolling moment. Figure 2.14c shows this variation in rolling moment coefficient. The last sub-figure, figure 2.14d shows the rolling moment with relation to the vertical separation. The changes are small but the mathematical models show no agreement with the wind tunnel results. It is clear that around zero vertical separation, although small, irregularities exist within the model.
Interesting to note is the difference between the drag coefficient determined by the wind tunnel and the extended lifting line theory. The wind tunnel results show a major increase in drag due

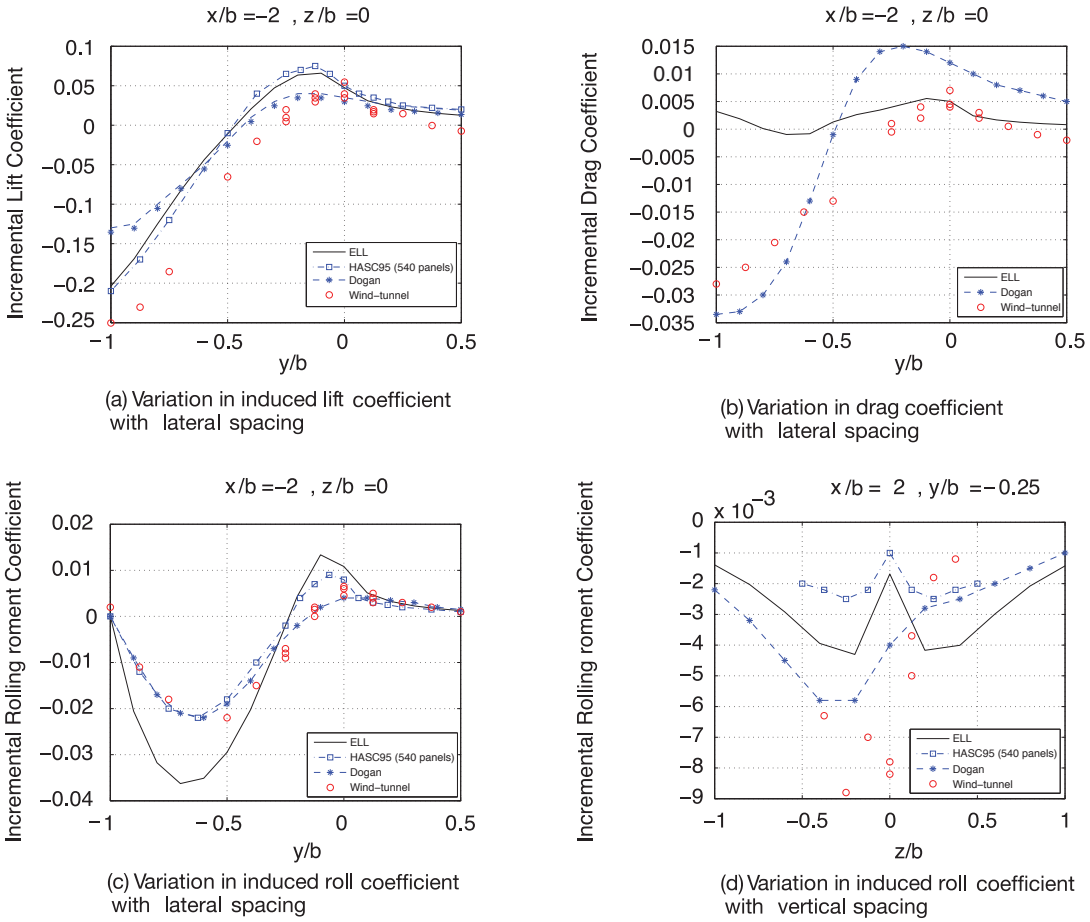

(a) Variation in induced lift coefficient with lateral spacing

(b) Variation in drag coefficient with lateral spacing

(c) Variation in induced roll coefficient with lateral spacing

(d) Variation in induced roll coefficient with vertical spacing

Figure 2.14: Variation of force and moment coefficients within a wake field for several lateral and vertical separation distances [34]

to the vortex-induced flow separation over the wing tip, as identified in earlier studies. As the lifting line theory does not include viscous and compressibility effects, this sudden increase is not properly modelled.

Nangia developed a design and analysis tool applicable to transport aircraft for the formation flight condition [23]. His study focusses on a Airbus A340 wing. The drag reduction achievable was determined to be between $15-20\%$, although destabilizing moments were also apparent. A different approach was used by not measuring and counteracting the vortex-induced moments, but by adjusting the wing design. The goal is to obtain a similar wing loading in the formation as out of the formation by changing camber and control surface deflections. An example of the results are shown in figure 2.15. The figure shows the wing at a wake position of $1.45x/b$, $0.0y/b$ and $-0.05z/b$, also made visible within figure 2.15. The left hand side shows the desired forces and moments, the target value, together with the actual forces and moments by placing the wing within the wake vortex field. The right hand side shows the result after 5 design iteration cycles.

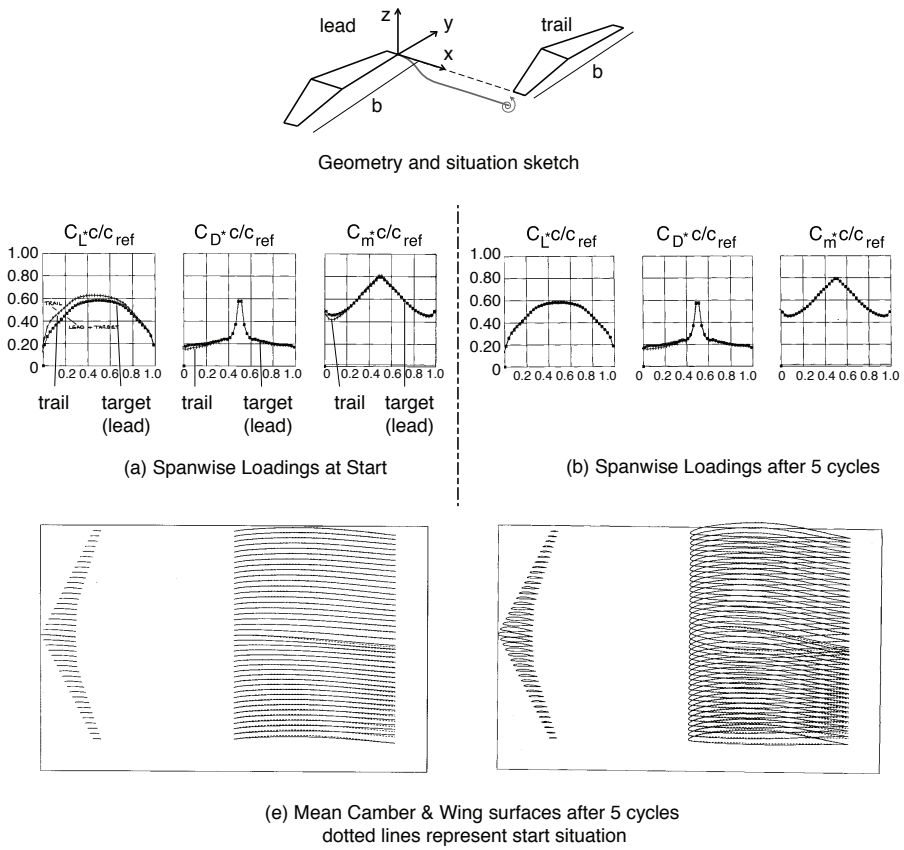

Figure 2.15: Variation of force and moment coefficients within a wake field for several lateral and vertical separation distances [23]

The results from the start position show how the interaction of the wake vortex field with the wing creates an asymmetric wing loading by increasing the lift on the left hand side. This reduces the drag on the left hand side, although also creating a local more negative pitching moment. This decrease in local pitching moment creates a positive rolling moment, one of the destabilizing moments. The redesigned case still shows the decrease in drag whilst removing the asymmetric loading and the local pitching moment.
The approach used by Nangia also shows an invasive change in camber to obtain an equilibrium at just one instance within the wake field. By moving around within the wake field, other equilibrium designs will occur. Not to forget that the aircraft must also be capable of flying out of the formation without an increased drag, or inherent moment that needs to be counteracted. Nevertheless the research of Nangia shows the asymmetric wing loading, which is at the basis of the destabilizing moments and forces, occurring when flying within the wake field. The correct modelling of the asymmetry of the wing loading ensures the capturing of the wake vortex interference effects.
Another important finding was the effect of the size of the lead aircraft upon the aerodynamic benefit of the trail aircraft. The larger the lead aircraft, the higher the vorticity of the wake vortex system, the more benefit can be obtained.

The importance of the position of the trail aircraft with relation to the lead aircraft has been shown as well as the need to distinguish and accurately measure the asymmetric local lift distribution over the span to properly model the forces and moments of the trail aircraft in a formation flight condition.

2.3 Flight dynamics

This section will change the focus from the aerodynamic perspective to the flight dynamical aspects of the aircraft when flying in the formation. The term flight dynamics is broad, and needs to be defined/narrowed to clearly grasp what is going to be discussed within this section.

The importance of the investigation of the behaviour of the aircraft within the wake field can be seen by discussing the results of Blake [19]. Blake investigated two delta wings theoretically and experimentally. The study revealed regions of positional stability, the ability of the aircraft to return back to the equilibrium condition after a disturbance (force or moment). These regions of positional stability are shown in figure 2.16. It can be seen that no region exists were all forces and moments show the tendency to return to the equilibrium position. The model used for this analysis lacks the presence of a vertical tail though. Disturbances including a yawing motion require a vertical tail to return to the original position. A yawing disturbance is removed as the vertical tail is turned into the flow, automatically creating a force to counter the yawing motion. The lack of a vertical tail make that it becomes difficult to create a static positional stable for yaw, although not impossible as the roll and yawing motion can be linked together.

The static position stability can be performed by subdividing the wake field into lateral and vertical instances. For all these instances the disturbance effects working upon the aircraft can

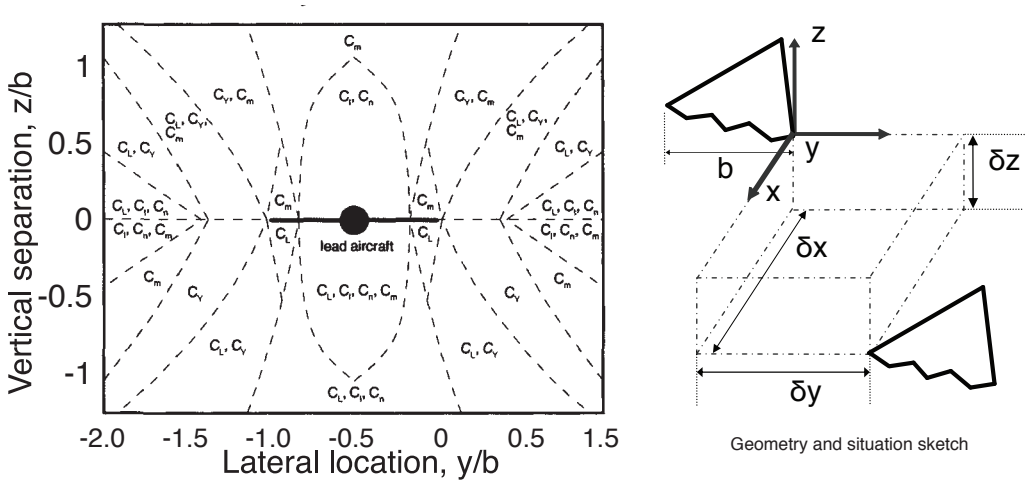

Figure 2.16: Regions of positional stability relative to the lead aircraft [19]

be identified. Afterwards a trim analysis can be performed to balance against the disturbances. Subsequently a dynamic analysis can be done by including variations in time to identify how the aircraft will behave within the wake field, after at the initial position where the disturbances were balanced. The dynamic analysis can include triggered motions, to identify the responses, to make conclusions regarding stability. To first obtain initial insight into the flight behaviour, it would be advised to investigate the wake field instance per instance. This approach only lacks the interaction behaviour when moving from one position to another, therefore a dynamic analysis is required to identify how the aircraft will respond. To primarily understand the behaviour of the aircraft due to the wake vortex field, the atmospheric interference effects, e.g. gusts, side-winds..., will also be neglected.
The cruise flight condition, which is under investigation, requires a steady straight flight condition. The behaviour of the aircraft, due to the wake vortex interferences, should thus be compensated for by using the control surfaces. The influence of using these control surfaces to retain cruise flight condition upon the aerodynamic benefit brings us back to the research question of this study. A brief overview will be presented concerning the general investigation of the trimmed flight condition.

2.3.1 Trim analysis

The aircraft in trimmed condition requires all forces to be balanced, no accelerations in all directions, and all moments to be zero [35]. A trimmed situation implies that the forces and moments are balanced in such a manner to obtain a desired flight condition. The aircraft attitude (angle of attack, side-slip angle, heading angle), control surfaces (aileron, elevator, rudder, spoilers) and engines (thrust) can be used to obtain this condition. The relation of the variations required to obtain the trimmed condition with relation to velocity provides insights into the influence of each parameter upon the aircraft. Relations like the angle of attack with relation

to velocity in trimmed condition prove to be interesting to investigate.
The formation flight condition introduces the positional aspect to the analysis. The disturbances vary throughout the wake field, thus also creating different trimmed conditions.

2.4 Trimmed formation flight

The effect of lateral trim on the formation flight condition was already researched by others, like Kless et al., from whom the results will be presented here briefly. The research of Kless investigated two configurations, two rectangular wings and two transonic wing fuselage models in the formation flight condition. The results of the transonic aircraft will be discussed here, of which a geometry model is shown in figure 2.17.

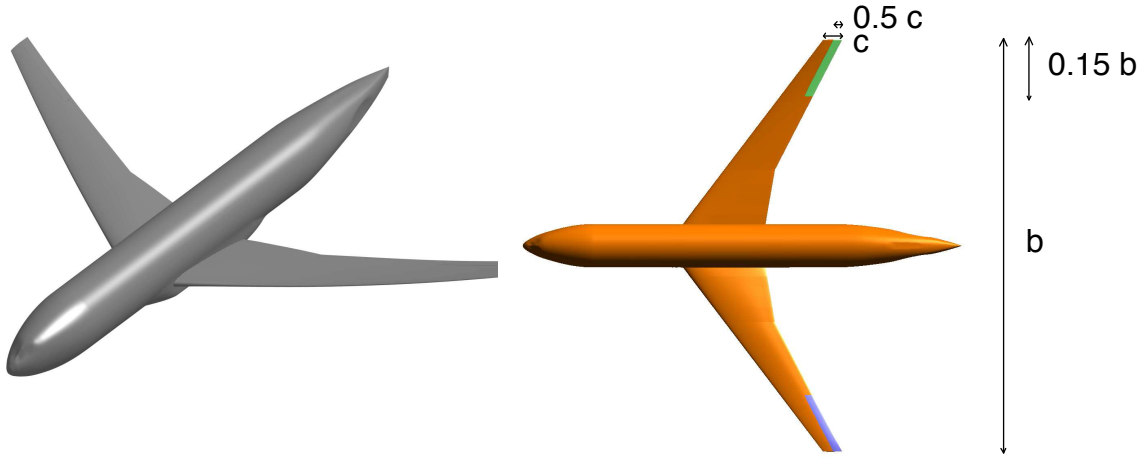

(a) CRM geometry (b) CRM geometry with ailerons

Figure 2.17: Transonic aircraft model used within the research of Kless [6]

The wake vortex interference forces and moments where determined using an extended Euler Solver, the NASA AERO package. Interesting was the analysis of the pressure distributions over the wing profile for the condition where the wing tip of the trail aircraft is positioned just within the wake vortex system. These results are shown in figure 2.18. The comparison is made between the pressure distribution of the lead aircraft and the trail aircraft, laterally trimmed and untrimmed. The aircraft is flying in cruise condition, $C_L = 0.5$ and $M = 0.83$, and normalized values are compared. Compressibility effects are included, although viscous effects are neglected (inviscid analysis). The differential aileron deflection for the trimmed configuration was determined to be at $1.8^{\cdot}$ degree and is not illustrated within the wing profiles shown in the figure.

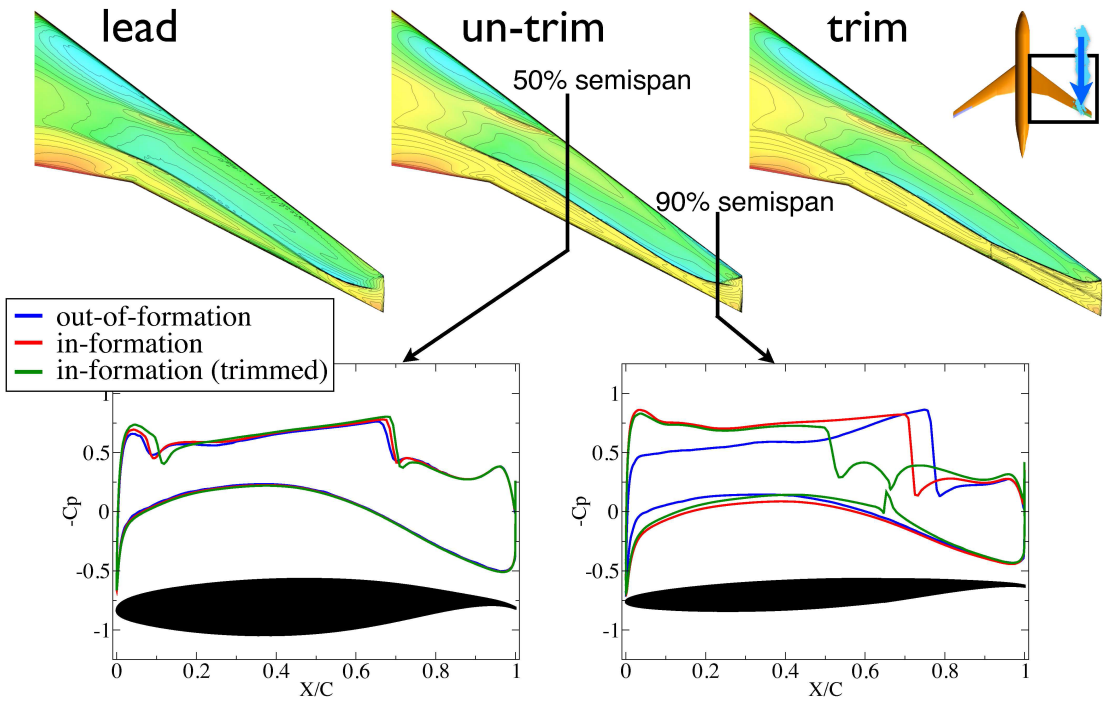

Figure 2.18: Pressure coefficient distributions on the in-vortex wing at 50% and 90% semispan for the lead aircraft, trail aircraft not trimmed and trail aircraft trimmed; where the vortex is positioned at the wing tip at a freestream Mach number of 0.83 and Lift coefficient of $C_L = 0.5$ [6]

At 50% semi-span the effect of the wing-vortex interaction only shows slight variations, affirming that the effects due to the up-wash region are only localized around the vortex system. Towards the trailing edge an adverse pressure gradient is present, appointed to a shock wave over the wing. At 90% semi-span the influence of the vortex and the trimming of the aircraft can be clearly identified. The out-of-formation case shows a shock wave aft of the wing profile, seen in the pressure distribution by an adverse pressure gradient. Due to the presence of the vortex, the shock wave is pushed forward on the wing profile, although a compensation is made by a higher constant pressure at the leading edge of the profile. The deflection of the aileron to $1.8^{\cdot}$ degree, reduces the adverse pressure and shock wave but pushes the it to half of the chord, retaining the pressure at the leading edge.
Trimming of the aircraft will thus locally lead to a reduction in lift. As the lift directly influences the induced drag benefit, due to the formation flight, the benefit will decrease. Remember that the induced drag is reduced by the formation flight due to the tilting the lift vector forward due to the up-wash, effectively creating aerodynamic thrust. As the lift decreases in magnitude, the benefit will also reduce.

Kless et al. identified a reduction in aerodynamic benefit of $3-5\%$ in subsonic conditions and $9-11\%$ in transonic conditions. The question could be raised whether small adjustments to the control surface and/or wing could affect the decrease in benefit.

2.5 General flight

Now that the aerodynamics and flight dynamics are introduced, it is time to move on to the operational part of the formation flight. A representative formation flight condition will be defined within this section, which will be used for the further analysis within this research.

The formation flight offers a drag reduction during flight. Obviously one wants to exploit this benefit as long as possible. Logically one would like to fly solo towards a way-point, create a formation for the cruise flight, after which the aircraft split up to go to their specific airports. The research of Dekkers [36] was focussed on how to optimize flight paths with relation to the creation and break-up of the formation flight, to which one is referred for further information regarding flight path optimisation. Dekkers shows that to create a formation is an ongoing process. Once a certain amount of aircraft is in the air (incorporating delays and non-take-offs), a formation can be created. The research of Van der Kleij [26] has a focus on the automated flight control system (AFCS) to retain the formation flight, with the aid of an autopilot system. One of the conclusions was to further investigate the effect of control deflections upon the total benefit of the formation, as his study revealed that a maximal control deflection was required to fly within the wake field. This suggests that one does not want to manoeuvre to much once in formation. The cruise flight offers a constant steady flight condition for a longer period of time, for which the AFCS and the flight path can be optimised to obtain the most of the induced drag benefit. The longer the cruise flight, the higher the benefit, thus long-haul flights would be best suited. An example of such a flight is the transatlantic route, as now aircraft fly in a sequence where one could fly in a formation. A configuration of two aircraft in this long haul cruise flight will

be investigated. Two aircraft where chosen to reduce complexity of the analysis with relation to interference and interaction of multiple bodies upon each other. When investigating two aircraft in a formation flight, only the echelon shape can be chosen. The cruise flight condition was fixed at $11,000$ meters.

New and upcoming long-range passenger aircraft are the Boeing B787 and the Airbus A350. Some older aircraft, used for transatlantic flight, are the Boeing B777-B747-B757 and the Airbus A330-A340 [37] [38]. The older models have already been analysed and researched, making that more (accurate) information regarding these aircraft is present. This makes them more suitable for the formation flight analysis, as less uncertainty is present regarding the aircraft parameters. From the latter aircraft, the Boeing 747 and the Airbus A330, have the most available data present.
The Boeing B777 and the Airbus A330-A340 are the ones with future prospects as the development and production on the Boeing B747-B757 have stopped. The Airbus A330 would provide enough information and be relevant for potential future usage of the formation flight condition. From the Airbus A330 family the A330-300 is the largest model, which is also the most sold [39]. For both reasons this aircraft was chosen to further analyse within this research.

The Airbus A330-300 top view is shown in figure 2.19. Normally the A330-300 has winglets mounted on the wing tips. The research of Fransen showed less reliable induced drag reduction values when winglets were included. The winglets increased the induced drag benefit, something that was not expected. Two effects can be distinguished. For a uniform formation, the winglets on a lead aircraft will actively reduce the strength of the incident vortex, also the effect in the wake field for the trail aircraft will be reduced. Secondly, the winglet on the trail aircraft will interact with the incident vortex (winglet-vortex interaction).
To reduce complexity and additional interference effects, the winglets where omitted from the geometrical model used within this research. Figure 2.19 shows the original aircraft wing on the left side and the version without winglets on the right side.

2.6 Conclusion

This chapter started off with a chronological overview of the developments and research studies concerning formation flight. Specific elements, characteristic for the formation flight, were singled out and discussed into more detail within the aerodynamic section. The wake vortex sheet and wing vortex interactions, as studied by literature, provided a qualitative insight into the actual flow behavioural aspects of the formation flight. The wake field analysis identified the rolling and pitching moment to have pronounced wake-induced interference effects. The sensitivity to lateral and vertical positioning within the wake field was discussed.

The flight dynamics of trimmed flight and important characteristics were discussed. The static analysis method (instance per instance) to analyse the wake field was deemed accurate enough to obtain insights into the flight mechanical behaviour of the trail aircraft. Studies also showed

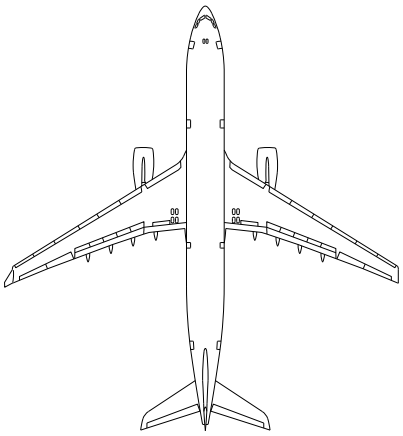

Figure 2.19: A330-300 aircraft in top view

the importance of the incorporation of compressibility effects, to accurately model the flow over a wing with deflected control surfaces.

Lastly the general flight condition is discussed, to obtain a representative case which can be analysed for wake field sensitivities and a flight dynamic and load analysis during the formation flight condition. The Airbus A330-300 was chosen for transatlantic a cruise flight, which will be further analysed within the upcoming chapters. Table 2.2 shows an overview of all papers and proceedings that were found and discussed within this chapter. The papers are categorized according to their topic: aerodynamics (Aero), control and operations (Oper). The aerodynamic papers can be subdivided into three more specific categories: vortex related (A-Vortex), wake field related (A-Wake) or related to the effect on the trail aircraft (A-Trail).

Reference	Year	Category	Main topic	Calc. method	aircraft	Key findings
Wieselsberger [1]	1914 1914	Aero	Formation flight benefit	-	-	- Initial identification of benefit by observing birds
Lissaman et al. [11]	1970 1914	Aero	Formation flight benefit		-	- Description aerodynamics of benefit
Speer et al. [16]	1971	Control	History of military formation flight	-	-	- Station Keeping Systems (SKS)
McMillan et al. [14]	1978	A-Vortex	Wing-vortex interaction	Wind tunnel	- Rect. wing	- Variations forces/moments wrt. lat. pos. to vortex
Hummel [12]	1983	A-Trail	Formation flight benefit	- HSV - Lifting surface	- Rect. wing	- Quantification of the induced drag benefit - Formation shape and relation to the benefit - Influence of (in)homogeneous formations
Hummel [40]	1995	A-Trail	Formation flight benefit	- HSV - Test flight	- Rect. wing - DO-28	- 15% power reduction trail aircraft - Comparison test flight Dornier DO-28 - Formation shape/composition impact on benefit - Distribution benefit upon all aircraft in formation
Rossow et al. [15]	1995	A-Vortex	Wing-vortex interaction	- Wind tunnel	Swept wing	- Variations forces/moments wrt. lat. pos. to vortex
Blake et al. [18]	1998	A-Trail	Formation flight benefit	- HSV	- Rect. wing	- Induced drag benefit calculation - Rectangular wings in formation flight - Variations forces/moments wrt. lat. pos. of vortex - 'Optimum' flight condition for formation flight
Blake [19]	2000	A-Wake	Formation flight Aerodynamic simulation	- VLM HASC95 - Wind tunnel	Delta wing	- Induced drag benefit calculation - Aerodynamic coupling effects - Positional stability analysis of wake field
Jacquin et al. [30]	2001	A-Wake	wake vortex propagation	- Wind tunnel	A300	- Vortex meandering within wake field - wake vortex sheet formation and properties - Unsteady properties of meandering vortices
Wagner et al. [20]	2001	A-Trail	Formation flight & trim	- VLM HASC95	T-38	- Induced drag benefit of 62% - Induced drag benefit trimmed condition of 59% - Third aircraft in the formation benefit of 67%
Hansen et al. [21]	2002	A-Trail	Formation flight induced effects	- Test flight	F/A-18	- Induced drag benefit calculation - variations with relation to long.-lat.-vert. pos. of trail aircraft
Ray et al. [22]	2002	A-Trail	Formation flight performance	- Test flight - Horseshoe vortex	F/A-18	- Evaluation performance benefits - Fuel flow reduction between $14 - 18\%$
Veldhuis et al. [31]	2003	A-Wake	wake vortex propagation	- PIV in towing tank	A340-300	- wake vortex decay - vortex meandering to 'stable' pos.
Blake et al. [41]	2004	A-Wake	Formation flight interference effects	- Wind tunnel - VLM HASC95	Delta wing	- Induced drag benefit calculation - Validation VLM - Mapping of variations in wake-induced effects
Nangia et al. [23]	2007	A-Trail	Formation flight variations size& spacing	- panel method	A340	- Design tool to optimise span loading and camber control against induced rolling
Saban et al. [34]	2009	A-Wake	Formation flight simulation wake vortex effect	- Ext. lifting line	Delta wing	- Validation ELL with wind tunnel results - Cross coupling effects in wake field
Ning et al. [24]	2011	A-Trail	Formation flight & compressibility effects	- Euler solver AERO package		- Formation induced shock wave propagation - Strong buffet and separation potential
Inasawa et al. [33]	2012	A-Vortex	Wing-vortex interaction	- Wind tunnel	- Rect. wing	- Induced drag benefit of 24% for -0.05 y/b - Incident & tip vortex interaction and propagation
Fransen [25]	2012	A-Wake A-Trail	Formation flight relation to wind tunnel modelling	- ext. VLM	- A330 - A380	- A330 total drag reduction of 26% at sweet spot - Interference forces and moments determination - Computational modelling of wind tunnel set-ups - Complete aerodynamic analysis of wake field
van der Kleij [26]	2012	Control	Formation flight control	- Ext. lifting line - simulation model RECOVER	B-747	- Identification of behaviour in wake vortex field - Dynamic behaviour and control authority
Pahle et al. [29]	2012	A-Trail	Formation flight	- Test flight	C-17	- Fuel flow reduction between $7 - 8\%$, possibly 10% - High workload in the formation according to pilots

Table 2.1: Overview of papers and proceedings as were found during the background research study

Reference	Year	Category	Main topic	Calc. method	aircraft	Key findings
Kless et al. [6]	2013	A-Trail	Formation flight & trim	- Euler solver AERO package	- Rect. wing - Transonic aircraft model	- 54% induced drag reduction, $3-5\%$ lower for trim in subsonic condition - 35% induced drag reduction, $9-11\%$ lower for trim in subsonic condition - Highest shock wave strength on out-of-vortex wing - Trim only out-of-vortex wing not beneficial to benefit
Barnes et al. [28]	2014	A-Vortex	Wing-vortex interaction	- Navier Stokes FDL3DI	- Rect. wing	- Wing-tip vortex-incident vortex interactions - Identification bipole-entrainment-bifurcation - Effect on forces and moments - Relation of wing flexibility on interaction
Garmann et al. [27]	2014	A-Vortex	Wing-vortex interaction	- Navier Stokes FDL3DI	- Rect. wing	- Wing-tip vortex-incident vortex interactions - Identification bipole-entrainment-bifurcation - Influence on forces and moments
Flanzer et al. [4]	2014	Oper	Operational analysis of formation flight	- Optimisation tool	C-17	- $5-10\%$ fuel flow reduction per mission - Identification problem fuel benefit, without reducing fuel carried - Variations on flight planning, 1 hour take-off flex. achieves 50% of maximal benefit - Heterogeneous formations preferred
Bieniawski et al. [3]	2014	A-Trail A-Wake	Formation test flight summary	- Test flight	C-17	- Redefining formation flight station keeping system - Summary of test flights and their data - $5-10\%$ fuel flow reduction - Structural impact, safety and wear - No structural or vibrational limits exceeded - Slight degradation of ride quality
Slotnick et al. [2]	2014	A-Wake A-Trail	Formation flight analysis	- VLM - Panel method - RANS CFD	C-17	- 25% drag benefit - Comparison between computational methods - Variations within wake vortex field
Halaas et al. [5]	2014	A-Wake A-Trail Control	Formation flight simulation tool	Simulation model - CFD data - Test flight data - VLM data		- Development control system - System level performance analysis - Wake development & meandering estimation incl. aerodynamic disturbances - Variations within wake vortex field - Incorporates wake-crossing simulation results

Table 2.2: Overview of papers and proceedings as were found during the background research study

CHAPTER

THREE

AERODYNAMIC ANALYSIS

This chapter is concerned with the aerodynamic analysis of the formation flight condition. The variation in forces and moments for multiple lateral and vertical positions of a trail aircraft flying within a wake field of a lead aircraft will be modelled and investigated. To be able to model the wake field and subsequently position the trail aircraft at multiple positions within that wake field, first an aerodynamic solver needs to be chosen. First a set of requirements is stated, after which the aerodynamic solver is chosen. The two first sections comprise these two steps. Afterwards the aerodynamic solver was subjected to three reference cases, to check its validity regarding the modelling of the formation flight condition. Finally at the end of this chapter, the wake field for the general flight condition, two A330-300 aircraft in a two aircraft echelon formation at a lift coefficient of $0.623[-]$ and Mach number of 0.6 at an altitude of $11,000$ meters, is analysed.
Figure 3.1 shows the two parts that are of interest within this chapter indicated in black.

3.1 Requirements

First the general requirements for the aerodynamic solver are stated. Obviously a first one is the ability to create a flow field, representing the wake field of a lead aircraft to recreate the formation flight condition. This can be done by implementing two aircraft within the model in a formation flight configuration or by first analysing the wake field properties behind an aircraft, after which these are super-imposed upon the free stream in front of an aircraft.
The initial analysis and the vortex wing interaction, as discussed in the previous section, showed that the location within the vortex field is of great influence on the formation flight condition. The local lift distribution is also of importance at each location within the wake field, as the induced angle of attack changes over the wing span.

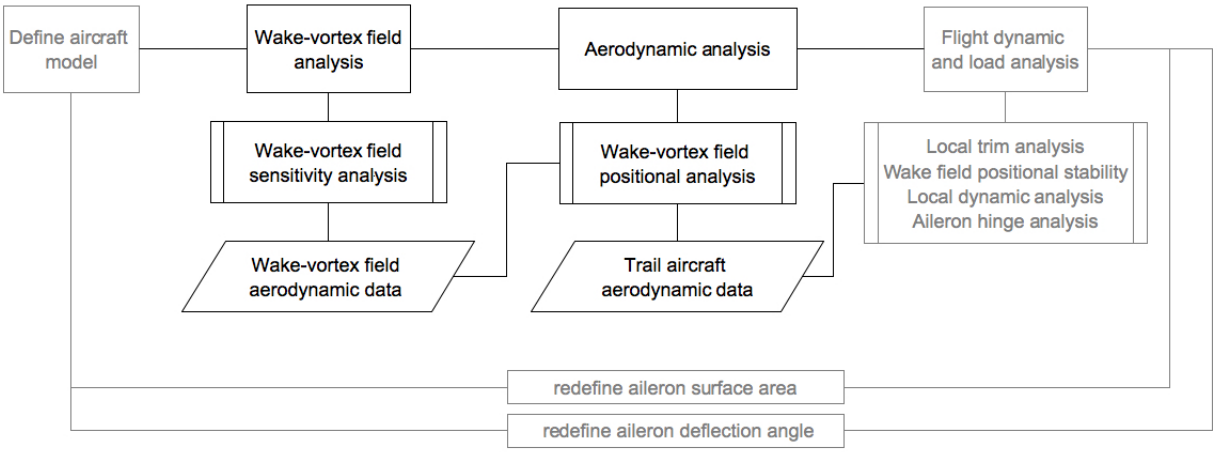

Figure 3.1: Outline of research into different topics, aerodynamic analysis highlighted

The above three characteristics can be redefined into more specific parameters to define the wake field and formation flight condition for further analysis. The wake field is defined by a vortex (pair) with a 'wake-sheet' in between. The total wake field can be defined by the total circulation strength Γ_0, where each vortex can be identified by its own circulation strength $\Gamma_{1,2}$ defined as 1 and 2 for the time being. Each vortex also has a core with specific radius and radial velocity, r_c and $V_{r,\theta}$. These last two parameters are of importance to theoretically recreate the vortex flow in strength.
The radius and velocity can also be related to the distance downstream of the lead aircraft, to incorporate the vortex decay. The two last parameters are the longitudinal and lateral separation distances between the two vortex cores, effectively the width and 'fall' of the wake sheet downstream. These variable changes directly behind the lead aircraft until they reach a steady value within the downstream wake, as was stated in the previous chapter concerning the aerodynamics of the formation flight and the wake field properties 2.2. Finally the model must be able to locally analyse forces and moments on the wing span, to incorporate the changes in effective angle of attack. The required properties of interest for the solver are:

- Wake sheet/vortex pair modelling (Γ_0 $\Gamma_{1,2}$ r_c $V_{r,\theta}$)
- Wake propagation downstream (wake-roll-up and vertical movement)
- Local force and moment analysis

A trade-off must be made between the accuracy concerning the properties of the solver and the computational time and the availability of the software. The remainder of this section is dedicated to an aerodynamic solver method related to specific a aerodynamic program. Aerodynamic solvers do not always include vortex models for (formation flight) analysis, so a way to model a vortex also requires some attention after the aerodynamic solver. The

combination of a vortex model together with an aerodynamic solver can be used to analyse the aerodynamic behaviour within the flow field.

3.2 Aerodynamic solvers

The aerodynamic solvers used throughout literature vary from Euler based, Navier-Stokes based solvers up and till Vortex Lattice Methods. The Navier-Stokes based solvers are only used for the specific wing-vortex interaction case, e.g. Garmann [27] and Barnes [28]. The Euler based solver were used within the studies upon compressibility effects, e.g. Ning [24] and Kless [6]. The investigations of the entire wake field were performed using Vortex Lattice Methods, which are based on the Horse Shoe Vortex model. These models are fast and prove to be accurate in the prediction of the wake vortex induced forces and moments. As this research is focussed on the wake field analysis for the trimmed formation flight condition, Horse Shoe Vortex based models would seem a good choice. The Horse Shoe Vortex (HSV) model is therefore elaborated and placed into context with the requirements as stated earlier. These models require a theoretical definition of the vortices used, of which three representations will also be discussed afterwards. Finally a list of assumptions is given.

3.2.1 Horse Shoe Vortex (HSV) model

The Horse Shoe Vortex model, further abbreviated to HSV, is a system of a bound vortex to represent the wing surface with two free vortices attached perpendicular at the edges to represent the tip vortices. The bound vortex recreates the lift and drag whilst the two free vortices recreate the wake field. The theory behind the force and moment calculations is based on the elementary potential flow theory, with as governing equation the equation of Laplace.

The Laplace equation makes use of the first compressible Euler equation, shown in the first part of equation 3.1. The first Euler equation is derived from the continuity equation. The continuity equation states mass can neither be created nor destroyed. By assuming and inviscid flow adiabatic flow, effectively neglecting boundary layer effects, the first Euler equation is obtained. If the flow is inviscid, it will also be irrotational and can be rewritten as is shown in the second part of equation 3.1. If the flow is assumed to be incompressible (lower than Mach 0.3), the dot product can be dropped. This finally brings us to the Laplace equation, shown in equation 3.2.

$$\nabla \cdot V = \nabla \times V = \nabla \cdot (\nabla \phi) = 0 \tag{3.1}$$

$$\nabla^2 \phi = 0 \tag{3.2}$$

Using the Laplace equation together with boundary conditions (flow tangency condition at the aerofoil), an inviscid, adiabatic and incompressible flow can be modelled. A compressibility correction can be used to estimate the behaviour at Mach numbers in the high subsonic

region. One method is the Prandtl-Glauert compressibility correction. The Prandtl-Glauert compressibility correction is only valid for thin aerofoils at small angle of attack. The stating and derivation can be found in books concerning aerodynamics like Anderson. The correction is based on the linearised velocity potential equation [42]. This limits the correction to Mach Numbers below 0.6, to be representative. An example of a wing and its corresponding HSV system is shown in figure 3.2.

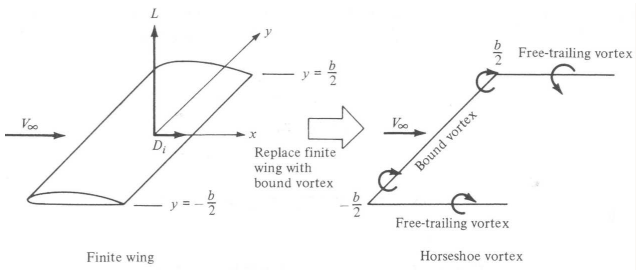

Figure 3.2: Horse Shoe Vortex model using a single vortex system [42]

Aircraft can be modelled using just one HSV or multiple. The Lifting Line (LL) theory consists of one or more HSV placed upon the lifting line to represent a three dimensional wing. The Extended Lifting Line (ELL) are series of HSV placed next to each other on a constant chordwise location across the span. When this spanwise distribution is extended to also include a chordwise distribution, multiple lifting lines parallel to one another to recreate the wing surface, it is called a Vortex Lattice Method (VLM). When comparing the required properties of interest to the HSV model, it becomes clear that multiple spanwise HSV are mandatory to accurately model the local effects across the span and downstream of the wing. By doing so the last requirement is satisfied.

Two programs where investigated for suitability within this research, the ELL developed and used by Van der Kleij [26] and the Athena Vortex Lattice (AVL) method developed by Drela [43] and extended by Fransen [25]. Obviously by using a chord and spanwise distribution of the HSV to recreate the wing surface, the accuracy of the local force/moment behaviour increases. Both programs offer results close to one another. The main advantage of AVL is that it has been made to serve the purpose of a general aerodynamic solver where Van der Kleij created a program to calculate only forces and moments using the theory of HSV models. AVL offers the possibility to analyse the forces and moments as well as their derivatives and incorporate control deflections as well as trim calculations. The purpose of AVL was intended for rapid aircraft configuration analysis where the ELL of Van der Kleij was to calculate the desired aerodynamic properties specific to his research.

The HSV model programs however do not model the incident vortex by default. The advantage lies within the fact that the aircraft are modelled as bound and free vortices. A HSV could thus be positioned in front of an aircraft to become an incident vortex. The VLM used and extended by Fransen includes the option to position multiple HSV models with relation to each other, effectively recreating the formation flight condition. The disadvantage lies within the fact that

the vortices are positional bound. Once the vortex is positioned within the y-z field, it will always flow parallel to the x-axis. Aircraft under angles of attack will receive a different vorticity as compensation, the vortices remain parallel (this is the case for the VLM extended by Fransen and not a general property). The merging and creation of the wake sheet can thus not be modelled, only the final state of a pair of counter-rotating vortices decaying whilst propagating downstream. After nine wingspans, due to the inward rolling of the wake sheet, the effective distance between both vortices can be set at $\frac{\pi}{4}b$ [31] (see section 2.2.1). The strength, decay and other characteristics of all of the vortices used within a HSV based model are defined by a vortex representation model. Several models exist of which three will de discussed now, all of which where implemented within the the VLM that was extended by Fransen.

3.2.2 Vortex representations

This section deals with different vortex representation models that can be used to define vortices, within for example HSV based models. The three analytical methods that will be described here are the Biot-Savart, Lamb Oseen model or Burnham Hallock vortex representations.

The major distinction between the three analytical models is the manner to model the vortex core radius and induced velocity, an unsteady behaviour in reality. The Biot Savart model makes use of the Laplace equation [25] to model the induced velocity, as shown in equation 3.3, with r being the distance from the center of the core to the point where the velocity is calculated. When using this model an artificial core velocity is required, to prevent a singularity at $r = 0$.

$$V_\theta = \frac{\Gamma}{2\pi r} \tag{3.3}$$

The Lamb-Oseen model in the other hand offers an extended version, shown in equation 3.4 [44]. An extra factor is the core radius that is included within the induced velocity. The core radius is in function of the kinematic viscosity ν, the Lamb-Oseen constant λ and the fraction of the effective viscosity $\frac{r^2}{r_c^2}$. The vortex core radius also changes as it is propelled downstream due to the time dependency, as can be seen from equation 3.5.

$$V_\theta = \frac{\Gamma}{2\pi r} \cdot \left[1 - e^{-1.256431\frac{r^2}{r_c^2}}\right] \tag{3.4}$$

$$r_c^2 = r_{c,0}^2 + 4\nu\lambda\left(1 + \frac{\mu_t}{\mu}\right) \cdot t \tag{3.5}$$

Reynolds effects are also incorporated in the growth of the vortex core radius, by the (effective) viscosity, $\frac{\mu_t}{\mu}$. If the effective viscosity contribution is neglected, the model is called laminar, when it is calculated, it is called turbulent.
The Burnham-Hallock model induced velocity relation is shown in equation 3.6 The core radius

representation has the same relation as Lamb-Oseen, only the Lamb-Oseen constant λ is replaced with another constant value. These models will thus model the vortex strength by defining the circulation of the system Γ.

$$V_\theta = \frac{\Gamma}{2\pi r} \cdot \frac{r^2}{r_c^2 + r^2} \tag{3.6}$$

As part of his research Fransen implemented these three models within the existing VLM of AVL. The option is included to choose which model to use to define all vortices of the HSV accordingly. The exact information of the vortex can thus be measured and adjusted, satisfying the first requirement. The validation with multiple reference cases studies showed that the best agreement was attained when using the Laminar Lam-Oseen vortex representation model. Comparing the three vortex representation methods, as presented here, showed only small differences. Consequently the laminar Lam-Oseen vortex representation model was chosen to be used throughout the rest of the analysis. No exact comparative analysis between the three models was made for this study.

3.2.3 Assumptions

Returning to the requirements and comparing them to the VLM extended by Fransen, it can be seen that all requirements are met. The VLM offers the possibility to model local forces over the wing, by setting enough HSV over the wing planform. The wake propagation is captured by retaining a minimal distance of nine wingspans, thus only encountering the steady decaying vortex pair, positioned at a constant distance with relation to one another. Finally the wake vortex modelling can be achieved by fine-tuning the vortex parameters from the vortex models implemented within the extended VLM of Fransen. The VLM of Fransen was therefore chosen for the aerodynamic analysis.

The disadvantages are that only an inviscid, adiabatic and incompressible flow can be analysed. To include compressibility effects an estimation can be made using the Prandlt-Glauert correction. This estimation shows high deviations however at a Mach number above 0.6. The usage is thus limited by this Mach number. The analytical wake vortex models, within AVL, do not identify the wing profile and bend accordingly. The vortex flow remains parallel to the initial condition specified, as stated before. A region of close proximity, direct vortex-wing flow interaction, will thus have questionable results due to the lack of viscous and compressible flow modelling, and the analytical vortex models with parallel vortex flow. A list of assumptions and short comings are:

- no viscous effects included
- no compressibility included
- compressibility correction (Prandtl-Glauert), maximal Mach number $0.6M$
- analytical vortex core radius and velocity approximation, four models included though

- rudimentary modelling of direct wing-vortex interaction (vortex flow parallel to x-axis)
- boundary layer interaction with vorticial flow is neglected
- homogeneous formation can be investigated (no heterogeneous)

This last assumption was not yet introduced and discussed. The VLM extended by Fransen makes use of just one geometry that is duplicated and translated with the analysis field. This imposes the condition of only homogeneous formations to be investigated. This should be kept in mind, although it does not impose problems with relation to the accuracy or validity of the program, it only limits the usage.

To gain initial insight into the behaviour of the flow within the wake field and the balancing of forces and moments, the extended program of AVL was chosen with the recommendation to do further research into the complex wing-vortex behaviour. A more detailed diagram showing the working of the entire aerodynamic module as adjusted and used subsequently used throughout this research is provided in Appendix A. The specifics concerning the extended VLM program of Fransen are not included, just a general overview of the functionality is provided here [25].

3.3 Reference cases

The extended VLM of Fransen was chosen for the aerodynamic analysis of the formation flight condition at hand here, with the laminar Lamb-Oseen vortex representation. To check whether or not this method provides enough accuracy for our research purposes, several cases from literature where recreated and the results compared. The cases where selected for different geometrical properties of wind tunnel tests and an Euler solver in the formation flight condition. To start with however, the coefficient and derivative data in the solo flight condition were observed to show initial accuracy of the chosen method. Finally the effect of sweep angle on the formation flight condition will be discussed briefly.

3.3.1 Solo condition of A330-300 using DATCOM

DATCOM is created by the United States Airforce with the goal to provide a systematic summary of methods for estimating stability and control characteristics in preliminary design applications. It is a program with the ability to provide a rapid estimation of aerodynamic stability and control characteristics [45]. The ‘older’ estimation method has been extensively used to determine the aerodynamics of missiles as well as of conventional aircraft designs.

To identify the accuracy of the coefficient derivatives from AVL, the A330-300 in solo flight condition was recreated in DATCOM. The results of AVL were compared to those obtained with DATCOM to see how the correlate. The solo flight condition was in the subsonic speed regime at cruise altitude. For the correlation between both, the results from DATCOM where used as the reference value. Table 3.1 shows the results of the comparison. The derivatives

are expressed per radian for angles, and dimensionless for roll-pitch-yaw rates. Only significant and comparable derivatives were represented within table 3.1.

	C_{D_α}	C_{Y_α}	C_{L_α}	C_{l_α}	C_{m_α}	C_{n_α}
AVL	-	-	*6.892*	-	*-2.093*	-
DATCOM	-	-	*5.866*	-	*-1.798*	-
Difference	-	-	17.49%	-	16.38%	-
	C_{D_β}	C_{Y_β}	C_{L_β}	C_{l_β}	C_{m_β}	C_{n_β}
AVL	-	*-0.747*	-	*-0.101*	-	*0.203*
DATCOM	-	*-1.112*	-	*-0.080*	-	*0.250*
Difference	-	-32.87%	-	26.24%	-	-18.65%
	C_{D_p}	C_{Y_p}	C_{L_p}	C_{l_p}	C_{m_p}	C_{n_p}
AVL	-	*-0.010*	-	*-0.492*	-	*-0.007*
DATCOM	-	*0.037*	-	*-0.504*	-	*-0.025*
Difference	-	$\lvert -72.97\% \rvert$	-	-2.39%	-	-73.58%
	C_{D_r}	C_{Y_r}	C_{L_r}	C_{l_r}	C_{m_r}	C_{n_r}
AVL	-	-	-	*0.125*	-	*-0.315*
DATCOM	-	-	-	*0.131*	-	*-0.323*
Difference	-	-	-	-4.18%	-	-2.67%
	$C_{D_{da}}$	$C_{Y_{da}}$	$C_{L_{da}}$	$C_{l_{da}}$	$C_{m_{da}}$	$C_{n_{da}}$
AVL	-	-	-	*-0.096*	-	*0.00028*
DATCOM	-	-	-	*-0.109*	-	*0.003*
Difference	-	-	-	-11.62%	-	-88.82%
	$C_{D_{de}}$	$C_{Y_{de}}$	$C_{L_{de}}$	$C_{l_{de}}$	$C_{m_{de}}$	$C_{n_{de}}$
AVL	-	-	*0.801*	-	*-2.893*	-
DATCOM	-	-	*0.902*	-	*-3.204*	-
Difference	-	-	-11.20%	-	-9.73%	-

Table 3.1: AVL validation of a A330-300 aircraft with DATCOM

In general the results show that AVL gives a good indication for the derivative values. Some results show remarkable differences, which will be further explained here. A general remark is that both programs do not use the same model of the A330-300. Although both models were created to match one another, differences might exist. The AVL model was de-constructed and drawn to identify all the values, using basic geometry rules.

The derivatives to the angle of attack show a deviation between $15 - 20\%$. AVL shows a higher trend, implying more lift can be attained at lower angles of attack. The assumptions used within AVL, neglecting viscous and compressibility effects for an adiabatic irrotational flow, could over-predict the lift. DATCOM makes use of statistical and empirical data, providing more realistic data. The manner of estimating lift could thus explain the difference as seen here.
The derivatives to the side slip angle show a shift in deviation ranging from 32% to 18%. The geometric model differences can create these differences, as the AVL model does not include a fuselage where the DATCOM model does include one. AVL has the possibility to include

slender bodies, i.e. a fuselage, although no extensive validation exists of the accuracy and validity when using this option. Within the manual of AVL it is stated that the usage of the option should be done with caution. It was chosen here not to model the fuselage within AVL to only have the formation flight condition as uncertainty, without having to worry about fuselage modelling, especially to omit extra uncertainty due to the interaction of the vortex flow with the fuselage on the entire model.

The roll rate derivative with relation to the rolling moment shows good agreement, a difference of 2%. The side force however shows a high deviation, but this value is small and is often neglected. The yawing moment coefficient also shows a high deviation, like the side force around 70%. The values again are small and could be assigned to the effect of adverse yaw. A positive rolling motion, the left wing (down-moving) will experience a higher angle of attack creating a forward oriented force. The right wing (up-moving) experiences the opposite. As the wings are swept, this contribution of forward and backward oriented force is reduced. AVL only looks at the induced drag components. The induced drag components due to the adverse yaw were already small, which even further decrease due to the sweep angle. The yawing motion due to the roll, as estimated by AVL will be small, as can be seen when comparing to the data from DATCOM. The latter higher value is more representative for the roll induced yawing.
The derivatives to the yaw rate show good agreement, both compared values have less than 5% deviation.

The derivatives to the aileron and elevator deflections show an overall good agreement. The rolling moment with aileron deflection has a 12% deviation and the lift force and pitching moment to elevator deflection show a deviation of around 10%. The yawing moment with relation to aileron deflection however, shows a high deviation of 89%. The value of this derivative is fairly small and could be neglected. The derivative is a quantification of the increase/decrease in drag due to an aileron deflection for the down/up-moving wing, creating a yawing moment. Obviously large values are undesirable. The difference here could also be linked to the difference in yawing moment derivative due to a roll rate change, which works on the same principle.

Overall the derivatives of a flight in solo condition of AVL compare well to those from DATCOM. Deviations present could be explained to differences in geometric models and small/negligible values.

3.3.2 Formation Flight of 3D rectangular wing using Euler solver

The first formation flight validation is for a three dimensional rectangular wing. The Euler solver, AERO analysis package of NASA, is used for this comparison as found in the work of Kless [6].

The NASA's AERO analysis package is an Euler solver, which makes use of three-dimensional Euler equations of a perfect gas to model the flow [24]. When looking at two aircraft flying in formation, the Euler method is used to model the flow around the lead aircraft. The vortex propagation from the lead towards the trail aircraft is approximated by the augmented Betz

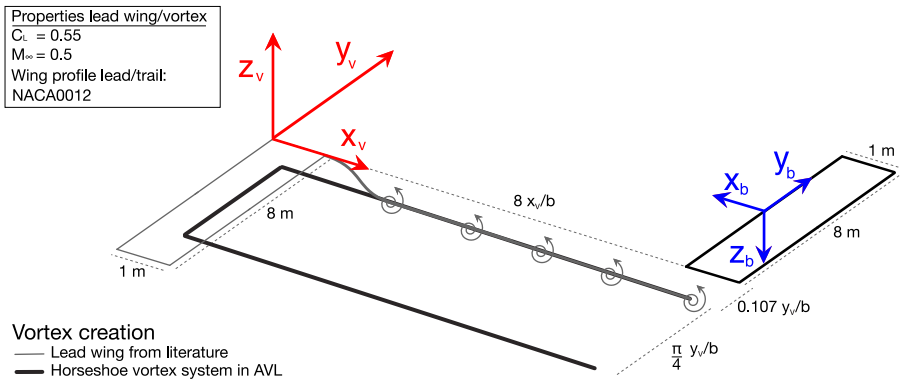

Figure 3.3: Geometry and situational sketch of the model as used in AVL and as used by Kless et al. within their research study [6]

method for computing far-field vorticity distribution [46]. The propagated vortex is then imposed as a boundary condition to the trail aircraft and again the Euler method is used to evaluate the trail aircraft.

The model used for validation purposes was a straight untapered wing of aspect ratio 8 with the NACA0012 profile at a free stream velocity of 0.5 Mach with a lift coefficient of 0.55. The formation flight model consists of two identical wings, as described, separated by 8 wing spans. A geometry and situational sketch is shown in figure 3.3.

The Euler solver uses the vortex shed by the identical lead wing for the formation flight calculation. AVL however does not use the augmented Betz method to determine the vortex strength and propagation, but the circulation of the lead aircraft to create the vortex system of the lead aircraft. Here it was assumed that AVL creates a similar vortex with relation to the Euler solver, in the absence of specific vortex distribution/strength information. All the different vortex models where tested and data was compared. The laminar Lamb-Oseen vortex model showed the best agreement and was therefore chosen for the comparison.

The validation of data consists of a comparison of the lift coefficients for the formation flight condition, at two vertical separation distances and multiple lateral separation distances. The Mach number, lift coefficient and atmospheric conditions were given for the rectangular wing. The lift coefficient was used subsequently to identify the angle of attack to attain a lift coefficient of 0.55. The lift coefficient for the rectangular wing to achieve a lift coefficient of 0.55 at Mach 0.5 and sea level conditions was identified to be $6.19^{\cdot}$ degrees.
The two wings were subsequently placed in a two wing formation at this fixed angle of attack, with 8 span longitudinal separation distance, where lift coefficients are shown in table 3.2. The formation flight condition was investigated for multiple lateral and vertical separation distances with relation to the oncoming vortex.

The formation flight condition, shown in table 3.2, shows the variation of the lift coefficient for multiple lateral separation distances (y/b). For the rectangular wing model used here,

C_L wrt. y/b		-0.2 y/b	-0.1 y/b	0.0 y/b	0.1 y/b	0.3 y/b
AVL	0.0 z/b	0.5736	0.6026	0.6133	0.5888	0.5695
Euler	0.0 z/b	0.5449	0.5436	0.5447	0.5480	0.5476
Difference	0.0 z/b	5.26%	10.86%	12.59%	7.46%	4.00%
AVL	-0.1 z/b	0.5664	0.5839	0.5902	0.5822	0.5684
Euler	-0.1 z/b	0.5481	0.5498	0.5483	0.5478	0.5480
Difference	-0.1 z/b	3.33%	6.20%	7.65%	6.29%	3.73%

Table 3.2: AVL validation of a 3D rectangular wing in formation for $\alpha = 6.19^{\cdot}$ at a Mach number of 0.5 at sea level conditions, using an Euler solver

the optimum exists around $0.0y/b$, the condition where the wing tips of both lead and trail aircraft are aligned. This condition is the close proximity condition, as the trail aircraft does not encounter the tip vortex due to the roll-up of the wake. (The vortex positioned on the wing tip of the trail aircraft occurs at $-0.1y/b$.) It can be noticed that AVL shows larger variations for lateral separation, compared to the Euler Solver. The possible explanation can be the vortex model representation used by AVL, the laminar Lamb-Oseen model. The vortex core velocity is approximated at a theoretical value. With zero vertical separation, the velocity of the core would flow over the wing profile, creating a different speed region. In reality first the core velocity would be different and second the vortex flow would bend over the wing, both effects making the speed and thus the lift coefficient differ.
Generally AVL predicts the trend for lateral separation, but around the wing-tip-vortex interaction an over-prediction is present for AVL due to the imperfections of the theoretical vortex model.

Table 3.2 is divided into two parts, designated to 0 and $-0.1z/b$ vertical separation distance. The theoretical effect of direct wing-vortex interaction can be investigated. As seen earlier AVL is limited and only can model a vortex travelling along a straight line, neglecting viscous effects and bending of the vortex path with streamlines around the wing. It will thus not be able to model the close proximity interaction of the vortex with the wing. A limit could be set to identify at what point AVL shows large deviations in results. Table 3.2 already shows that for $-0.1z/b$, the deviation of the results of AVL decrease. The largest deviation is present around wing-tip-vortex interactions, as expected. The behaviour for the wing tip aligned with the vortex is the most pronounced, as was shown for the wing-vortex interaction study in section 2.2.2. Figure 3.4 shows the wing loading for both vertical separation distances.

Overall the comparison of AVL with the Euler solver of the NASA aeropackage shows that AVL gives an accurate indication for the solo flight condition and a good approximation for the formation flight condition. However in the case of the formation flight it must be investigated when the wing-vortex interaction results in unrealistic deviations from reality. The next sections will therefore compare the data from AVL to wind-tunnel measurements.

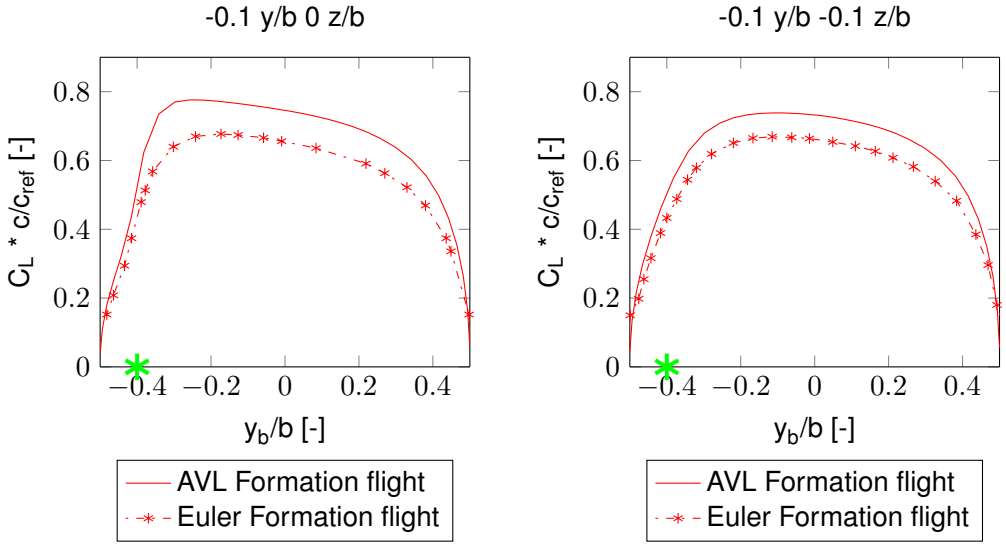

(a) tip aircraft aligned with vortex for $0z/b$

(b) tip aircraft aligned with vortex for $-0.1z/b$

Figure 3.4: Lift distribution over rectangular wing in solo and formation flight, for zero vertical separation with tip aligned with oncoming vortex

3.3.3 Formation flight of 3D rectangular wing using wind tunnel

This section deals with a rectangular wing model placed behind a vortex generator in the NASA Ames Research Center wind tunnel facility. The research was done by McMillan et al. [14] in the late seventies to investigate the accuracy of theoretical prediction methods, strip theory and vortex lattice methods, for forces and moments in a trailing aircraft in wake vortex field. The main goal was to evaluate theoretical methods to calculate forces and moments induced by a vortex wake field. This within the vortex hazard problem of aircraft encountering a wake vortex, helicopter rotors operating within a wake and lifting surfaces being subjected to vortex interactions.

The wind tunnel test set-up consists of a generator wing, placed vertically from the tunnel floor up till the height of the model. The trailing aircraft is mounted to the traversing system of the wind tunnel by means of a small fuselage. Two identical geometrical models of trail aircraft were used for measuring the data, one using a force based and the other pressure based measuring. As the names already suggest, the first one has built in force balances to measure forces and moments where the second one utilizes pressure taps. The pressures were measured using differential transducers mounted in Scanivale modules, after which the data was converted to forces and moments.
Both models have a NACA-0012 wing profile. Important to note here is that this configuration cannot be reproduced by AVL. The vortex mount in AVL will be placed horizontally instead of vertically, which affects the wing when it is positioned within the wake field. The vortex generator

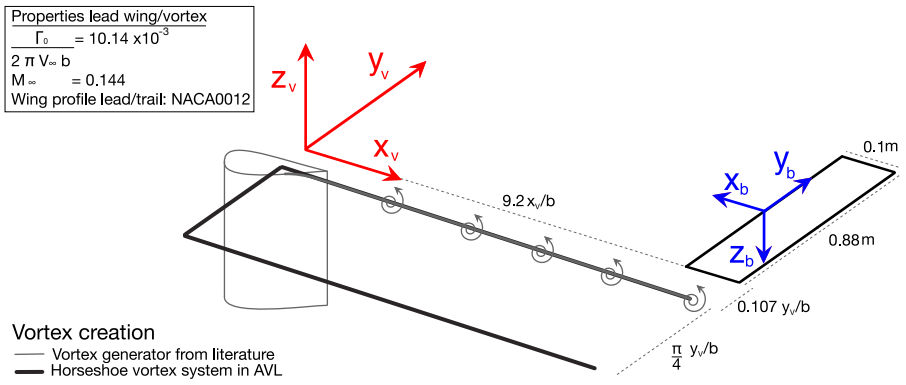

Figure 3.5: Geometry and situational sketch of the model as used in AVL and as used by McMillan et al. within their wind tunnel test [14]

will create a side-wash instead of a region of up- and down-wash. For small vertical separation distances this does not matter, as the trail wing will mostly only encounter the tip vortex. Due to the rotational effect of the tip vortex, its orientation with relation to the wake field does not matter. The region of side-wash below the trail wing will slightly affect the lower pressure distribution. This was neglected. Positions where the trail aircraft wing tip would be positioned within the wake field, require a correction to include the region of down-wash, present within the wake field. When discussing the local wing loading, further explanations will be given concerning the estimation of the down-wash in the wake field.
Figure 3.5 gives a geometry and situation sketch of the model as it is used within AVL and within the wind tunnel research.

The total circulation strength of the vortex generator was compared to that of AVL, to recreate the test set-up. The formula for total circulation is shown in equation 3.7. The value was made non-dimensional by the last term in equation 3.7.

$$\frac{\Gamma_0}{2\pi b V} = \frac{C_L V S}{\frac{\pi}{2} b} \frac{1}{2\pi b V} \tag{3.7}$$

As AVL does not have the circulation as input variable or constraint, several runs where made after which the circulation was calculated. The condition under which the lead aircraft produces the correct amount of circulation was deduced using interpolation and reasoning. An exact match to the data in literature was not obtained, nonetheless the difference was made as small as possible. The value from AVL was $\Gamma_0 = 10.13 \circ 10^{-3}[-]$, where the wind tunnel had a total circulation of $\Gamma_0 = 10.14 \circ 10^{-3}[-]$.
The trail aircraft was positioned behind the vortex system at multiple lateral and vertical separation distances, whilst being at a zero angle of attack condition.
The local lift distribution at one position, and the lift and rolling moment coefficient at multiple lateral separation distances will be compared to the results from the recreated model in AVL.

The results are stated below in figure 3.6, 3.7 and 3.8.

The local lift distribution was chosen at a small positive vertical separation, $0.0083z/b$ distance and a lateral separation such that the vortex is at the center of one wing, $-0.375y/b$. The results for both wind tunnel data and AVL are shown in figure 3.6.

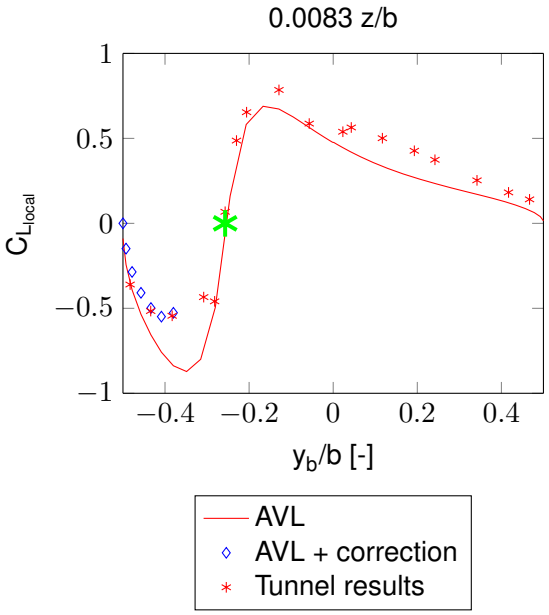

Figure 3.6: Local lift distribution over rectangular wing in formation flight condition (for zero angle of attack) at $0.0083z/b$, wind tunnel validation

Figure 3.6 shows the local lift distribution ($0.0083z/b$, $-0.357y/b$). The vortex is identified by the green star. First the up-wash region, to the right of the vortex is slightly under-predicted by AVL. However the down-wash region, on the left side of the vortex, is over-predicted, by 54% increase at $0.38y_b/b$. The reason can be the horizontal wake field (side-wash), as was mentioned earlier. An approximation of the change in lift due to this horizontal wake field can be made using basic wake field equations from Anderson [42]. Using equation 3.8 the downward velocity distribution with relation to vertical separation in the wake field can be estimated. The velocity can be used to estimate the induced angle of attack, to eventually determine the change in lift, using both relations in equation 3.9 and equation 3.10.

$$w(y) = -\frac{\Gamma}{4\pi}\frac{b}{\left(\frac{b}{2}\right)^2 - y^2} \tag{3.8}$$

$$\alpha_i = tan^-1\left(-\frac{w(y)}{V_\infty}\right) \cong -\frac{w(y)}{V_\infty} for \alpha \cong 0 \tag{3.9}$$

$$\delta C_L = \alpha_i C_{L_\alpha} \tag{3.10}$$

Equation 3.8 to 3.10 where used to calculate the difference in lift due to the wake field, for -0.5 until -0.4 y_b/b. Effectively until the vortex core radius is reached, assuming that the region before is only affected by the wake field and not the vortex itself. The core radius by the Lamb-Oseen laminar model in this case is $0.025y_b/b$, making the wake field influence from the wing tip until $-0.4y_b/b$. By subtracting this extra decrease in lift, due to down-wash of the wake field in AVL, the trough of the down-wash almost coincides with the wind tunnel data as shown in figure 3.6. The difference reduces to -3.24% at $-0.38y_b/b$. This shows that AVL accurately predicts the local lift distribution at $0.0083z/b$, as the down-wash over-prediction can be subscribed to the presence of the wake field in AVL and not in the wind tunnel.
Due to the fact that the down-wash is over-predicted by AVL, the total lift and rolling moment coefficients will show other results than the wind tunnel data. It is expected that the total lift will also be over-predicted and the rolling moment to be less 'severe' (as the larger down-wash balances the up-wash better).

The lift coefficient comparison can be seen in figure 3.7. The lift coefficient values for two constant vertical separation of $0.0083z/b$ and $-0.05z/b$ are shown for a range of lateral separation distances. The x-axis within the graphs show how the position of the trail aircraft is altered, from the vortex positioned on the fuselage ($-1y/b$) to the vortex on the left wing (-1 to $0y/b$) and finally no vortex on the body (0 to $0.6y/b$), all for a constant vertical separation.
As identified for the local lift distribution, the down-wash region was over-predicted by AVL. This effect can be seen in figure 3.7a where the total lift is (negatively) over-predicted. At $-0.375y/b$ a 79% decrease in lift is measured between AVL and the wind tunnel data. The trough location on the other hand is accurate. By 'crude estimation' the lift coefficient with the correction for the wake field was determined by calculating the area under the local lift coefficient graph, as seen in figure 3.6, for $-0.375y/b$. After the correction, the results show a closer agreement with the tunnel data from McMillan, a difference of 68% was measured at $-0.375y/b$. The difference remains large but the calculation method used is only a crude approximation, nevertheless it does show that wake field orientation could explain the difference. For larger vertical separation distances, the peaks and trough diminish in strength, as seen when comparing figure 3.7a and 3.7b. This was expected, however due to the limited amount of data the accuracy of the direct interaction prediction by AVL could not be assessed.

Finally the rolling moment coefficient results of AVL are compared to the wind tunnel data. As for the lift coefficient, two values of constant vertical separation of $0.0083z/b$ and $-0.05z/b$ are shown for a series of lateral separation distances in figure 3.8. Figure 3.8a shows a lower rolling moment than expected. The rolling moment is induced by the unequal up- and down-wash distribution. The results from AVL will have more down-wash present for a similar amount of up-wash, creating a better balance between both resulting in a lower trough for the rolling moment with relation to the lateral separation. The corrected value using the local lift distribution at $-0.375y/b$ is marked and shows a closer agreement to the results from McMillan. Again use is made of a 'crude estimation' taking the local lift distribution over both wings and calculating

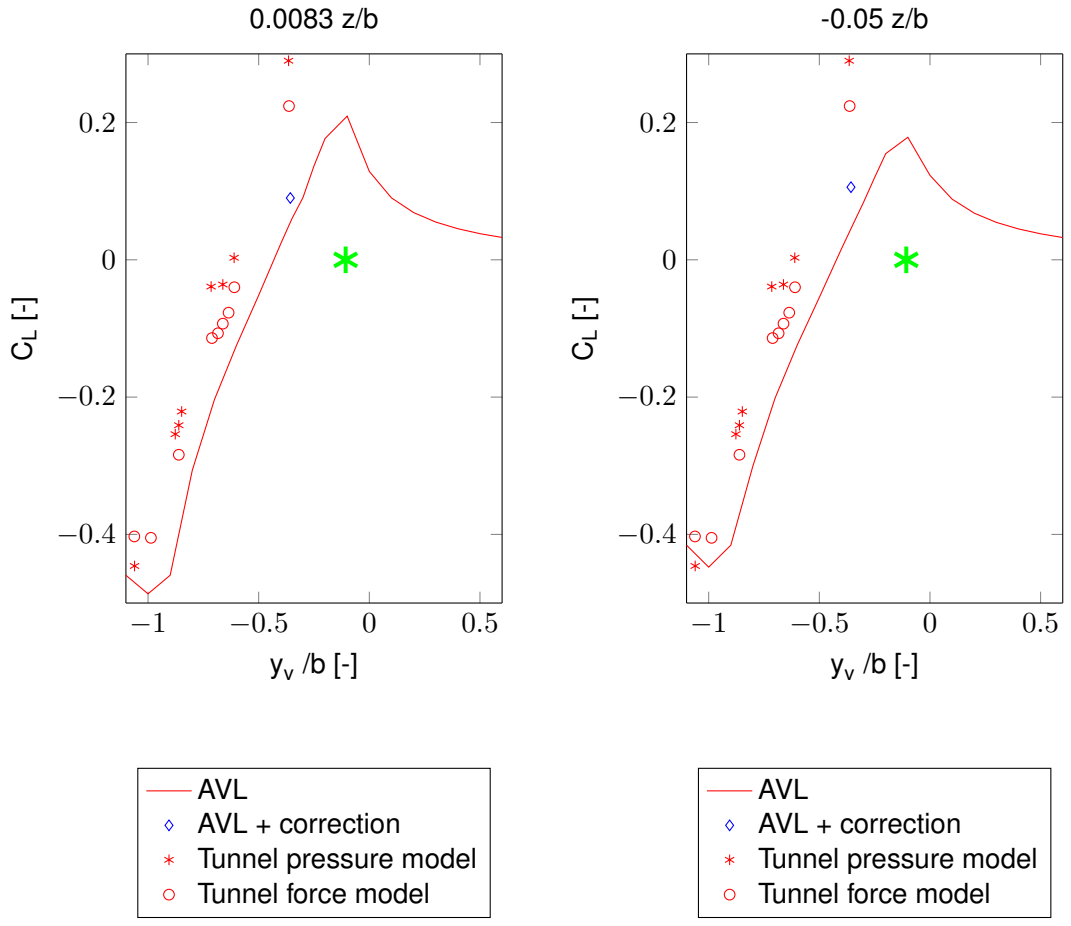

(a) Zero vertical separation with vortex, $0.0083z/b$

(b) Negative vertical separation with vortex, $-0.05z/b$

Figure 3.7: Lift coefficient with relation to lateral separation over rectangular wing in formation flight condition (for zero angle of attack), wind tunnel validation

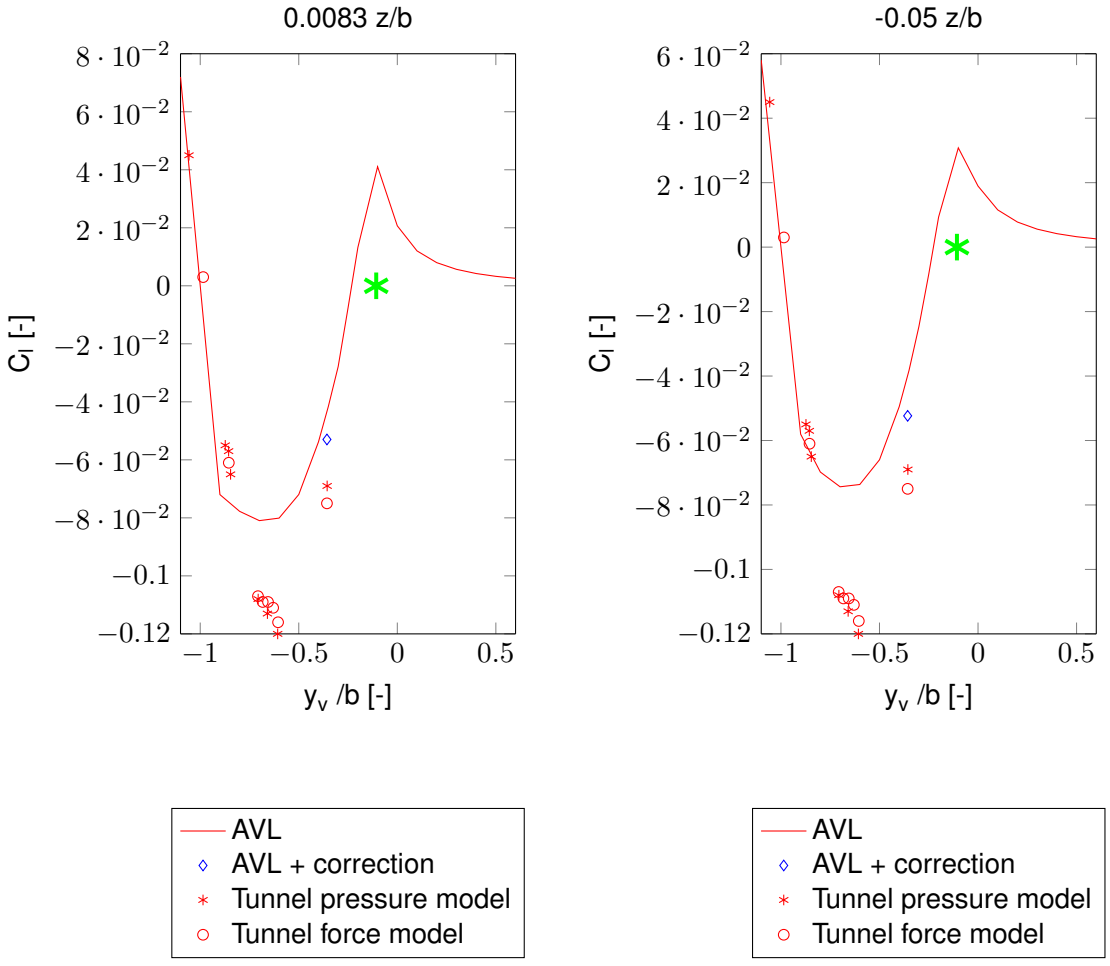

(a) Zero vertical separation with vortex, $0.0083z/b$

(b) Negative vertical separation with vortex, $-0.05z/b$

Figure 3.8: Rolling moment coefficient with relation to lateral separation over rectangular wing in formation flight condition (for zero angle of attack), wind tunnel validation

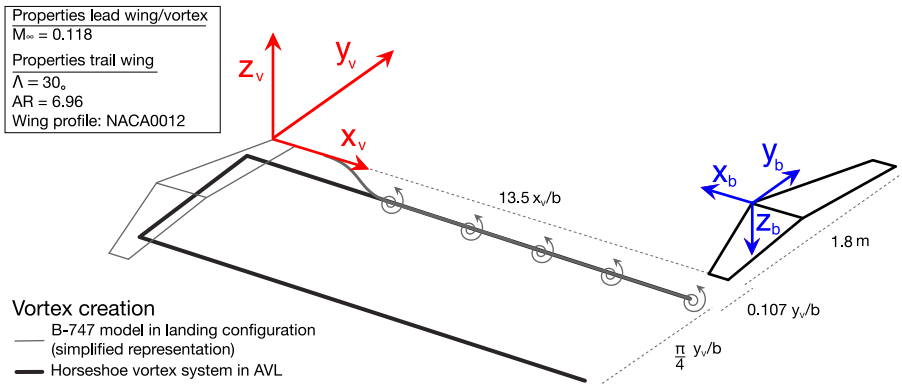

Figure 3.9: Geometry and situational sketch of the model as used in AVL [15]

the area of the graph. The initial difference at $-0.375y/b$ - $0.0083z/b$ is -40% which reduces to -23% after making the crude estimation correction.
The difference in vertical separation, figure 3.8a and 3.8b, show no major differences. As the peaks diminish in strength when their for indirect vortex-wing interaction. As for the lift coefficient, due to the limited amount of data and the wake field interference the accuracy of the direct interaction prediction by AVL could not be assessed here.

Concluding the results of AVL show to be accurate for the local lift distribution over the wing in the formation flight condition for direct $(0.0083z/b)$ wing-vortex interaction when compared to wind tunnel results. The total lift and rolling moment coefficient show deviations, but those are explicable due to a mismatch in wake field orientation of the model recreation by AVL. A comparison with the rectangular wing of the Euler Solver in section 3.3.2 was not possible as no data was present around for wing-tip-vortex interaction, only for wing overlap $(< -0.1y/b)$.

3.3.4 Formation flight of 3D swept wing using wind tunnel

Another wind tunnel test was performed for a swept wing model encountering a vortex and wake system. The test was done by Rossow et al. [15], regarding the accuracy of vortex lattice methods to predict loads due to lift-generated wakes. Similar to the research of McMillan, it is performed to identify potential dangerous situations when encountering a wake vortex of a preceding aircraft.

The wind tunnel research and test where performed in the 80 by 120 foot wind tunnel of the NASA research center. The wake was generated by a 0.03 scale model of a Boeing 747 aircraft. Behind this model at a fixed longitudinal position, a swept wing model was placed at multiple vertical and lateral positions within the wake field. The model used by AVL is shown in figure 3.9.

As the wake generator model and the trail wing differ in geometry, some problems arise with the remodelling in AVL. AVL can only model two identical geometries within a formation flight condition. It was chosen to use the geometry of the trail aircraft, after which the angle of attack (consequently also the lift) of the lead aircraft was varied to match the vortex behaviour from the B-747. From the research of Rossow, the induced velocity distribution is known. By comparing these results to AVL, the vortex produced by the B-747 could be 'matched' to the vortex created in AVL. This comparison is shown in figure 3.10.

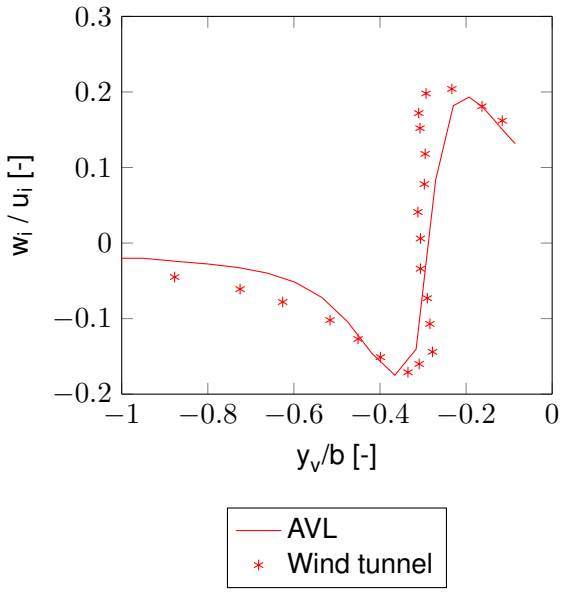

Figure 3.10: Up and down-wash distributions along a lateral traverse through the vortex centers, wind tunnel validation

Figure 3.10 shows no perfect match, as is expected due to the vortex core radius and velocity approximations made within AVL. However the information and trend around the vortex core show good agreement. The only discrepancy present is at the fuselage-vortex interaction around $-1.0y/b$. The wind tunnel results and AVL move to a different negative value. It is thus assumed that the results of AVL become inaccurate when the fuselage is in close proximity of the vortex system.
Using the AVL model with approximated vortex strength, the lift and rolling moment coefficients with relation to lateral separation are compared to the wind tunnel data for multiple vertical separation instances, as was done in the previous section. First the lift coefficient with relation to lateral separation for $0.0z/b$ and $-0.05z/b$ vertical separation are shown in figure 3.11.

Although no perfect match was made for velocity distribution of the vortex, the lift coefficient agrees rather well with the wind tunnel results. A difference exists in proximity of the vortex, marked by the green star, and at the position when both fuselage of lead and trail aircraft are aligned. The maximal difference for wing-tip-vortex proximity is around 17% and for fuselages aligned 16%. When increasing the vertical separation distance, these differences start to

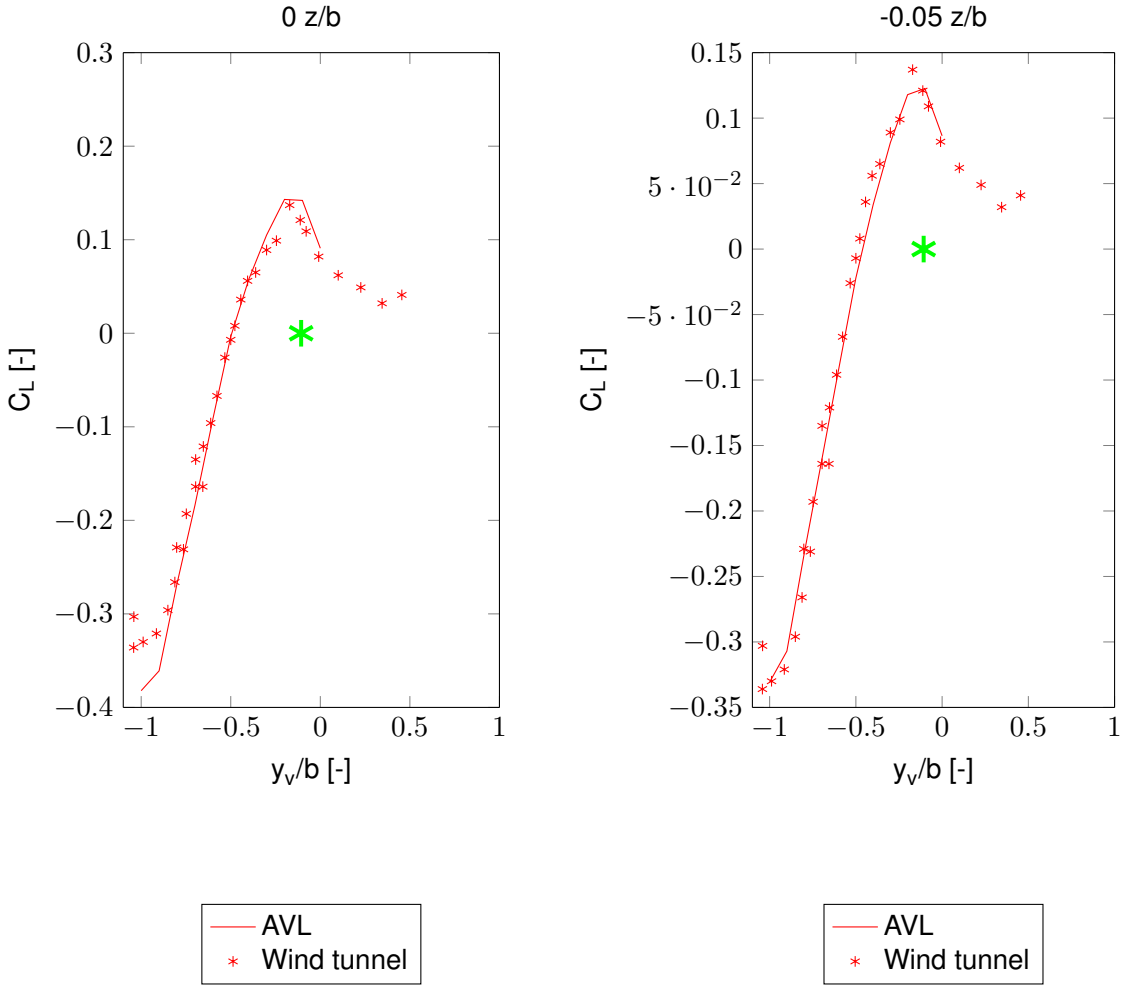

(a) Zero vertical separation with vortex, $0.0z/b$

(b) Negative vertical separation with vortex, $-0.05z/b$

Figure 3.11: Lift coefficient with relation to lateral separation over swept wing in formation flight condition, wind tunnel validation

diminish to 1.32% and 0.21% respectively. At $-0.05z/b$ the least difference between data points is present, shown in figure 3.11b.
The overall trend is as expected and for the inboard travelling vortex the results of AVL compared to the wind tunnel agree well. around the wing-tip-vortex interaction and moving further inboard where the fuselage starts to interact with the incident vortex, AVL will over-predict the lift. The best matching results where obtained for a vertical separation of $-0.05z/b$. Important to note is that in the region of lateral separation away from the wing-tip-vortex and fuselage-vortex interaction, $-0.15y/b$ till $-0.90y/b$ the values agree well with only small margins of error.

Next the rolling moment coefficient was compared with relation to the lateral separation where the results for two vertical separation distances, $0.0z/b$ and $-0.05z/b$, are shown in figure 3.12. For zero vertical separation, figure 3.11a, the region where the vortex is travelling inboard (< $-0.1y/b$), the results from AVL agree rather well. It appears as if a small shift to the left is present within the data, but the local minima is reached. The region around the wing-tip-vortex interaction however shows an over-prediction of the local maxima.

The values at a vertical separation of $-0.05z/b$, shown in figure 3.11b, are expected to show better accuracy as the lift coefficient comparison, however this is not the case. Where the lift coefficient showed a discrepancy for $-1.0y/b$, the opposite is happening for the rolling moment. At $-0.05z/b$ vertical separation, the region around the wing-tip-vortex interaction shows better agreement, however the rolling moment local minima becomes under-predicted. Overall only at the direct wing-tip interaction ($-0.1y/b$) at $0.0z/b$ a difference in value of 98% compared to the tunnel data is present. At $-0.05z/b$ the difference is already diminished to 48%. The best agreement for the rolling moment at the wing-tip-vortex interaction is for a vertical separation of $-0.1z/b$ with a -4.2% difference, which is not shown here. The inboard vortex locations at $0.0z/b$ show a fairly good agreement. By increasing/decreasing the vertical separation the values start deviating more, as was seen by the under-prediction of the local minima in figure 3.11b when compared to figure 3.11a. The largest difference at $0.0z/b$ is -38% at $-0.5y/b$, not considering the lateral shift. Again important to note is that only the lateral region around the vortex, $-0.05y/b$ till $-0.15y/b$, show large deviations. The other lateral separation instances show a rather good agreement.

The lift coefficient analysis could identify a 5% region of (small) deviation in values, where AVL shows inaccurate results. The differences however are small at $0.0z/b$ and large at $-1.0z/b$. The rolling moment analysis identifies a 10% deviation region around the wing-tip-vortex interaction, $0.0z/b$, where the trough around $-1.0z/b$ is well approximated. This margins of error of 5% for the lift and 10% for the rolling moment show to be circumferential. Laterally moving from the vortex core at zero lateral separation, reduces the error. For the lift coefficient the error returns however from $-0.90y/b$, for when both tips show vortex interaction. This could be explained that once the vortex travels over the wing surface, the left and right adjoining wing regions, vortex to tip and vortex to root, balance the inaccuracy. The reappearing error arises when the vortex reaches the other wing tip, effectively removing the balance of the region vortex to tip.

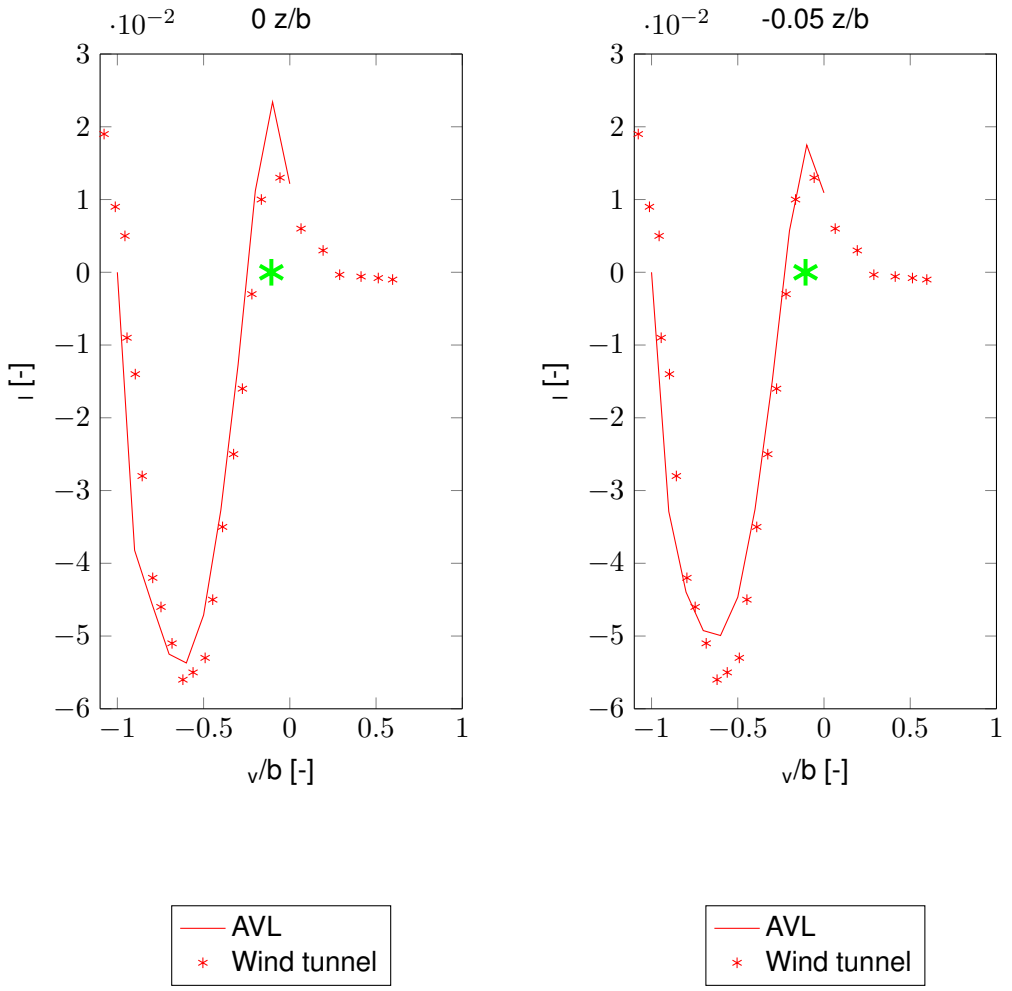

(a) Zero vertical separation with vortex, $0.0z/b$

(b) Negative vertical separation with vortex, $-0.05z/b$

Figure 3.12: Rolling moment coefficient with relation to lateral separation over swept wing in formation flight condition, wind tunnel validation

3.3.5 Effect of sweep on Formation Flight

The previous two reference studies could be used to compare the influence of the addition of sweep angle on the aircraft in the formation flight. Both show the results of AVL compared to wind tunnel results for a rectangular wing to a swept wing model. However no direct relation can be made between the two models, as the vortex strength does not coincide, general remarks could be made. For better comparison, the model of the rectangular wing from section 3.3.3 was adjusted to incorporate a sweep angle of 30 degrees. Figure 3.13 shows the comparison for lift coefficient and rolling moment coefficient for a vertical separation distance of $-0.05z/b$.

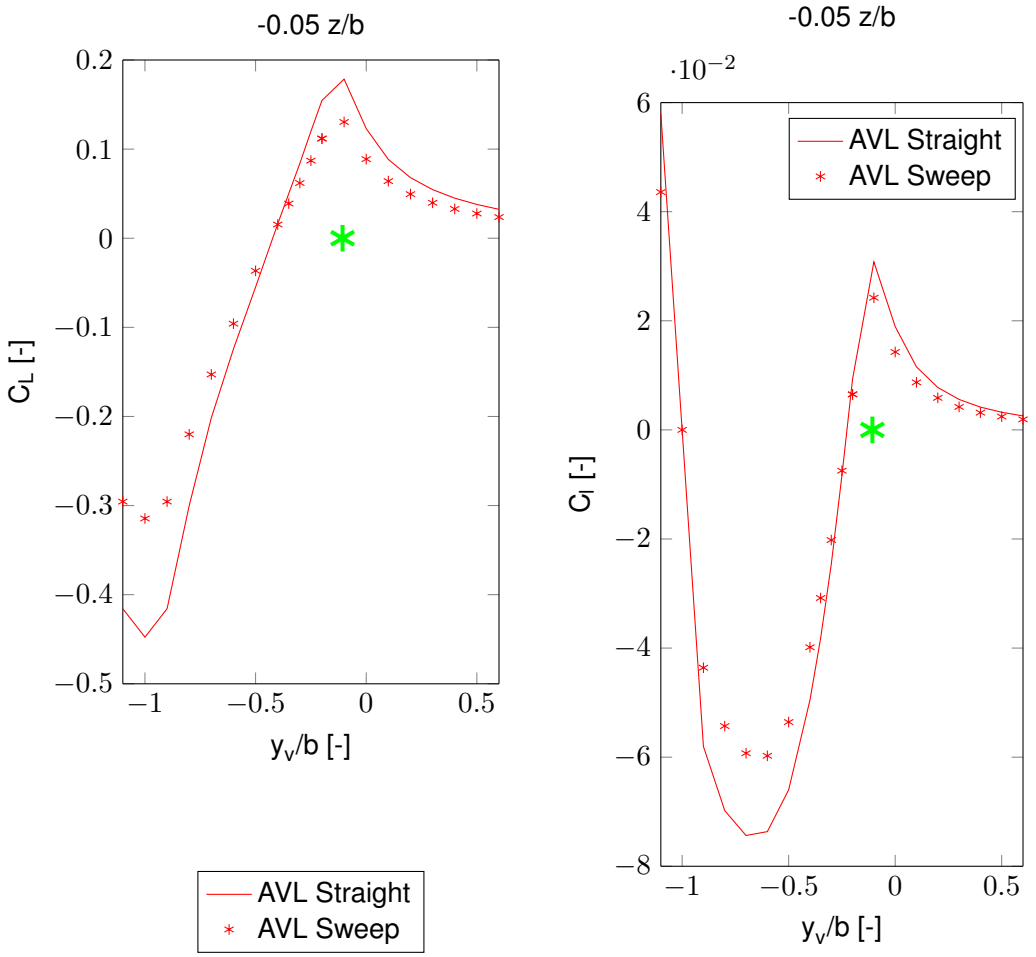

(a) Lift coefficient for $-0.05z/b$

(b) Rolling moment coefficient for $-0.05z/b$

Figure 3.13: Effect of sweep angle on swept wing for lift and rolling moment coefficient, model of rectangular wing McMillan with 0 and 30 degrees sweep angle

This initial analysis shows that both the lift and rolling moment are affected by the introduction of a sweep angle, as was expected. Due to the introduction of sweep, the lift coefficient will

diminish slightly, although the wing area remains the velocity creating lift will be positioned under the sweep angle [47]. For the swept wing, the peaks become less severe. This also directly affects the rolling moment and its peaks, as shown in figure 3.13b, which is beneficial from a control perspective as less trim would be required. The wing-tip-vortex interaction region, around $-0.1y/b$, remains virtually unaffected however when compared to the difference when moving the vortex inboard. Important to note is the difference at this low speed and altitude with a maximum difference of -30% for the lift and -20% for the rolling moment coefficient.

The sweep angle generally, as initially investigated here, has a positive effect on the induced rolling moment within the wake field, by decreasing the local maxima. The negative lift coefficient is reduced within the wake field, requiring less actions to be undertaken to retain the flight path. The region of wing-tip-vortex interaction however does not show great influence to the introduction of sweep, however even small reductions could be positive effect.

3.4 Formation Flight aerodynamic analysis

Within this section a first analysis is done of the A330-300 aircraft within a two aircraft formation flight, echelon shape, using the extended program of AVL as created by Fransen. Two aircraft in the echelon formation, as defined earlier, are separated by $10x/b$, or 10 wing spans longitudinal separation. First an aircraft model of the A330-300 needs to be defined. A comparison between the actual A330-300 and the model used by the VLM extended by Fransen is shown three dimensionally in figure 3.14 and from top view in figure 3.15.

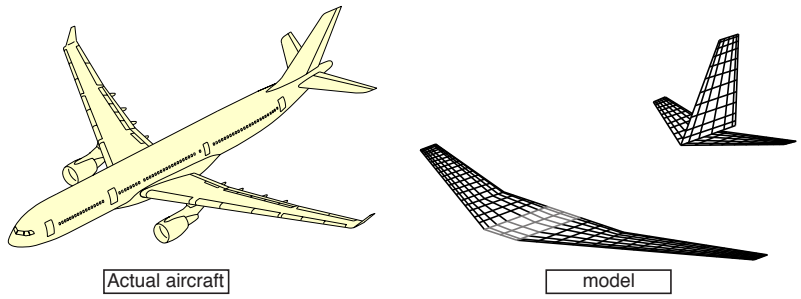

Figure 3.14: Clarification aircraft axis system and aircraft positioning

The remainder of this section shows the angle of attack and the forces and moments within the wake field, together with their variations. All data is for the aircraft in an untrimmed condition, where the lift coefficient of the trail aircraft is fixed at $0.623[-]$. The lift coefficient value was determined using the maximal take-off weight of $242,000kg$, for the condition of $L = W$ for a Mach number of 0.82. The maximal take-off weight was chosen to mimic the start of the cruise condition, where no estimation was tried for weight reduction after take-off. The vortex lattice method used by AVL however uses a compressibility correction, only reasonable accurate up till $0.6M$. To remain within the limits imposed by AVL, the Mach number was lowered to 0.6

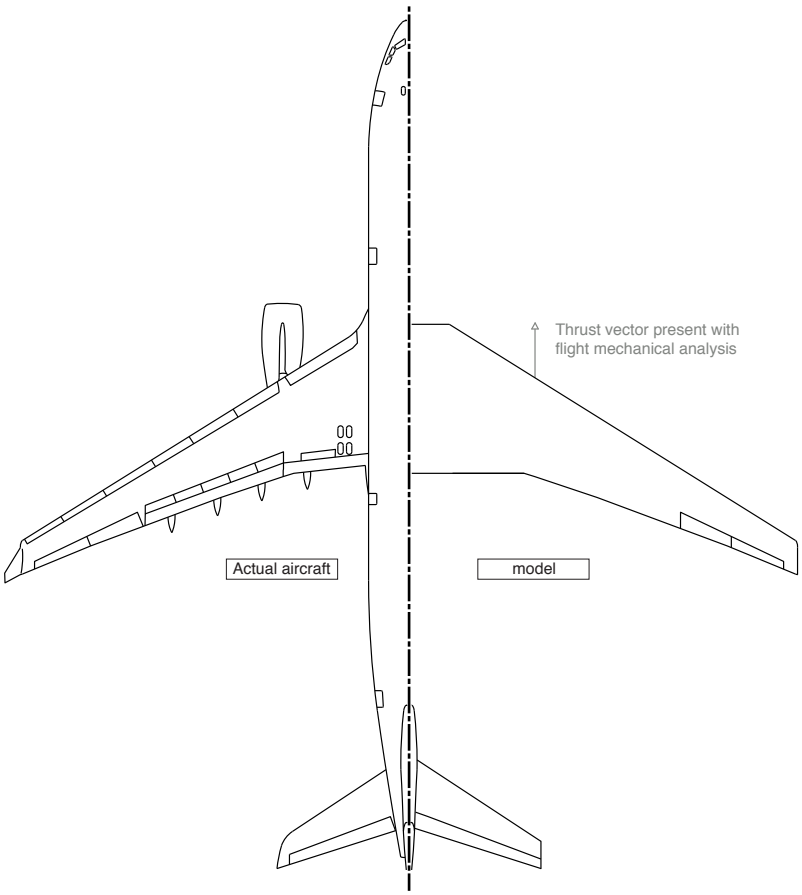

Figure 3.15: Clarification aircraft axis system and aircraft positioning

retaining the lift coefficient of $0.623[-]$. As a consequence the weight was reduced to a value of $129,566kg$ to retain the lift coefficient at a lower speed. The altitude was kept at cruise height, $11,000$ meters.

All graphs of the wake field are under the influence of an oncoming vortex, shed from the lead aircraft, which is located at $-0.107y/b\ 0.0z/b$. The vortex is indicated by the black star within the graphs. A situational sketch is given in figure 4.7 (based on the axis system in figure 2.1). Within the previous section, concerning the validation of the extended VLM of Fransen, a margin of error was identified. Within this margin, the values of the VLM compared to wind tunnel results showed deviation. The deviation was assigned to the direct wing-vortex interaction, not properly modelled by the VLM. The error margin comprises of two regions at $-0.1y/b$ and $-1y/b$ for $0.0z/b$ around which a 10% distance shows questionable results. The highest error was that of 10% for the rolling moment, where the 5% of the lift coefficient is included within this region.

The first region is deep within the wake field, were it was already identified by the literature that retaining formation flight is not desired. The second region is around the vortex core, were the formation flight sweet spot is located according to Fransen [25]. The deep wake field region is of less interest as the theoretical sweet spot, determined from literature, is in close proximity and not deep within the wake field. The analysis will focus on the region from -0.5 to $0.3y/b$ and -0.5 to $0.5z/b$. Only the region of error around the vortex core will thus be highlighted. Each graph also provides a geometry and an explanatory sketch of the most pronounced effect. This sketch is for one wake field position, marked by the red dot in the wake field graphs.

First the changes of angle of attack within the wake field are presented in figure 3.17. The graph shows a region where the angle of attack is reduced to attain a constant lift coefficient throughout the wake field. This shows again increased effective angle of attack effect due to the vortex interaction, basic formation flight principle as explained before. As the effective angle of attack is increased, the required angle of attack can be reduced. In solo flight condition the angle of attack is 2.81 degrees, meaning that the entire wake field depicted here has a beneficial influence of the oncoming vortex. The highest effect is when the vortex is located just above inboard of the wing tip at $-0.15y/b\ 0.0z/b$. Figure 3.17 also gives a geometry sketch for the wake field position marked by the red spot.

This increased effective angle of attack, resulting in a reduction of required angle of attack of the aircraft, creates a beneficial region for drag. Figure 3.18 shows the reduction of the induced drag coefficient within the wake field. The values shown are reduction due to the formation flight with relation to the solo condition of only the trail aircraft (equation 2.1 for the induced drag only). Similar behaviour as for the angle of attack can be seen where the vortex inboard of the wing tip results in the highest induced drag reduction. Whether the vortex is positioned above or below the wing does not affect the reduction value much (approximate symmetrical behaviour). The highest reduction value is a decrease of 83.5%, compared to solo flight induced drag, again at $-0.15y/b\ 0z/b$. This value however is questionable as the direct wing-tip-vortex interaction, 10% wing span in all directions around the vortex core, showed questionable results with the reference case analysis. The optimal is within that region. When looking at the surrounding

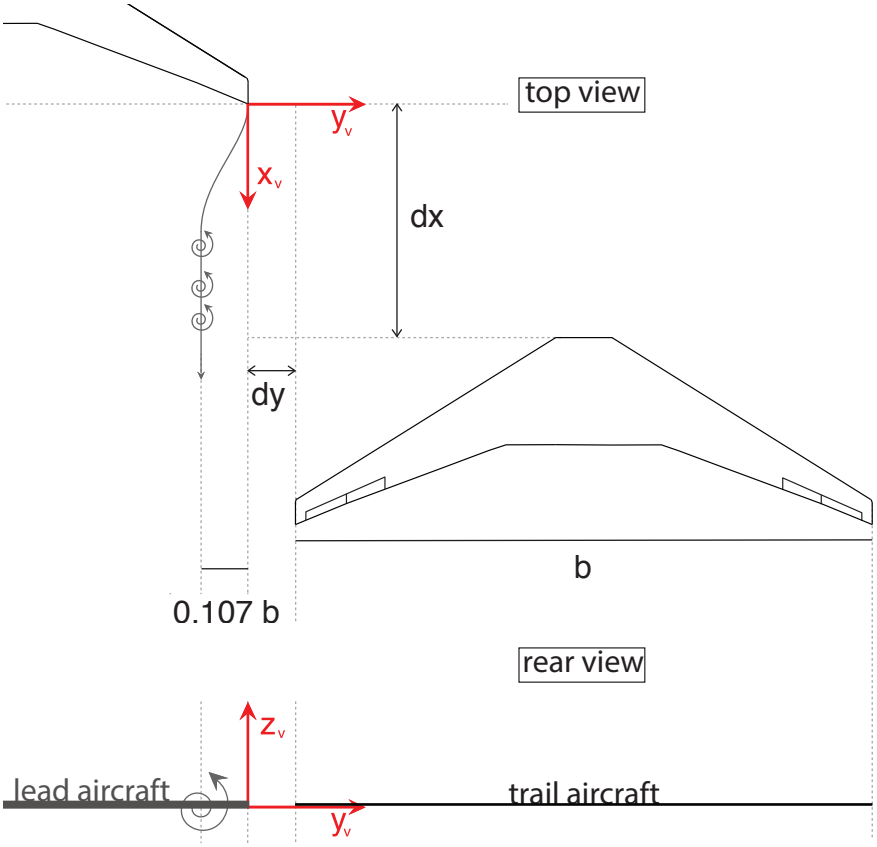

Figure 3.16: Clarification aircraft axis system and aircraft positioning

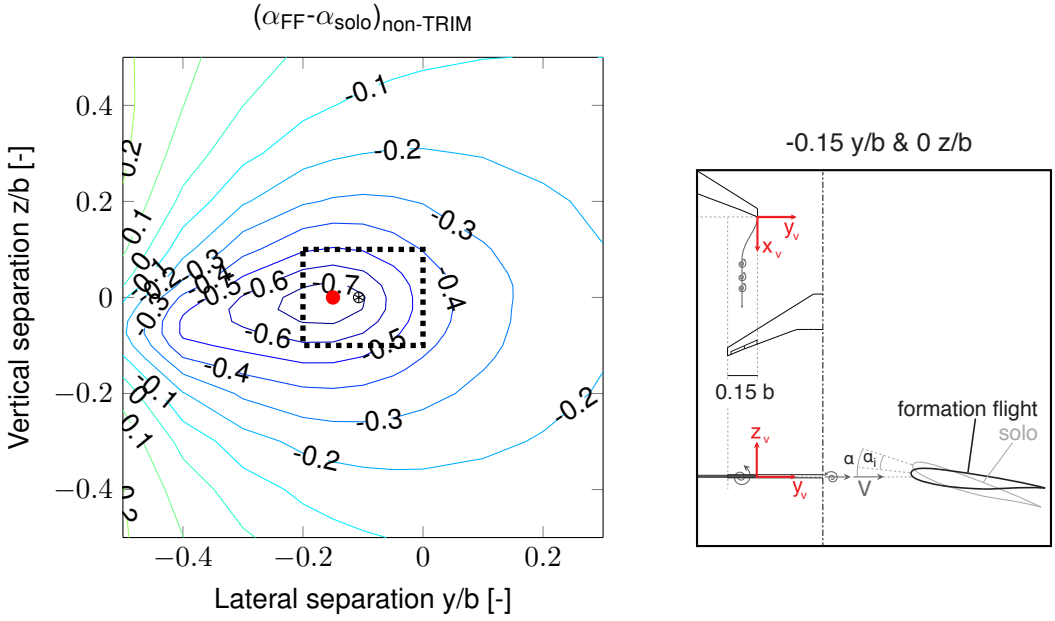

(a) Variation in wake field

(b) Geometry sketch situation position red dot

Figure 3.17: Wake field analysis with relation to angle of attack of A330-300 aircraft in a two aircraft echelon formation (black star indicates vortex location)

values however, the highest reduction becomes 70.1% at $-0.2y/b\ 0z/b$, outside of that region. It can be identified from the graph that a small region of 'unrealistic' high values remains to the left of the vortex. The direct wing-vortex interaction could still cause these values, although the margin of error from the validation of the VLM was applied. Further research is thus still required. When looking at the values to the right and below/above the margin, lower values can be seen, ranging from 49.8% at the upper left corner ($-0.20y/b\ 0.1z/b$) to 40.3% at the lower right corner ($0y/b\ -0.1z/b$). These value lies more within the expectation pattern of induced drag reductions, when comparing to results from test flights e.g. Ray et al. who measured a highest induced drag reduction of between $40 - 50\%$ around the vortex core[22]. It was chosen to use the position $-0.15y/b$ laterally and $0.1z/b$ vertically with a drag benefit of 52.6% as a reference point away from the direct wing-vortex interaction. Here the induced drag reduction shows the highest value outside of the margin of error, neglecting the left boundary for questionable results.

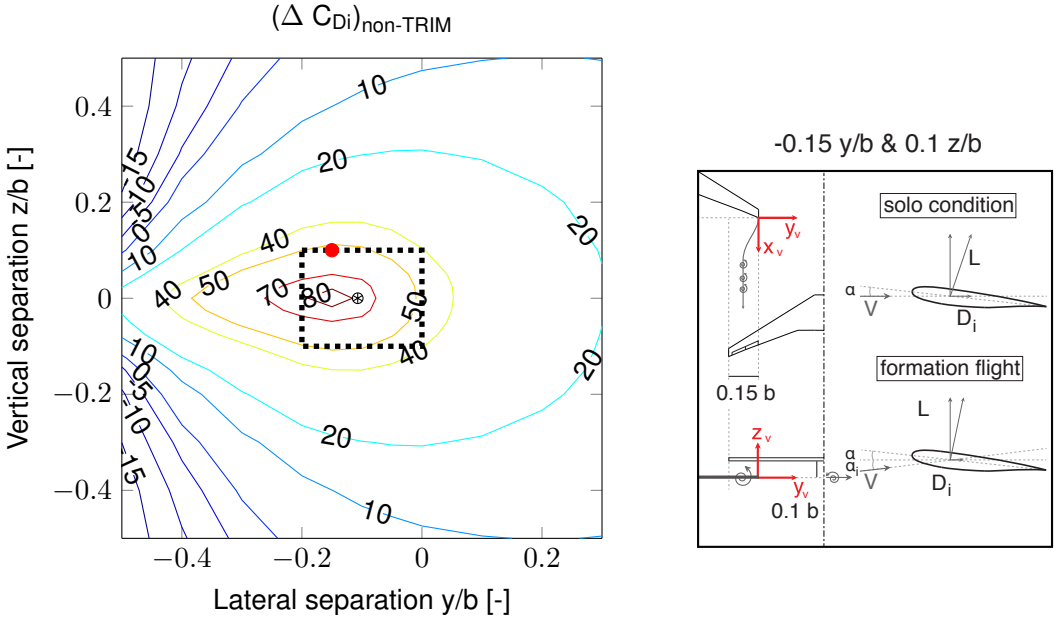

(a) Variation in wake field

(b) Geometry sketch situation position red dot

Figure 3.18: Wake field analysis with relation to induced drag coefficient of an A330-300 aircraft in a two aircraft echelon formation (black star indicates vortex location)

The side-force coefficient throughout the wake field is show in figure 3.19. The difference in pattern compared to the induced drag reduction is apparent. The side-force values shown are the ones of only the formation flight condition, as the side-force in the solo flight condition is zero within this case.
The region were the wing tip of the trail aircraft is aligned with the fuselage of the lead wing, $-0.5y/b$, at a vertical separation of $-0.3z/b$ shows the highest side force of the wake field, $0.0238[-]$. Almost parallel within the wake field a region of zero side-force is present, at a

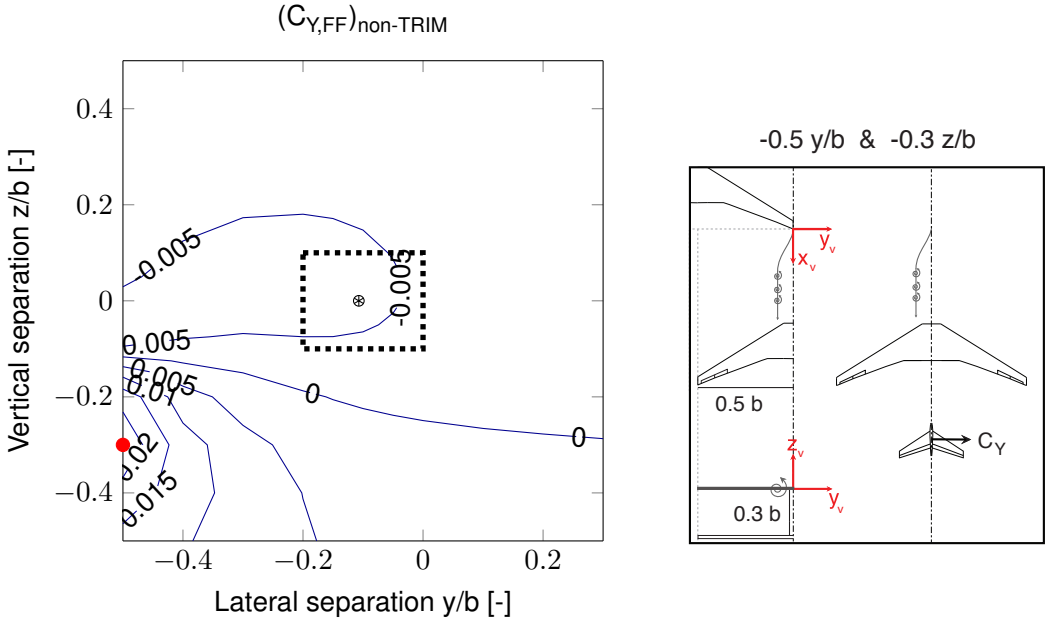

(a) Variation in wake field

(b) Geometry sketch situation position red dot

Figure 3.19: Wake field analysis with relation to side-force coefficient of an A330-300 aircraft in a two aircraft echelon formation (black star indicates vortex location)

vertical separation of $-0.1z/b$ to $-0.2z/b$. This overall change in side-force is induced by the rolling moment, created due to the change in effective angle of attack over the wing. If the aircraft rolls, the vertical tailplane will create a side-force, the adverse yaw. The region of highest difference could be created due to the proximity of the vertical tailplane with the incident vortex, as for $-0.5y/b$ the vertical tail is positioned at $0.1y/b$ away from the vortex core. The side-force at the location of highest induced drag reduction is $-0.0080[-]$ at $-0.15y/b$ and $0z/b$. Including the 10% error margin region the value at $-0.15y/b$ $0.1z/b$ of the side force becomes $-0.0061[-]$.

Next to the induced drag reduction, a large rolling moment will be present. The rolling moment interference has a large impact on the steady horizontal flight. The results as obtained by the VLM are shown in figure 3.20. The advantage of the reduction also creates the non-symmetrical wing loading. This will create a positive rolling moment, effectively rolling the aircraft out of the formation. The in-vortex wing receives more lift where the lift on the out-of vortex wing remains the same. The wing-tip-vortex interaction region shows the highest rolling moment. A shift in sign can also be noticed to the left of the vortex core (around $-0.25y/b$), stretching parabolic towards the edges of the wake field. The rolling moment changes sign as the vortex moves further inboard.
The vortex will create a region of up-wash, creating the benefit, but also one of down-wash, reducing the benefit. Outside of the vortex core the region of up-wash is present and inside of the wake field a region of down-wash is present. When moving the in-vortex wing further into the wake field, parts of the wing will be in the down-wash region and others within the up-wash region. The down-wash region decreases the effective angle of attack and thus the lift. A tipple point exists when the increase in lift does not outweigh the decrease in lift, this happens for positions where the in-vortex wing is further within the wake field. At the vertical separation of $0.0z/b$ this occurs at mid wing, $-0.25y/b$. Further decreasing the lateral separation, the in-vortex wing will create less lift compared to the out-of-vortex wing shifting the positive rolling moment to a negative one.
Where the solo condition had a zero rolling moment coefficient, the formation flight condition shows values. The region for highest induced drag reduction was at $-0.15y/b$ and $0.0z/b$. The rolling moment coefficient at this location is one of the highest in the wake field, namely $0.0120[-]$. Including the 10% margin of error the value at $-0.15y/b$ $0.1z/b$ of the rolling moment coefficient becomes $0.0036[-]$. Interesting to note is that this location is near the zero rolling moment region. The highest rolling moment coefficient was measured at $-0.5y/b$ and $0.0z/b$ with a value of $-0.0286[-]$.

The pitching moment change, shown in figure 3.21, also shows a behavioural shift running parallel. The shift is located around $0z/b$ across the wake field, shifted up when compared to the side-force coefficient. The pitching moment coefficient within the solo flight does already have a value, namely a negative one of $-0.0266[-]$. In solo condition the aircraft thus has a pitch down tendency.
The formation flight condition condition shows a region running parallel through the wake field, around zero vertical separation and wrapping itself around the vortex core, where no change in

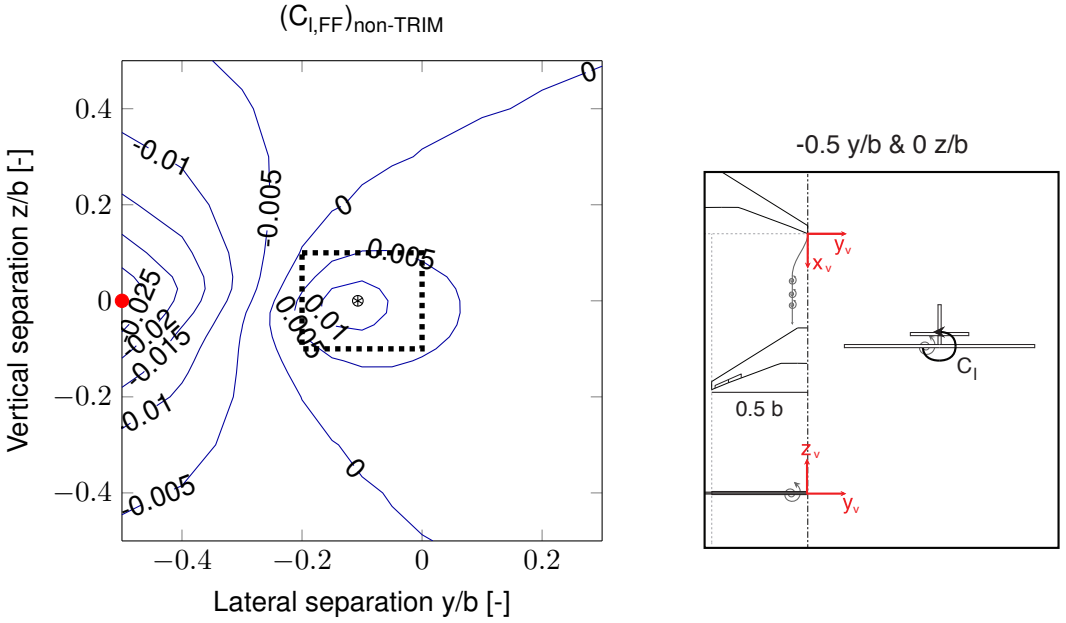

(a) Variation in wake field

(b) Geometry sketch situation position red dot

Figure 3.20: Wake field analysis with relation to rolling moment coefficient of an A330-300 in a two aircraft echelon formation (black star indicates vortex location)

pitching moment is present. Flying at positive vertical separation distances makes the pitching moment become less pronounced, where negative vertical separation distances negatively increase the the pitch down.
The interaction of the vorticial flow with the horizontal tailplane contributes to these changes. The positive vertical separation distances makes the vortex flow below the horizontal tail, creating a force on the lower side of the tailplane pointing downward. This force effectively relieves the pitch down tendency, explaining the decrease in negative pitching moment. Similarly the negative vertical separation distances create a force over the horizontal tailplane upper surface, pointing upward, inducing more pitch down and thus a more negative pitching moment.
At the highest induced drag reduction point, $-0.15y/b$ and $0.0z/b$, the difference in pitching moment becomes $\Delta 0.0025[-]$. Including the 10% margin of error the value at $-0.15y/b\ 0.1z/b$ of the side force becomes $\Delta 0.0093[-]$.

Compared to the solo condition, the aircraft flying in the formation will be forced to roll out of the formation. Remember that at $0.0z/b$ for longitudinal separations of $-0.25y/b$ towards positive, the aircraft responds by rolling away from the lead. For separations of $-0.25y/b$ towards negative the aircraft will roll behind the lead aircraft. A change in pitch is also induced, depending on the vertical separation lowering or increasing the pitch down tendency.
At the position for zero rolling moment and zero pitching moment difference, at $-0.25y/b$ and $-0.1z/b$, the induced drag reduction is 49.3%. The highest pitching moment coefficient change was measured to be $-0.0576[-]$ at $-0.4y/b$ and $-0.1z/b$.

Finally the yawing moment is shown in figure 3.22. The changes can be assigned due to the rolling moment changes, creating a side force and yawing moment as stated before. The contour patterns do resemble the side-force contour pattern. As for the rolling and pitching moment a series of positions exist where the difference between the solo flight and formation flight condition is zero. This region is located underneath the aircraft running almost parallel within the wake field, in accordance with the side-force as discussed earlier, logical as the side-force drives the yawing moment.

By looking at the side-force and the three moments, no location exists where all difference are zero. As stated earlier the rolling moment and pitching moment show small deviations around $-0.25y/b$ and $-0.1z/b$. The side-force and yawing moment have a region for trail wing tip aligned with lead fuselage and a negative vertical separation. The region for highest induced drag reduction was at $-0.15y/b$ and $0.0z/b$. The difference in yawing moment coefficient at this location is $0.0045[-]$. Including the 10% margin of error the value at $-0.15y/b\ 0.1z/b$ of the rolling moment coefficient becomes $0.0031[-]$. The highest rolling moment coefficient was measured at $-0.5y/b$ and $-0.3z/b$ with a value of $-0.0121[-]$.

An overview of all the values identified within the aerodynamic analysis are gathered in table 3.3. The table is subdivided into three parts: the first comprises of the values at the sweet spot (highest induced drag reduction) and the second of the sweet spot when excluding values

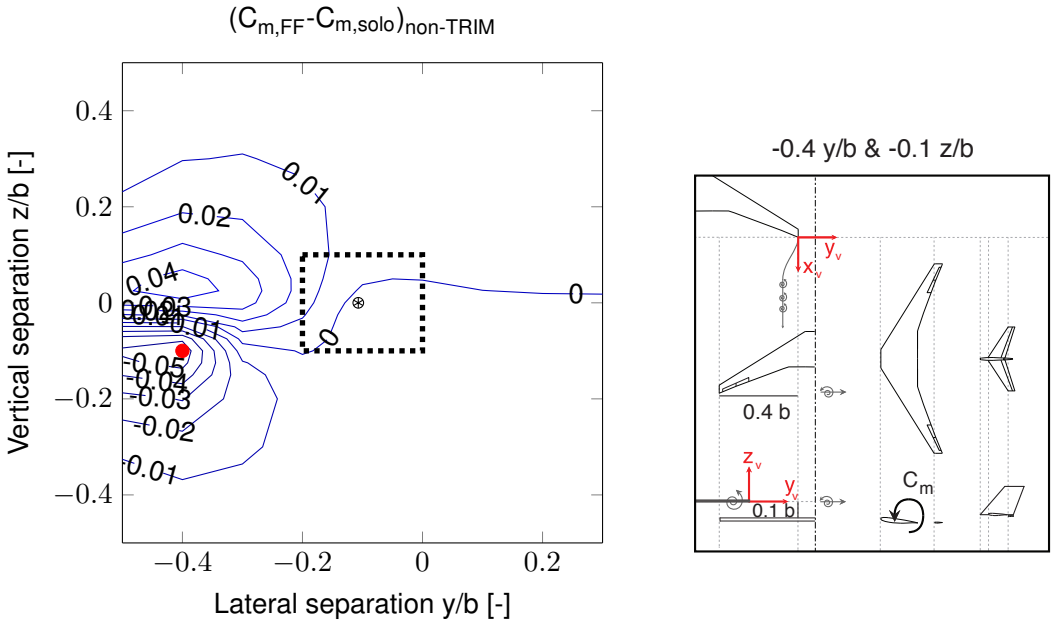

(a) Variation in wake field

(b) Geometry sketch situation position red dot

Figure 3.21: Wake field analysis with relation to pitching moment coefficient of an A330-300 in a two aircraft echelon formation (black star indicates vortex location)

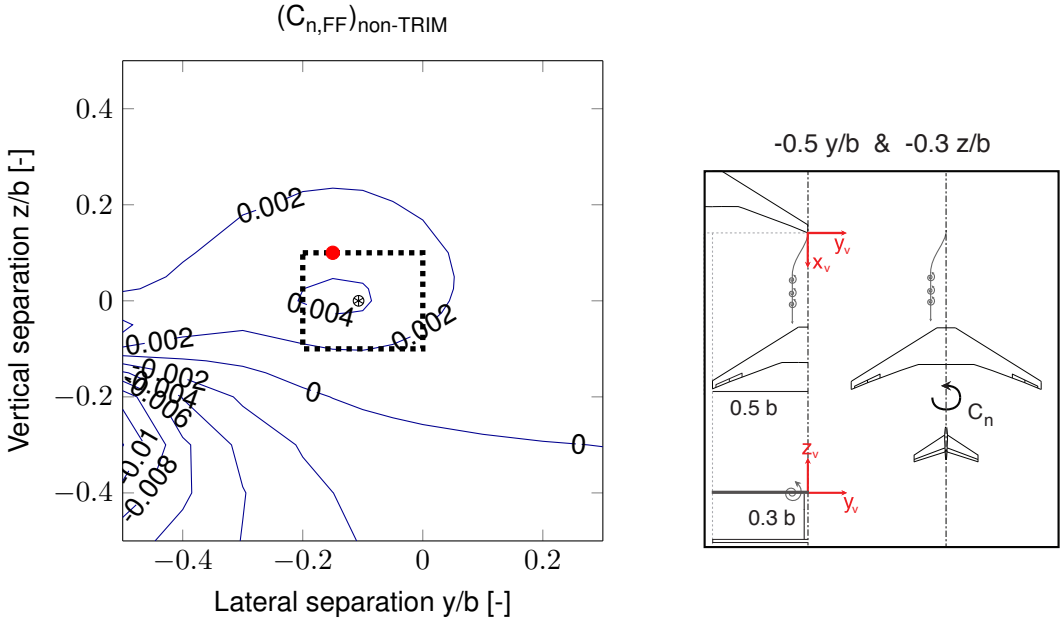

(a) Variation in wake field

(b) Geometry sketch situation position red dot

Figure 3.22: Wake field analysis with relation to yawing moment coefficient of an A330-300 aircraft in a two aircraft echelon formation (black star indicates vortex location)

within the margin of error, identified as the reference point. The third column comprises of the highest value and its location, for side-force and the three moments.

	Solo value	*Sweet spot* $-0.15y/b$;$0.0z/b$	*reference point* $-0.15y/b$;$0.1z/b$	*Highest value*	*Location*
C_{D_i}	0.010	$\Delta 83.5\%$	$\Delta 52.6\%$	$\Delta 83.5\%$	$-0.15y/b$; $0.0z/b$
C_Y	0	-0.0080	-0.0061	0.0238	$-0.5y/b$;$-0.3z/b$
C_l	0	0.1020	0.0036	-0.0286	$-0.5y/b$;$0.0z/b$
C_m	-0.027	-0.0241	0.0173	-0.0842	$-0.4y/b$;$0.1z/b$
		$\Delta 0.0025$	$\Delta 0.0093$	$\Delta - 0.0576$	$-0.4y/b$;$-0.1z/b$
C_n	0	0.0045	0.0031	-0.0121	$-0.5y/b$;$-0.3z/b$

Table 3.3: Overview changes in forces and moments obtained during aerodynamic analysis of Formation Flight at the sweet spot, sweet spot excluding values within margin of error and highest values in wake field, for assumed cruise condition: $M = 0.6$, $h = 11,000 meters$, $C_L = 0.623$

The effect of the rolling and pitching moment within the wake field are the most pronounced as wake vortex induced separation, as was already expected from literature. The entire wing loading is affected by incident vortex and will thus have a major impact on the aircraft stability and control. The asymmetric wing loading creates a rolling moment and the vortex flow creates the pitching moment, which both need to be counteracted by the control surfaces to retain steady straight flight. The investigation of trim and its effect on the aerodynamic benefit of the formation flight will be analysed within the next chapter.

3.5 Conclusion

At the beginning of this chapter, an aerodynamic solver method was chosen to analyse the formation flight condition. This aerodynamic solver was a vortex lattice based method extended by Fransen to include the formation flight condition. Validation of the analytical method with an Euler based solver and two wind tunnel tests proved that the VLM extended by Fransen is rather accurate. Nevertheless a region ranging from $5 - 10\%$ vertical separation shows inaccuracies, for positions where a wing tip is aligned with the vortex core. The discrepancy is highest for wing-tip vortex interaction. Positions in between both wing tips show rather good agreement on the other hand. The effect can be assigned to the inaccurate modelling of the direct vortex wing interaction present, a region of high viscous flow, not modelled within the VLM.

The wake field analysis of the A330-300 aircraft in cruise flight condition at a lift coefficient of $0.623[-]$ and a Mach number of 0.6 at an altitude of $11,000$ meters, was analysed. The vortex core was located at $-0.1y/b$ and $0.0z/b$ within the wake field.
The angle of attack varies within the wake field, as is expected due to the effective angle of

attack change within the up- and down-wash regions. The highest reduction in angle of attack, related to the solo flight condition, is located for the vortex positioned on the wing tip. This location positions the entire wing within the up-wash field, where moving left or right positions the wing away from the up-wash region or inside the down-wash region, effectively lowering the overall effect.
The highest induced drag reduction was 83.5% obtained at $-0.15y/b\ 0z/b$. Including the 10% margin of accuracy around the vortex core and neglecting the direct wing-vortex interaction values, a reference point was chosen. The point was located at the wake field position $-0.15y/b$ $0.1z/b$ with an induced drag reduction of 52.6%, showing a more realistic result when comparing to literature. This point at the edge of the erorr margin will further be referred to as the new sweet spot. Both side force and yawing moment showed a similar pattern in contour plots, with low values although not zero. The rolling and pitching moment coefficients showed larger deviations. The VLM used does properly model the wake vortex induced effects as well as the aerodynamic benefit, although around the vortex core the values are overestimated. An overview of the results of the aerodynamic analysis can be found in table 3.3, which was shown at the end of the last section and is therefore not repeated here.

CHAPTER

FOUR

FLIGHT DYNAMIC AND LOAD ANALYSIS

After determining the aerodynamic behaviour within the wake vortex field and identifying the major interference effects, it is time to look at the response of an aircraft flying within this wake field. The aerodynamic data as derived earlier can be used for the analysis. The analysis of the wake field is to attain insights into the aircraft behaviour when flying in the formation. Before an analysis can be executed, a simulation model is required.
A set of objectives and requirements is created to choose and determine the fidelity of the simulation model. The model is subsequently investigated and extended to meet the objectives. Important aspects include the aircraft model implementation, hinge moment estimation and total drag estimation.The assumptions regarding the simulation model are stated to wrap up the section. Once the model satisfies the requirements, it can be chosen to perform the analysis.
The simulation model will be used in four analysis parts: local trim analysis, wake field positional stability analysis, local dynamic analysis and a wake field hinge moment analysis. The entire analysis is set for the formation flight condition of the A330-300 aircraft in cruise condition, with a lift coefficient of $0.623[-]$ and a Mach number of 0.6 at an altitude of $11,000$ meters.
The last section discusses the analysis performed, followed by a conclusion. Figure 4.1 shows the two parts that are of interest within this chapter indicated in black.

4.1 Requirements

The formation flight condition and its flight dynamic and load analysis covers a broad topic. Therefore it is narrowed into four specific parts, which will be analysed here. The research study focusses on the effect of aircraft trim upon the formation flight, specifically the probable reduction of the drag benefit. To gain insights into the effects of trim in the formation flight for positions throughout the wake field, a trim analysis needs to be performed. Furthermore

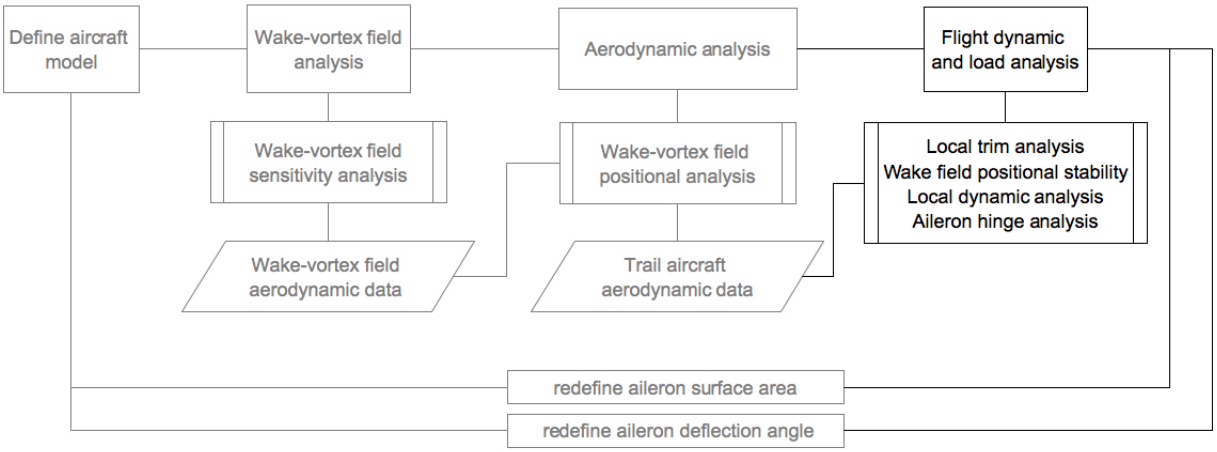

Figure 4.1: Outline of research into different topics, flight mechanic analysis highlighted

by looking at the trimmed aircraft within the wake field, a positional static stability analysis will provide insights into the aircraft responses, according to different wake field positions. The possibility to simulate and analyse the dynamic behaviour of the aircraft when trying to retain steady straight flight provides information into the feasibility of the flight within a wake field during the formation flight. Finally a specific load analysis upon the aileron hinge system needs to be investigated. The rolling moment disturbance was already identified as the largest interference within the wake field. The wake induced roll needs to be counteracted by the ailerons, where in solo flight condition no such counteraction is required. The ailerons systems will thus have a increased loading, which needs to be investigated to identify if limits are exceeded.
To analyse the formation flight condition, the simulation model thus needs to perform four types of analysis. These form the objectives that the simulation model needs to satisfy.

- Trim analysis at a wake field position
- Positional static stability analysis of entire wake field
- Dynamic analysis at a wake field position
- Aileron hinge moment analysis of entire wake field

The trim analysis and positional static stability analysis investigate the behaviour of the trail aircraft positioned throughout the wake field, without influence of time. For each position, the loads upon the trail aircraft need to be determined and analysed. Trim deflections should subsequently be used to balance the forces and moments to attain a predefined flight setting, a steady straight flight in this case. To deflect the control and trim surfaces, a module needs to be present to vary deflection angles. The load analysis and deflections required can be grouped within the aerodynamic module of the simulation model. Depending on the model, if an engine

module is present, the thrust can also be used to to balance the aircraft. An engine module would be required when investigation of fuel flow and propulsive efficiency is desired.
The influence of trim to balance the loads upon the forces of the aircraft can be quantified for each position within the wake field. Similarly the hinge moment is determined using the loads for the static analysis. The hinge moment value can be compared to the design limit value. The design limit value, as will be defined in section 6.2.3, is related to the maximal roll rate at a speed near stall at sea level conditions for the aircraft in solo condition. To determine the design limit, a dynamic simulation and analysis in solo condition is required. This opens the possibility to also briefly investigate the dynamic behaviour of the trail aircraft in formation flight at one position within the wake field. The purpose of the dynamic analysis at one wake field position is to see how the aircraft will respond to when moving within the wake field.

The wake field behind a lead aircraft is an unknown and volatile region to fly in. The earlier studies for wake vortex interaction during the landing phases show that until recently, more effort was placed into avoiding the wake region, as was discussed within chapter 2.2. During the landing phase dangerous situations can arise when an aircraft interacts with a wake field, which have previously resulted in crashes or serious damage to an aircraft. The complex nature of the aircraft response and behaviour after and/or during a wing-vortex interaction needs to be properly modelled. The simulation model should thus be based on the non-linear equation of motions, to be able to fully simulate all motions (symmetric and asymmetric ones).

The formation flight has specific aerodynamic characteristics and a definition of control to analyse the trimmed flight, for an A330-300 aircraft with specific dimensions and structural properties. It is therefore important that the simulation model incorporates the aerodynamics (aircraft and controls) and the aircraft structure in detail. The total flight analysis requires a propulsion definition within the model, to relate the induced drag benefit to fuel savings. Effectively this leads to a simulation model with an extended aerodynamic module, propulsion module and a detailed aircraft model definition. All must be able to be adjusted to specifically fit the formation flight condition.
A list of required characteristics for the simulation model can be set up. The aircraft model definition was left out, as obviously this is dependent on assumptions and geometrical data that is known. The level of detail is thus not linked to the simulation model itself, but to the data available and what is implemented.

- Non-linear equations of motion
- Extended aerodynamic module, with possibility for adaptation
- Propulsion module for total flight analysis

The accuracy of the simulation results depends on the fidelity of these modules as well as the input used to define the aerodynamics and geometry of the aircraft.

Recently a simulation model was created and extended by US air force and NASA for the Surfing Aircraft Vortices for Energy program. The model is briefly explained by Halaas et al [5]. The simulation model makes use of different types of datasets, ranging from data of vortex lattice methods to actual flight tests. The model includes the aerodynamic disturbances and

the vortex meandering of the wake field as generated by the lead aircraft. The exact built up of the model is unknown, only the specific addition of one module to estimate the influence of the wake is elaborated within the paper. The wake module includes the wake state, strength and position with relation to the trail aircraft.

4.2 Flight simulation model

Within the group of Flight Performance and Propulsion of the faculty of Aerospace Engineering of the Delft University of Technology, a flight mechanical model was already present called the Flight Mechanic Toolbox (FMT). This model was written in the Matlab software package by Mark Voskuijl et al. and makes use of the non-linear equations of motion. The program connects software modules created for conceptual aircraft design, aerodynamics and flight mechanics. The main focus of the program is to link these analysis components together for the purpose of the investigation of novel aircraft designs [48]. An example where the model was used, was the investigation of the Prandtl plane aircraft configuration by van Ginneken et al. [49] and Voskuijl et al. [50]. A subsonic blended wing body was also investigated for distributed propulsion, featuring boundary layer ingestion by Kok et al. [51]. The model now includes the following aspects, were only relevant aspect are listed:

- Prandtl plan aircraft model
- Aerodynamic and control surface module (using data VSAero)
- Engine module (three spool turbofan)
- Flight control system module (daisy chain)
- Non linear equations of motion based on rigid multi body dynamics
- Dynamic and static simulation and analysis scripts

The Flight Mechanic Toolbox has a modular built up. Each aircraft model is built up out of separate modules for aerodynamics, drag, engine, flight control system and structural data. Each module can be as extensive as information is present. Depending on information that is known, several assumptions need to be made. Similarly to the aircraft model, the simulation and analysis tools also have a modular built up. Aircraft components can be added or removed and minimized or extended to optimally suit the level of detail of the aircraft model. Similarly a choice can be made into which type of analysis one wants to execute.
The FMT simulation module can both perform static and dynamic simulations. Multiple analysis scripts are present to post process the simulation data into stability. Due to the modular built up, modules can be altered, created, deleted to better suit the simulation case and aircraft model at hand. An analysis module for the formation flight can be created and implemented, by adjusting the existing modules of aerodynamics and the aircraft.

The FMT simulation model thus satisfies the first three objectives, trim analysis positional static wake field analysis and local dynamic wake field analysis. The aileron hinge moment analysis

is not present now, but due to the nature of the model, an extension is easily made to use the simulation data to approximate the aileron hinge moment.
The required characteristics are also present, the non-linear equations of motion based on a rigid multi body dynamics are used. The simulation model is built up in separate modules that can be added or removed during simulations, e.g. one could simulate a landing gear and/or engines present or only look at the aircraft body. As the model is built within the MATLAB environment, it can easily be adjusted and tailored to ones needs.

The model as it is now can however not be used for the formation flight analysis. Changes and additions to existing modules as well as additional analysis scripts need to be written. First of all the aircraft model needs to be created. The structural, drag and aerodynamic information was obtained using the key dimensions provided by Airbus [52] and the results of the extended vortex lattice method. The engines were modelled using information already present for a three spool turbofan engine, as was created by Jan de Klerk. A pre-set daisy chain flight control system was reused within the Airbus A330-300 simulation model. An extension to the reference frame definition, located within the equation of motion module, needs to be made to include the vortex reference frame. The vortex reference frame is required to link the aerodynamic data to the aircraft position within the wake field, as the wake field shows variations in aerodynamic forces and moments. The aerodynamic and control surface modules were extended to be able to simulate both the formation flight as the solo flight condition. Additional analysis scripts also need to be created to determine the aileron hinge moments and to analyse the formation flight condition. The required extensions are listed for clarity:

- A330-300 aircraft model (aerodynamic-drag-structure)
- Extension aerodynamic and control surface module
- Vortex reference frame inclusion in equations of motion module
- Creation Formation flight analysis script
- Creation aileron hinge moment analysis script

The remainder of this section will discuss the additions to the simulation modules and their key features. The aileron hinge moment and formation flight analysis script will also be discussed. First the aircraft model is discussed together. Second, the adaptation for the formation flight to the aerodynamic, control surface and the equations of motion module together with the formation flight analysis script is elaborated. Third, the aileron hinge moment analysis script is discussed, followed by a total drag estimation. Finally a list is provided of all assumptions of the model.

4.2.1 Aircraft model

The aircraft module was reconfigured to suit the Airbus A330-300 aircraft. The aircraft model has five important parts: the geometry together with the aerodynamic and control

surface data and their incorporation within the aircraft model. Both aspects will be discusses subsequently.

The geometry was defined using the information of the key dimension data sheet as was provided by Airbus [52]. The Prandtl plane aircraft configuration from a previous study [50] was adapted to fit the rest of the A330-300 aircraft model. The engines of the Prandtl plane aircraft were relocated from the fuselage for the Prandlt aircraft to a position on the wing for the A330-300 aircraft. The control system was adjusted, where only the amount of surfaces and allocation definitions were adjusted. The control allocation principle and actuator systems from the Prandlt aircraft were used for the A330-300 aircraft. The control system was approximated using a daisy chain control allocation and standard control deflection limitations [53]. Actuators are implemented by modelling them as second order systems, as already defined in a previous study concerning the Prandtl plane aircraft configuration.

The structure was defined using again the information provided by the key dimension data sheet and rules of thumb for inertia estimations. Identified within chapter 2.2.2 was the effect of flexible wings upon the wing-vortex direct interaction problem. A complex interaction between a flexible wing, its tip vortex and the incident vortex was identified, without considering control surface deflections. The addition of a control surface deflection for flexible wings in solo condition will impose aerodynamic twist on the wing. The interaction of the (un-)steady aerodynamics and structural dynamics of the control surfaces when deflected creates complex aero-servo-elastic effects in solo condition. These effects encompass the dynamic interactions among wing loading, structural deformation and the automated flight control system [54] [55]. The formation flight condition, with an incident vortex, would possibly add to the unsteady aerodynamics and dynamic interactions. The incident vortex entangling with the tip vortex will create a complex unsteady aerodynamic behaviour over the wing tips, where the ailerons are located. The asymmetric wing loading, created by the incident vortex, will affect the wing loading and add to the structural deformation. The in-vortex wing will have a higher wing loading and thus probably more deformation will be present. Both effects could make the aero-servo-elastic effects more pronounced. Further research is required to obtain a clear insight into this behaviour, but due to the specific nature of the effect and the thorough local investigation required, it was omitted within this research.
A rigid wing model was therefore used within this research study. The wing was assumed not to bend and/or deform due to the loads imposed and/or control surface deflections. The effect of aero-servo-elasticity is therefore also neglected.

The aerodynamic data, required for the flight mechanic analysis, was obtained from the VLM extended by Fransen. Important to note is the fact that the aerodynamic data calculated does not incorporate aerodynamic disturbances like gusts and variations in wind velocity components.
The aerodynamic data is needed to determine the behaviour of forces and moments within the wake field. The aerodynamic data can be a function of the angular rates, p, q, r, the angle of attack, α, the side-slip angle, β, Mach number, M and the control surface deflections, $\delta a, \delta e, \delta r$. Depending on linear relation between the aerodynamic coefficients and the above mentioned 'changes', derivative values can be introduced to reduce the magnitude of the aerodynamic data

table. A derivative value effectively reduces the relation between the aerodynamic coefficient and the 'change' to a single value, instead of a variation of the 'change' with coefficient values to grasp the behaviour. As one can imagine, the use of the derivative values greatly reduces the magnitude and complexity of the aerodynamic data table. It is possible that a linear behaviour can be identified, but that the zero function variable value is not equal to a zero force or moment value. This implies that a zero-value needs to be added. The best known example is the zero-lift addition required when assuming linear behaviour of the lift coefficient with relation to angle of attack.

As stated before to obtain total forces and moment variations for the function variables implies a large dataset. For example if for each function variable two values need to be calculated, this would imply 2^8 function variables $= 256$ aerodynamic iterations required. Each iteration calculates all forces, moments and derivative values for one input set of function variables. As the formation flight wake field is analysed, three extra variables come into play, the longitudinal-lateral-vertical separation distances. As identified in chapter 3.4 the force and moment relations change with position within the wake field. The longitudinal distance was fixed at ten wingspans, making that the lateral and longitudinal separation distances remain as two extra variational parameters. The 256 iterations thus also need to be made for the set of points within the wake field, further enlarging the data set.
The use of derivative values would significantly lower the amount of iterations, as just one iteration per wake field position would be required for that function variable, instead of the minimal of two. The use of these derivatives is possible if a linear behaviour can be identified for a force or moment, with relation to the function variables. An example are the control derivatives, which show a linear behaviour which go through the origin, not requiring a zero value addition. In solo condition, the angular rates also show a linear behaviour that go through the origin. The angle of attack also has a linear behaviour for a small range of angles of attack, away form the stall angle. As a zero lift value needs to be added it was decided to disregard the linear behaviour and retaining the function variable for the forces and moments. The side-slip and Mach number show a non-linear behaviour in the solo condition.
The formation flight condition identified that for each position, small changes in linearity were present. For the initial investigation, it was chosen to adhere to the linearity relations of the solo condition. The aerodynamic data set thus becomes a function of the angle of attack, the side-slip angle and the Mach number. The option was added to drop the relation with the Mach number, further reducing the complexity and magnitude of the dataset. This simplification is only valid when the analysis is at a fixed Mach number.

Equation 4.1 shows the mathematical representation of the aerodynamic data set, not incorporating the Mach number. These equations determine the data required, and their variations. Important to note are the lateral and vertical separation distances, denoted as subscript to each matrix to simplify the equations. These equations where incorporated within the aircraft aerodynamics module to be able to analyse the formation flight condition. They form the aerodynamic basis for the entire analysis performed in section 4.3.

$$\begin{bmatrix} C_X \\ C_Y \\ C_Z \\ C_l \\ C_m \\ C_n \end{bmatrix} = \begin{bmatrix} C_{X_{tot}}(\alpha,\beta) \\ C_{Y_{tot}}(\alpha,\beta) \\ C_{Z_{tot}}(\alpha,\beta) \\ C_{l_{tot}}(\alpha,\beta) \\ C_{m_{tot}}(\alpha,\beta) \\ C_{n_{tot}}(\alpha,\beta) \end{bmatrix}_{y,z} + \begin{bmatrix} C_{X_{\delta a}} & C_{X_{\delta e}} & C_{X_{\delta r}} \\ C_{Y_{\delta a}} & C_{Y_{\delta e}} & C_{Y_{\delta r}} \\ C_{Z_{\delta a}} & C_{Z_{\delta e}} & C_{Z_{\delta r}} \\ C_{l_{\delta a}} & C_{l_{\delta e}} & C_{l_{\delta r}} \\ C_{m_{\delta a}} & C_{m_{\delta e}} & C_{m_{\delta r}} \\ C_{n_{\delta a}} & C_{n_{\delta e}} & C_{n_{\delta r}} \end{bmatrix}_{y,z} \cdot \begin{bmatrix} \delta a \\ \delta e \\ \delta r \end{bmatrix} + \begin{bmatrix} C_{X_p} & C_{X_q} & C_{X_r} \\ C_{Y_p} & C_{Y_q} & C_{Y_r} \\ C_{Z_p} & C_{Z_q} & C_{Z_r} \\ C_{l_p} & C_{l_q} & C_{l_r} \\ C_{m_p} & C_{m_q} & C_{m_r} \\ C_{n_p} & C_{n_q} & C_{n_r} \end{bmatrix}_{y,z} \cdot \begin{bmatrix} p \\ q \\ r \end{bmatrix} \tag{4.1}$$

The option was added to also include an extended dataset where the aerodynamic data is a function of angular rates, deflection angles, angle of attack, side-slip angle and Mach number. Similarly a minimal dataset option was included only making use of the derivative values, added with the zero values. Although this option was added, the differences in results were not investigated within this research report.

4.2.2 Formation flight adaptation

The FMT program now includes the aircraft model. The modules for aerodynamics, control surfaces and the equations of motion need to be extended to incorporate the aircraft model and the vortex reference frame. The vortex reference frame is required for the use of the aerodynamic dataset, which is linked to the position of the aircraft within the wake field.

The equations as defined earlier for the aircraft model were included within both aerodynamic and control surface module, to determine the changes in forces and moments using the datasets form the VLM of Fransen. The forces and moments are determined using a linear interpolation method, reading out data from the aerodynamic property table. The aerodynamic and control surface module work to find a balance of aircraft forces and moments within the wake field, by changing the attitude of the aircraft and the control deflections. Thereby the aircraft can be trimmed to a predefined flight condition. Still required for both modules to function are the relative locations within the wake field. The dependency of the aerodynamic data to the positions within the wake field was already made apparent. The positions are however not yet defined within the FMT model.

The equation of motion module was expanded by a transformation matrix to implement the link of the earth reference frame to a ‘second body’ reference frame, representing the wake vortex sheet. A situational sketch is provided in figure 4.2, highlighting all coordinate reference frames present. The vortex reference frame is fixed in lateral and vertical direction, travelling at the same velocity as the aircraft (retaining a constant longitudinal separation). First the user defines the position of the aircraft within the wake vortex field as input. As the aircraft moves, the changes within the earth reference frame are determined. These changes are subsequently transformed into the changes in vortex reference frame coordinates. The initial position and the changes are added to obtain the new position within the vortex reference frame.

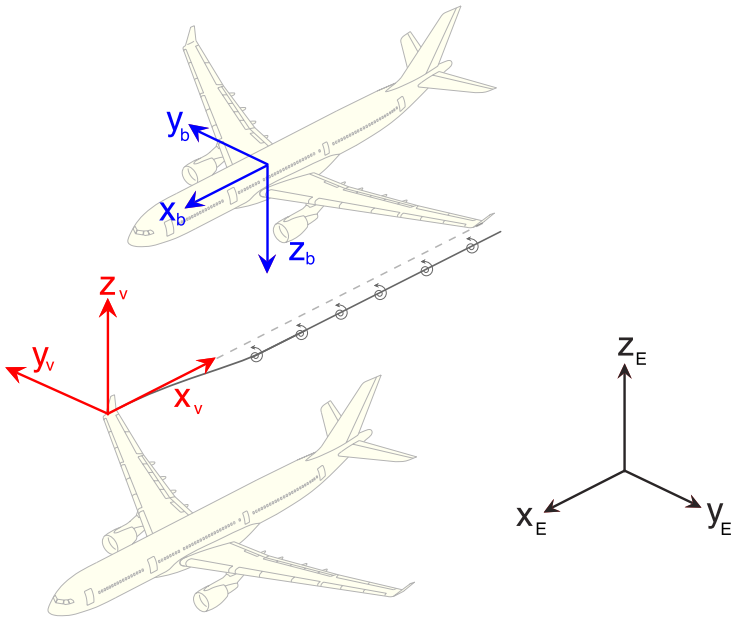

Figure 4.2: Coordinate reference frames identified

The transformation matrix, as was used to convert the earth reference frame coordinates to the vortex reference frame coordinates is shown in equation 4.2, in its condensed formulation. The first addition represents the initial position within the wake field, as defined by the user as input. The second term contains the velocity and initial altitude, to retain the constant longitudinal separation at the correct altitude. Equation 4.3 shows the entire transformation matrix, where the bold signs are the changes with relation to a standard transformation matrix.

$$\mathbf{x}_v = \mathbb{T}_{ve} \cdot \mathbf{x}_e + \mathbf{x}_{e,initial} + \begin{bmatrix} V_e * t \\ 0 \\ h_{initial} \end{bmatrix} \tag{4.2}$$

$$\mathbb{T}_{ve} = \begin{bmatrix} \mathbf{-}\cos\theta\cos\psi & \cos\theta\sin\psi & -\sin\theta \\ \sin\phi\sin\theta\cos\psi \mathbf{+} \cos\phi\sin\psi & \mathbf{-}\sin\phi\sin\theta\sin\psi + \cos\phi\cos\psi & \mathbf{-}\sin\phi\cos\theta \\ \cos\phi\sin\theta\cos\psi \mathbf{-} \sin\phi\sin\psi & \mathbf{-}\cos\phi\sin\theta\sin\psi - \sin\phi\cos\psi & \mathbf{-}\cos\phi\cos\theta \end{bmatrix} \tag{4.3}$$

Finally a small adjustment was made to the flight control system module. The option to set a predefined deflection for left and right aileron separately was included. This option allows the user to play with non-differential aileron deflections in a direct and clear manner, without having to alter the control allocation vector and/or system. These angles can be defined within the aerodynamic data tables, if not present they are set to zero automatically.

Apart from all these adjustments and extensions to the simulation modules of the FMT model, an analysis script was written to automatically perform calculations within the entire wake field. The formation flight analysis script creates a loop to run the simulation at all wake field positions. The simulation results are processed, used in calculations and made non-dimensional, to create the final analysis plots and saved into the formation flight dataset. Appendix B gives a general overview of the formation flight analysis module.

4.2.3 Hinge moment

The hinge moment and hinge moment coefficient are a measure of the aerodynamic force exerted on a trailing edge device as it is deflected during flight. The moment is created as the deflection at the trailing edge will create lift on the deflected section. The extra lift force will create a moment on the hinge around which the trailing edge device is deflected. This hinge is also the connection point to the main wing. The hinge has a structural limitation, which the moment force may not exceed.

In chapter 3.4 the highest disturbance moment due the wake field, was the rolling moment. Steady straight flight in the wake field thus requires an increased aileron deflection to retain the flight condition when compared to the solo flight. The pitching and yawing moment only show a small disturbance moment in the wake field, creating the assumption that the aileron deflection angles will show the largest deviation when compared to the solo condition. The highest hinge moment during steady straight flight (cruise condition) is thus expected on the aileron hinges.
The ailerons are not designed to constantly be deflected during the cruise flight, which is required during the formation cruise flight. In most cases not even ailerons, but spoilers are used for roll control during cruise flight. It was already identified within chapter 2 that the elevated aileron deflections during cruise flight might become critical upon the aileron control system. From a control perspective, the question arises if enough margin for control deflections still exist, i.e. the remainder angle that can be made with the control surface before reaching the design limit after deflection for the disturbance moments.

The aileron hinge moments are assumed to become critical before the elevator and rudder hinge moments. The analysis here will focus on the aileron hinge moment only. When considering the aileron deflection and its hinge moment, the assumption of a rigid wing was used neglecting the aero-servo-elastic effects.
Within this section first a method to estimate the hinge moment will be derived, for solo and formation flight condition, using an empirical/analytical method as derived by the Engineering Sciences Data Unit (ESDU). Next a statistical limit load, as defined by the Federal Aviation Authority (FAA) within the Federal Aviation Regulations (FAR), is determined for comparison with moment forces estimated during the formation flight condition.

4.2.3.1 Hinge moment estimation

Obtained from the ESDU repository, a prediction method for the hinge moment derivatives of trailing edge controls on wings at subsonic speeds was used to determine the hinge moment value [56] [57]. The method is suited for full- and part-span sealed trailing edge control surfaces. It makes use of the data for two dimensional flow, corrected with induced angle of attack and induced camber based on the lifting-surface method. Compressibility effects are included using the Prandtl-Glauert compressibility correction, effectively limiting the Mach number to a value lower then 0.6. The part-span controls require a correction, using empirical data which is extracted from literature. The estimation method shows an accuracy of 0.05 per radian with control deflections when compared to reference cases, for the tested geometries. The geometries ranged in aspect ratio from 2 to 8, with half chord sweeps up to $50^{\cdot}$ degrees and a thickness to chord ratio ranging from 0.06 to 0.14.

The aerodynamic analysis was already limited to high subsonic velocities, therefore the method suitable for subsonic estimation was chosen. The derivation is divided into two parts, the hinge moment derivative with relation to change in angle of attack due to the rolling motion, parameter b_1, and the hinge moment derivative with relation to change in trailing edge deflection, parameter b_2. Both derivatives can be combined to obtain the final hinge moment relation. The derivations make use of basic flow conditions and geometrical wing plan-form parameters. The geometrical parameters found in the A330-300 key dimension and data document as provided by Airbus [52]. A schematic representation of the aileron and hinge is shown in figure 4.3. The limitations of the method are stated below:

- Rigid wing model
- Sealed control surface with stream-wise side-edges
- Mach number under 0.6
- Sweep angle,Λ, between $0 - 50^{\circ}$ [degrees]
- Aspect ratio,AR, between $2 - 8[-]$
- Thickness to chord ratio,t/c, between $0.06 - 0.14[-]$
- Control surface chord to total chord ratio,c_f/c, between $0.2 - 0.4[-]$
- trailing edge sweep angle,τ, between $6 - 20^{\circ}[degrees]$
- span-wise distance from center-line to inboard limit of surface over semi-span, η_i, between $0 - 0.8[-]$

The aircraft is modelled as a rigid wing model within FMT. The edges of the control surfaces are assumed to be stream-wise oriented with sealed connections to the wing. The aircraft and flow parameters used were a Mach number of 0.6, Λ of 30° degrees, an aspect ratio of 10 [-], t/c of 0.13 [-], c_f/c of 0.3 [-], τ of 17.8° degrees and η_i of 0.77 [-]. All values are within the limitations, with the exception of the aspect ratio. It was assumed that the small deviation from the limitation value for the aspect ratio would not affect the results to much.

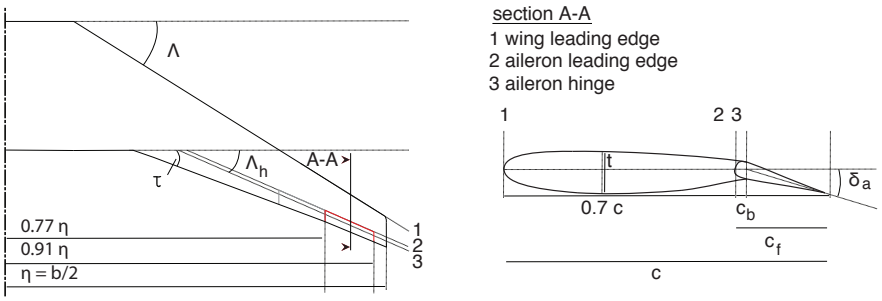

Figure 4.3: Schematic representation of aileron and hinge as used to estimate the hinge moment, specific to the A330-300 aircraft

Two other interesting parameters are related to the geometry of the aileron and its hinge. First is the location of the hinge with relation to the chord of the control surface, c_b/c_f, which is equal to 0.3 [-]. Second is the span-wise distance from the center-line of the aircraft to the outboard end of the control surface divided by semi-span, η_n, which is equal to 0.91 [-], where η_i was equal to $0.77[-]$.

The estimation method for the hinge moment determines the hinge moment derivatives with relation to angle of attack, b_1, and with relation to the aileron deflection angle, b_2. The method also uses the rates of change of lift due to the angle of attack, a_1, and due to the aileron deflection a_2.
During the estimation method subscripts and superscripts appear. The superscript 'star' denotes the assumption for a standard plain section. The standard plain section implies that empirical values are used, determined by the general geometric properties of the aileron size and hinge location, as if the aileron would be a stand-alone surface. The subscript 'zero' denotes the assumption of a two dimensional wing in an incompressible flow. Whenever the subscript 'T' is used, it implies that the value was determined theoretically instead of empirically.

The determination requires the derivatives of the lift coefficient to the angle of attack and the control deflection angle, identified by the symbol a. Similarly to the derivatives for the hinge moment, the derivative of the lift coefficient with relation to the angle of attack is identified by 1 (a_1) and the one with relation to control deflection angle is identified by 2 (a_2). The derivatives of the lift coefficient are determined using empirical relations. They are required to determine the values for a two dimensional wing profile, identified by subscript zero, of the standard plain section, identified by superscript star. The symbols in this condition become $(b_{1,2})_0^\star$ and $(a_{1,2})_0^\star$, for the derivative of the hinge moment and the derivatives of the lift coefficient.

The rates of change of lift have both a theoretical value as well as an empirical one. Both the theoretical value and the empirical rate of change of lift are determined using the fraction of the aileron chord with relation to the mean chord, c_f/c , and the thickness to chord ratio, t/c [58] [59]. Similarly the hinge moment derivative values are determined using the thickness to chord and aileron chord with relation to the mean chord [60] [61]. These derivative values together

with the trailing edge sweep angle and the thickness to chord ratio are used to determine the hinge moment derivatives for the two dimensional wing in an incompressible flow. Equation 4.4 and 4.5 show the relations that were used.

$$(b_1)_0 = (b_1)_0^\star + 2\left[(a_1)_{0,T}^\star - (a_1)_0^\star\right](tan\left((0.5\tau) - t/c\right) \tag{4.4}$$

$$(b_2)_0 = (b_2)_0^\star + 2\left[(a_2)_{0,T}^\star - (a_2)_0^\star\right](tan\left((0.5\tau) - t/c\right) \tag{4.5}$$

These relations can be refined when the control is not strict but balanced. Balancing of the control surface can be done by making use of aerodynamic solutions like a nose balance or an Irving balance. Essentially both make use of an aerodynamic force distribution to alleviate the moment on the hinge. Where multiple other solutions can be used for balancing only those are considered within this estimation method. As it is unknown if a form of balancing is present, it was chosen to omit the balancing factor. The purpose to make a comparison between hinge moments between formation flight and solo condition would not be affected by the absence of the balance, as a constant factor would be multiplied to the derivative values in both conditions to include the balancing.

As the hinge moment derivatives are still for a two dimensional wing in an incompressible flow, further calculations are required. The sweep angle, λ, is introduced together with the derivative of the lift coefficient to angle of attack, $dC_L/d\alpha$. Three empirical values are used, $G_{1,2,3}$, to refine the estimation. The empirical values are determined using the sweep angle, Mach number and aileron location upon the wing with relation to the semi-span ($\eta_{i,n}$). The hinge moment derivatives for the actual aileron surface can be defined using equation 4.6 and 4.7. The sweep angle at a quarter chord, $\Lambda_{1/4}$ is the only variable not yet introduced within equation 4.7.

$$b_1 = \frac{(b_1)_0}{(a_1)_0}\left(\frac{dC_L}{d\alpha}\right)cos\left(\Lambda_h\right) + G_1 + G_2 \tag{4.6}$$

$$b_2 = \left((b_2)_0 - \frac{(a_2)_0}{(a_1)_0}(b_1)_0\right)\frac{cos\Lambda_h}{\sqrt{\sqrt{1-M^2}tan^2\Lambda_{1/4}}} + \frac{(a_2)_0}{(a_1)_0}(b_1 + G_3) \tag{4.7}$$

The final step is to make the derivatives specific to the changes due to the flow at one instance e.g. within the wake field. To transform the derivative relations to hinge moment relations, equation 4.8 is required, including specific aerodynamic control derivative data. This relation was obtained from the flight dynamics course of the Delft University of Technology [35]. The equation relates the derivative data obtained to moment force components by multiplying them with angle of attack due to the control deflection and control deflection itself.

$$(C_H)_{left,right} = b_1\alpha_{left,right} + b_2\delta_{a_{left,right}} = \frac{dC_H}{d\alpha_{left,right}}\alpha_{left,right} + \frac{dC_H}{d\delta_{left,right}}\delta_{a_{left,right}} \tag{4.8}$$

The control deflection angles are known, the change in angle of attack due to the control deflection however is not. The value could be approximated by making use of the actual angle of attack and the average effective change of angle of attack due to the rolling motion over the span of the aileron, identified by $\Delta\alpha_a$. The relation for the change in angle of attack is shown in equation 4.9 and equation 4.10, for left and right aileron respectively.

$$\alpha_{left} = \alpha - \Delta\alpha_a \tag{4.9}$$

$$\alpha_{right} = \alpha + \Delta\alpha_a \tag{4.10}$$

The average effective change of angle of attack due to the rolling motion can be determined using the roll rate and the distance of the mid-point of the control surface to the center line, in this case $y_m = 0.87\eta = 0.435b$. Equation 4.11 shows this relation, where the contribution of the roll rate can be substituted by equation 4.12, revealing only aerodynamic parameters and control deflections for left and right aileron respectively.

$$\Delta\alpha_a = \frac{pb}{2V}\frac{2y_m}{b} \tag{4.11}$$

$$\left(\frac{pb}{2V}\right)_{left,right} = -\delta_{left,right}\frac{C_{l_{\delta_a}}}{C_{l_p}} \tag{4.12}$$

By making the combination of all equations above, the change in angle of attack due to the control deflection can be determined. The hinge moments for left and right aileron respectively can be calculated.

All equations as derived now can be implemented within a MATLAB script to work alongside with the aerodynamic data set and flight mechanical module to use the force and moment coefficient values together with attitude settings in both formation flight and solo condition to estimate the hinge moments. To wrap up an overview of the assumptions that where made are stated:

- Specific geometric data for A330-300
- Specific control data obtained from empirical relations for A330-300 geometry $a^\star_{1,20}$, $b^\star_{1,20}$
- Hinge moment derivative, $b_{1,2}$, estimated using empirical relations of ESDU
- Estimation of change in angle of attack due to control deflection, $\Delta\alpha_a$, using $C_{l_{\delta_a}}$ and C_{l_p}

4.2.3.2 Limit value determination

The hinges of the control surfaces are limited by a maximal moment and force, before becoming prone to loosing structural rigidity. The structure is designed to withstand a certain load in a certain condition, called the design limit. This design limit is elaborated within this paragraph. It is based upon the maximal roll rate of the aircraft at sea level conditions and 1.67 times the stall speed, where the constant 1.67 is a design load factor chosen empirically. The limit value is defined within the Federal Aviation Regulations [62] [63].

The limit value is related to the roll rate. The roll rate of an aircraft will increase/decrease due to a control deflection until it reaches a maximal value in time. The design guideline, stated within the $FAR - 25.349$ regulations for commercial transport aircraft, limits the hinge moment during cruise flight by the maximal roll rate value.
The maximum roll rate is determined during a full control deflection at sea level conditions. The speed is set to a load factor times the stall speed, where the load factor is defined as n_z and is equal to 1.67. The velocity, defined as $V_A = n_z V_{stall}$ as obtained from Lomax structural loads [62]. For sea level conditions and V_A it is determined that the aircraft is required to make a full control deflection without breaking. This maximal roll rate, related to the maximal control deflection for V_A at sea level is subsequently set as a boundary condition to the cruise flight. If during cruise flight the maximal roll rate is obtained due to a control deflection, than that control deflection angle poses the limit value. The relations are shown in equation 4.13.

$$\begin{aligned} p_{max} = \dot{\phi}_{max} &= \left(\dot{\phi}\right)_{V_A} \\ \dot{\phi}_{max} &= \left(\dot{\phi}\right)_{V_C} \end{aligned} \tag{4.13}$$

In the cruise condition, the maximal roll rate for a full control deflection at V_A at sea level thus determines a limit aileron deflection angle. This aileron deflection angle is in its term used to determine the limit hinge moment. The limit hinge moment is only determined for solo flight condition, regarding the regulations withhold for an aircraft in solo flight condition.

Using the previous paragraph, the aileron hinge moment is calculated for the entire wake field within the formation flight condition. The obtained values are compared to the limit value as was just determined in solo flight condition, to identify if the limit is exceeded.

4.2.4 Total drag estimation

A single aircraft its induced drag value, as calculated in chapter 3.4, only represents part of the total drag value, as stated within the aerodynamic analysis. The total drag value of an aircraft is of more interest when investigating the total flight, as will be done within the feasibility analysis in chapter 6. The total drag has multiple contributions, due to aerodynamics and the body itself. Figure 4.4 shows an overview of the contributors to the total drag as was obtained from Raymer

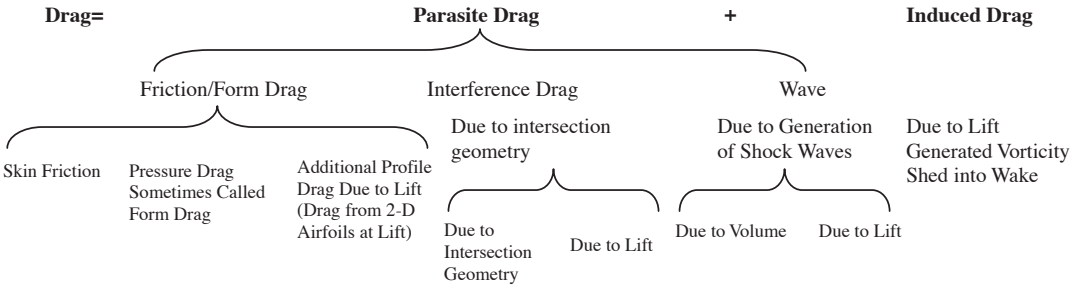

Figure 4.4: Build up of total drag of an aircraft as determined by Raymer [65]

[64]. Multiple equations could be formed using different contributing factors stated within figure 4.4. The equation used within this research is stated in equation 4.14

$$C_D = C_{D_{friction}} + C_{D_{pressure}} + C_{D_{induced}} = C_{D_{parasite}} + C_{D_{induced}} \tag{4.14}$$

The induced drag is calculated by the VLM extended by Fransen, the parasite drag thus remains. A crude estimation can be made by using the equivalent skin friction method, shown in equation 4.15. The value for the equivalent skin friction coefficient, $C_{f,e}$, can be taken from empirical data when assuming that the parasite drag will mostly consist of skin-friction drag plus a small separation pressure drag factor. This holds only for subsonic conditions. The value of $C_{f,e}$ for subsonic transport aircraft was set at 0.0030 [-].

$$C_{D_{parasite}} = C_{f,e}\frac{S_{wetted}}{S_{ref}} \tag{4.15}$$

A more elaborate method of determining the parasite drag was already present within the flight mechanic model. This method, also from Raymer, is dependent on the specific flight parameters like velocity and altitude. The aircraft geometry is included with the thickness to chord ratio, sweep angle, mean aerodynamic chord, wing area and wetted area. Using this information the Reynolds number is determined to make an estimation of the laminar and turbulent skin friction coefficients. The condensed equation to determine the parasite drag is shown in equation 4.16. Both skin friction coefficients are determined according to the relations shown in equation 4.17.

$$C_{D_{parasite}} = \left(C_{f,laminar} \left(\frac{x}{c}\right)_{laminar\,flow} + C_{f,turbulent} \left(\frac{x}{c}\right)_{turbulent\,flow} \right) \frac{S_{wetted}}{S_{ref}} \tag{4.16}$$

$$C_{f,laminar} = \frac{1.328}{\sqrt{Re}}$$
$$C_{f,turbulent} = \frac{0.455}{\sqrt{\left[(M^2 0.144)^{0.65}+1\right](\log Re)^{2.58}}} \tag{4.17}$$

By making the distinction into laminar and turbulent skin friction a new variable is imposed, namely the percentage of laminar flow in function of the chord where the turbulent region is defined as the rest of the chord. The wing profile is transonic for a swept wing in high-subsonic conditions, making the presence of laminar flow unlikely. The value was thus assumed to be zero. A good insight into the displacement and momentum thickness of the boundary layer is required to use accurate approximations to determine the transition point, like e.g. Thwaites method for laminar-turbulent transition and separation [66]. This was out of the scope of the research presented here.

Both methods discussed here make use of the wetted area. An estimation was made by using two estimation methods, one for the lifting surfaces using Raymer [64] and a second one for the fuselage by Nita [67]. The lifting surfaces include the wings, horizontal and vertical tail. In order to obtain a a parasite drag value as close as possible to reality, the wetted area for the fuselage was included for the calculation. The formula for lifting surfaces as, obtained from Raymer, is to determine the wetted area of a surface with thickness, by relating the top view to the thickness to chord ratio of the profile by empirical factors. The fuselage wetted area estimation relates the surface area of a cylinder with small manipulations to incorporate nose and tail. The final formula for the wetted area is shown in equation 4.18.

$$S_{wetted} = S_{fuselage} + S_{wing} + S_{tail}$$

$$S_{fuselage} = \left[\pi d_f l_f \left(1 - \frac{2d_f}{l_f}\right)^{2/3} \left(1 + \frac{d_f}{l_f}^2\right)\right]$$
$$S_{wing} = 2 * \left[S_{exposed,wing} \left(1.977 + 0.52\frac{t}{c}\right)\right] \tag{4.18}$$
$$S_{tail} = 2 * \left[S_{exposed,HT} \left(1.977 + 0.52\frac{t}{c}\right)\right] + \left[S_{exposed,VT} \left(1.977 + 0.52\frac{t}{c}\right)\right]$$

The variables d_f and l_f represent the diameter and length of the fuselage and $S_{exposed}$ is the top view exposed area by both wings. Figure 4.5 shows the exposed areas highlighted. The factor two for wing and horizontal tail is to compensate for both surfaces.

With the wetted area value known, the parasite drag estimations can be completed. The comparison between both methods, discussed earlier, is shown in the list below for the A330-300 aircraft in solo flight condition.

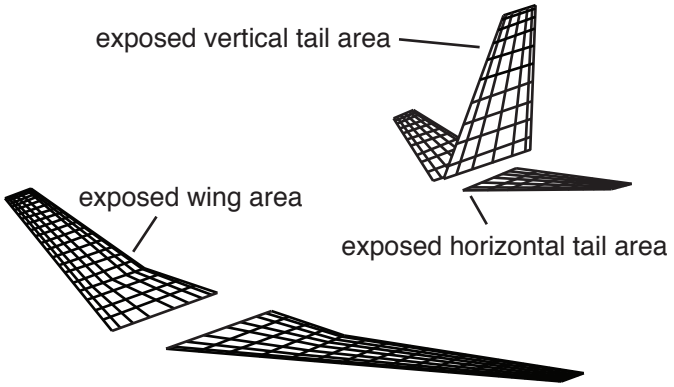

Figure 4.5: Exposed areas as present within the geometrical model used during the aerodynamic analysis

- Equivalent skin friction coefficient method: $C_{D_{parasite}} = 0.0206$
- Raymer method: $C_{D_{parasite}} = 0.0186$

A difference of 10.7% between both methods is identified. As the flow effects are included within the second method of Raymer, it was chosen to be used to determine the parasite drag.

4.2.5 Assumptions

The simulation model chosen was the flight mechanic toolbox. It met all the requirements set up within the beginning of this chapter. It has a modular built up and was extended to incorporate a formation flight analysis. Its strenght also lies in the use of an aerodynamic property table. As the model now uses the results of the VLM extended by Fransen, it can easily make use of the results of a CFD analysis or even wind tunnel results. This flexibility makes that the aerodynamic data can be made more accurate and precise without requiring specific adjustments to the model. Even though limitations of the model exist.

A list of the assumptions used by the model is given below. The power of the model however lies within the modular built up. By extending and adding modules, the limitations can be refined/redefined.

- Rigid wing model
- No aero-servo-elastic effects
- No aerodynamic disturbances included (e.g. gusts, wind velocity changes)
- Variational behaviour of forces and moments with relation to velocity, angle of attack and side-slip angle

- Linear behaviour of forces and moments with relation to changes in roll-pitch-yaw rate
- Linear behaviour of forces and moments with relation to changes in aileron-elevator-rudder deflection

The assumptions introduced within the model by the use of the aerodynamic data of the VLM extended by Fransen are also listed.

- Analysis for (high)subsonic condition, Mach number lower than 0.6
- Margin of error of 10% around vortex core, laterally and vertically

If the hinge moment is also determined, the assumptions made for the estimation should also be adhered to. The assumptions of the hinge analysis module are listed again below.

- Specific geometric data for A330-300
- Specific control data obtained from empirical relations for A330-300 geometry $a^{\star}_{1,2^0}$, $b^{\star}_{1,2^0}$
- Hinge moment derivative, $b_{1,2}$, estimated using empirical relations of ESDU
- Estimation of angle of attack change using $\delta a_{left,right}$, $C_{l\alpha}$ and C_{lp}

Appendix B includes a basic flow diagram of the extended FMT program module, as was created to perform the flight mechanical analysis. An overview of the settings of the flight mechanic model for all calculations and simulations performed is provided within appendix C.

4.3 Formation flight mechanic analysis

Using the FMT simulation model, the formation flight condition is analysed. The flight conditions and wake field region under investigation are identical to those in chapter 3.4, which are restated here. The lift coefficient was determined to be $0.623[-]$ for the maximal take of weight in cruise condition, $242,000$kg for $0.82M$ at $11,000$ meters. To fulfil the limitation of maximal Mach of 0.6 in the FMT and AVL programs, the weight was lowered whilst retaining the lift coefficient. The cruise conditions become an altitude of $11,000$ meters at a lift coefficient of $0.623[-]$ for a cruise speed of Mach 0.6 for two A330-300 aircraft of $129,566$kg in echelon formation condition. The trail aircraft is under the influence of an oncoming vortex, shed from the lead aircraft, which is located at $-0.107y/b$ $0.0z/b$. A wake field region of -0.5 to $0.3y/b$ and -0.5 to $0.5z/b$ is analysed as the close proximity formation flight condition is of interest. A region of error around the vortex core of 10% is included and marked by a dotted black line in the result graphs.

A trim analysis was performed for changing formation velocities the sweet spot, position of highest drag reduction. The entire wake field analysis is executed afterwards for the assumed cruise condition. The wake field analysis is subdivided into a part on positional static analysis of the entire field and a dynamic analysis at the sweet spot, defined outside of the margin of error, at $-0.15y/b$ and $0.1z/b$ as defined in chapter 3.4. Finally the hinge moments of the ailerons are

investigated, first by determining the limit and comparing that to positions within the wake field. All comparisons and computations are performed only including the induced drag component, the profile drag estimation is included in the final stage of this research discussed in chapter 6.

4.3.1 Trim analysis

The trim analysis is first performed at one instance within the wake field, namely the position of highest induced drag reduction, the sweet spot, as was determined in chapter 3.4. The sweet spot is located at $-0.15y/b$ and $0.1z/b$, when incorporating the margin of error. The angle of attack and the induced drag coefficient with their relation to velocity for trimmed formation flight and solo flight condition will be discussed.

The angle of attack relation, shown in figure 4.6a, show a decrease in angle of attack with increasing velocity. By decreasing the velocity in solo condition, for a constant weight, the angle of attack needs to increase to create enough lift to retain straight flight. It is immediate evident that the formation flight condition allows a decrease in angle of attack due to the favourable wake vortex flow field. The wake vortex shed by the lead aircraft of the formation will create a region up-wash, increasing the effective angle of attack. This allows the aircraft to lower its angle of attack to obtain a similar lift coefficient.

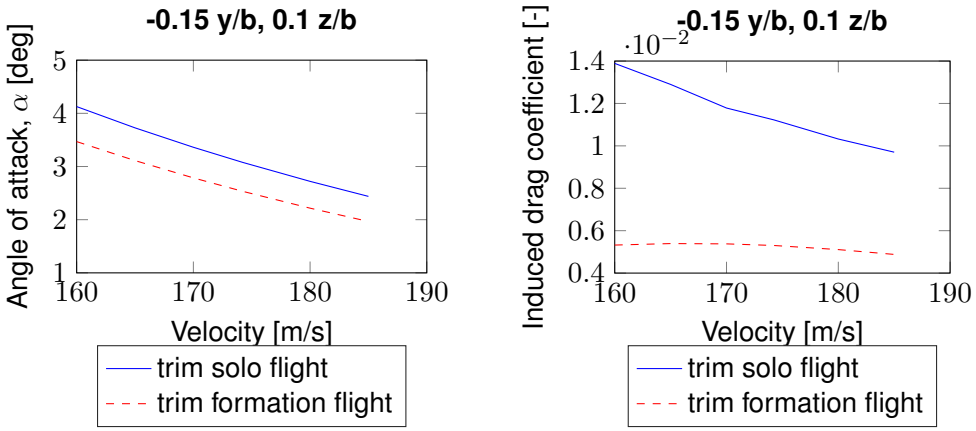

(a) Angle of attack to velocity

(b) Induced drag coefficient to velocity

Figure 4.6: Relations to velocity of an A330-300 aircraft for trimmed solo and formation flight condition at the sweet spot, $-0.15y/b$ and $0.1z/b$ in wake field

The induced drag coefficient however, shows a different trend. Important to note is that these results are only for the induced drag, not the total drag of the aircraft. This explains the lower values. The induced drag in solo flight condition shows a decreasing value. As the angle of attack becomes lower, the induced drag will also decrease. The formation flight condition on the other hand shows an almost constant behaviour, with only a slight decrease with velocity. For

increasing velocity the induced drag moves towards the value of $0.005[-]$. Compared to the solo condition, the induced drag almost remains constant. The slightly higher value at low speeds can be due to the larger angle of attack that is attained at the lower speeds. This creates the most benefit for the formation flight condition. The highest angle of attack will tilt the lift vector forward, creating the most 'aerodynamic thrust'. However flow transition and separation are neglected here. A point will exist when the angle of attack will become to high, lowering the lift and consequently also the benefit of the formation flight condition. Some key values obtained at the sweet spot in assumed cruise conditions are shown in table 4.1, with the solo condition values as comparison.

Solo condition		*Formation flight sweet spot*	
α	$3.08^{\cdot}$	α	$2.53^{\cdot}$
δa_{right}	$0^{\cdot}$	δa_{right}	$2.32^{\cdot}$
δe	$-0.80^{\cdot}$	δe	$-0.61^{\cdot}$
δr	$0^{\cdot}$	δr	$0.74^{\cdot}$
$C_{D_{itrim}}$	0.0112	$C_{D_{itrim}}$	0.0053
$C_{D_{inon-trim}}$	0.0101	$C_{D_{inon-trim}}$	0.0048

Table 4.1: Key data values of trimmed formation flight analysis at the sweet spot, $-0.15y/b$ $0.1z/b$, for assumed cruise condition: $M = 0.6$, $h = 11,000meters$, $C_L = 0.623$, $W = 129,566$kg

4.3.2 Positional static stability analysis

By making the trim analysis at all instances within the wake field, overall result plots can be made concerning the changes in attitude, forces and moments. This is a static analysis, it thus does not include the changes with relation to time. The calculations are performed for multiple positions throughout the wake field, a positional analysis. A situation and geometry sketch is provided within figure 4.7 to relate the results to the position within the wake field.

Each graph shows the changes between solo and formation flight condition. The following comparative rules have been adhered to, differences for angles shown in equation 4.19 and percentages when forces where discussed equation 4.20. If one value is very small and/or close to zero, than the actual value is plotted instead of the comparative value. Within each graph the above title shows what comparative rule has been used. Important to note is that all results are for the 'trimmed configuration', i.e. control deflections are used to retain the aircraft in a steady straight flight. The control deflections are determined for each wake field position separately.

$$\Delta angle = angle_{FormationFlight} - angle_{Solo} \tag{4.19}$$

$$\Delta C_{xx} = 100\left(1 - \frac{C_{xx_{FormationFlight}}}{C_{xx_{Solo}}}\right) \tag{4.20}$$

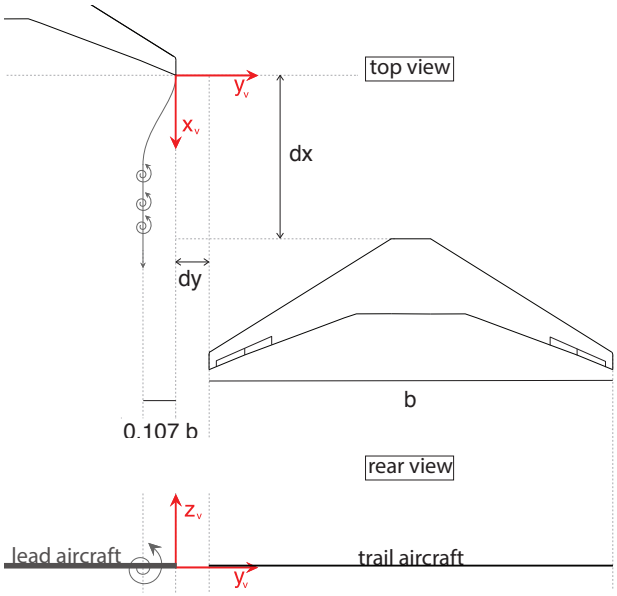

Figure 4.7: Situation and geometry sketch for A330-300 model with relation to positions within the wake field

Figure 4.8 shows the difference in angle of attack within the wake field for the assumed cruise flight. The influence the wake vortex shed by the lead aircraft creates an overall decrease in angle of attack. The increase in effective angle of attack for the trail aircraft results in a reduction of angle of attack to attain the same lift coefficient. This was also seen when discussing the relation of the angle of attack to velocity. The highest decrease is for the region close to the vortex, where direct vortex-wing interaction occurs (black star indicates vortex location). As for the results of chapter 3.4, a margin is highlighted where the accuracy of the VLM is questionable. When moving closer towards the boundaries of the wake field the decrease moves towards zero, again returning to the solo flight condition away from the wake vortex sheet. The highest change in angle of attack is -0.80 degrees and is located at $-0.15y/b$ and $0.0z/b$. This indicates the identical sweet spot as was seen for the aerodynamic analysis. Again looking outside of the margin to the location of $-0.15y/b$ and $0.10z/b$, the value becomes -0.54 degrees of change. A small increase in value can be observed. The trimming of the aircraft increases the angle of attack, compared to untrimmed condition. A comparison was made between the angle of attack change at $-0.15y/b$ and $0.10z/b$ between the solo flight condition, the untrimmed condition and the trimmed condition. The explanatory sketch is shown alongside in figure 4.8.

Figure 4.9 shows all the required changes to the control deflections due to the formation flight condition. Alongside all wake field variations a situation sketch is shown and the change has been made visual, for the sweet spot position outside of the margin of error at $-0.15y/b$ and $0.1z/b$ (marked by red dot). The aileron deflection shows the most remarkable changes.

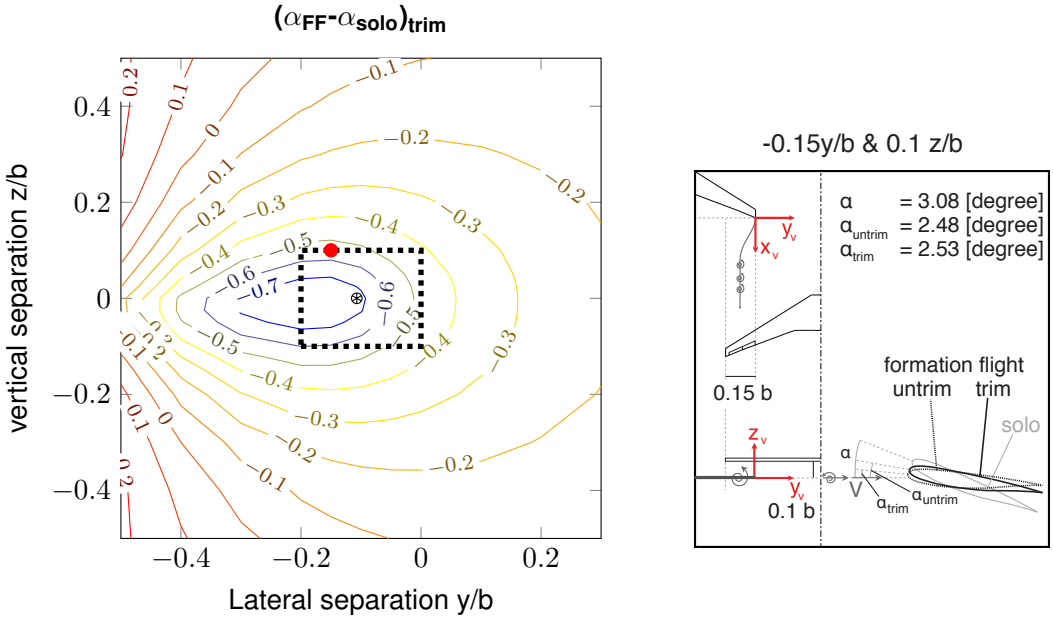

(a) Angle of attack variation in wake field

(b) Geometry sketch situation position red dot

Figure 4.8: Wake field analysis of the change in angle of attack in trim due to formation flight condition for A330-300

Figure 4.9a shows the right aileron deflection values within the wake field for the assumed cruise flight. A high value exists around the incident vortex location, as was expected due to the high wake vortex induced rolling moment, identified within chapter 3.4. A value for zero aileron deflection is marked around $-0.25y/b$ and $0z/b$.
Lets take a closer look when he trail aircraft moves in the wake vortex field, going from $0y/b$ towards $-0.5y/b$. When the wing tip of the trail aircraft is aligned with the incident vortex, around $-0.1y/b$, the region between the incident vortex and wing root will be placed in a region of up-wash. This effectively increases the lift over the wing locally. The local increase in lift on the tips will create a positive rolling moment, for which a positive right aileron deflection angle is required. If the vortex is positioned on the wing however, a 'second region' will exist between the vortex and the tip. This region will be positioned within the down-wash of the wake vortex, effectively decreasing the lift locally. The decrease in lift will lower the positive rolling moment, until it eventually reaches a zero value at approximately $-0.25y/b$ for $0z/b$. The zero aileron deflection coincides with the zero rolling moment found in chapter 3.4. Once the positive rolling motion is cancelled, the decrease in lift locally will induce a negative rolling moment. The moment will require a negative right aileron deflection. Within literature and the aerodynamic analysis the deep wake field positions were identified as dangerous with high interference moments and forces. These range from -0.5 to $-1.5y/b$, i.e. if one wing of the trail aircraft is immersed within the wake field. The region, under investigation here, has its highest value at the edge of this region. An required aileron deflection of $-15.4^{\cdot}$ degrees was identified at $-0.5y/b$ and $0z/b$. This highlights the dangers when flying too deep wake field positions.

To compensate for the overall change in lift, due to the vortex, extra deflections from the elevator and rudder are required. These deflections remain moderate however and are shown within figure 4.9c and 4.9e. Both elevator and rudder show a region of zero change, when compared to the solo condition, running parallel through the wake field around $0z/b$.

The change in induced drag coefficient, the effective benefit from the formation flight condition, is shown in figure 4.10a.The pattern of reduction is similar to the angle of attack reduction, which affirms the link between the increased effective angle of attack and the decrease in induced drag. A maximal decrease of 83.85% is identified at $-0.15y/b$ and $0z/b$. This value is almost identical to the maximal drag reduction as was identified for the untrimmed condition, as determined in the aerodynamic analysis in section 3.4. The high value lies within the margin of error of the VLM program, as did the value in untrimmed condition. The high value could thus again be assigned to the unrealistic modelling of the direct wing-vortex interaction by the VLM. When looking at the sweet spot for the untrimmed condition, outside of the margin of error at $-0.15y/b$ and $0.10z/b$, the value becomes 47.5%. This value is more realistic when looking at other results from literature. Ray et al. performed a test flight in 2002 using two F/A-18 aircraft to measure the induced drag reductions [22]. Although two completely different aircraft types are compared, it can be reasoned that the induced drag difference between the lead and the trail aircraft is comparable in general trend. The results of the test flight are shown in figure 4.10c. The sweet spot has moved down, due to the wake vortex propagation longitudinally, 'vortex meandering' [30] [31]. This effect was already discussed within chapter 2.2.1 and was

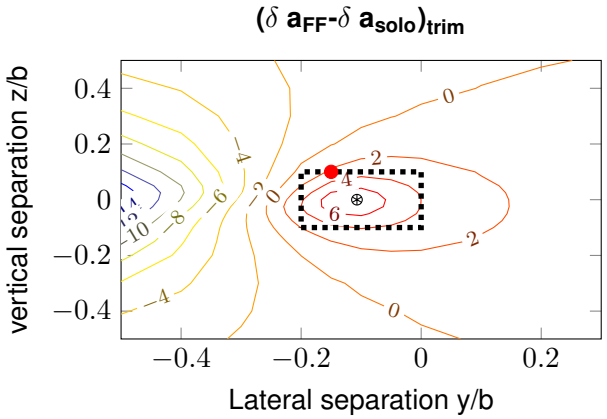

(a) Aileron variation in wake field

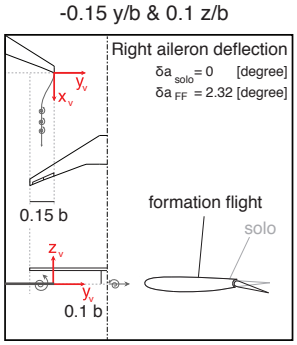

(b) Situation sketch aileron at position red dot

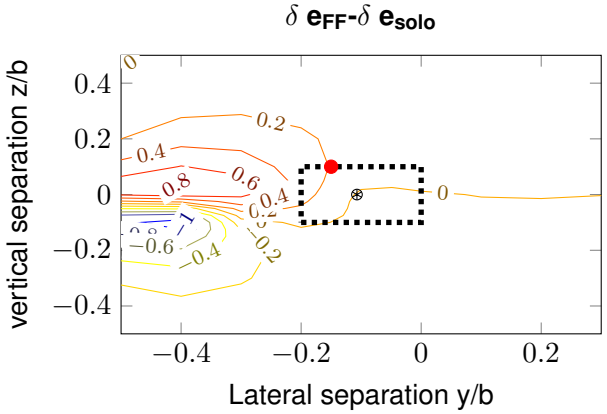

(c) Elevator variation in wake field

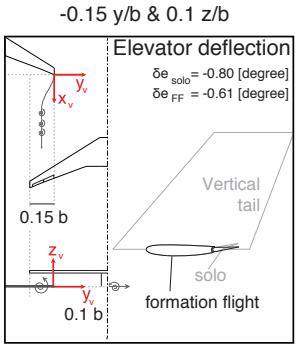

(d) Situation sketch elevator at position red dot

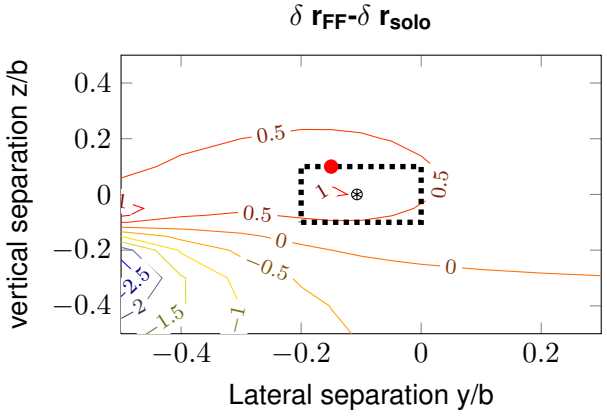

(e) Rudder variation in wake field

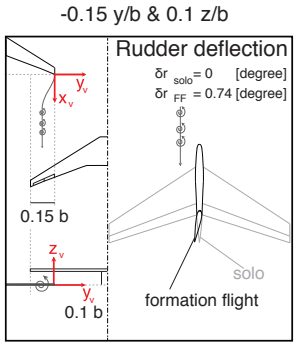

(f) Situation sketch rudder at position red dot

Figure 4.9: Wake field analysis of the control deflection due to trim in formation flight condition for A330-300

neglected within the VLM, which assumed a parallel vortex flow at zero vertical separation. When comparing the test flight results for position in close proximity the results agree rather well. For wing tips aligned, $0y/b$ and $0z/b$, the test flight results show a reduction of estimated around 30% where the results of FMT show a value of around 40%. For the close proximity case, $0.3y/b$ and $0z/b$, the values of the test flight and the FMT model are around 10%.

The effect of trim on the decrease in induced drag and thus also thrust and the quantification of this effect was one of the goals of this research. The values of the aerodynamic data of the wake field for the untrimmed condition, at the current cruise conditions, were compared to the values as obtained by the FMT model. The result is shown in figure 4.11a, where the induced drag reduction in untrimmed condition is subtracted from that in trimmed condition, both in assumed cruise flight.

Within the direct vicinity of the vortex core, where also the highest induced drag reduction occurs, difference in drag reduction tends towards zero. This implies that around the vortex core, none of the benefit is lost due to trimming of the aircraft. An explanation could be that the unrealistic wing-vortex interaction for the data of the VLM creating such high forces (lift and drag), that the control surface deflection component is to small to show any influence. The unrealistic wing-vortex interactions consists of high vorticity flow, with high vortex core velocity. In reality the airflow would interact and would possibly create separation bubbles and induce flow separation, increasing the drag and affecting the influence of the aileron control surface. The creation of separation bubbles on the wing tip for direct wing-vortex interaction, with the vortex positioned inboard, was identified by Garmann et al. [27]. A graphical representation is shown in figure 4.11b, where the separation bubble is marked. Due to the rigid wing model and the neglecting of the aero-servo-elastic effects, the drag differences due to aerodynamic bending is also neglected.
At the sweet spot within the margin, at $-0.15y/b$ and $0z/b$, the difference in induced drag becomes $83.9\%-83.5\% = 0.4\%$, an increase as expected. Outside of the margin at the location of highest benefit, at $-0.15y/b$ and $0.10z/b$, the difference becomes $52.6\% - 47.5\% = 5.1\%$. Kless et al. identified that in subsonic conditions $3 - 5\%$ and in transonic conditions $9 - 11\%$ at the sweet spot would be lost due to aircraft trim, using an Euler solver including compressibility effects [6]. The estimation By the VLM thus provides a fair estimation, when upholding the margin of error within the results.
Upon the rest of the wake field, the trimmed condition reduces the aerodynamic benefit of the formation flight. Interesting to note is that the difference keeps on increasing, and does not go to zero. This is due to the comparison of the induced drag reduction from trimmed and untrimmed flight. The untrimmed flight condition will always show a lower induced drag when compared to the trimmed flight condition. For a larger field it is expected that the difference value moves towards a constant value, which can not be clearly identified within the wake field slice shown here.

Table 4.2 gives an overview of the results, similar to the one from the aerodynamic analysis. Both the sweet spot inside and outside the margin of error are indicated, as well as the highest values and their location respectively.

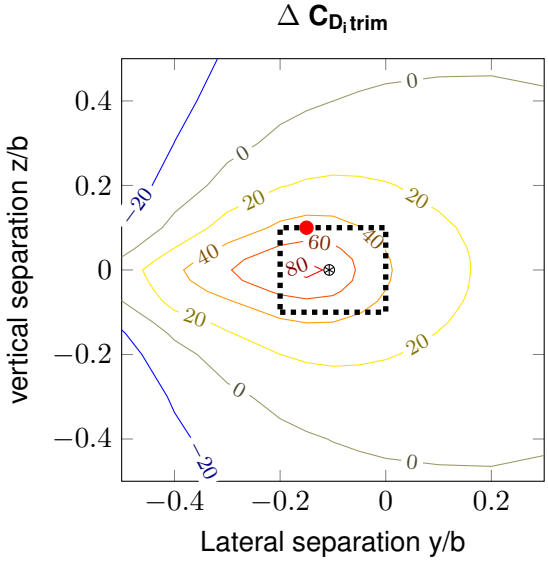

(a) Induced drag variation in wake field

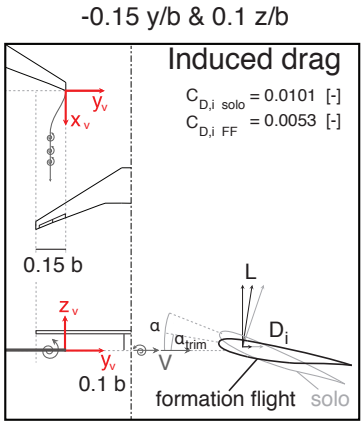

(b) Situation sketch at position red dot

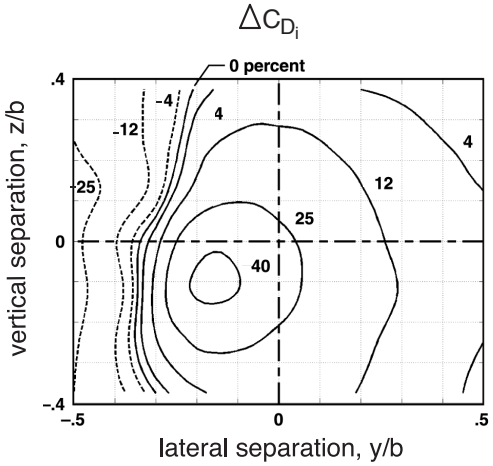

(c) F/A-18 test flight results

Figure 4.10: Wake field analysis of the induced drag coefficient in trim due to formation flight condition, accompanied by situation skecth and comparison with test flight results [22]

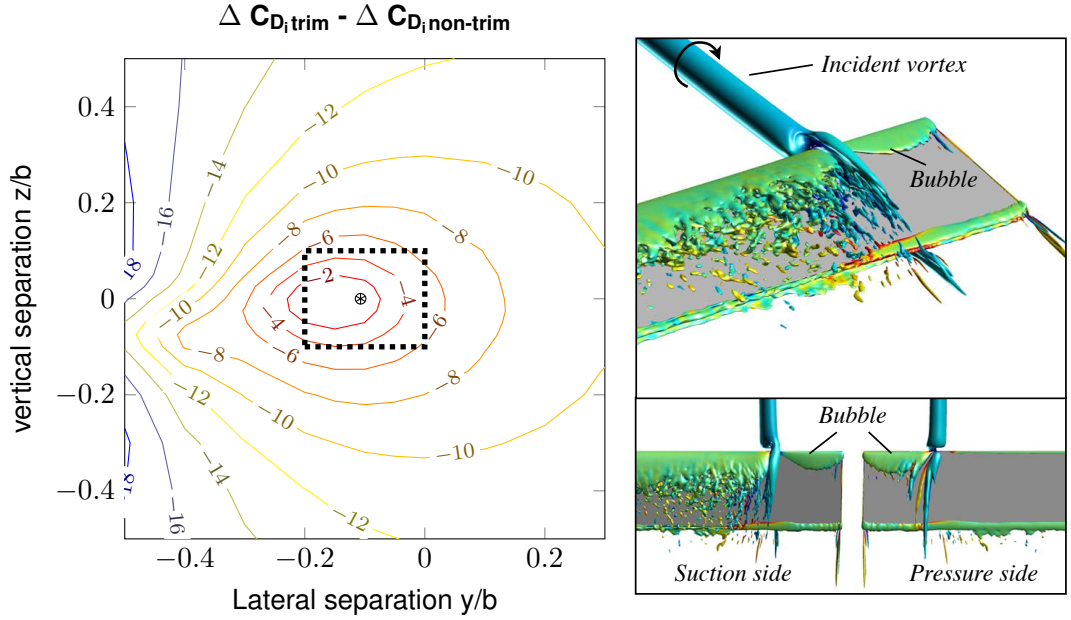

(a) Difference induced drag benefit

(b) Direct vortex interaction maginification

Figure 4.11: Wake field comparison of difference in induced drag of aerodynamic data in untrimmed condition (VLM) and the trimmed condition (FMT) in formation flight for A330-300, alongside a magnification of the direct wake vortex interaction as obtained from a RANS CFD method [27]

	Sweet spot $-0.15y/b\ 0.0z/b$	*reference point* $-0.15y/b\ 0.1z/b$	*Highest value*	*Location*
$C_{D_{itrim}}$	83.9%	47.49%	83.9%	$-0.15y/b\ 0.0z/b$
α	$2.28^{\cdot}$	$2.53^{\cdot}$	$2.28^{\cdot}$	$-0.5y/b\ -0.3z/b$
FF - solo	$\Delta - 0.80$	$\Delta - 0.54$	$\Delta - 0.80$	
δa_{right}	$7.08^{\cdot}$	$2.32^{\cdot}$	$-15.4^{\cdot}$	$-0.5y/b\ 0.0z/b$
δe	$-0.72^{\cdot}$	$-0.61^{\cdot}$	$-1.87^{\cdot}$	$-0.4y/b\ -0.1z/b$
FF - solo	$\Delta 0.089$	$\Delta 0.19$	$\Delta - 1.07$	
δr	$1.03^{\cdot}$	$0.74^{\cdot}$	$-2.96^{\cdot}$	$-0.5y/b\ -0.3z/b$

Table 4.2: Overview changes in induced drag and angles obtained during flight mechanic analysis of Formation Flight at the sweet spot, sweet spot excluding values within margin of error and highest values in wake field, for assumed cruise condition: $M = 0.6$, $h = 11,000 meters$, $C_L = 0.623$

4.3.3 Dynamic analysis at $-0.15y/b$ and $0.1z/b$

The sweet spot outside of the margin of error was chosen as a start point to perform a brief dynamic analysis of the formation flight condition within the wake field. The purpose is to identify if the aircraft is able to retain a steady straight flight, after being statically trimmed at the position, or is constant control/re-trimming required. An important assumption is the constant longitudinal separation distance of 10 wingspans. A change in speed during the simulated flight, would reposition the aircraft longitudinally, what is not included within the aerodynamic data at this time. An extension can be made however to perform a more accurate analysis. The dynamic analysis is done first by simulating a steady straight flight in solo and formation flight condition for 20 to 25 seconds, where the formation flight simulation is at one wake field position. Secondly the eigenvalues of the aircraft are compared in solo condition to those of the formation flight at one specific position within the wake field. By comparing the eigenvalues, changes and instabilities can immediately be identified.

The position within the wake field was chosen to be $-0.15y/b$ and $0.1z/b$, as this is the spot for highest induced drag reduction outside of the margin of error. The margin of error was determined due to the improper modelling of the direct wing-vortex interaction within the extended VLM of Fransen. The cruise conditions, as assumed before, are used also for this analysis. The altitude is set at $11,000$ meters for a lift coefficient of 0.623 [-] and a Mach number of 0.6.

To start off a brief simulation was performed of 25 seconds to identify the changes in Euler angles and roll-pitch-yaw rates. Both the solo condition and formation flight case variations are shown in figure 4.12. A clear change in behaviour can be seen, where the solo flight condition does not show variations for the 25 second simulation. The constant behaviour in solo flight was expected as no disturbances are present in the simulation model.

The initial pitch angle shows the effect of the formation flight, lowering the required angle of attack of the aircraft due to the increased effective angle of attack due to the region of up-wash. The Euler angles start to show a behavioural shift from 15 seconds onwards. All angles show an initial diverging behaviour, although no final conclusion can be drawn. The pitch angle firsts shows an increase followed by a decrease, not like the roll and yaw angle. The roll-pitch-yaw rates show a similar shift from 15 seconds onward. A small plateau exists for the pitch rate around 22-23 seconds, explaining the shift from pitch up to pitch down tendency.
The aircraft starts its simulation above the incident vortex with a small overlap, as the location of the vortex is $-0.107y/b$ & $0z/b$ and the trail aircraft wing tip is located at $-0.15y/b$ & $0.1z/b$. The wake field creates interference forces and moments, which differ per position in the field. A small deviation could lead to change in balance, for which the aircraft is not trimmed. Here this occurs around 15 seconds, when the aircraft starts to roll behind the lead aircraft and initiate and adverse yaw due to the rolling motion. The yaw angle and yaw rate are small compared to the change in roll rate and roll angle though. Due to the rolling motion, the left wing (closest to the vortex) will loose lift where the right wing will create more lift. The aircraft was already trimmed such that more lift on the right wing is created and less lift on the left wing, due to the induced roll this is enhanced. The overall lift will decrease slightly creating a pitch up tendency.

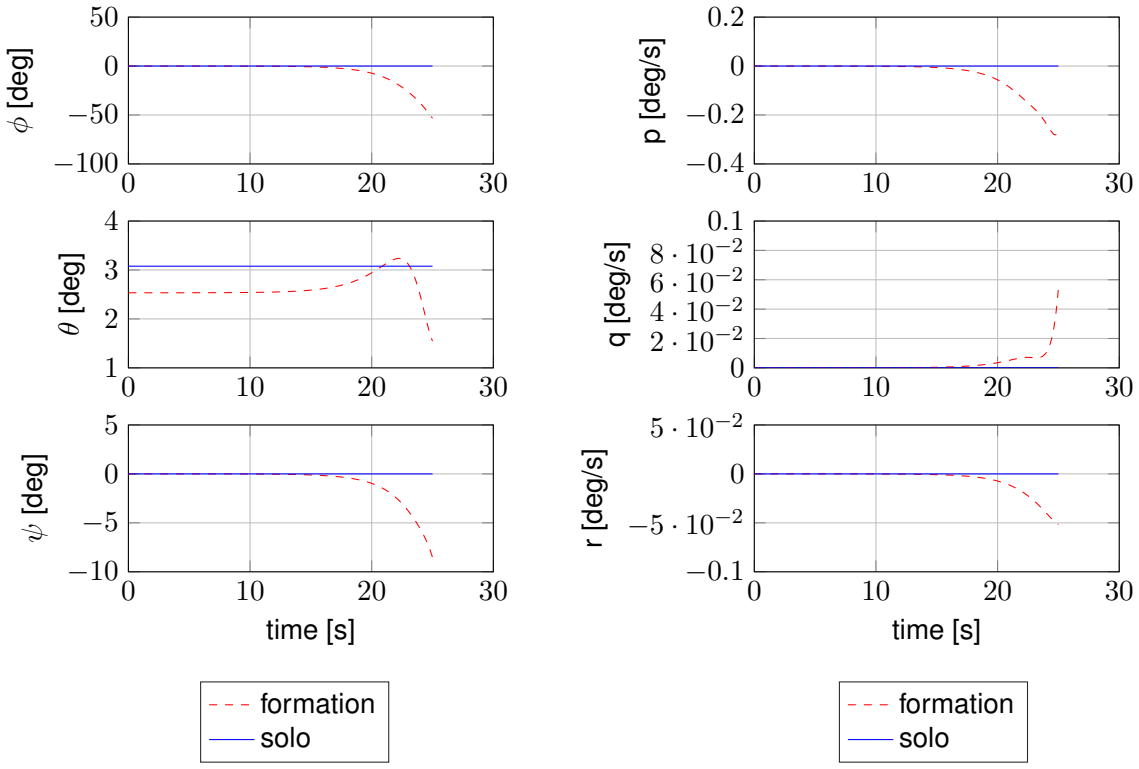

(a) Euler angles

(b) roll-pitch-yaw rates

Figure 4.12: Graphs representing variations of an A330-300 aircraft in solo fligt and formation flight condition at Mach 0.6 for an altitude of $11,000$ meters and a lift coefficient of 0.623 [-] for a wake field start position of $-0.15y/b$ and $0.1z/b$

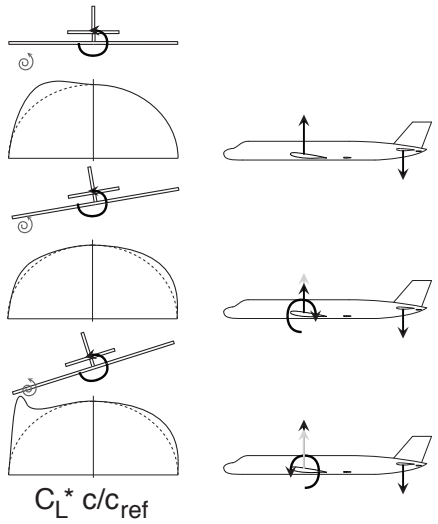

Figure 4.13: Skecth roll and pitch behaviour of an A330-300 aircraft in formation flight condition at Mach 0.6 for an altitude of $11,000$ meters and a lift coefficient of 0.623 [-] for a wake field start position of $-0.15y/b$ and $0.1z/b$

However as the left wing moves down, it will come closer to the incident vortex. The closer the left wing is, the higher the benefit will be, again increasing the overall lift of the wing. The increase of lift will create a pitch down tendency. Figure 4.13 shows a sketch explaining what is happening for the wake field position.

Important to note are the limitations of the aerodynamic data, used within the simulation model. The error of margin of 10% around the vortex core was not removed from the dataset, creating the possibility that during the simulation the aircraft will move into the region. For the simulation presented here, this is the case. The initial divergence is questionable. Nevertheless it can be concluded that the aircraft is unstable, as it should not have deviated from its original position in the first place.
It was already identified by literature that an aircraft in the formation flight condition, requires constant control input and/or trim to retain its position. Pahle et al. [29] identified during a test flight of a C-17 transport aircraft that the workload on a pilot is high, confirming that a large effort is required to retain a position, if no automatic formation flight control system is present.

A second analysis is done by looking at the eigenvalues of the dynamic motions in solo and formation flight condition. The eigenvalues of the complete state-space matrix, of the simulation model, is shown in figure 4.14 for both conditions. Clearly shifts are present, creating instability during the formation flight condition. Table 4.3 shows all values of eigenvalues plotted in figure 4.14

The eigenvalues presented are for both asymmetric and symmetric motions, they represent the linear solution of the complete state-space matrix of the simulation model. The state-space

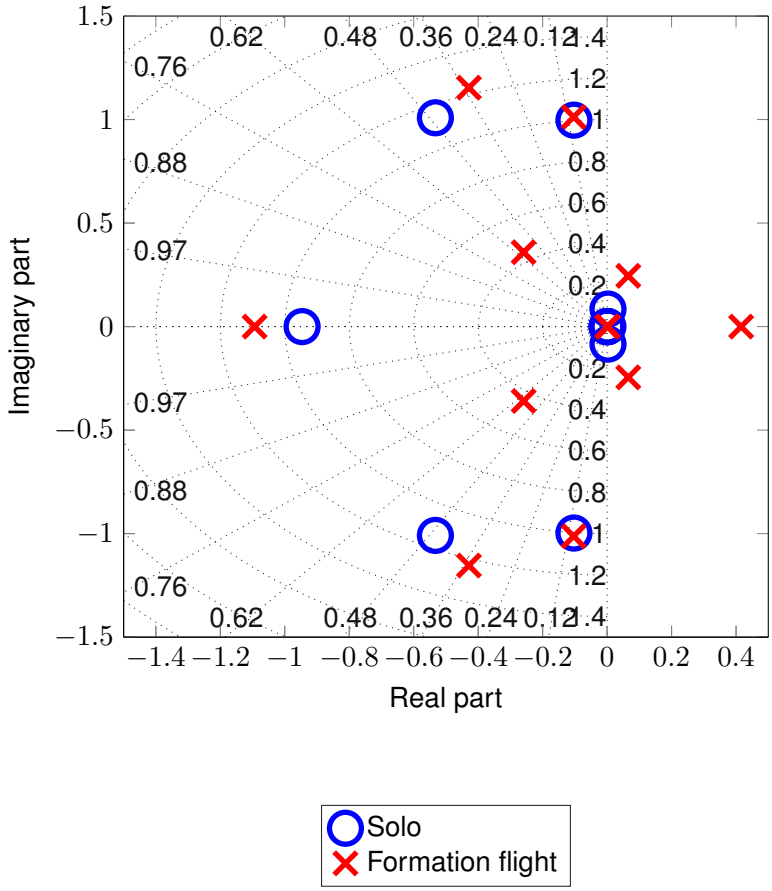

Figure 4.14: Root locus plot total state-space matrix of an A330-300 aircraft in solo fligt and a formation flight condition at Mach 0.6 for an altitude of $11,000$ meters and a lift coefficient of 0.623 [-] for a wake field start position of $-0.15y/b$ and $0.1z/b$

	simplified		*state-space total*	
Motion	*solo*	*formation*	*solo*	*formation*
Phugoid	$0.0025 \pm 0.0770i$	$0.0015 \pm 0.0674i$	$0.0028 \pm 0.0847i$	$-0.2590 \pm 0.3592i$
-	-	-	-	$0.0657 \pm 0.2451i$
Short period	$-0.5325 \pm 1.0083i$	$0.4194 \pm 1.1553i$	$-0.5327 \pm 1.0086i$	$-0.4288 \pm 1.1541i$
Roll mode	-0.9129	-1.0385	-0.9463	-1.0935
-	-	-	-	0.4158
Spiral	0.0253	0.0265	0.0025	0.0024
Dutch roll	-0.1310 ± 0.2911	$0.1398 \pm 0.2693i$	$-0.1029 \pm 0.9972i$	$-0.1038 \pm 1.0125i$

Table 4.3: Eigenvalues of an A330-300 aircraft in solo flight and a formation flight condition at Mach 0.6 for an altitude of $11,000$ meters and a lift coefficient of 0.623 [-] for a wake field start position of $-0.15y/b$ and $0.1z/b$

matrix can also be simplified to subdivide the symmetric and asymmetric motions, to identify typical motions like phugoid, short period, spiral, roll mode and dutch roll. To retain the full picture, the entire state space matrix was used for the graph, where the simplified eigenvalues were also calculated to identify by approximation which motion is which behaviour in the total state-space matrix. The formation flight condition has two additional eigenvalue responses in the total state-space response, which show unstable behaviour.
The short period, spiral and dutch roll show fairly good agreement between the simplified and total state-space eigenvalues. The formation flight condition shows small variations for the short period, where the spiral and dutch roll are almost identical. The period of the short period motion, related to the imaginary part, decreases whilst the time to damp to half the amplitude, related to the real part, increases. More important are the two additional eigenvalues. No specific research was performed into the origin of their motion and behaviour. Using deduction and the time simulation results as presented earlier, both were linked to the phugoid and roll mode. Pitch and roll were identified to initially diverge, making the aircraft unstable. Further research is required however into the dynamic motion behaviour of the aircraft in the formation flight condition.

4.3.4 Hinge moment

Using the method derived earlier in section 6.2.3, the hinge moment and design limit for both solo and formation flight condition where determined. The A330-300 in solo condition was simulated during a flight of 4 seconds. The first run was to identify the maximal roll rate during a full aileron deflection at sea level conditions, to obtain the maximal design roll rate [62]. This 'design' condition was at a Mach number of 0.31 and altitude of zero and a lift coefficient of 0.623 [-]. The second run implied the deflection of the ailerons at cruise condition until the maximal roll rate is attained, resulting in a cruise limit deflection value. The cruise condition was again the assumed one as used before, at Mach 0.6 for an altitude of $11,000$ meters and a lift coefficient of 0.623 [-].
The calculation was performed for the entire range of aileron deflections, from 0 until 30 degrees with an accuracy of 0.1 degrees. For each deflection the maximal roll rate was compared if it met the maximal design roll rate within 5%. Eventually a cruise limit aileron deflection value was obtained.

Figure 4.15a shows the roll rate for both conditions. The rate for the cruise flight is limited by the maximal roll rate for the 'design condition'. Figure 4.15b shows the right aileron deflection in both conditions indicating the cruise limit deflection for the aileron. Figure 4.15c shows the hinge moment in function of the right aileron deflection angle, with the limit value also indicated. The limit deflection and the build up of the hinge moment in time is shown in figure 4.15d.

Figure 4.15c shows how the hinge moment has a linear behaviour with the aileron deflection. The black dotted lines indicate the location where the maximal aileron deflection is reached, as is determined from figure 4.15b using the maximal roll rate from figure 4.15a. The hinge moment has a negative value as the right aileron is deflected upward, where a positive moment

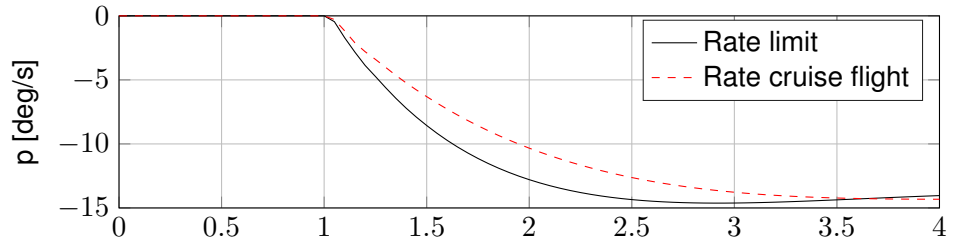

(a) Roll rate limit determination

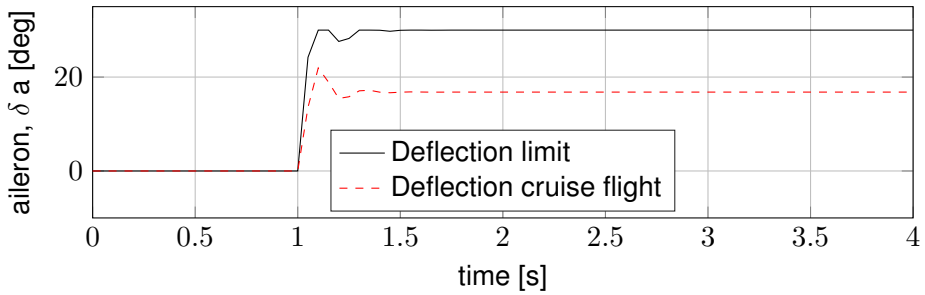

(b) Aileron deflection limit determination

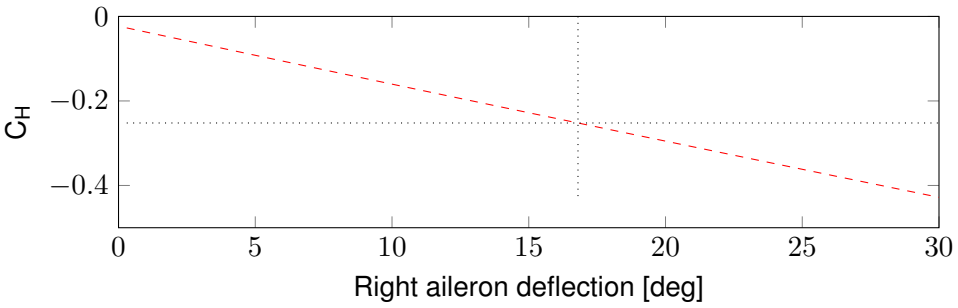

(c) Hinge moment wrt right aileron deflection in cruise condition

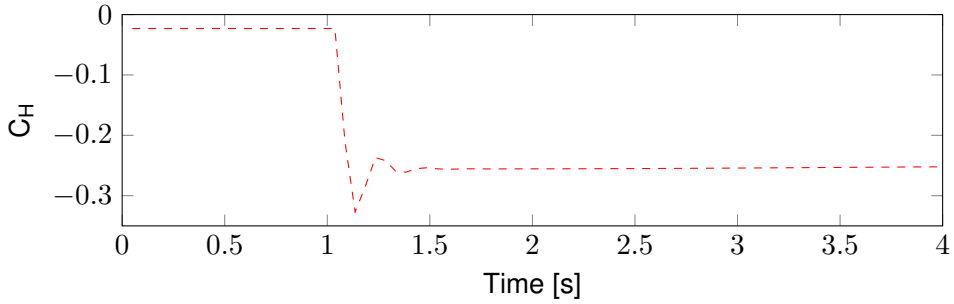

(d) Hinge moment wrt maximal right aileron deflection in cruise condition

Figure 4.15: Aileron hinges at Mach 0.31 at sea level conditions, compared to the deflection during cruise flight at Mach 0.6 for an altitude of $11,000$ meters and a lift coefficient of 0.623 [-], of the A330-300 in solo flight condition

is for a deflecting downward. The hinge moment with relation to time for the maximal deflection, as was determined from figure 4.15b, shows a peak in hinge moment. This peak afterwards settles to a constant value. This peak is similar and linked to the aileron deflection that first peaks before reaching a constant value in figure 4.15b. As the limit is determined using the maximal roll rate, without specifying the possible peaks due the initial deflection and before reaching a steady state, the peaks are neglected. For the hinge moment analysis, the constant limit hinge moment value is used.
The cruise limit deflection as identified here became the limitation upon the aileron deflection. The limit aileron deflection was set at the steady deflection value of $16.8^{\cdot}$ degrees. Subsequently the limit hinge moment, $C_{H,max}$, for the left and right aileron become $0.2516[-]$ and $-0.2522[-]$ respectively. Both values are not identical, due to the sign differences of deflection for the left and right aileron, where the change due to angle of attack component is identical in both cases. Effectively in equation 4.8 the first component is identical in both cases, where the difference in left and right aileron creates and addition or subtraction to that value.

The hinge moment was calculated for the entire wake field, using the estimation method as determined in section 6.2.3. The left and right aileron show a an increase in discrepancy. Figure 4.16a and figure 4.16b show the behaviour. Alongside in the figure a situation sketch for the highest hinge moment on the left aileron is shown, at $-0.5y/b$ and $0z/b$. As explained before, the sign of left and right aileron determine the difference in hinge moment. As the aileron deflection angles are increasing, the difference also increases.
Important to remark is the lower cruise speed, due to the limitations within the aerodynamic model and the hinge moment estimation. The assumption of a rigid wing model and neglecting aero-servo-elastic effects makes that this is an estimation of the moment upon the hinge just due to the deflection itself. Higher speeds, flow transition and separation, wing bending and aero-servo-elastic effects will possibly create extra stresses upon the aileron surface and its hinges.
For the left aileron it can be seen that the limit hinge moment is just exceeded within the deep wake field. The highest hinge moment value is also located in the deep wake field. This corresponds to a high positive (downward) deflection angle of $15.4^{\cdot}$ degrees of the left aileron for zero vertical separation, at $-0.5y/b$ and $0z/b$, reaching a hinge moment value of $-0.2688[-]$, 6.8% above the design limit. The limit value was set at 0.2516 for the left aileron. Interesting to note is that the limit hinge moment is reached at a lower aileron deflection angle. The change in aerodynamic parameters create that a lower angle induces a hinge moment that reaches the limit value. The limit deflection is redefined to a positive angle of $14.3^{\cdot}$ degrees. As the highest aileron deflections are required in the deep wake field, the exceeding of the limit was expected to occur within this region.
The same high negative deflection angle on the right aileron shows a lower value in hinge moment. On the right aileron the limit is never exceeded within the deep wake field region. This apparently shows that a high negative deflection has a lower impact upon the aileron hinge moment, this due to the contribution of the angle of attack change due to the rolling moment, again the first component in equation 4.8. The positive deflection creates an addition, where a negative deflection creates a subtraction of the value, leading to the difference.

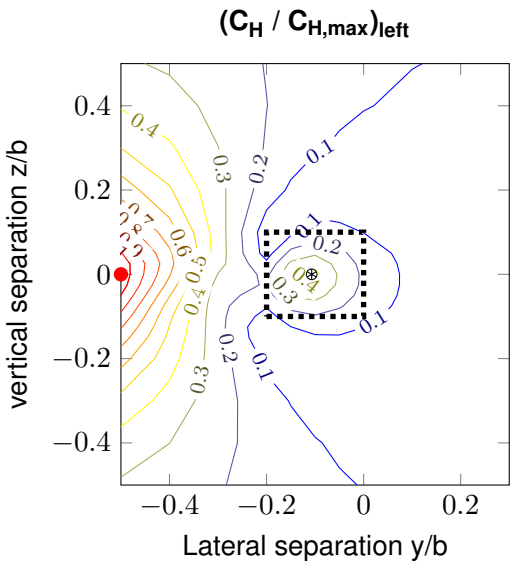

(a) Variation hinge moment left aileron in wake field

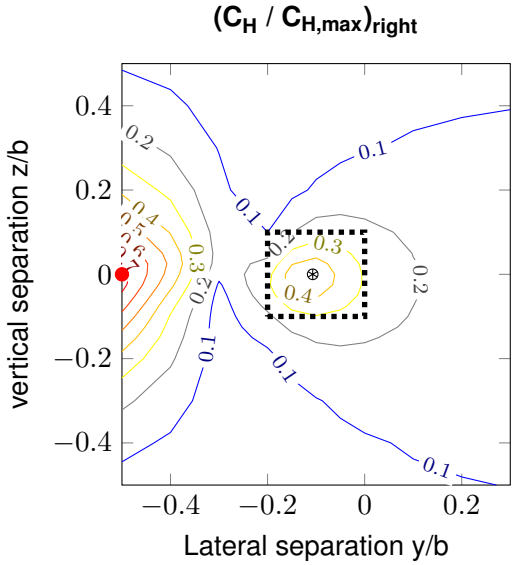

(b) Variation hinge moment right aileron in wake field

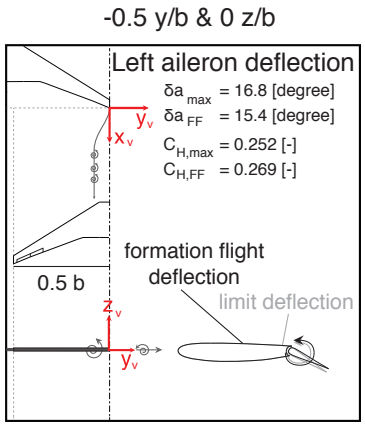

(c) Situation sketch at position red dot

Figure 4.16: Wake field analysis of difference in hinge moment left aileron with relation to limit value

The region around the vortex core is neglected as being inaccurate in aerodynamic modelling due to the direct wing-vortex interaction. The hinge moment estimation makes use of the aerodynamic data and therefore the margin of error should also be applied here. For the left aileron the hinge moment at the sweet spot, $-0.15y/b$ and $0z/b$, is $0.0937[-]$. The value at $-0.15y/b$ and $0.1z/b$, excluding the margin of error, becomes $0.0189[-]$.
The close proximity case does not exceed the design limits of both of the aileron hinges. Within the deep wake field only the left aileron, with high positive deflection, create a hinge moment that exceeds the value. High positive deflections could thus lead to exceeding the design limit for the aileron hinge moment, where high negative deflections do not create such high hinge moments.

4.4 Conclusion

This chapter included the flight mechanic analysis of the formation flight of the A330-300 aircraft in an assumed two aircraft formation cruise flight. First a computational model was chosen, using a set of requirements. These requirements were the non-linear equations of motion and the opportunity to perform both static and dynamic positional stability analysis. A modular program, the Flight Mechanics Toolbox, was chosen as it met all requirements. Due to the modular built up it also provided the possibility to easily adapt and extend the program. A hinge moment estimation was added and a formation flight analysis tool was implemented. Some assumptions were present however. The model makes use of a rigid wing and at neglects the aero-servo-elastic effects. Due to the inclusion of the aerodynamic data, created by the VLM, also their assumptions need to be kept in mind. The most pronounced are the limitation of velocity to Mach 0.6 and the absence of viscous and compressibility effects.
The flight dynamic and load analysis of the formation flight was subdivided into four parts: a local trim analysis, a positional static stability analysis, a dynamic analysis at the sweet spot and the hinge moment analysis. The results for all parts are shown in table 4.4 to 4.7.

The local trim analysis showed the relation of the aerodynamics with relation to velocity at one position within the wake field, $-0.15y/b$ $0.1z/b$. The induced drag benefit of the formation flight slightly increases with increasing velocity. Compared to the solo condition, the induced drag almost remained at a constant level for the formation flight condition. The local trim also revealed that the highest control surface deflection required is that of the aileron, as was expected.

The positional static stability analysis showed the magnitude of the required control deflections to retain a steady straight cruise flight. Thee variations throughout the wake field were the largest for the ailerons, followed by the elevators and with only minor changes to the rudder, when the formation flight is compared to the solo flight condition. Remarkably the aileron deflection even reaches a maximal value of $15.4^{\cdot}$ degrees in the deep wake field $-0.5y/b$ $0z/b$. This position implies that almost the entire left wing is immersed within the wake field, specifically the down-wash field between both vortex cores. The highest benefit is achieved within the close proximity case, where the aileron deflection reaches a value of $2.32^{\cdot}$. Due to

Solo condition		*Formation flight sweet spot* $-0.15y/b\ 0.1z/b$	
α	$3.08^{\cdot}$	α	$2.53^{\cdot}$
δa_{right}	$0^{\cdot}$	δa_{right}	$2.32^{\cdot}$
δe	$-0.80^{\cdot}$	δe	$-0.61^{\cdot}$
δr	$0^{\cdot}$	δr	$0.74^{\cdot}$
$C_{D_{itrim}}$	0.0112	$C_{D_{itrim}}$	0.0053
$C_{D_{inon-trim}}$	0.0101	$C_{D_{inon-trim}}$	0.0048

Table 4.4: Trim Analysis Key data values of trimmed formation flight analysis at the sweet spot, $-0.15y/b\ 0.1z/b$, for assumed cruise condition: $M = 0.6$, $h = 11,000$ meters, $C_L = 0.623$, $W = 129,566$kg

the control deflections, an increase in drag was expected. The induced drag at the sweet spot outside the margin of error, at $-0.15y/b$ and $0.1z/b$, becomes 47.5% where it was 52.6% in untrimmed flight. The benefit on the induced drag is reduced by 5.1%.

	Sweet spot $-0.15y/b\ 0.0z/b$	*Reference point* $-0.15y/b\ 0.1z/b$	*Highest value*	*Location*
C_{D_i}	83.9%	47.49%	83.9%	$-0.15y/b\ 0.0z/b$
α	$2.28^{\cdot}$	$2.53^{\cdot}$	$2.28^{\cdot}$	$-0.5y/b\ -0.3z/b$
FF - solo	$\Delta - 0.80$	$\Delta - 0.54$	$\Delta - 0.80$	
δa_{right}	$7.08^{\cdot}$	$2.32^{\cdot}$	$-15.4^{\cdot}$	$-0.5y/b\ 0.0z/b$
δe	$-0.72^{\cdot}$	$-0.61^{\cdot}$	$-1.87^{\cdot}$	$-0.4y/b\ -0.1z/b$
FF - solo	$\Delta 0.089$	$\Delta 0.19$	$\Delta - 1.07$	
δr	$1.03^{\cdot}$	$0.74^{\cdot}$	$-2.96^{\cdot}$	$-0.5y/b\ -0.3z/b$

Table 4.5: Positional static stability analysis Overview changes in induced drag and angles obtained during flight mechanic analysis of Formation Flight at the sweet spot, sweet spot excluding values within margin of error and highest values in wake field, for assumed cruise condition: $M = 0.6$, $h = 11,000$ meters, $C_L = 0.623$

The dynamic analysis at the sweet spot, defined outside of the margin of error at $-0.15y/b$ and $0.1z/b$, investigated the flight within the wake field by performing a brief simulation of 25 seconds and the linear eigenvalue results using the state-space equations of the simulation model. It becomes apparent that the aircraft is unstable in pitch and roll. The eigenvalue analysis of the total state-space revealed two additional motions, possibly related to the phugoid and roll mode. Further research into the dynamic behaviour is required though.

In solo flight condition the limit hinge moment was defined. This limit deflection was set at $16.8^{\cdot}$ degrees for a maximal aileron hinge moment of $C_H = 0.2516[-]$ for the left and $C_H = -0.2522[-]$ for the right in cruise condition. The hinge moment throughout the wake field was determined and compared to this design limit. The hinge moment of the left aileron during the

	simplified		*state-space total*	
Motion	*solo*	*formation*	*solo*	*formation*
Phugoid	$0.0025 \pm 0.0770i$	$0.0015 \pm 0.0674i$	$0.0028 \pm 0.0847i$	$-0.2590 \pm 0.3592i$
-	-	-	-	$0.0657 \pm 0.2451i$
Short period	$-0.5325 \pm 1.0083i$	$0.4194 \pm 1.1553i$	$-0.5327 \pm 1.0086i$	$-0.4288 \pm 1.1541i$
Roll mode	-0.9129	-1.0385	-0.9463	-1.0935
-	-	-	-	0.4158
Spiral	0.0253	0.0265	0.0025	0.0024
Dutch roll	-0.1310 ± 0.2911	$0.1398 \pm 0.2693i$	$-0.1029 \pm 0.9972i$	$-0.1038 \pm 1.0125i$

Table 4.6: Dynamic analysis Eigenvalues of an A330-300 aircraft in solo flight and a formation flight condition at Mach 0.6 for an altitude of $11,000$ meters and a lift coefficient of 0.623 [-] for a wake field start position of $-0.15y/b$ and $0.1z/b$

formation flight just exceeded the limit value, within the deep wake field at $-0.5y/b$ and $0z/b$. Within close proximity of the vortex core a region of increased hinge moment can be identified, although the values are 'far' below the limit. A difference between left and right aileron hinge moments was identified.
The highest value was obtained on the left aileron deep within the wake field at $-0.5y/b$ and $0z/b$ with a value of $C_H = -0.2688[-]$ for an angle of $15.4^{\cdot}$ degrees. The maximal hinge moment is achieved at a lower deflection angle when compared to the solo condition. The changes in aerodynamic parameters due to the formation flight limit the maximal attainable deflection angle to a value of $14.3^{\cdot}$ degrees.
At the sweet spot, outside of the margin of error at $-0.15y/b$ and $0.1z/b$, the hinge moment reaches a value of $C_H = 0.0189[-]$. The results again highlight the danger of flying deep within the wake vortex field, creating a large disturbance in rolling moment, requiring moderate to large aileron deflections, pushing its hinge towards and over the design limit. The close proximity case also shows high values, but considerably lower compared to the deep wake field. As this is the region of interest, it can be assumed that the formation flight is possible using the current aileron hinges. Although further research into aero-servo-elastic effects is mandatory to fully grasp the dynamic motions and behaviour of the control surfaces and their hinge moments.

	C_{Hleft}	C_{Hright}	δ_{aleft}	δ_{aright}
limit solo	0.2516	-0.2522	$-16.8^{\cdot}$	$16.8^{\cdot}$
Formation				
$-0.15y/b\&0.0z/b$	0.0937	-0.1129	$-7.08^{\cdot}$	$7.08^{\cdot}$
$-0.15y/b\&0.1z/b$	0.0189	-0.0500	$-2.32^{\cdot}$	$2.32^{\cdot}$
$-0.50y/b\&0.0z/b$	-0.2688	0.1882	$15.4^{\cdot}$	$-15.4^{\cdot}$

Table 4.7: Hinge moment analysis Aileron hinge moments and deflections of an A330-300 aircraft in solo flight and a formation flight condition at Mach 0.6 for an altitude of $11,000$ meters and a lift coefficient of $0.623[-]$ for a multiple wake field positions

CHAPTER

FIVE

DATA SENSITIVITY ANALYSIS

Within this chapter two sensitivity analyses were performed. The purpose is to identify design parameters sensitive to the trimmed formation flight condition, where possible optimisation of the design could be performed. As was identified within chapter 4.3, the aileron surface requires the largest control deflection. Therefore it was chosen to focus upon the aileron control surface systems for this sensitivity analysis.

Two parameters of interest are the aileron surface and the aileron control allocation. The formation flight condition creates an asymmetric wing loading, which induces a rolling moment (among small other disturbances). By increasing the area of the ailerons, they should become more effective and should require less deflection angles. By changing the control allocation, the asymmetric wing loading can be counteracted locally. The in-vortex wing with increased wing loading should receive a higher deflection angle and the out-of-vortex wing with similar wing loading a lower one. Both approaches effectively try to reduce deflections to lower their drag contribution. The main goal is to reduce the drag benefit lost due to the trimmed configuration. The aileron surface is investigated by including the inboard aileron surface and the outboard aileron surface, where only the outboard aileron surface was investigated earlier. The control allocation was investigated by changing the differential control deflection tot a non-differential one. The in-vortex wing will be given a predefined aileron deflection angle to only locally counter the effect of the vortex, instead of using both ailerons to the same extend.

First both parameters and conditions are clearly stated. Afterwards the flight mechanic analysis is redone for both cases and their results are compared subsequently. Finally this chapter ends with a conclusion on the parameter sensitivity analysis as well as an overview table of the results for both cases, with relation to the original case of chapter 4.3.

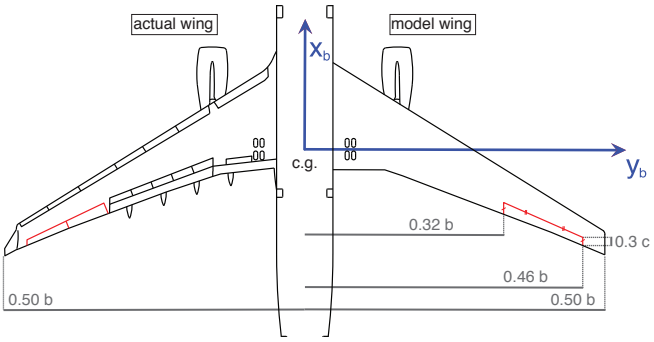

Figure 5.1: Schematic representation A330-300 model with increased surface area

5.1 Parameter analysis

The highest disturbance within the wake field is the rolling moment. Due to this rolling moment disturbance, the ailerons need to be deflected to maintain steady straight flight. As was seen in chapter 4.3, this induces a higher hinge moment and a part of the potential benefit is lost. It was identified in chapter 4.3.2 that 5.1% of the potential induced drag benefit is lost due to aircraft trim. The plan-form and control allocation of the aircraft were redefined to identify their impact upon the potential reduced benefit due to trim.

The first case is that of a change in aileron plan-form. When looking at the plan-form wing of the A330-300 aircraft, shown in figure 5.1, it can be seen that both inboard and outboard ailerons are located near the wing tip, next to one another. The ailerons are marked in red in figure 5.1. Up an till now the analysis was performed only using the outboard ailerons. To investigate the effect of plan-form area on the formation flight analysis, the inboard ailerons were also included within the aerodynamic and simulation model. To reduce complexity, both inboard and outboard ailerons were assumed to deflect by an identical angle. By using both inboard and outboard aileron as one surface, less deflection would be expected. This would result in less reduction of the induced drag advantage due to trim. The forces on the surface could however become larger, affecting the hinge moment.

The second case is that of a change of control allocation of the aileron control system. The disturbance in rolling moment is created due to an asymmetrical distribution of local lift, created by the span-wise variation of effective angle of attack. An asymmetrical control deflection would seem an appropriate solution. It was not chosen to alter the control allocation scheme here, to obtain an initial insight into the effect. A lower induced drag coefficient will be expected by giving a predefined aileron deflection on the in-vortex aileron to balance the rolling moment. A predefined angle setting for the in-vortex wing implies that ideally only one aileron is deflected to counteract the disturbances, the aileron of the in-vortex wing. From this predefined angle on the in-vortex wing, both ailerons are deflected asymmetrically to control the aircraft during manoeuvres.

The two previously explained cases, of plan-form area increase and predefined control deflection, will be analysed using the same general flight conditions as defined before. The assumed cruise flight is at a velocity of Mach 0.6 and a cruise altitude of $11,000$ meters with a lift coefficient of $0.623[-]$.
The results are compared to the A330-300 in solo condition, without the use of inboard and outboard ailerons or the predefined deflection angle. This makes that the results can be compared to those from chapter 4.3.

5.2 Case 1: Surface area

The first case that was investigated was the increase of the aileron control surface area, by using inboard and outboard ailerons simultaneously. Figure 5.1 shows the aircraft with both inboard and outboard ailerons and some key dimensions.

Important to note before moving on towards the analysis of the results. Whilst adjusting the aircraft model and running the FMT model for the formation flight analysis, a region was unveiled were no solution was possible. The region around the lateral separation distance $-0.4y/b$ showed a high rolling moment, as was expected when comparing the rolling moment in the wake field at this location, as was shown in figure 3.20. To compensate this high rolling moment a large aileron deflection was required. By increasing the area of the aileron surface, a large pitch up moment was generated by the in-vortex aileron, requiring compensation by the elevators and angle of attack. This resulted in a situation where the aircraft could not be trimmed, around the zero vertical separation distances from $-0.025z/b$ up and till $0.2z/b$. The aircraft trim within this region required in a too high angle of attack, resulting in an unrealistic value making the aircraft being not able to trim.
The interest for the formation flight lies within the close proximity case, between $-0.1y/b$ up and till $0y/b$, and less for trail aircraft positioned within the wake field. It was therefore justifiable to neglect the data points for the lateral separation around $0.4y/b$ and assuming a linear behaviour between $-0.5y/b$ and $-0.3y/b$. Further investigation is required into this region when further exploring the use of inboard and outboard ailerons.

The angle of attack results are shown in figure 5.2. The values of the wake field variations for the base case outboard ailerons are shown alongside to the case of inboard and outboard ailerons. As with previous results a margin of error has been introduced within all results. A situational sketch is provided alongside to clarify the change in angle of attack due to the use of inboard and outboard ailerons at the position where the largest change occurs, at $-0.5y/b$ and $0z/b$.
The behaviour shows a shift running through the center of the wake field. The close proximity positions, $-0.1y/b$ and higher, show a similar trend when compared to the base case. The positions within the wake vortex field show an increase in angle of attack is desired. This would imply not enough lift is generated, forcing the aircraft to increase the angle of attack to attain the desired lift coefficient. The increase in the area of the ailerons and the negative deflection of

the in-vortex aileron could explain the behaviour. The aileron would remove more of the benefit over a larger wing span, effectively reducing the formation flight advantage.

The difference in lift due to the control deflections is also noted by the control deflections to trim the aircraft within the wake field. Figure 4.9 shows all control deflections for the base case alongside with the results for the case of inboard and outboard ailerons. A large difference exists between the aileron and elevator deflections. The values for the aileron deflections are half the value they were before. This is due to the aileron area that was doubled by using the inboard and outboard ailerons.
The elevator differences are larger and more pronounced. The increased angle of attack for the region within the wake vortex field, from $-0.5y/b$ to $-0.1y/b$, will shift the elevator from a negative deflection to a positive deflection. The increase in angle of attack, due to the change in lift by the ailerons to counteract the rolling moment, will create a pitch up tendency within the wake vortex field. To balance the pitch up a large positive elevator deflection is required. The rudder deflection remains virtually unaffected by the use of both ailerons. An increase is noticed though, but compared to the aileron and elevator changes, it is small. This shows that the use of both ailerons does hardly disturb the rolling or yawing influences, but imposes problems for the lift force and pitching moment.

The changes show what was already discussed before, the reduction of the aileron deflections by a factor of two. The rudder deflection differences are small. The largest interest was identified for the change in elevator deflection within the wake field behind the lead aircraft. As identified before, an increase in angle of attack was required to obtain the desired lift coefficient after lift is lost due to the large surfaces of the ailerons. The larger aileron affect more span-wise lift distribution, making that the most lift will be generated by the wing root, rather than evenly distributed. The aerodynamic center gets pushed forward due to the control deflection, moving in front of the center of gravity. This induces a pitch up behaviour, which needs to be counteracted.
This is highly unwanted as the aircrafts aerodynamic center is moved in front of the center of gravity, implying a statically unstable condition. Luckily this behaviour is only present for deeper wake field positions. The flight dynamic and load analysis already revealed the disadvantages of the flight within the wake field, which for this case become detrimental. The wake field, stretching from $-0.5y/b$ to $-0.2y/b$ and $0.3z/b$ to $-0.3z/b$ should be avoided to prevent the high pitch up tendency. Although if encountered, using quick elevator correction could prevent potential dangerous situations, which was not investigated at this time though.

Figure 5.4 shows explanatory sketches for what happens at the sweet spot and at the deep wake field position with highest change in values.

The region of induced drag benefit is greatly reduced by the increase of the aileron surface. Figure 5.5 shows the induced drag benefit contour plot for positions within the wake field. The region of positive towards zero benefit, where the formation flight creates equally induced drag as in the solo condition, shrinks more around the vortex core region. The change in aileron area will affect more of the lift advantage, as created over the in-vortex wing. The highest value for induced drag reduction is attained at $-0.3y/b\ 0z/b$ with 72.4%. The induced drag reduction

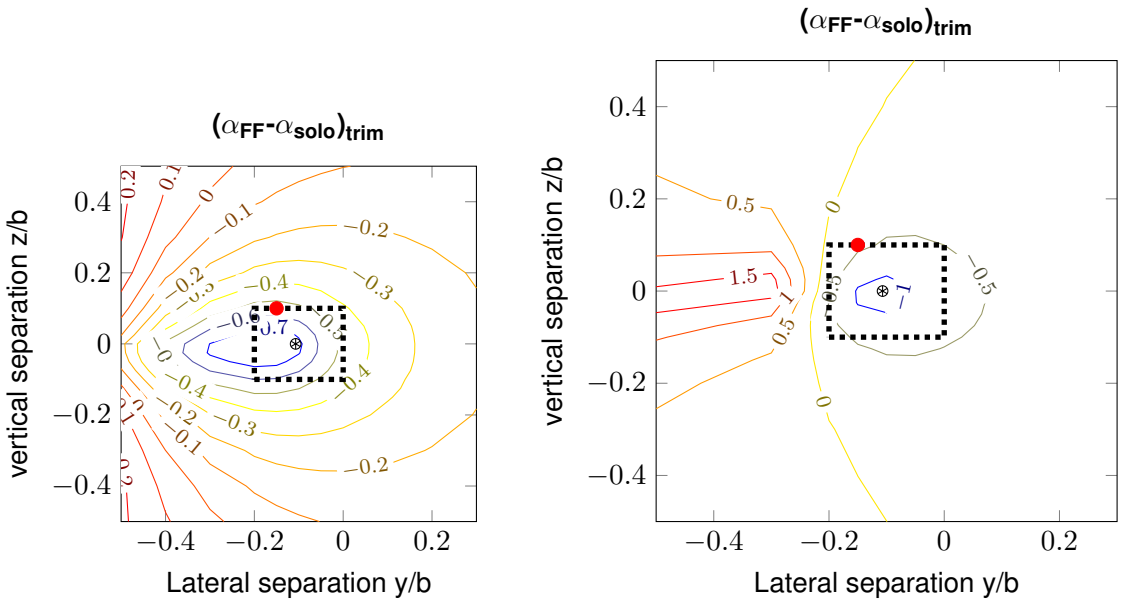

(a) base case: A330-300 analysis

(b) Case 1: inboard & outboard ailerons

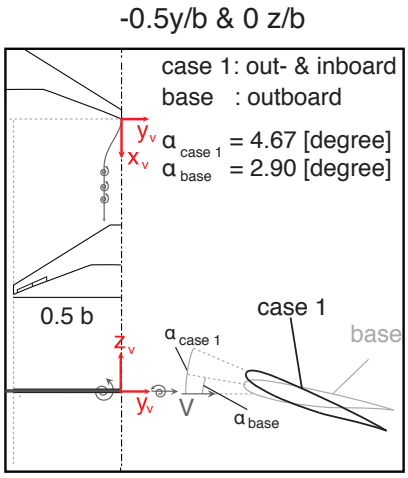

(c) Situation sketch at position red dot

Figure 5.2: Wake field analysis of the change in angle of attack in trim due to formation flight condition for the case of inboard and outboard ailerons compared to the case of only outboard ailerons

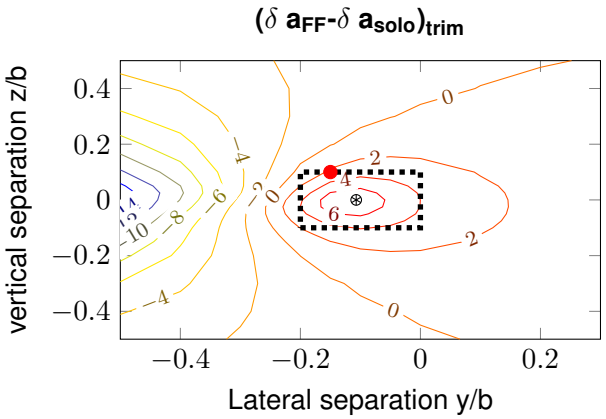

(a) base case: A330-300 analysis

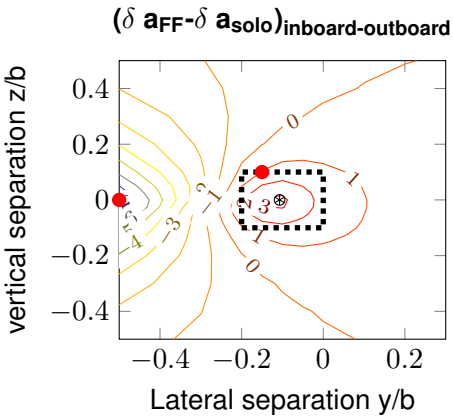

(b) Case 1: inboard & outboard

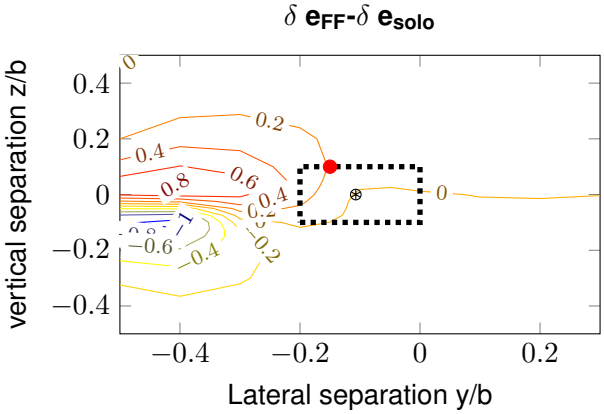

(c) base case: A330-300 analysis

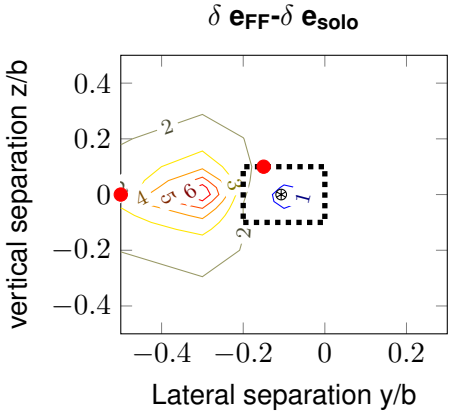

(d) Case 1: inboard & outboard

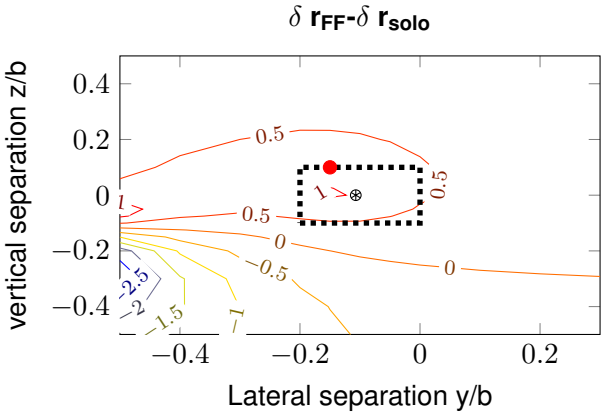

(e) base case: A330-300 analysis

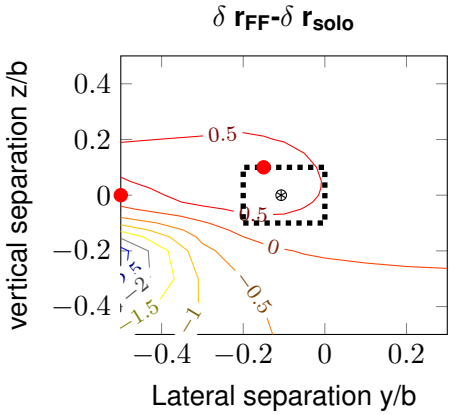

(f) Case 1: inboard & outboard

Figure 5.3: Wake field analysis of the change in control deflections in trim due to formation flight condition for the case of inboard and outboard ailerons compared to the case of only outboard ailerons

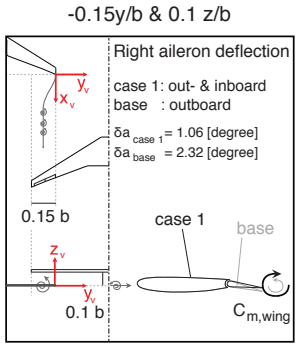

(a) Sketch at sweet spot

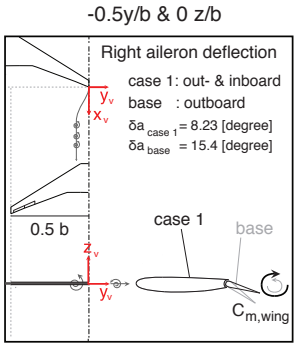

(b) Sketch at Highest value

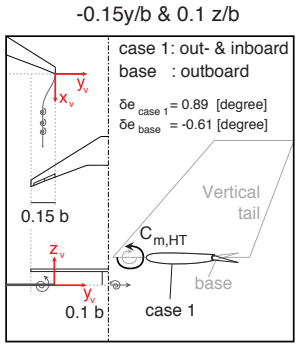

(c) Sketch at sweet spot

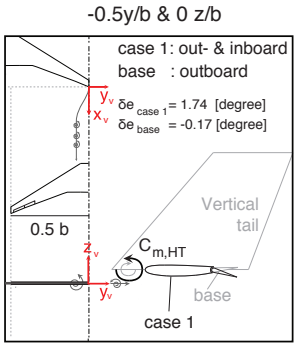

(d) Sketch at Highest value

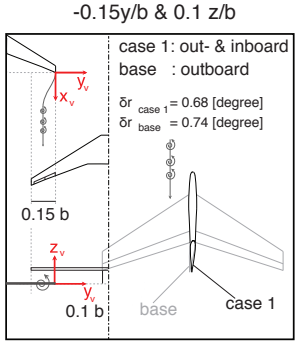

(e) Sketch at sweet spot

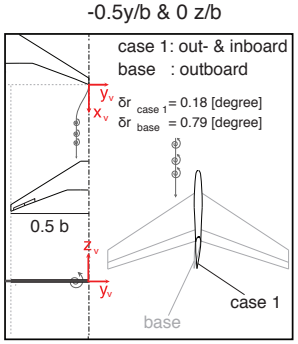

(f) Sketch at Highest value

Figure 5.4: Explanatory sketches of the difference in control deflections at $-0.15y/b$ and $0.1z/b$ & $-0.5y/b$ and $0z/b$ of in trim due to formation flight condition for the case of inboard and outboard ailerons

at the sweet spot, as was defined earlier at $-0.15y/b$ $0z/b$ shows an induced drag reduction of 37.50%. The sweet spot outside of the margin of error, previously defined at $-0.15y/b$ and $0.1z/b$ becomes 18.2%.
The increased aileron area thus moves the position for highest induced drag reduction more into the wake field, where disturbances are higher. The point for highest drag reduction is already outside of the margin of error, nevertheless it is questionable if the high value would still be present when including pressure drag components due to the larger elevator deflections. The increase in aileron area is thus not beneficial for the induced drag benefit, as the highest attainable benefit decreases, and the trail aircraft is forced to fly deeper within the wake vortex field. Figure 5.5 shows the the induced drag reduction in trimmed condition for both cases, the case of the use of inboard and outboard ailerons compared to the case of only outboard ailerons. The difference between both cases is also shown, alongside to a sketch marking the difference between both cases at a deep wake position, $-0.5y/b$ and $0z/b$.

Remarkable is that the increase of the aileron area reduces the benefit to such extend that, compared to the base condition, only a small area can be identified where the area change is desired. This area is located deep within the wake field at $-0.5y/b$ and $0.025z/b$ reaching a value 43.7%. This in contrast with the value of 1.89% benefit in the base condition. It must be noted that a rigid wing is assumed and no other drag components are included within this analysis. The addition of the pressure drag could reverse this result, as the lower aileron deflection will create a lower contribution. From a structural perspective a lower aileron deflection would also be desired, as the forces upon the aileron and wing tips will be lowered.

Figure 5.7 shows the hinge moment variation in wake field. The figure shows that the hinge moment is still well below the design limit value. The deep wake field, where the design limit was exceeded in the normal condition, shows no values exceeding the design limit. The difference between left and right aileron hinge moment remains, where in general the left aileron shows a higher moment compared to the left aileron.

At the sweet spot outside the margin of error,$-0.15y/b$ and $0.1z/b$, the hinge moment for left aileron becomes 0.0025 and for the right aileron -0.0258. At this position both moment show a remarkable decrease compared to the earlier obtained values of 0.0189 and -0.0500 for left and right aileron respectively. The increased area relieves the ailerons, as the doubled area requires a lower deflection angle. The in-vortex, left, aileron shows the highest benefit of the reduced aileron deflection angle. Two clarification sketches were also provided alongside to visualize the difference between both cases, at the sweet spot located at $-0.15y/b$ and $0.1z/b$.

The use of both inboard and outboard ailerons to counteract the disturbances within the wake vortex field results in a change of benefit as well as attitude. A larger pitching moment will be generated, which the elevators need to counteract by making larger deflection angles. The wake vortex region even showed that the pitch down tendency switched to a pitch up, potentially posing a dangerous environment to fly in. When compared to the base case, only using outboard ailerons, the benefit is greatly reduced. An overall advantage is still present to a

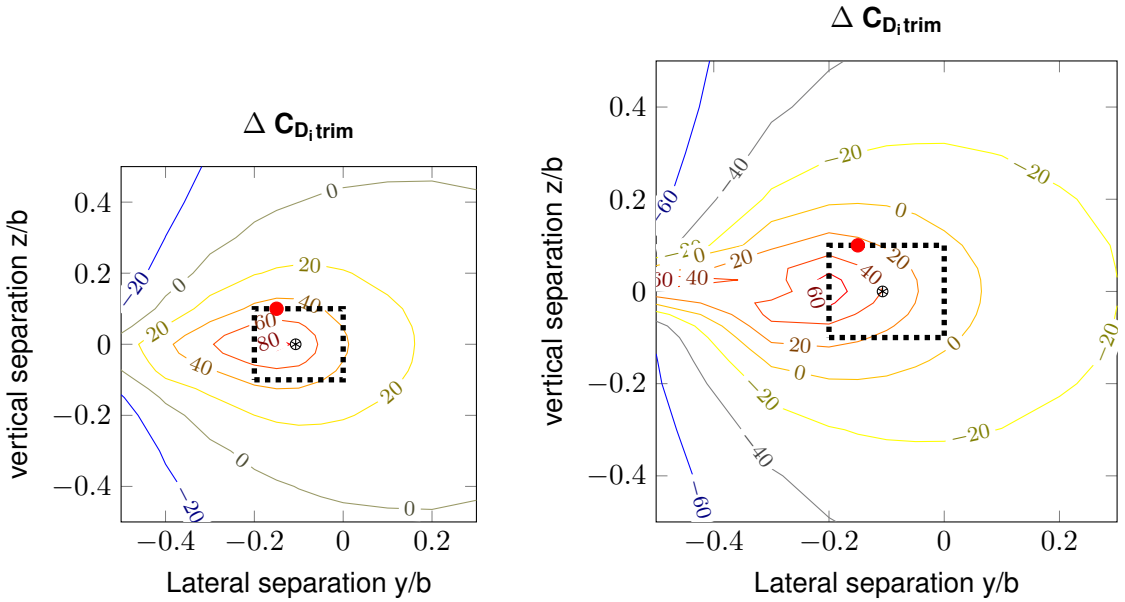

(a) base case: A330-300 analysis

(b) Case 1: inboard & outboard

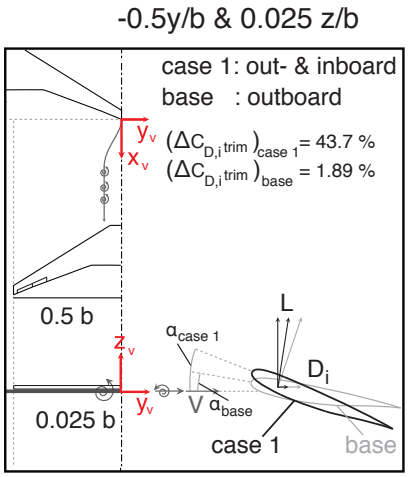

(c) Situation sketch at position red dot

Figure 5.5: Wake field analysis of the difference in induced drag in trim due to formation flight condition for the case of inboard and outboard ailerons compared to the case of only outboard ailerons

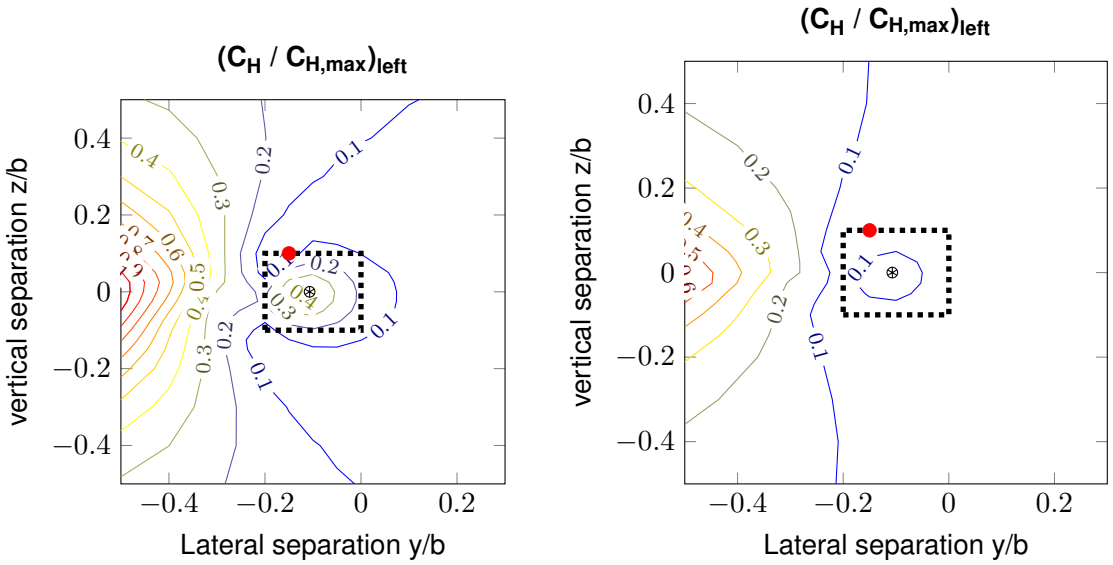

(a) Left aileron base case: A330-300 analysis

(b) Left aileron case 1: inboard & outboard

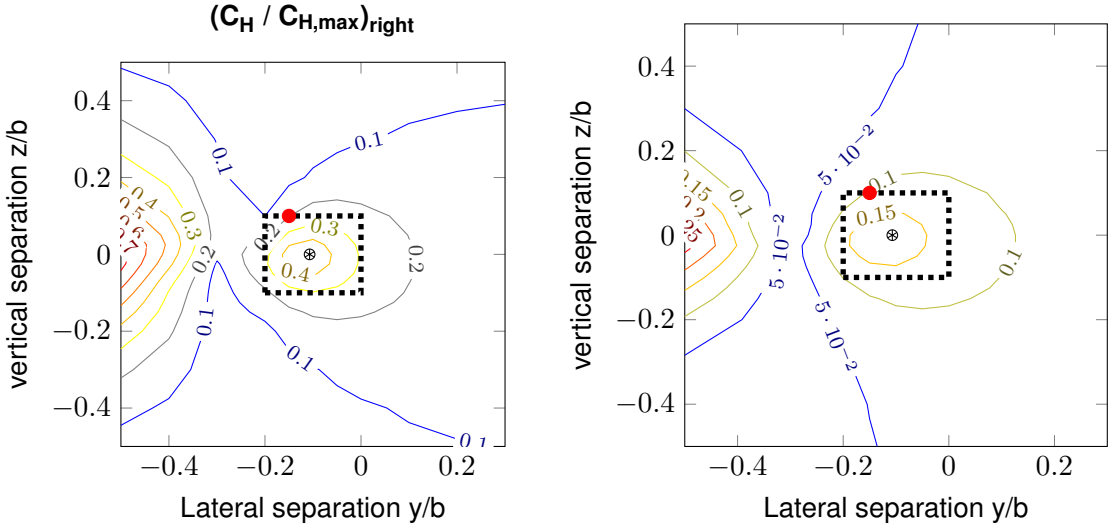

(c) Right aileron base case: A330-300 analysis

(d) Right aileron case 1: inboard & outboard

Figure 5.6: Wake field analysis of the difference in hinge moment in trim due to formation flight condition for the case of inboard and outboard ailerons compared to the case of only outboard ailerons

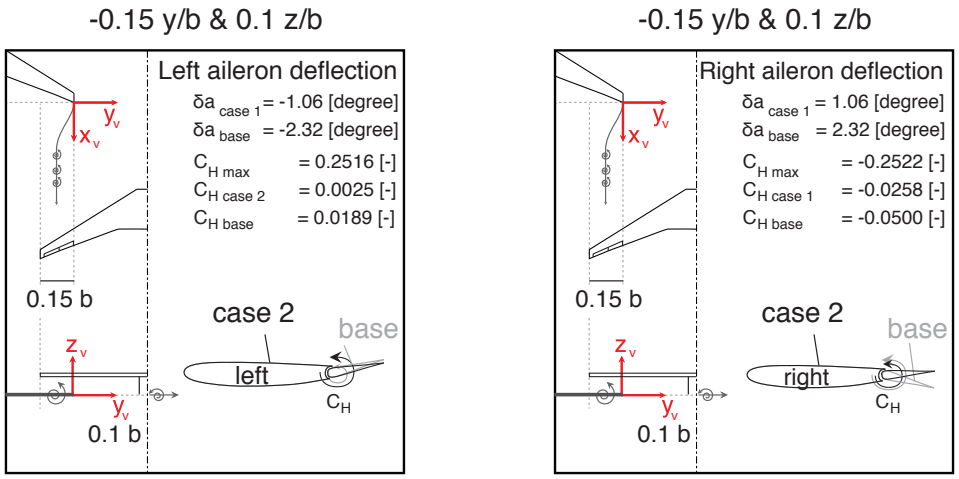

(a) Situation sketch left aileron at position red dot

(b) Situation sketch right aileron at position red dot

Figure 5.7: Explanatory sketches of hinge moment at $-0.15y/b$ and $0.1z/b$ in trim due to formation flight condition for the case of inboard and outboard ailerons compared to the case of only outboard ailerons

much lower extend. Deep within the wake field, at $-0.5y/b$ and $0.025z/b$, an advantage was measured. The volatile environment of this region, requiring high aileron deflections, elevator and rudder deflections make this region not advisable to fly in.
The wake vortex region should further be researched as it poses uncertainties and could present potential dangerous situations. This was also identified within chapter 4.3. By including a more elaborate drag estimation, not only the induced component, might prove that the use of both inboard and outboard ailerons is beneficial. The lower aileron deflections required will create less drag and pose lower forces upon the wing and aileron structures.

Again a brief dynamic analysis was performed to identify the behaviour of the aircraft. At the sweet spot outside of the margin, at $-0.15y/b$ and $0.1z/b$, the eigenvalues of the state-space matrix were determined. Figure 5.8 shows the eigenvalues of the solo flight compared to the base case, as was shown in chapter 4.3. Added are the eigenvalues as were determined for the aircraft with the usage of inboard and outboard ailerons.

state-space total			
Motion	*solo*	*formation outboard*	*formation inboard-outboard*
Phugoid	$0.0028 \pm 0.0847i$	$-0.2590 \pm 0.3592i$	$-0.1184 \pm 0.5006i$
-	-	$0.0657 \pm 0.2451i$	$0.2086 \pm 0.2375i$
Short period	$-0.5327 \pm 1.0086i$	$-0.4288 \pm 1.1541i$	-0.3462
Roll mode	-0.9463	-1.0935	-1.1031
-	-	-	-1.0776
-	-	0.4158	0.5418
Spiral	0.0025	0.0024	0.0069
Dutch roll	$-0.1029 \pm 0.9972i$	$-0.1038 \pm 1.0125i$	$-0.0942 \pm 0.9558i$

Table 5.1: Eigenvalues of total state space of an A330-300 aircraft in solo flight and a formation flight condition for outboard ailerons and inboard and outboard ailerons at Mach 0.6 for an altitude of $11,000$ meters and a lift coefficient of 0.623 [-] for a wake field start position of $-0.15y/b$ and $0.1z/b$

From the table and the figure it can be seen that the aircraft is also unstable, even 'more' unstable compared to the base case. Remarkable to note is the introduction of another eigenvalue, that was assumed to be connected to the roll mode, located completely to the left of the eigenvalue plot. According to the simulation model the short period transformed into a non-oscillatory motion. This gives the indication that more research needs to be performed into the identification of all dynamic motions. What can be concluded is that the usage of both inboard and outboard ailerons within the formation flight condition at that spot, shows highly unstable behaviour.

The first case regarding the use of both inboard and outboard ailerons revealed a change in attitude. Due to the increased aileron area their deflection to counteract the interference rolling moment in the wake field creates a large pitching moment. The elevators need to compensate

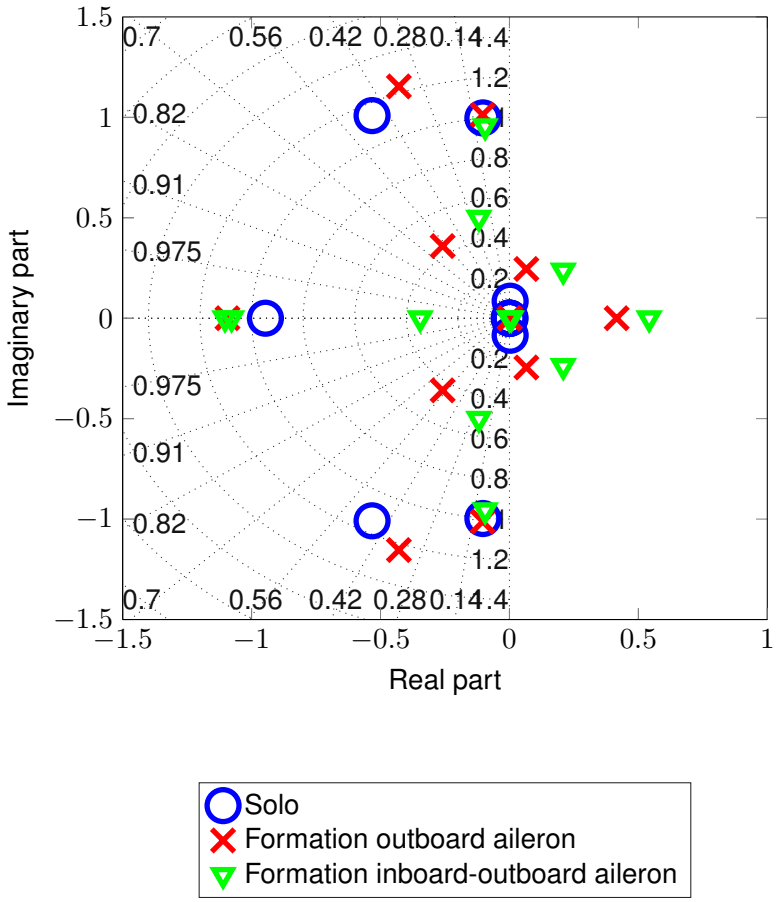

Figure 5.8: Root locus plot total state-space matrix of an A330-300 aircraft in solo flight and a formation flight condition for both only outboard and inboard-outboard aileron case at Mach 0.6 for an altitude of $11,000$ meters and a lift coefficient of 0.623 [-] for a wake field start position of $-0.15y/b$ and $0.1z/b$

radically even by changing from upward to a downward deflection at certain positions within the wake field. The region for induced drag benefit in the wake field is reduced by the use of both ailerons, due to the change in pitching moment. The aircraft becomes more dynamically unstable and a new eigenvalue is present within the state-space solution. The complex behaviour arising from the usage of both inboard and outboard ailerons at the same time, with identical deflection, requires more detailed study. The results as presented here show a benefit for aileron hinge moments, due to the reduction in aileron deflection angle. A possible benefit can be present from an induced drag perspective.

5.3 Case 2: Control allocation

The second case to be analysed is the predefined control deflection for the in-vortex wing. Figure 5.9 gives a schematic overview of the situation. The aileron of the in-vortex wing was given a predefined angle of $-2.32^{\cdot}$ degrees, implying an upward deflection. The out-of-vortex wing was not given a predefined deflection. The aileron control system still makes use of a differential control mechanism. The difference lies in the fact that the in-vortex wing is not balanced around $0^{\cdot}$ degrees but around $-2.32^{\cdot}$ degrees. The base condition without predefined deflection, showed a value of $-2.32^{\cdot}$ degrees at $-0.15y/b$ and $0.1z/b$. The $-2.32^{\cdot}$ degrees was chosen to approximate the aileron deflection around this spot, trying to remove the differential deflection required. The aileron deflection is required to counter the rolling moment due to an asymmetric wing loading. The asymmetry is created upon the in-vortex wing, thus by using a predefined deflection, possibly a much lower differential aileron deflection would be expected. The method of a predefined angle could be extended to make use of a non-differential aileron control deflection. This would imply that both left and right aileron would work independently to create and balance the rolling moments. The extension required a complex redefinition of the control allocation vector, which was not done here. The predefined deflection of the in-vortex wing should offer a good insight in whether or not it could be beneficial to use non-differential control deflections for the formation flight condition.
A flight mechanic analysis was performed to identify how the formation flight is affected by this predefined deflection upon the in-vortex aileron. The assumed cruise condition from section 5.2 and chapter 4.3 were adhered again. A Mach number of 0.6 at an altitude of $11,000$ for a lift coefficient $0.623[-]$ were used as flow conditions.

By making use of a predefined deflection angle the aileron of the in-vortex wing will be deflected to locally counter the effect of the incident vortex. The out-of-vortex wing will thus not create extra drag at the expense of the formation flight. As only one predefined angle is defined for the entire wake field, this can only be achieved at one point for the assumed cruise condition investigated here. Other positions within the wake field or other flight conditions will require a different angle. This makes the link to the extensive control allocation system that would be needed to automatically adjust itself to optimally trim the aircraft, according to moments and location within the wake field.
To first identify the actual benefit, an investigation of one position in one flight condition is tested

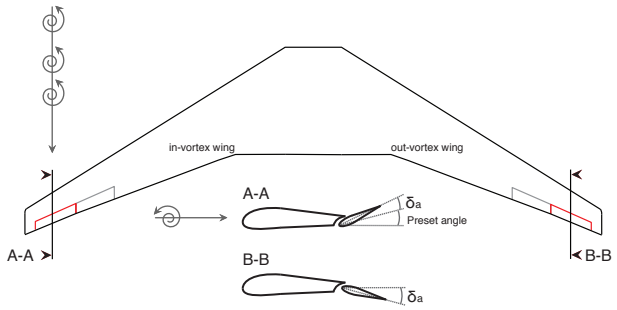

Figure 5.9: Schematic representation of aileron and hinge as used to estimate the hinge moment, specific to the A330-300 aircraft

here. The sweet spot outside of the margin of error, as was identified earlier to be at $-0.15y/b$ and $0.1z/b$, was chosen. The predefined deflection of $-2.32^{\cdot}$ on the in-vortex aileron resulted in a change of other control deflections, which are listed in table 5.2. Table 5.2 also contains the flight specific data of angle of attack and the induced drag.

$-0.15y/b$ $0.1z/b$	*Solo Condition*	*Formation Flight base case*	*Case 2 predefined* δ_a	*Difference solo & case 2*
C_{D_i}	0.0101	0.0048	0.0048	$\Delta 52.6\%$
$C_{D_i trim}$	0.0112	0.0053	0.00529	$\Delta 47.5\%$
Difference	0.0011	0.0005	0.00049	$\Delta - 5.09\%$
α	$3.08^{\cdot}$	$2.53^{\cdot}$	$2.53^{\cdot}$	$0.55^{\cdot}$
δa_{right}	$0^{\cdot}$	$2.32^{\cdot}$	$-0.32^{\cdot}$	$0.32^{\cdot}$
δa_{left}	$0^{\cdot}$	$-2.32^{\cdot}$	$-2.00^{\cdot}$	$2.00^{\cdot}$
δe	$-0.80^{\cdot}$	$-0.61^{\cdot}$	$-0.61^{\cdot}$	$-0.19^{\cdot}$
δr	$0^{\cdot}$	$0.74^{\cdot}$	$0.78^{\cdot}$	$-0.78^{\cdot}$
$C_{H left}$	$max = 0.2516$	0.0189	0.0375	-0.0186
$C_{H right}$	$max = -0.2522$	-0.0500	-0.0342	0.0158

Table 5.2: Overview for the case of predefined in-vortex aileron deflection angle compared to the base condition, for assumed cruise condition: $M = 0.6$, $h = 11,000$ meters, $C_L = 0.623$

The data shows that the right aileron deflection is almost reduced to zero. Further refinement of the predefined deflection could reduce the right aileron deflection completely to zero. The benefit for induced drag remains almost identical to the normal trimmed condition. A slight difference does exist though. This difference shows that the predefined angle does improve the reduction of induced drag benefit due to trim, as the difference between the trimmed and untrimmed case becomes lower. The attitude of the other control surfaces remains, with only a small difference in rudder deflection. Graphical representations of the three control surfaces and their changes at the sweet spot are shown in figure 5.10. The base case condition value is compared to the newly obtained value for the predefined in-vortex aileron case.

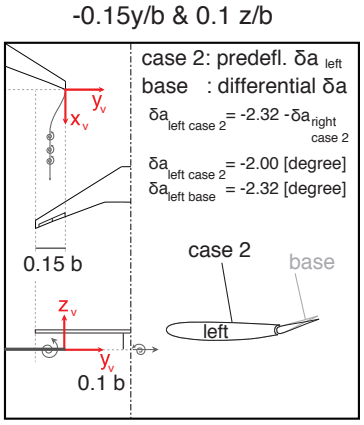

(a) Left aileron deflection, with $-2.32^{\cdot}$ degrees predefined angle

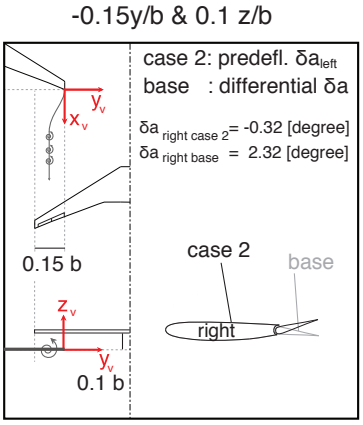

(b) Right aileron deflection, with $0^{\cdot}$ degrees predefined angle

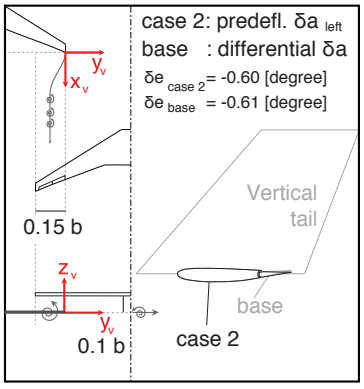

(c) Elevator deflection

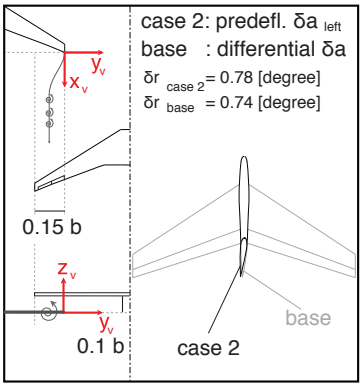

(d) Rudder deflection

Figure 5.10: Situational sketches at the sweet spot outside margin of error, $-0.15y/b\ 0.1z/b$, for the difference in control deflections in trim due to formation flight condition for the case of inboard and outboard ailerons compared to the case of no predefined deflection

The difference in induced drag, as seen here, was expected to be larger in magnitude. The difference between the trimmed and untrimmed condition is 5.09% reduction of the benefit compared to the 5.10% found for the base case (without the predefined deflection). The small deflection of the out-of-vortex aileron was expected to have reduced the drag component significantly. An explanation can be found by discussing the induced drag and its contributions. The induced drag is the component of the drag related to the lift force, effectively the flow component of the lift created by tilting the vector. By deflecting the aileron surfaces in solo condition, the lift on both wings is altered to create a rolling moment. The forces required however, are small compared to the overall lift force of the wing. The effectiveness of the forces created by the ailerons lie in their moment arm, to counter the rolling moment. Their contribution to the induced drag would thus be low as lift changes are small.
Within the formation flight condition, an asymmetric lift distribution is created inducing a interference rolling moment. The ailerons need to be deflected, to counteract the interference rolling moment. The deflection itself will not contribute much to the induced drag, as explained before. On the in-vortex wing however, due to the negative deflection of the aileron, the lift created by the wake vortex will be destroyed. This explains the difference identified when comparing the induced drag benefit in trimmed and untrimmed condition. The contribution of the deflection of the out-of-vortex wing is small however and explains the small values as seen in figure 5.11. The sketch shows a graphical representation of the effect as it was just described. The small change in drag is also noticed by the rudder. The difference in drag creates a small positive yawing moment that needs to be counteracted by a small reduction in rudder deflection, as was identified before and was seen in figure 5.10.

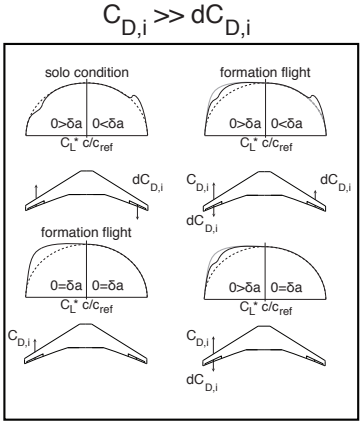

Figure 5.11: Explanatory sketch induced drag benefit due to predefined deflection at $-0.15y/b$ and $0.1z/b$, in trim due to formation flight condition for the case of inboard and outboard ailerons compared to the case of no predefined deflection

The benefit of the predefined aileron setting is prosperous. Only the induced drag is investigated here, for which control deflections show small contributions. In reality the viscous and

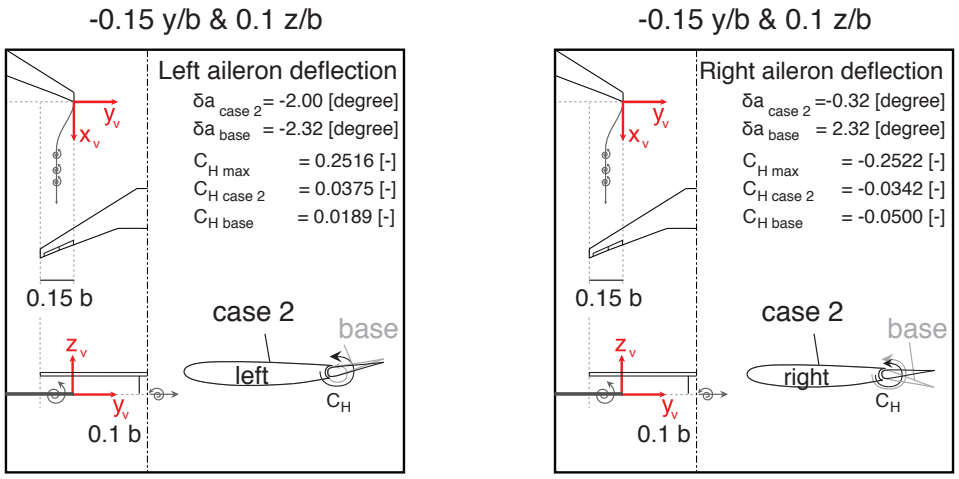

(a) Left aileron hinge moment

(b) Right aileron hinge moment

Figure 5.12: Situational sketches at the sweet spot outside margin of error, $-0.15y/b\ 0.1z/b$, for the difference of aileron hinge moment in trim due to formation flight condition for the case of inboard and outboard ailerons compared to the case of only outboard ailerons

compressibility effects at a Mach number of 0.6 will create other drag components due to a control deflection, e.g. pressure drag. The small difference noticed within this research probably could become higher. The smaller out-of-vortex deflections will also impose less aerodynamic bending and aero-servo-elastic effects, which will pose less strain upon the aileron system and the effectiveness of the surface.
The benefit is only local however. Optimally an adjustable system would be preferred to change the predefined angle according to the position within the wake field, which could be under the form of a custom made control allocation scheme.

The hinge moments of both left and right aileron finally show an interesting behaviour. Two explanatory sketches are provided within figure 5.12. Both hinge moments stay well below the design limit at the position under investigation. However an increase upon the left aileron can be identified, where the right aileron sees a reduction. Left and right aileron hinge moment are close in value, closer than was the case for the regular aircraft. Although the left ailerons was increased by 98%, the right aileron was reduced by 32%. The right aileron becomes alleviated. Interesting to note is the lower deflection angles of aileron that do create a higher hinge moment value. The change in angle of attack due to the rolling moment, related to the aileron deflection, shifts the constant first term of equation 4.8 to a higher value. The shift in constant value, shifts the overall aileron hinge moment to a higher value.

Finally a brief dynamic analysis was performed for the sweet spot location outside of the margin of error, at $-0.15y/b$ and $0.1z/b$. As for previous cases, the eigenvalues of the total state-space

matrix were determined and plotted. Figure 5.13 shows the eigenvalue results for solo flight condition, the base case of the aircraft without predefined aileron deflection and the one with a predefined aileron deflection of $-2.32^{\cdot}$. The plot almost shows no difference, when compared to the case of no predefined deflection of the in-vortex aileron. The eigenvalues in table 5.3 highlight minor changes in behaviour.

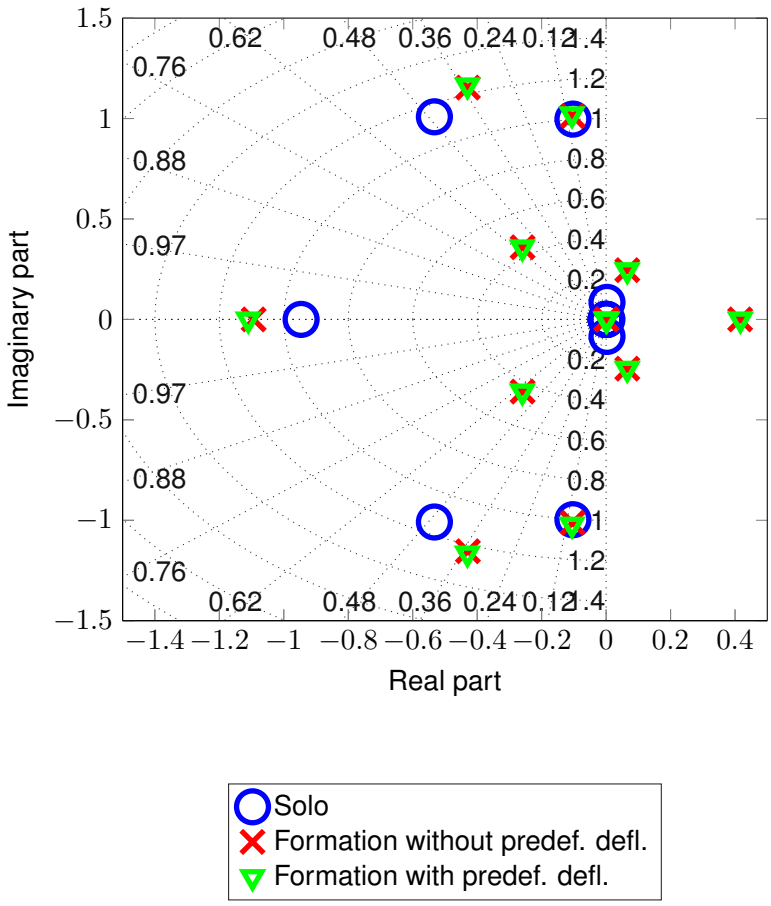

Figure 5.13: Root locus plot total state-space matrix of an A330-300 aircraft in solo flight and a formation flight condition with and without predefined in-vortex aileron ($-2.32^{\cdot}$) deflection at Mach 0.6 for an altitude of $11,000$ meters and a lift coefficient of 0.623 [-] for a wake field start position of $-0.15y/b$ and $0.1z/b$

The second case, setting a predefined aileron deflection upon the in-vortex wing, showed a small benefit regarding the trimmed formation flight condition at the position $-0.15y/b$ and $0.1z/b$. Due to the predefined angle on the in-vortex aileron, the out-of-vortex aileron deflection was almost reduced to zero. The angle of attack remained identical to the case were no predefined angle was used. The rudder showed a small change in angle, due to the lower in induced drag due to the decreased deflection angle upon the out-of-vortex aileron. The contributions of the aileron deflections to the induced drag are small however. This created

state-space total			
Motion	*solo*	*formation without predf.defl.*	*formation with predef. defl.*
Phugoid	$0.0028 \pm 0.0847i$	$-0.2590 \pm 0.3592i$	$-0.2598 \pm 0.3587i$
-	-	$0.0657 \pm 0.2451i$	0.0654 ± 0.2453
Short period	$-0.5327 \pm 1.0086i$	$-0.4288 \pm 1.1541i$	$-0.4303 \pm 1.1654i$
Roll mode	-0.9463	-1.0935	-1.1101
-	-	0.4158	0.4166
Spiral	0.0025	0.0024	0.0024
Dutch roll	$-0.1029 \pm 0.9972i$	$-0.1038 \pm 1.0125i$	$-0.1058 \pm 1.0215i$

Table 5.3: Eigenvalues of total state space of an A330-300 aircraft in solo flight and a formation flight condition with and without predefined in-vortex aileron ($-2.32^{\cdot}$) deflection at Mach 0.6 for an altitude of $11,000$ meters and a lift coefficient of 0.623 [-] for a wake field start position of $-0.15y/b$ and $0.1z/b$

only a small benefit regarding the loss of induced drag benefit due to trimming of the aircraft. The low out-of-vortex aileron deflection would probably significantly reduce the pressure and wave drag. It would also lower the structural disadvantages of deflecting the out-of-vortex wing during cruise. The in-vortex aileron deflection would create a higher hinge moment upon the aileron. However this model assumes a rigid wing and neglects aero-servo-elastic effects, so no conclusive answer can be given regarding the actual structural advantages. Further research would be required. The dynamic analysis still showed an unstable behaviour, although the predefined aileron deflection does not worsen the eigenvalue results in the formation flight condition.

5.4 Conclusion

Two sensitivity studies were performed, to potentially reduce the loss in benefit due to trimming the aircraft within the formation flight condition. The rolling moment, induced within the wake field due to the asymmetrical wing loading, has the highest value. Previously it was already identified that the largest control deflections were required for the ailerons within the wake field. The sensitivity analysis was therefore focussed on the aileron control system. First the area of the aileron was increase, by using both inboard and outboard ailerons simultaneously. Secondly the control allocation was rudimentary altered by setting a predefined angle to the in-vortex aileron. The purpose was to only locally counteract the asymmetric wing loading, instead of using differential aileron control.

The first case was for the increased area of the aileron, by using both inboard and outboard ailerons simultaneously. The general attitude of the aircraft was altered, as the increase in area created a pitch up tendency. The elevator deflection changed sign within the wake field and

showed remarkable high values within the deep wake field. The region for potential induced drag benefit is greatly affected. Remarkable is the creation of a beneficial region in the deep wake field for zero vertical separation. This region is however shows rapid changes and should be avoided during flight. The region around the vortex core, close proximity, retains a part of the benefit however. The dynamic analysis showed a highly unstable behaviour, compared to the solo condition and the condition of only using outboard ailerons. The advantage lies in the much lower aileron hinge moments. Although only approximated, a major reduction was identified, which in turn could reduce wear and safety upon their systems.
Generally further research into the dynamic behaviour of the use of both inboard and outboard ailerons is required before it could be considered during the formation flight, to lower the aileron hinge moments.

The second case consisted of a predefined aileron deflection on the in-vortex wing of $-2.32^{\cdot}$ degrees. The angle was determined according to the required deflection in normal formation flight condition at the sweet spot, $-0.15y/b$ and $0.1z/b$. The angle of attack and elevator deflection remained similar to the case without predefined aileron deflection. The aileron angle shows a shift, where the out-of-vortex, right, aileron is reduced to an deflection of almost zero. The in-vortex aileron is also lower compared to the base case without predefined deflection. The lower deflection angles of the ailerons was seen in the induced drag component. As the aileron deflection itself does not contribute much to the induced drag, the difference is small. The total drag, when incorporating wave and pressure drag, would probably further decrease. The dynamic behaviour was similar to the condition without predefined deflection, remaining unstable though.
By locally using predefined aileron deflections, the loss in potential induced drag benefit can be reduced. Probably the loss can be significant, although no conclusive results can be presented as no pressure and wave drag are incorporated.

Both cases also highlighted the need for an active trim control system. The dynamic instability and the variations in forces and moments highlight a local trim approach within the wake field. The predefined aileron angle showed how much can be gained by optimizing for one position. The possibility must remain however to change angles, when manoeuvring within the wake field or when aerodynamic disturbances change the position of the lead and/or trail aircraft. This was also identified for the base condition in chapter 4. An overview of the results for both cases and the base condition is given in table 5.4 for the sweet spot outside of the margin of error, at $-0.15y/b$ and $0.1z/b$.

$-0.15y/b$ $0.1z/b$	*Solo* *Condition*	*Formation Flight* *Base condition*	*Formation Flight* *in-out-board*	*Formation Flight* *predefined* δ_a
C_{D_i}	0.0101	$\Delta 52.6\%$	$\Delta 52.6\%$	$\Delta 52.6\%$
$C_{D_i trim}$	0.112	$\Delta 47.49\%$	$\Delta 18.2\%$	$\Delta 47.50\%$
$_{D_i}$	0.0011	$\Delta - 5.10\%$	$\Delta - 34.4\%$	$\Delta - 5.09\%$
α	$3.08^{\cdot}$	$2.53^{\cdot}$	$2.67^{\cdot}$	$2.53^{\cdot}$
δa_{right}	$0^{\cdot}$	$2.32^{\cdot}$	$1.06^{\cdot}$	$-0.32^{\cdot}$
δa_{left}	$0^{\cdot}$	$-2.32^{\cdot}$	$-1.06^{\cdot}$	$-2.00^{\cdot}$
δe	$-0.80^{\cdot}$	$-0.61^{\cdot}$	$0.89^{\cdot}$	$-0.61^{\cdot}$
δr	$0^{\cdot}$	$0.74^{\cdot}$	$0.68^{\cdot}$	$0.78^{\cdot}$
$C_{H left}$	$max = 0.2516$	0.0189	0.0025	0.0375
$C_{H right}$	$max = -0.2522$	-0.0500	-0.0258	-0.0342

Table 5.4: Overview for the sensitivity analysis results compared to the base condition, for assumed cruise condition: $M = 0.6$, $h = 11,000$ meters, $C_L = 0.623$

CHAPTER

SIX

FEASIBILITY ANALYSIS

Within this chapter the focus will be on the total benefit of an aircraft in the formation flight. First the assumptions of both models, aerodynamic and simulation, used within this research study are restated. Afterwards the results of the formation flight are analysed. The parasite drag estimation is added to obtain the total drag benefit of the formation flight. Finally an overview of the state-of-the-art research is given, using information obtained by test flights performed in the period of 2012-2013 and the current ongoing research. The study upon the effect of trim is positioned within the current ongoing research to clearly identify the added value. The goal is to identify the total benefit with relation to fuel savings of the formation flight condition.

6.1 Assumptions

All assumptions that where used throughout this research study are restated here. The assumptions are subdivided into the aerodynamic and flight mechanic model within this chapter. The purpose is to give a clear overview of the limitations and assumptions of both models used, before moving into the feasibility analysis of the formation flight condition.

6.1.1 Aerodynamic analysis

The list of assumptions from chapter 3.2.3 is restated here for clarity. All results obtained are under the influence of these assumptions. Possible effects that are disregarded due to these assumptions where also clearly stated when discussing the results.

- no viscous effects included
- no compressibility included

- compressibility correction (Prandtl-Glauert), maximal Mach number 0.6
- analytical vortex core radius and velocity approximation, four models included though
- rudimentary modelling of direct wing-vortex interaction (vortex flow parallel to x-axis)
- boundary layer interaction with vorticial flow is neglected
- homogeneous formation can be investigated (no heterogeneous)

6.1.2 Flight dynamic and loads analysis

The list of assumptions from chapter 4.2.5 are listed below. Obviously for the flight dynamic and load s analysis the aroedynamic assumptions also hold, as the data of the aerodynamic analysis is used by the simulation model.

- Rigid wing model
- No aero-servo-elastic effects
- No aerodynamic disturbances included (e.g. gusts, wind velocity changes)
- Variational behaviour of forces and moments with relation to velocity, angle of attack and side-slip angle
- Linear behaviour of forces and moments with relation to changes in roll-pitch-yaw rate
- Linear behaviour of forces and moments with relation to changes in aileron-elevator-rudder deflection

A second list of assumptions is created when using the hinge moment estimation tool. These assumptions are also stated again to obtain the full overview.

- Specific geometric data for A330-300
- Specific control data obtained from empirical relations for A330-300 geometry $a^{\star}_{1,20}$, $b^{\star}_{1,20}$
- Hinge moment derivative, $b_{1,2}$, estimated using empirical relations of ESDU
- Estimation of angle of attack change using $\delta a_{left,right}$, $C_{l\alpha}$ and C_{lp}

6.2 Flight analysis

The aerodynamic and flight mechanical analysis of the formation flight condition for the A330-300 aircraft proved that much is to gain with the application of this operational technique. The local benefit upon the aircraft forces and moment balance was shown, but not the effect for a total flight condition. The first paragraph will focus on the total flight benefit with relation to

drag and fuel flow. Up until now only the induced drag benefit was investigated, as the benefit is mainly created due to a difference in induced drag.

The A330-300 aircraft in its normal formation flight condition will be considered, as both sensitivity studies did not resulted in a conclusive significant benefit. The increased aileron surface area showed a relieving of the aileron hinge moments and the predefined deflection angle showed a reduction in potential induced drag benefit loss due to control deflections. Both do initially show a benefit that is worth to further research and potentially exploit. The second and third paragraph will discuss the control authority and hinge moment, focussed on the normal formation flight condition, using information attained within the sensitivity analysis. Finally a general overview for the potential benefit of the formation flight condition for an unadjusted A330-300 aircraft is given.

6.2.1 Total drag and fuel flow

The results from former chapters show a high induced drag reduction attainable for the assumed cruise flight at $11,000$ meters at a velocity of 0.6 Mach and a lift coefficient of $0.623[-]$. The induced drag reduction implies a total drag reduction that can be attained, also creating a fuel saving. To obtain the entire picture for the A330-300 aircraft during the formation flight, the total drag is now determined, using the FMT model and its estimation for parasite drag, where parasite drag and induced drag form the total drag of the aircraft. The estimation method discussed within chapter 4.2.4, included within the FMT model, was used for the estimation.

The attitude of the aircraft remained identical, after adding the parasite drag contribution. The only difference lied in the maximal attainable drag reduction, which lowered in value from 83.85% until 29.47% at the sweet spot in trimmed condition, $-0.15y/b$ and $0z/b$. The sweet spot on the edge of the margin of error, at $-0.15y/b$ and $0.1z/b$ the benefit further reduces to 16.59%, compared to the 52.6% induced drag reduction. Both induced drag reduction as the total drag reduction graphs are shown in figure 6.1. The total drag reduction as obtained here, corresponds roughly to what was expected from the literature described, within the background in chapter 2. The drag presented here is only of the trail aircraft and not the total formation. This is unconventional, when compared to some literature. The reason lies in the fact that the lead aircraft will be trimmed differently. To gain insight into the specific trimmed situation, the drag contribution of the lead aircraft is not incorporated to obtain the total drag of the formation.

The fuel flow difference of the formation flight with relation to the solo flight condition, as determined within the flight mechanical model is shown in figure 6.2. This is the fuel flow reduction achieved for the normal A330-300 aircraft. Figure 6.2b shows the result of a test flight using a Dornier Do-28 fighter aircraft, flown in a two aircraft formation in 2002 and analysed by Ray et al. [22]. Although both aircraft are of a different type, the comparison was made to affirm similarities in pattern and global magnitude of the fuel flow reduction. When comparing the results to those from the test flight, a difference exists. First again the sweet spot for the test flight has moved with relation to the sweet spot defined by the FMT model. The movement is

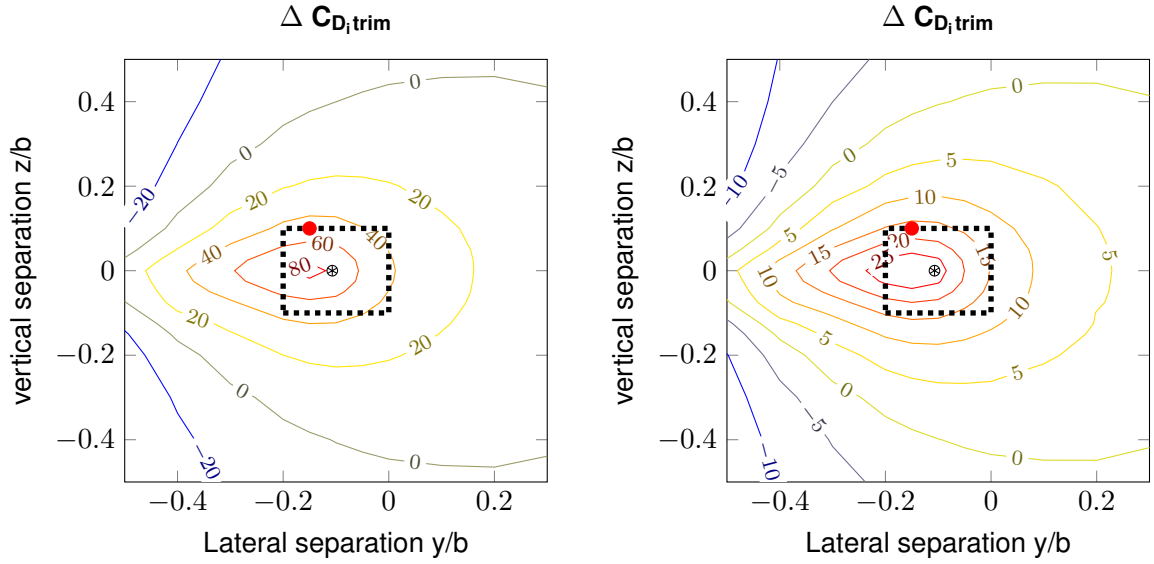

(a) Induced drag coefficient

(b) total drag coefficient

Figure 6.1: Wake field analysis in trim and due formation flight condition for un-adjusted A330-300

due to the wake vortex field that does not remain parallel but shifts down vertically, as was seen and described earlier. The effect of vortex meandering vertically, was not accounted for by the aerodynamic model used and thus also not by the FMT model. The aerodynamic model also poses a margin of error within the wake field. Within this margin, the VLM used here is not able to accurately model the direct wing-vortex interaction, resulting in unrealistic values.

The maximal fuel flow reduction achievable is 37.10% reduction at $-0.15y/b$ and $0z/b$, the earlier defined sweet spot. Including the margin of error, the value at the sweet spot becomes 18.27% at $-0.15y/b$ and $0.1z/b$. Both results identify a larger region of benefit. Even if the sweet spot would not be maintained, reductions in fuel flow could still be obtained, neglecting the impact of possible constant trim control required to fly within the formation. Comparing the close proximity case of wing tips aligned, at $0y/b$ and $0z/b$, a reduction of 16.24% was measured by the FMT model were the flight test results show a reduction of 12%. This would imply that within the close proximity case a fairly good assumption is made by the models used here. Again note that two different aircraft are compared, so no conclusive comparison can be made. It does offer confidence in the model used.

The aerodynamic model used within this study does not include the viscous effects and uses the estimation of Prandtl-Glauert to include compressibility effects, limiting the research to high subsonic Mach numbers. The complex interaction between the incident vortex, wake field and the wing is complex and requires further attention. The flight mechanic model also assumes a rigid wing that does not deform due to control deflections. The structural impact upon the direct

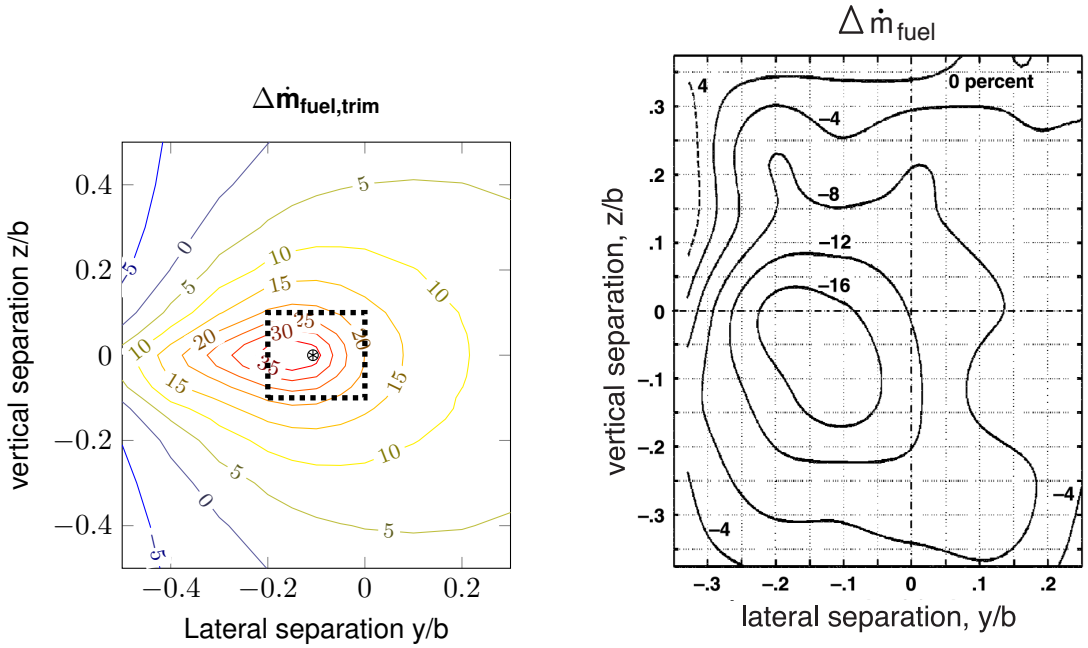

(a) FMT model

(b) Test flight 2 Do-28 aircraft

Figure 6.2: Wake field analysis of the fuel flow reduction in the formation flight condition, results FMT compared to test flight results of a two aircraft formation of Dornier Do-28 fighter aircraft at Mach 0.56 and an altitude of $7,600$ meters [22]

wing-vortex interaction and the dynamic behaviour due to the flexibility of the wing should also be further investigated. All these effects could further affect the benefit as identified here.

6.2.2 Control authority

The United States Air Force performed test flights using C-17 transport aircraft. Military transport aircraft are able to fly within formation using advanced systems. The flight is thus feasible. The pilots described the task of retaining one position within the wake field as feasible, by making use of the enhanced auto pilot present in the aircraft. The pilots identified a slight degradation of the ride quality in close proximity of the vortex system. Overall no remarks of an unattainable flight position where made during test flights within the wake field [3]. How do these results relate to the analytical models used here.

The formation flight condition was investigated dynamically by briefly simulating steady straight flight and by comparing the eigenvalues with relation to the solo flight condition. The analysis revealed an unstable flight condition. The eigenvalues of the total state-space matrix showed two extra motions, one oscillatory and one periodic. The brief dynamic simulation revealed an initial divergence in roll and pitch, possibly linking the eigenvalues to the phugoid and roll mode. Controls could be used to actively make the aircraft stable.
It must be noted that the dynamic simulation performed here assumes one trimmed condition. It is known that the variations in interference moments and forces are strongly related to position within the wake field. A small change in position could require a new trimmed condition. A constant re-evaluation of control deflections required for trim would be mandatory. Further research into the exact behaviour is mandatory however to obtain conclusive findings regarding the dynamic behaviour.

At the high subsonic Mach number, 0.6, the aileron hinge moment was below its design limit throughout the wake field, with exemption of the deep wake field for zero vertical separation. The limit was only exceeded on the in-vortex aileron though. The out-of-vortex aileron does see an increased hinge moment around the vortex core.
In general deep wake field positions should be avoided during the formation flight. The variations in moments and forces are not gradual. Actuator speeds also come into play, as changing an aileron deflection from e.g. $10^{\cdot}$ degrees to $-3^{\cdot}$ will not be instantly. As the close proximity region of the wake field offers benefits, the large disturbances can be avoided whilst still attaining the benefit. The trumping of the aileron hinge moment should thus not pose a problem as preferably the entire deep wake vortex field is avoided.
As the hinge moment stays well within the design limit, with exemption of the deep wake field for the left aileron, it could be implied that enough leeway is present for control. Although to be conclusive the aero-servo-elastic effects, neglected here, need to be included to identify the effectiveness of the aileron control deflection. Nevertheless, the results as identified here show good potential regarding control authority.

It remains inconclusive what happens when for example an aerodynamic gust forces the aircraft to change position. Possibly the aileron deflections required, do surpass the design limit. The

changes could also come suddenly, making that control deflections are delayed, forcing the aircraft out of the formation before it can trim for the new position. Van der Kleij [26], who investigated an automated formation flight control system, showed what would happen when the trail aircraft would move from left tip aligned ($0.0y/b$) towards right tip aligned ($-2.0y/b$) at zero vertical separation ($0z/b$), moving across the region of high aileron deflection and hinge moment values. The trail aircraft would experience a change from positive rolling moment to a high negative rolling moment within the down-wash region of the wake field. The down-wash would create a pitch-down tendency for the trail aircraft. Both pitch-down and high negative rolling moment would force the aircraft out of the formation, despite disturbing, without creating an unsafe situation. A remark is that the aircraft was flown into the wake field to identify what would happen, without forcing the aircraft to retain a position deep within the wake-field. It remains inconclusive if a current passenger aircraft can respond fast enough to cope with the sudden changes in destabilizing forces and moments.

The test flight identified the feasibility, question marks remain to describe and understand the behaviour when flying within the formation. Before commercial aircraft can switch to the formation flight as a manner of fuel saving, further research is required into the dynamic behaviour and the impact upon the control systems. It must be researched if static and dynamic stability can be achieved, with constant trimming throughout the formation flight. The divergence in pitch, as identified, should be avoided during flight. The question remains open whether or not this is achievable and/or if by trying another dynamic divergence motion is initiated.

6.2.3 Hinge moments

The hinge moment estimation showed a difference in value for left and right aileron. The solo condition also revealed minor changes, which grew larger for the formation flight condition. It was already identified that this was due to the constant factor present within equation 4.8, that shifts the balance point. The highest values are obtained when the aileron is deflected downward, the deep wake field for the left aileron and around the vortex core for the right aileron. The hinge moments remain within the design limit value in the wake field. The only exemption was the deep wake field positions for zero vertical separation on the in-vortex, left, aileron. As this region is generally one to avoid, due to the more brutal changes in destabilizing forces and moments. Important to note is the assumed cruise speed of Mach 0.6, considerably lower than the normal cruise Mach number of the A330-300, which is Mach 0.82. The hinge moment as was obtained is restated within figure 6.3. A higher velocity creates shock waves and partial turbulent flow over the aileron control surface, possibly affecting the forces and moments acting upon the aileron control surface including the hinge moment.

The assumption of a rigid wing as well as the neglecting of aerodynamic twist due to a control deflection and the aero-servo-elastic effects could also make the hinge moment to be larger than estimated here. By incorporating these effects, possibly higher aileron deflections might be needed to attain a similar result or similar deflections create higher forces and moments acting on the surface. Both cases would imply an increase in hinge moment. The dynamic

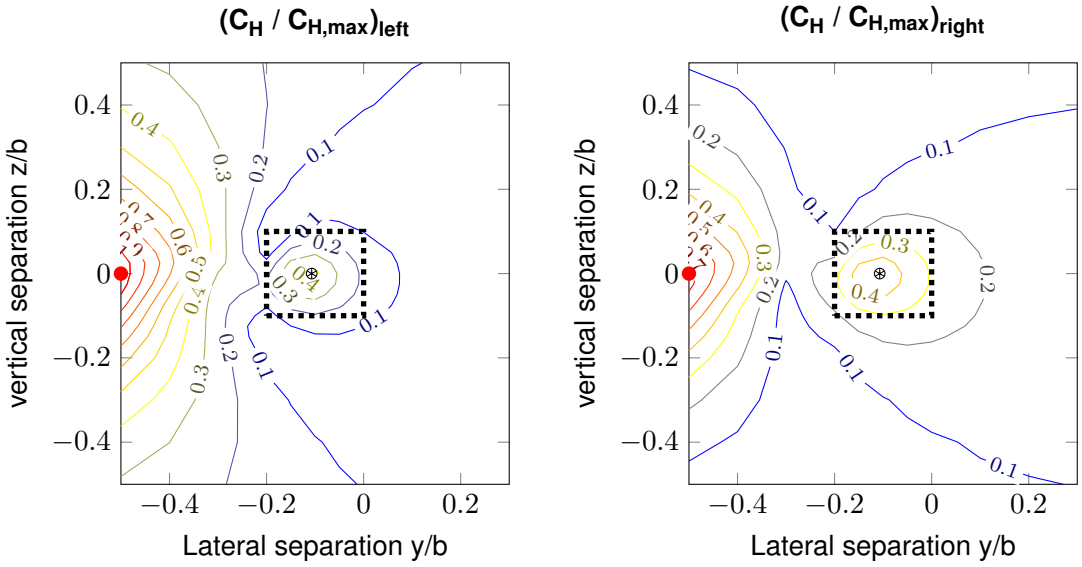

(a) Left aileron hinge moment

(b) Right aileron hinge moment

Figure 6.3: Wake field analysis of difference in hinge moment with relation to limit value

behaviour of the deflections of the wing as well as the aerodynamic twist due to the aileron deflection could create structural oscillations that might endanger the integrity of the ailerons and wing tips. Further research into the structural properties of the aileron deflections and wing tip deflections is required to identify potential problems.

6.2.4 Benefits

The formation flight offered a 18.27% reduction in fuel flow located at the sweet spot outside the margin of error, $-0.15y/b$ and $0.1z/b$. The flow conditions where set to the assumed cruise flight at $11,000$ meters at a velocity of 0.6 Mach and lift coefficient of $0.623[-]$. The position was chosen on the boundary of the margin of computational error, imposed by the aerodynamic model 10% around the vortex core.

This reduction comes at the cost of an disturbance in loads which requires extra control deflections to retain steady straight flight at the sweet spot. The most pronounced interferences are in roll and pitch. The aileron deflection shows the largest required change in value, where the surface was not designed to retain large deflection angles during cruise flight. Depending on position within the wake vortex field, the required deflection angles change. Small changes in position thus require a different setting, making that active control is required to retain a steady straight flight.
The dynamic analysis already identified an unstable behaviour within the formation flight condition. Only the eigenvalues were studied of the total state-space representation of the

equations of motion. The unstable behaviour stems from the variations throughout the wake field, related to the positions. If the position is altered, the defined trim balance changes. The aircraft will be forced out of the formation if no action is undertaken. The analysis as presented now even shows that the aircraft moves into a roll and pitch divergence, if no counteracting control deflection is performed. Further research into the behaviour is required however to obtain conclusive results concerning the behaviour of the formation flight condition.
The loads upon the hinge moment of the aileron are increased due to the deflections. The design limit load was even exceeded on the in-vortex aileron in the deep wake field. This 'new' way of using the ailerons will have an effect on the structural life-time of the hinge, which should be further investigated.
Important to remember are the subsonic flow assumption, together with the rigid wing neglecting aero-servo-elastic effects. Moving into the transonic flow region and incorporating wing deformations could further aggravate the loads and dynamic behaviour.

In general the total benefit would offer great fuel savings for long-haul flights in the formation flight condition. Current aircraft could be used, although constant control is required to retain one position within the wake field. A new automated flight control system could alleviate the loads on the pilot and more accurately position the aircraft in the wake field. A reinforcing of the aileron control systems would better cope with the loads, requiring less maintenance.

6.3 State-of-the-art

The last couple of years the interest into the formation flight topic grew. Since 2012 the U.S. Air Force in cooperation with NASA started to investigate its benefits within the SAVE program, identifying Surfing Aircraft Vortices for Energy. One of the major goals was to reduce the risks and uncertainties associated with the formation flight condition, to possibly be used within a fleet of military aircraft to reduce the fuel consumptions.

The first test flight before the real kick-off of the SAVE project was performed in 2012 by the NASA Dryden research center with two regular C-17 aircraft [29]. The C-17 aircraft where chosen due to their advanced station keeping capability, more often called Formation Flight System (FFS). Speer described the development of this technology for formation flight avionics in air mobility aircraft. An 'additional' flight control system was developed to relax the task of pilots whilst trying to retain a formation from a military protective perspective, disregarding the potential aerodynamic benefit [16]. The initial flight test already showed fuel flow reductions ranging from 6.8% till 7.8%. The workload on the pilots to retain test positions within the wake field was high, however not infeasible. It was concluded that the task was not operationally representative.
The changes of forces and moments within the wake field, creating disturbances, were also identified within this research. Control deflections are required to balance these disturbances to retain a desired flight path. As the disturbances throughout the wake field varied, constant trim would be mandatory to retain a position within the wake field. Some positions of lower benefit do offer lower disturbances or regions of constant disturbance. This could relieve the

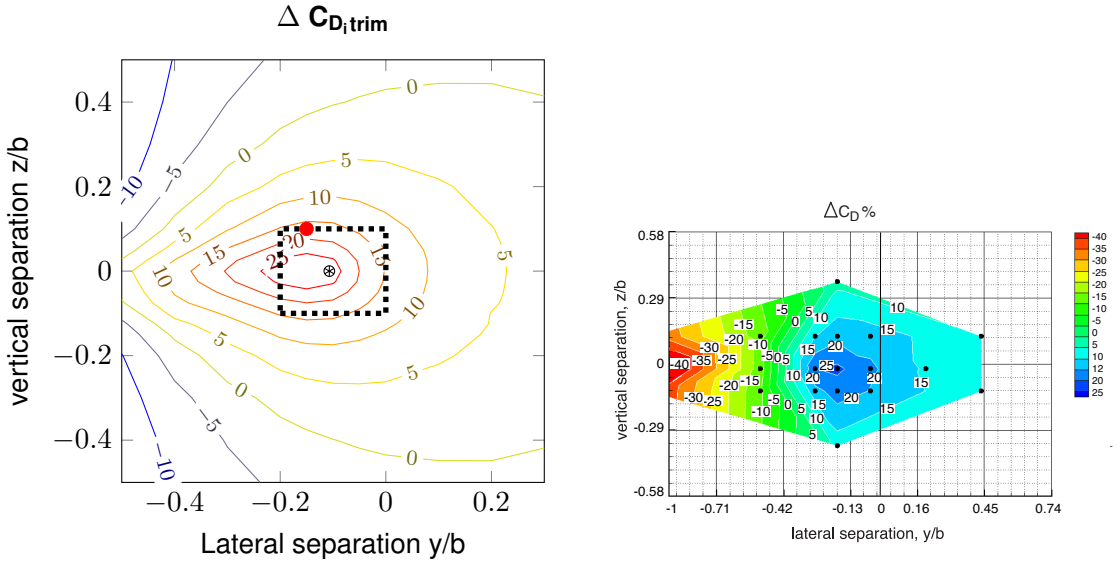

(a) Induced drag results A330-300 by FMT

(b) Induced drag results of C-17 aircraft by RANS CFD solver

Figure 6.4: Induced drag savings, Formation flight condition related to solo flight condition

workload upon the pilots if no automatic station keeping system is present.
The test flights performed with the C-17 military cargo aircraft already offered the automatic station keeping system, developed for military purposes, making it ideal to perform tests with. Possibly the system could be extended to better suit the station keeping within the formation flight condition.

Slotnick et al. developed a computational aerodynamic analysis tool to be used to analyse the flow before further developing the formation flight technology for the C-17 program [2]. A high-fidelity approach was used with a hybrid CFD method, based on the Reynolds Averaged Navier Stokes (RANS) equations. To compare our induced drag results, both the results obtained by the high fidelity approach and the results from FMT are plotted in figure 6.4. Although different aircraft where used, the difference for induced drag should be comparable in pattern and magnitude, as both can de defined as large transport aircraft of different configuration though. Noting the assumptions made by both the aerodynamic and flight mechanical analysis, the drag reduction is fairly well predicted. Again the values around the vortex core deviate more compared to the results obtained by Slotnick et al. The general behaviour is similar, and the values agree better within close proximity condition. Within the wake vortex field and the direct vortex interaction conditions, discrepancies are identified.

The results obtained were subsequently used by Halaas et al. [5] to create a formation flight simulation tool, to obtain a better insight into the formation flight condition and the aerodynamic benefit. The research was positioned within the technology development phase of the SAVE program. The goal was to create and validate a dynamic simulation tool, which includes the

aerodynamic wake effects with enough accuracy. The simulation tool could afterwards be used to support and develop a control system capable of aiding an aircraft to fly within the formation flight. An accurate dynamic wake development model was created, to simulate the wake vortex sheet as it is shed by the lead aircraft. Subsequently the effects of positioning could be simulated.
The final model incorporated the effects of wake descent and meandering downstream of the lead aircraft. Atmospheric disturbances were also included as well as the decay of the vortex pair downstream. The model relied on results from multiple computational solvers combined with test flight data to accurately simulate the wake behaviour.

The simulation model was used to further investigate and elaborate the station keeping system of the C-17 aircraft before performing a new test flight in 2013. A summary of the actual flight tests is given by Bieniawski et al. [3]. The station keeping system was extended by a wake-crossing prevention and accurate positioning system was developed, installed and tested to position the trail aircraft within the wake field. The wake-crossing prevention prevented the trail aircraft to be forced within the wake field of the lead aircraft, increasing forces and creating pitch-down out of the formation, as was seen earlier. Nevertheless also wake crossings were flown to quantify the dangers present.

A series of short and long test flights was performed to measure the reduction in fuel flow as well as investigating the impact on the aircraft structure. Regarding the safety and wear of the aircraft, no exceeding of structural or vibration limits where detected. 60% of design limit was reached in worst case scenario, a longitudinal wake crossing creating a large rigid body response on the outboard wing of the trail aircraft as it is rolling through the wake field. In general the probability of weak crossings should be limited, to reduce wear and fatigue of the aircraft structure. The direct interactions of the aircraft with the vortex core and wake field were identified as dangerous and should be avoided to reduce the rigid body roll response on the outboard part of the trail aircraft wing. The wake-crossing prevention assisted the pilot to avoid these regions.
The region of worst case scenario was also identified within the aerodynamic wake analysis presented here, where the forces and moments proved to reach a maximal value at the center of the wake vortex field at $-0.5y/b$. Similarly the aileron hinge moments showed their highest values at this location. The quantification of the forces, moments and the aileron hinge moments together with the hinge design limitation offers a fast estimation tool to further investigate the effects of design changes. The fuel flow reductions during the long test flights showed fuel flow reductions varying from $5 - 10\%$, considerably lower then estimated here.

The tool extended for this master thesis work, the FMT model, could be compared to the simulation model of the SAVE project. The difference lies within the flexibility of the FMT model. Multiple aircraft can easily be implemented due to the modular structure of the program. The level of accuracy can also be extended by including more accurate data next to the already existing data, as was obtained using the VLM. The option to quantify the effect of trim upon the formation flight condition could further be exploited to optimise the design to better suit the formation flight.
Although the values are over-predicted, not all drag components were included. Also

aerodynamic and structural deformation effects were not included. The possibility to further develop and extend the FMT model could increase the reliability of the model to obtain more insight into the formation flight analysis.

6.4 Conclusion

The FMT model showed a total drag reduction of 16.59% at $-0.15y/b$ and $0.1z/b$, corresponding to the sweet spot outside the margin of error imposed by the aerodynamic data used. The total drag reduction at that location corresponds to a fuel flow reduction of 18.27%. Using an empirical estimation method, it was identified that the hinge moment was not exceeded within the wake field, with exemption of the deep wake field for zero vertical separation on the left aileron. As this region shows large and sudden variation in interference forces and moments, it should be avoided. A difference between left and right aileron hinge moments was present, which could be assigned to the downward deflection creating a higher moment in the formation flight condition. Regions of high values were identified around the vortex core, within the margin of error. The initial dynamic analysis showed an unstable behaviour of the aircraft, for which further research is required to obtain conclusive results concerning the dynamic behaviour within the wake field.a position
The simulation model extended for this master thesis offers a flexible simulation tool to further investigate the aerodynamic and flight mechanic behaviour within the formation flight condition. The modular structure also offers the incorporation of structural analysis tools to investigate the impact of the dynamic behaviour upon the airframe.

CHAPTER

SEVEN

CONCLUSIONS

The goal of this research was to provide a quantitative analysis of aircraft trim upon the trail aircraft and its lateral control system when flying within the wake vortex generated by a lead aircraft during formation flight. Several questions were identified to obtain this goal. A wake field analysis into the sensitivity of the interference forces and moments is required first. Thereby insight is gained into the wake vortex field before a trail aircraft is positioned within this field. The positioning of the trail aircraft in the wake vortex field as well as the balancing of the forces and moments on the trail aircraft, for a desired flight condition, was subsequently investigated. The aircraft balanced for multiple positions resulted in the quantification of the aircraft trim throughout the wake vortex field. Similarly an analysis of the aileron hinge moment throughout the wake field was investigated, related to the design limit in solo flight condition. Finally a brief dynamic eigenvalue analysis was performed at one position of interest. The positioning, balancing, trim quantification, dynamic and aileron hinge moment analysis was repeated for two cases studies to identify relations between the lateral control surface and the trimmed condition.

To start off a literature review was performed. The literature review had as primary purpose to identify what was already done regarding formation flight analysis, trimmed flight and those two combined. The secondary purpose was to identify aircraft behaviour under formation flight conditions, i.e. what to expect. Research into formation flight stretches back to 1914. In formation flight, a trail aircraft flies within the wake vortex field of another aircraft. The wake vortex field consists of a region of downwash, behind the lead aircraft, and a region of upwash, outside of the tips. By positioning the trail aircraft within the region of upwash, the lift vector is locally tilted forward. The effective angle of attack is increased, reducing the induced drag component locally. The region of downwash however does the opposite.
As only locally the effect is noticed, an asymmetric force distribution will appear and interference moments will be generated on the aircraft. The pitching and rolling moment were identified as

largest contributors to the interference effects, where the deep wake vortex field shows the highest values of disturbance.

Two models were used within the research: an aerodynamic solver and a simulation model. Both models introduced assumptions and limitations to the results. The most important ones are listed:

- Free stream lower than Mach 0.6
- Aerodynamic data error 10% at $-0.107y/b\ 0z/b$ & 5% at $-0.5y/b\ 0z/b$
- Rigid wing model
- Aileron hinge empirical estimation
- Tailored to Airbus A330-300, with option to add other models

The research analysis is performed for an assumed cruise flight of Mach 0.6 at a normal cruise lift coefficient of $0.623[-]$ and altitude of $11,000$ meters.

The aerodynamic analysis identified the disturbance forces and moments for a series of instances within the wake field. Important remarks are:

- Sweet spot shifts due to margin of error to $-0.15y/b$ and $0.1z/b$
- Induced drag reduction at sweet spot 52.7%
- Deep wake field shows highest interference loads (around $-0.5y/b$)

The disturbances were in accordance with what was identified in literature, with the highest disturbances located at the center of the wake vortex field. The disturbance forces and moments that were obtained were used in the simulation model. Through analysis of flight dynamics and loads, the value of induced drag reduction after trimming the aircraft into a steady straight flight was obtained. Throughout the wake field, aileron deflection is increased, compared to solo flight condition, and the potential induced drag benefit is reduced, although only slightly. The assumptions of the models probably underestimate the reduction of benefit due to trim. The local dynamic eigenvalue analysis at the sweet spot showed an unstable roll and pitch mode. The aileron hinge moment remained within its design limits, except for the deep wake field positions of the in-vortex aileron were the limit was exceeded by a few percent. It was identified that a positive deflection angle results in the highest hinge moment, where the larger the deflection result in higher moments.
The most remarkable changes due to trim at the sweep spot, $-0.15y/b$ and $0z/b$, are:

- Induced drag benefit from 52.7% to 47.5%
- Angle of attack from $3.08^{\cdot}$ degree to $2.53^{\cdot}$ degree (decrease)
- Aileron deflection from $0^{\cdot}$ degree to $2.32^{\cdot}$ degree (increase)
- Elevator deflection from $-0.81^{\cdot}$ degree to $-0.61^{\cdot}$ degree (decrease)
- Rudder deflection from $0^{\cdot}$ degree to $0.74^{\cdot}$ degree (increase)

- Dynamic eigenvalue analysis shows unstable behaviour
- In-vortex aileron hinge moment of $0.0189[-]$ with limit set at $0.2516[-]$
- Out-of-vortex aileron hinge moment of $-0.0500[-]$ with limit set at $-0.2522[-]$

Two design sensitivity studies were performed. First an increase in aileron size was investigated by using both the inboard and outboard ailerons as a means of lateral control. The purpose was to lower the deflection angle to possibly lower the drag created by the surface. The aileron deflection could be lowered by using both ailerons at the same time, although a large pitch up tendency was created. This created a stronger pitch instability and mandatory change in direction of elevator deflection. The potential induced drag benefit for the case was lower at the sweet spot.
The second case was that of the predefined aileron deflection at the in-vortex wing. The approach was to reduce the out-of-vortex aileron deflection to zero, to reduce impact of trim drag on the potential benefit. The approach is affected by the position within the wake field, as for each position one specific angle is optimal. The sweet spot was chosen as the focus of the second case. The angle was set at the normal deflection required at this position, namely $2.32^{\cdot}$ degrees. The analysis revealed a slight reduction in loss of benefit due to trim. The induced drag however does not capture the drag created due to a control deflection. The pressure drag does see the influence of a control deflection, but was not included within this study. This implies that more is to gain by the approach of a predefined angle to optimize formation flight. Overall the predefined aileron deflection showed a noticeable benefit, albeit small.
Table 7.1 shows a summary of the simulation results, as was shown at the end of chapter 5.

$-0.15y/b$ $0.1z/b$	*Solo* *Condition*	*Formation Flight*	*Formation Flight* *in-out-board*	*Formation Flight* *predefined* δ_a
C_{D_i}	0.0101	$\Delta 52.6\%$	$\Delta 52.6\%$	$\Delta 52.6\%$
$C_{D_i trim}$	0.112	$\Delta 47.49\%$	$\Delta 18.2\%$	$\Delta 47.50\%$
$_{D_i}$	0.0011	$\Delta -5.10\%$	$\Delta -34.4\%$	$\Delta -5.09\%$
α	$3.08^{\cdot}$	$2.53^{\cdot}$	$2.67^{\cdot}$	$2.53^{\cdot}$
δa_{right}	$0^{\cdot}$	$2.32^{\cdot}$	$1.06^{\cdot}$	$-0.32^{\cdot}$
δa_{left}	$0^{\cdot}$	$-2.32^{\cdot}$	$-1.06^{\cdot}$	$-2.00^{\cdot}$
δe	$-0.80^{\cdot}$	$-0.61^{\cdot}$	$0.89^{\cdot}$	$-0.61^{\cdot}$
δr	$0^{\cdot}$	$0.74^{\cdot}$	$0.68^{\cdot}$	$0.78^{\cdot}$
C_{Hleft}	$max = 0.2516$	0.0189	0.0025	0.0375
C_{Hright}	$max = -0.2522$	-0.0500	-0.0258	-0.0342
eigenvalues'Stable'		*unstable* *roll/pitch*	*unstable* *roll/pitch*	*unstable* *roll/pitch*

Table 7.1: Overview of flight dynamic and load analysis results, for assumed cruise condition: $M = 0.6$, $h = 11,000$ meters, $C_L = 0.623$

Finally the formation flight benefit was positioned within the total flight picture, looking at the total drag and fuel flow. At the sweet spot outside of the margin of error, at $-0.15y/b$ and $0.1z/b$, the benefit is:

- Potential total drag reduction of 16.59%
- Reduction of fuel flow of 18.27%

Reduction pattern and magnitude are in agreement with results from other research studies.

The control allocation and its influence on the formation flight condition is hypothetically discussed, as no specific and conclusive results could be presented within this research work. The hinge moment estimation did identify an exceeding of the design limit within the deep wake field, which is not a region of interest for positioning the trail aircraft. The region in close proximity to the vortex core, which is of interest, showed hinge moments that were well below the design limit.
The simulation model used during this research offers a good platform to start more research on the topic of formation flight. It is modular, it can therefore be extended and adjusted easily to obtain a powerful tool for simulation and analysis of the formation flight condition.

The research study provided an analysis of the wake vortex field, shed by a lead aircraft, identifying the interferences within. Subsequently a trail aircraft was positioned in that wake vortex field to quantify the aircraft responses to the interferences. The aircraft was trimmed for the desired steady straight cruise flight and the aileron hinge moment was investigated at each position within the wake field separately, using a simulation model. A dynamic eigenvalue analysis was performed to identify stability of the formation flight condition. Finally the sensitivity of size and deflection of the lateral control system were investigated. Changes in deflection and control allocation showed to be the most promising area of interest for further improvements in drag reduction.
Thus, a tool was provided to quantify the aircraft trim on the trail aircraft and its lateral control system while in formation flight. It also opens the possibility to undertake further research into the aerodynamic and flight dynamic behaviour of aircraft in formation flight.

CHAPTER

EIGHT

RECOMMENDATIONS

It has been proven that a potentially large benefit can be gained by flying in the formation flight condition for long haul flights. Current passenger aircraft initially do not show problems due to the formation flight condition, although more research into the wear and safety of control systems and aircraft structure are required primarily. Even if the theoretical benefit is overestimated, still a benefit can be gained by implementing an operational change.
To conclude the research as presented here, recommendations are made. These recommendations illuminate further fields of interest as well as possibilities to extend the current research, to gain insight into the behaviour of the formation flight condition. Topics that were not tackled within this study are also listed among the recommendation. These recommendations are grouped into three categories, conform to the division within the report: the aerodynamics, flight dynamic and loads and finally the general flight aspects.

The aerodynamic recommendations related to the formation flight research and the extended vortex lattice method are listed primarily:

- Research into the different aerodynamic data tables
- Research into the direct wing-vortex interaction
- Research into the aero-servo-elastic effects
- Extension of the aerodynamic data tables (incorporate compressibility and viscous effects)

The first three points are concerning the aerodynamic effects that are dominant for the trimmed formation flight condition. The effect of the vortex acting directly on the wing(tip) structure has a complex nature, also relating to an aileron deflection. Previous research has investigated the effect of direct wing-vortex interactions and compressibility effects [28] [27], even related to aileron deflections [6]. The complex behaviour primarily needs to be understood before control

systems and structural adaptations can be made to aircraft to suit the formation flight condition. The results should be incorporated within the aerodynamic data tables to extend them and provide a more complete picture of the formation flight condition within the simulation model. By improving the understanding of the interactions present within the lead aircraft wake-vortex field, the formation flight and the responses of the trail aircraft can be refined. Simulation models can be extended to more accurately recreate the formation flight condition.

The flight dynamic and load recommendations related to the formation flight research and the simulation model used are listed secondly:

- Fine tuning simulation model for wake field positioning and load variation
- Research into dynamic behaviour and responses
- Extension simulation model for pressure and wave drag
- Extended research and simulation model for control authority

The model should be further extended to simulate other aspects of the formation flight. The extension of the aerodynamic property table together with fine tuning of the aerodynamic definitions within the model will result in more accurate results of the formation flight simulation. The simulation model can be used to do further research into the dynamic behaviour and responses of the trail within the formation flight condition. The current model or an extended version can be used for the analysis. The incorporation of pressure and wave drag will result in a more accurate simulation, resulting in an elaborate tool to analyse the formation flight condition for multiple aircraft. Finally by extending and changing the control module, more specific solutions to counter the load changes in the wake field can be researched. Within this study an approximate method for control allocation was incorporated, using a predefined aileron deflection. The option to specifically design a control allocation scheme, suited to the formation flight and relation to the aircraft geometry, would further extend the simulation tool.

The general formation flight recommendations are listed finally, incorporating aspects of the total formation flight picture:

- Validation of trimmed formation flight results, using CFD - wind tunnel - test flight data
- Extension simulation model to perform further analysis into formation flight condition
- Extension by adding multiple geometries in the aerodynamic and simulation model

The simulation results as presented here should be further investigated using other test methods, like CFD and/or wind tunnels. Fransen already presented a research how to test the formation flight in a wind tunnel [25]. The tests would validate the findings of the simulation model and could possible further extend its aerodynamic data table, to simulate the formation flight more accurately. Secondly extensions can be made to perform extra analysis of the formation flight, comparable to the extension of the hinge moment estimation added for this research. Finally by incorporating extra geometries in both aerodynamic and the simulation model, more research can be done concerning different aircraft and possibly also heterogeneous formations.

Both models as presented and used within this report offer prospects to perform further research into the formation flight topic. The aerodynamic model does not incorporate all effects, but offers a basic aerodynamic property table, to be further extended with extra data. The simulation model for the flight dynamic and load analysis offers the option to keep on extending. This could result in an extended model to simulate the formation flight condition for multiple aircraft geometries, further developing insights and possible (re)designs to better suit the formation flight. The simulation model would become comparable to that of the United States Air Force for the Surfing Aircraft Vortices for Energy program, partially presented by Halaas et al. [5], only here it would be for commercial aircraft and development research.

BIBLIOGRAPHY

[1] Carl Wieselsberger. Beitrag zur erklärung des winkelfluges einiger zugvögel. *Z. Flugtechnik u. Motorluftschiffahrt*, 5:225–229, 1914.

[2] J.P. Slotnick, R.W. Clark, D.M. Friedman, Y. Yadlin, D.T. Yeh, J.E. Carr, M.J. Czech, and S.R. Bieniawski. Computational aerodynamic analysis of formation flight for aerodynamic benefit program. In *AIAA 52nd Aerospace Sciences Meeting*, number AIAA 2014-1458, 2014.

[3] S.R. Bieniawski, R.W. Clark, S.E. Rosenzweig, and W.B. Blake. Summary of flight testing and results for the formation flight for the aerodynamic benefit program. In *AIAA 52nd Aerospace Sciences Meeting*, number AIAA 2014-1457, 2014.

[4] T. Flanzer, S.R. Bieniawski, and W.B. Blake. Operational analysis for the formation flight for aerodynamic benefit program. In *AIAA 52nd Aerospace Sciences Meeting*, number AIAA 2014-1460, 2014.

[5] D.J. Halaas, S.R. Bieniawski, D.T. Whitehead, T. Flanzer, and W.B. Blake. Formation flight for aerodynamic benefit simulation development and validation. In *AIAA 52nd Aerospace Sciences Meeting*, number AIAA 2014-1459, 2014.

[6] James E Kless, Michael J Aftosmis, S Andrew Ning, and Marian Nemec. Inviscid analysis of extended-formation flight. *AIAA Journal*, 51(7):1–13, July 2013.

[7] Hermann T Schlichting and Erich A Truckenbrodt. *Aerodynamics of the Airplane*. McGraw-Hill Companies, 1979.

[8] H. Schlichting. Leistungserparnis in verbandsflug. In *Mitt. Deutsch. Akad. Luftfahrtforsch. no.2*, pages p. 97–139, 1942.

[9] D. Hummel. Die leistungserparnis beim verbandsflug. In *J. Ornithol. 114*, pages 259–282, 1973.

[10] D. Hummel. Die leistungsparnis in flugformationen von vögeln mit unterschieden in gröbe, form und gewicht. In *J. Ornithol. 119*, pages p. 52–73, 1978.

[11] PBS Lissaman and Carl A Shollenberger. Formation flight of birds. *Science*, 168(3934): 1003–1005, 1970.

[12] Dietrich Hummel. Aerodynamic aspects of formation flight in birds. *Journal of theoretical biology*, 104(3):321–347, 1983.

[13] Markus Beukenberg and Dietrich Hummel. Aerodynamics, performance and control of airplanes in formation flight. In *ICAS, Congress, 17 th, Stockholm, Sweden, Proceedings.*, volume 2, pages 1777–1794, 1990.

[14] 0 J McMillan, RG Schwind, JN Nielsen, and MF E. Dillenius. Rolling moments in a trailing vortex flowfield. *Journal of Aircraft*, 15(5):280–286, 1978.

[15] Vernon J Rossow. Validation of vortex-lattice method for loads on wings in lift-generated wakes. *Journal of aircraft*, 32(6):1254–1262, 1995.

[16] TK Speer, EC Mills, and JL Tate. Formation flight technology. *Aircraft Engineering and Aerospace Technology*, 43(7):4–8, 1971.

[17] F.J. Overcash. Aircraft station keeping and terminal navigation system. Lockheed Aircraft corp, August 31 1965. US Patent 3204237.

[18] William Blake and Dieter Multhopp. Design, performance and modeling considerations for close formation flight. *CLJ*, 150:2, 1998.

[19] William B Blake. An aerodynamic model for simulation of close formation flight. In *Proceedings of AIAA Modeling and Simulation Technologies Conference and Exhibit*, number 4304. AIAA, August 2000.

[20] Geno Wagner, Dave Jacques, Bill Blake, and Meir Pachter. An analytical study of drag reduction in tight formation flight. *AIAA paper*, 4075, 2001.

[21] Jennifer L Hansen and Brent R Cobleigh. Induced moment effects of formation flight using two f/a-18 aircraft. In *Proceedings of AIAA flight mechanics conference and exhibit*, number 4489. National Aeronautics and Space Administration, Dryden Flight Research Center, 2002.

[22] Ronald J Ray, Brent R Cobleigh, M Jake Vachon, and C St. John. Flight test techniques used to evaluate performance benefits during formation flight. In *NASA CONFERENCE PUBLICATION*, number 4492. NASA, AIAA, 2002.

[23] RK Nangia and ME Palmer. Formation flying of commercial aircraft–variations in relative size/spacing–induced effects & control. *AIAA Journal*, 4163:2007, 2007.

[24] S Andrew Ning and IM Kroo. Compressibility effects of extended formation flight. In *29th AIAA Applied Aerodynamics Conference*, number 3812. AIAA, June 2011.

[25] Bert Fransen. Formation flight: Theoretical investigation regarding applicability of wind tunnel tests for the validation of theoretical formation flight benefits for long range transport aircraft. Master's thesis, Delft University of Technology, March 2012.

[26] C.A. van der Kleij. Close formation flight control with applications in commercial aviation. Master's thesis, Delft University of Technology, September 2012.

[27] Daniel J Garmann and Miguel R Visbal. Interaction of a streamwise-oriented vortex with a wing. *Submitted, AIAA SciTech*, 2014.

[28] Caleb J Barnes, Miguel R Visbal, and Raymond E Gordnier. Investigation of aeroelastic effects in streamwise-oriented vortex/wing interactions. 2014.

[29] J. Pahle, D. Berger, M. Venti, C. Duggan, J. Faber, and K. Cardinal. An initial flight investigation of formation flight for drag reduction on the c-17 aircraft. In *AIAA Atmospheric flight mechanics conference*, number AIAA 2012-4802, 2012.

[30] L Jacquin, D Fabre, P Geffroy, and E Coustols. The properties of a transport aircraft wake in the extended near field: An experimental study. *AIAA Paper 2001-1038*, 2001.

[31] LLM Veldhuis, Fulvio Scarano, and C Van Wijk. Vortex wake investigation of an airbus a340 model using piv in a towing tank. In *21st Applied Aerodynamics Conference, American Institute of Aeronautics and Astronautics*, 2003.

[32] Flow field behind aircraft.

[33] Ayumu Inasawa, Fumihide Mori, and Masahito Asai. Detailed observations of interactions of wingtip vortices in close-formation flight. *Journal of Aircraft*, 49(1):206–213, 2012.

[34] Deborah Saban, James F Whidborne, and AK Cooke. Simulation of wake vortex effects for uavs in close formation flight. *Aeronautical Journal*, 113(1149):727–738, 2009.

[35] J.A. Mulder, W.H.J.J. van Staveren, J.C. van der Vaart, and E. de Weerdt. *Flight dynamics lecture notes*. Delft University of Technology, February 2007.

[36] Maurits Dekkers. virtual hubs in the sky: Discrete-event simulation of an operational set-up for formation flight in commercial aviation. Technical report, Delft University of Technology, 2013.

[37] AIRBUS. Airbus aircraft family, . URL `www.airbus.com`.

[38] BOEING. Boeing aircraft family. URL `www.boeing.com/commercial`.

[39] AIRBUS. Airbus orders and deliveries, . URL `www.airbus.com/company/market/orders-deliveries`.

[40] Dietrich Hummel. Formation flight as an energy-saving mechanism. *Israel Journal of Zoology*, 41(3):261–278, 1995.

[41] William Blake and David R Gingras. Comparison of predicted and measured formation flight interference effects. *Journal of aircraft*, 41(2):201–207, March-April 2004.

[42] John D Anderson. *Fundamentals of Aerodynamics*, volume Fourth edition. McGraw-Hill, New York, NY, 2007.

[43] M. Drela. Athena vortex lattice.

[44] A.C. de Bruin and G Winckelmans. Cross-flow kinetic energy and core size growth af analytically defined wake vortex pairs, nlr. Technical report, report NLR-CR-2005-412, 2005.

[45] John E Williams and Steven R Vukelich. The usaf stability and control digital datcom. volume i. users manual. Technical report, DTIC Document, 1979.

[46] Albert Betz. *Behavior of vortex systems*. National Advisory Commitee for Aeronautics (NACA), 1933.

[47] Ed Obert. *Aerodynamic design of transport aircraft*. Ios Press, 2009.

[48] Till Pfeiffer, B Nagel, D Böhnke, A Rizzi, and M Voskuijl. Implementation of a heterogeneous, variable-fidelity framework for flight mechanics analysis in preliminary aircraft design. In *German Aeronautics and Space Congress, DLRK, 2011, Bremen, Germany*, 2011.

[49] DAJ Van Ginneken, Mark Voskuijl, Michel JL van Tooren, and Aldo Frediani. Automated control surface design and sizing for the prandtlplane. In *6th AIAA Multidisciplinary Design Optimization Specialist Conference, Orlando, Florida*, number 2010-3060, 2010.

[50] Mark Voskuijl, Jan de Klerk, and Daan van Ginneken. Flight mechanics modeling of the prandtlplane for conceptual and preliminary design. In *Variational Analysis and Aerospace Engineering: Mathematical Challenges for Aerospace Design*, pages 435–462. Springer, 2012.

[51] HJM Kok, Mark Voskuijl, and Michel JL van Tooren. Distributed propulsion featuring boundary layer ingestion engines for the blended wing body subsonic transport. In *6th AIAA Multidisciplinary Design Optimization Specialist Conference, Orlando, Florida*, 2010.

[52] Airbus. Airbus a330-300 dimensions and key data, 2013. URL `http://www.airbus.com/aircraftfamilies/passengeraircraft/a330family/a330-300/specifications/`.

[53] Jan Roskam. *Airplane flight dynamics and automatic flight controls*. DARcorporation, 1995.

[54] Ashish Tewari. *Aeroservoelasticity*. Springer, 2015.

[55] Helmut Zimmermann. Aeroservoelasticity. *Computer Methods in Applied Mechanics and Engineering*, 90(1):719–735, 1991.

[56] ESDU. Example of procedure in calculation of control hinge moments. Engineering Sciences Data Unit, August 1989.

[57] ESDU. Hinge moment coefficient derivatives for trailing-edge controls on wings at subsonic speeds. Engineering Sciences Data Unit, July 1989.

[58] ESDU. Slope of lift curve for two-dimensional flow. Engineering Sciences Data Unit, 1949.

[59] ESDU. Rate of change of lift coefficient with control deflection in incompressible two-dimensional flow. Engineering Sciences Data Unit, 1956.

[60] ESDU. Rate of change of hinge moment coefficient with incidence for a plain control in incompressible two-dimensional flow. Engineering Sciences Data Unit, 1956.

[61] ESDU. Rate of change of hinge moment coefficient with control deflection for a plain control in incompressible two-dimensional flow. Engineering Sciences Data Unit, 1956.

[62] Ted L. Lomax. *Structural loads analysis for commercial transport aircraft: theory and practice*. Aiaa, 1996.

[63] Federal Aviation Regulations. Airworthiness standards part 25.349. *Transport Category Airplanes, Retrieved May*, 2015.

[64] Daniel P Raymer. Aircraft design: A conceptual approach, american institute of aeronautics and astronautics. *Inc., Reston, VA*, 1999.

[65] Ohad Gur, William H Mason, and Joseph A Schetz. Full-configuration drag estimation. *Journal of Aircraft*, 47(4):1356–1367, 2010.

[66] Bryan Thwaites. *Approximate calculation of the laminar boundary layer*. Royal Aeronautical Society, 1949.

[67] M Niţă and D Scholz. From preliminary aircraft cabin design to cabin optimization. In *Deutscher Luft-und Raumfahrtkongress*, 2010.

APPENDIX

A

APPENDIX: AERODYNAMIC MODULE FLOW DIAGRAM

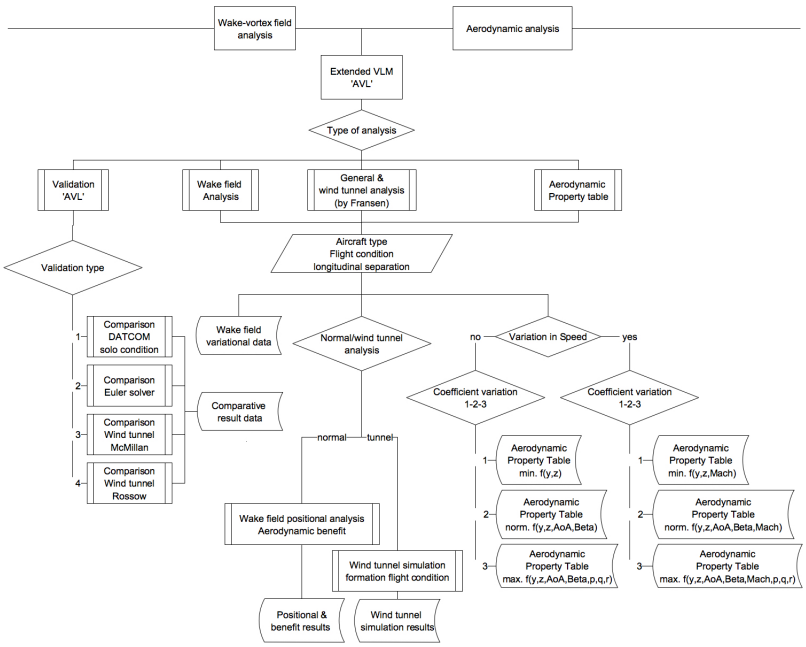

Figure A.1: Basic flow chart aerodynamic module

APPENDIX

B

APPENDIX: FLIGHT MECHANIC MODULE FLOW DIAGRAM

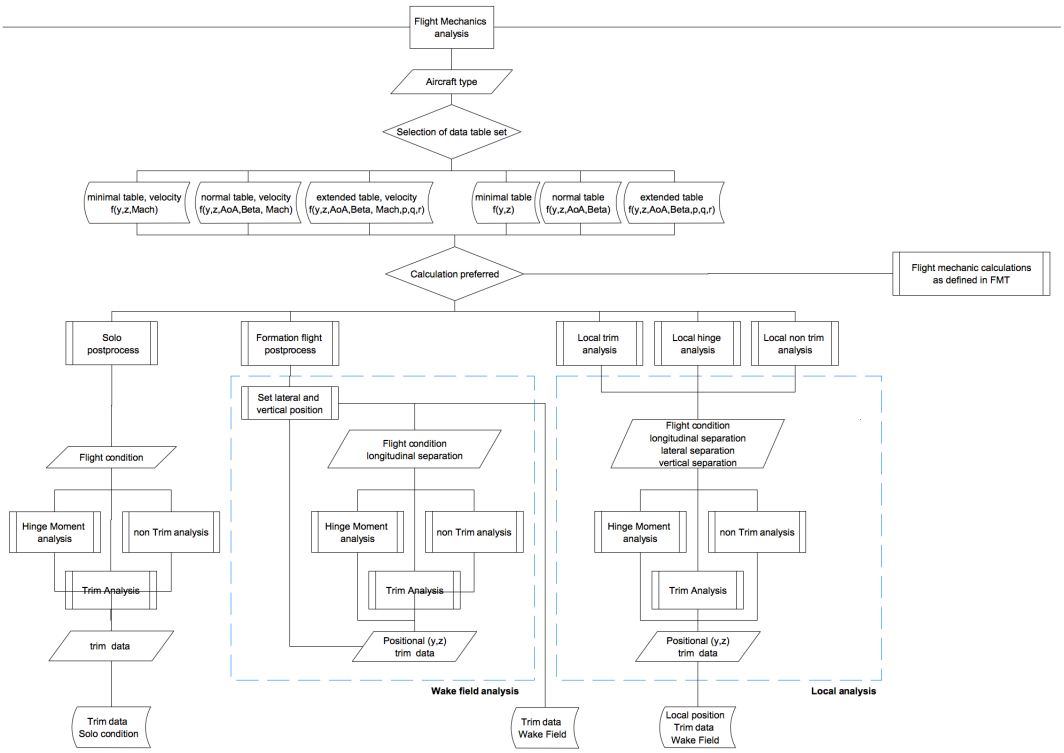

Figure B.1: Basic flow chart aerodynamic module

APPENDIX

C

APPENDIX: FMT CALCULATION OVERVIEW

This appendix contains an overview list of the settings, as were used during the creation of the results of the FMT simulation model. The difference between settings for the data sensitivity analysis are chosen by loading a different aircraft model at the start. This is indicated in the list by the addition of two aileron or control allocation to their geometry names. The remainder of the steps are identical. All results are gathered in the folder named Results under the geometry name. The data is saved in the folder of the geometry name in the aircraft model folder

The formation flight analysis requires a reference condition of the solo flight. First the solo flight analysis needs to be determined, before the formation flight analysis can be executed. The solo flight analysis requires the aerodynamic data table with relation to velocity due to the aileron hinge design limit determination, performing simulations at multiple velocities. The formation flight analysis is set at one velocity, not requiring the relation to velocity.

The list as presented here shows briefly which choices were made when creating the data using the FMT simulation model, for the A330-300 aircraft in formation flight condition. The list is divided into two parts, first the solo, reference condition is determined. Secondly the formation flight analysis is performed.

- SOLO condition
- Initiate simulation model, $create\_aircraft\_model$ in folder $aircraft\_models$
- Choose aircraft, solo A330-300 without winglets ($A330noWL$)
- Optional to choose aerodynamic data table, default is the 'normal' table as explained in chapter 4.2.1 (with velocity)
- Loading aircraft model
- Run solo analysis script, $SOLO\_PostProcess$

- Result figures in Results folder under geometry name and as $postprocess\_solo$ variable
- Result data in $aircraft\_models$ under geometry name and data
- FORMATION FLIGHT condition
- Initiate simulation model, $create_aircraft_mode$l in folder $aircraft\_models$
- Choose aircraft, solo A330-300 without winglets in formation flight condition ($A330noWL\_FF$)
- Optional to choose aerodynamic data table, default is the 'normal' table as explained in chapter 4.2.1(without velocity)
- Loading aircraft model
- Run solo analysis script, $FF\_PostProcess$
- Results in Results folder under geometry name and as postprocess variable
- Result data in $aircraft\_models$ under geometry name and data

APPENDIX

D

APPENDIX: LITERATURE OVERVIEW TABLE

Reference	Year	Category	Main topic	Calc. method	aircraft	Key findings
Wieselsberger [1]	1914 1914	Aero	Formation flight benefit	-	-	- Initial identification of benefit by observing birds
Lissaman et al. [11]	1970 1914	Aero	Formation flight benefit		-	- Description aerodynamics of benefit
Speer et al. [16]	1971	Control	History of military formation flight	-	-	- Station Keeping Systems (SKS)
McMillan et al. [14]	1978	A-Vortex	Wing-vortex interaction	Wind tunnel	- Rect. wing	- Variations forces/moments wrt. lat. pos. to vortex
Hummel [12]	1983	A-Trail	Formation flight benefit	- HSV - Lifting surface	- Rect. wing	- Quantification of the induced drag benefit - Formation shape and relation to the benefit - Influence of (in)homogeneous formations
Hummel [40]	1995	A-Trail	Formation flight benefit	- HSV - Test flight	- Rect. wing - DO-28	- 15% power reduction trail aircraft - Comparison test flight Dornier DO-28 - Formation shape/composition impact on benefit - Distribution benefit upon all aircraft in formation
Rossow et al. [15]	1995	A-Vortex	Wing-vortex interaction	- Wind tunnel	Swept wing	- Variations forces/moments wrt. lat. pos. to vortex
Lomax et al. [62]	1996	Struct	Aileron design limits	- Empirical	-	- Design deflection limit of aileron during cruise
Blake et al. [18]	1998	A-Trail	Formation flight benefit	- HSV	- Rect. wing	- Induced drag benefit calculation - Rectangular wings in formation flight - Variations forces/moments wrt. lat. pos. of vortex - 'Optimum' flight condition for formation flight
Blake [19]	2000	A-Wake	Formation flight Aerodynamic simulation	- VLM HASC95 - Wind tunnel	Delta wing	- Induced drag benefit calculation - Aerodynamic coupling effects - Positional stability analysis of wake field
Jacquin et al. [30]	2001	A-Wake	Wake-vortex propagation	- Wind tunnel	A300	- Vortex meandering within wake field - Wake-vortex sheet formation and properties - Unsteady properties of meandering vortices
Wagner et al.	2001	A-Trail	Formation flight & trim	- VLM	T-38	- Induced drag benefit of 62%

Table D.1: Overview of all papers and proceedings which contained relevant information regarding formation flight, from an aerodynamic and flight mechanic point of view as well as for the general case, that were used within this master thesis

Reference	Year	Category	Main topic	Calc. method	aircraft	Key findings
[20]				HASC95		- Induced drag benefit trimmed condition of 59% - Third aircraft in the formation benefit of 67%
Hansen et al. [21]	2002	A-Trail	Formation flight induced effects	- Test flight	F/A-18	- Induced drag benefit calculation - variations with relation to long.-lat.-vert. pos. of trail aircraft
Ray et al. [22]	2002	A-Trail	Formation flight performance	- Test flight - Horseshoe vortex	F/A-18	- Evaluation performance benefits - Fuel flow reduction between $14 - 18\%$
Veldhuis et al. [31]	2003	A-Wake	Wake-vortex propagation	- PIV in towing tank	A340-300	- wake-vortex decay - vortex meandering to 'stable' pos.
Blake et al. [41]	2004	A-Wake	Formation flight interference effects	- Wind tunnel - VLM HASC95	Delta wing	- Induced drag benefit calculation - Validation VLM - Mapping of variations in wake-induced effects
Nangia et al. [23]	2007	A-Trail	Formation flight variations size& spacing	- panel method	A340	- Design tool to optimise span loading and camber control against induced rolling
Saban et al. [34]	2009	A-Wake	Formation flight simulation wake vortex effect	- Ext. lifting line	Delta wing	- Validation ELL with wind tunnel results - Cross coupling effects in wake field
Ning et al. [24]	2011	A-Trail	Formation flight & compressibility effects	- Euler solver AERO package		- Formation induced shock wave propagation - Strong buffet and separation potential
Pfeiffer et al. [48]	2011	Flight Mech.	Flight Mechanics Toolbox	FMT	-	- Flight mechanic tool within FMT explanation and implementation
Voskuijl et al. [50]	2012	Flight Mech.	Flight Mechanics Toolbox	FMT	Prandtl plane	- Built up and functioning of FMT - Explanation Prandtl plane simulation model
Inasawa et al. [33]	2012	A-Vortex	Wing-vortex interaction	- Wind tunnel	- Rect. wing	- Induced drag benefit of 24% for -0.05 y/b - Incident & tip vortex interaction and propagation
Fransen [25]	2012	A-Wake A-Trail	Formation flight relation to wind tunnel modelling	- ext. VLM	- A330 - A380	- A330 total drag reduction of 26% at sweet spot - Interference forces and moments determination - Computational modelling of wind tunnel set-ups - Complete aerodynamic analysis of wake field
van der Kleij [26]	2012	Control	Formation flight control	- Ext. lifting line - simulation model RECOVER	B-747	- Identification of behaviour in wake-vortex field - Dynamic behaviour and control authority
Pahle et al. [29]	2012	A-Trail	Formation flight	- Test flight	C-17	- Fuel flow reduction between $7 - 8\%$, possibly 10% - High workload in the formation according to pilots
Kless et al. [6]	2013	A-Trail	Formation flight & trim	- Euler solver AERO package	- Rect. wing - Transonic aircraft model	- 54% induced drag reduction, $3 - 5\%$ lower for trim in subsonic condition - 35% induced drag reduction, $9 - 11\%$ lower for trim in subsonic condition - Highest shock wave strength on out-of-vortex wing - Trim only out-of-vortex wing not beneficial to benefit
Barnes et al. [28]	2014	A-Vortex	Wing-vortex interaction	- Navier Stokes FDL3DI	- Rect. wing	- Wing-tip vortex-incident vortex interactions - Identification bipole-entrainment-bifurcation - Effect on forces and moments - Relation of wing flexibility on interaction
Garmann et al. [27]	2014	A-Vortex	Wing-vortex interaction	- Navier Stokes FDL3DI	- Rect. wing	- Wing-tip vortex-incident vortex interactions - Identification bipole-entrainment-bifurcation - Influence on forces and moments
Flanzer et al. [4]	2014	Oper	Operational analysis of formation flight	- Optimisation tool	C-17	- $5 - 10\%$ fuel flow reduction per mission - Identification problem fuel benefit, without reducing fuel carried - Variations on flight planning, 1 hour take-off flex. achieves 50% of maximal benefit - Heterogeneous formations preferred
Bieniawski et al. [3]	2014	A-Trail A-Wake	Formation test flight summary	- Test flight	C-17	- Redefining formation flight station keeping system - Summary of test flights and their data - $5 - 10\%$ fuel flow reduction - Structural impact, safety and wear - No structural or vibrational limits exceeded - Slight degradation of ride quality
Slotnick et al. [2]	2014	A-Wake A-Trail	Formation flight analysis	- VLM - Panel method - RANS CFD	C-17	- 25% drag benefit - Comparison between computational methods - Variations within wake vortex field
Halaas et al. [5]	2014	A-Wake A-Trail Control	Formation flight simulation tool	Simulation model - CFD data - Test flight data - VLM data		- Development control system - System level performance analysis - Wake development & meandering estimation incl. aerodynamic disturbances - Variations within wake vortex field - Incorporates wake-crossing simulation results
Tewari [54]	2015	Aero -elasticity	Aero-servo	-	-	- Definition

Table D.2: Overview of all papers and proceedings which contained relevant information regarding formation flight, from an aerodynamic and flight mechanic point of view as well as for the general case, that were used within this master thesis